SURFACE MODIFIED SENSORS FOR THE DETERMINATION OF BIOMOLECULES/DRUGS

Ph.D. THESIS

by

MAMTA RAJ

DEPARTMENT OF CHEMISTRY
INDIAN INSTITUTE OF TECHNOLOGY ROORKEE
ROORKEE-247667 (INDIA)
APRIL, 2019

SURFACE MODIFIED SENSORS FOR THE DETERMINATION OF BIOMOLECULES/DRUGS

A THESIS

Submitted in partial fulfilment of the requirements for the award of the degree

of

DOCTOR OF PHILOSOPHY

in

CHEMISTRY

by

MAMTA RAJ

DEPARTMENT OF CHEMISTRY
INDIAN INSTITUTE OF TECHNOLOGY ROORKEE
ROORKEE–247667 (INDIA)
APRIL, 2019

INDIAN INSTITUTE OF TECHNOLOGY ROORKEE
ROORKEE

CANDIDATE'S DECLARATION

I hereby certify that the work which is being presented in the thesis entitled **"SURFACE MODIFIED SENSORS FOR THE DETERMINATION OF BIOMOLECULES/DRUGS"** in partial fulfilment of the requirements for the award of the Degree of Doctor of Philosophy and submitted in the Department of Chemistry of the Indian Institute of Technology Roorkee, Roorkee is an authentic record of my own work carried out during the period from December, 2014 to April, 2019 under the supervision of Dr. R.N. Goyal, Emeritus Professor and Dr. U.P. Singh, Professor, Department of Chemistry, Indian Institute of Technology Roorkee, Roorkee.

The matter presented in this thesis has not been submitted by me for the award of any other degree of this or any other Institute.

(MAMTA RAJ)

This is to certify that the above statement made by the candidate is correct to the best of my knowledge.

(U.P. Singh) **Supervisor**

(R.N. Goyal) **Supervisor**

The Ph.D. Viva-Voce Examination of **Ms. Mamta Raj**, Research Scholar, has been held on .....**.**

Chairperson, SRC **Signature of External Examiner**

This is to certify that the student has made all the corrections in the thesis.

(U.P. Singh) **Supervisor**

(R.N. Goyal) **Supervisor**

Head of the Department

Dated:

Chapter 1

General Introduction

1.1 ELECTROCHEMISTRY: OVERVIEW AND SIGNIFICANCE

Electrochemistry is a field of science, which deals with the interrelation of electrical and chemical processes. The electrochemical studies can encompass the electricity production from the released energy by the spontaneous chemical reactions and the applicability of electrical energy to accomplish non-spontaneous chemical transformations. The potent applications of electrochemistry in day to day life comprises energy conservation and storage devices, pollution control, biomedical research, corrosion, electrophoresis, fuel cells, electroplating etc. [1-5]. Electrochemistry also comprises further applications in the determination of mechanism of the electrode reactions as well as redox properties of biomolecules/drugs, which can also furnish insights on their metabolic products and pharmaceutical activities [6].

Firstly, in the year 1791, Luigi Galvani examined the impact of atmospheric electric discharge on a frog's leg, which was considered as the foundation experiment of electrochemistry. Further research in this area was started by Michael Faraday in 1832 and new electrochemical terminology was introduced by him, such as, cathode, anode, electrode, cation, anion and two fundamental laws of electrolysis. In the year 1888, Walther Hermann Nernst drawn out a theory relating the electromotive force to the energy of a chemical reaction in an electrochemical cell and derived an important equation known as "Nernst Equation". In 1923, "Father of electroanalytical chemistry", Czech scientist Jaroslav Heyrovsky, discovered the polarographic method of analysis, where current was measured as a function of the applied electrode potential and received Nobel Prize in 1959. This discovery of polarography resulted in the development of advanced electroanalytical methods, modern instruments, processors of analytical data and evolution of biosensors used in the electrochemical analysis of biomolecules [7,8]. The electrochemical methods are facile approach in direct analysis of analytes in pharmaceutical formulations and physiological fluids due to the capability of fast determining the drug content in blood, serum, plasma and urine samples without involving any pre-separation steps with good accuracy and selectivity. Electrochemical methods provide countless advantages such as rapid analysis, high accuracy, good sensitivity and selectivity, eco-friendly, long term stability and reproducibility, no requirement of pre-analysis steps and expensive instruments and hence, electrochemical analysis is considered as Green chemistry. Electrochemical techniques usually employ a three electrode system, which contains a reference electrode, a counter or auxiliary electrode and a working electrode. The oxidation and reduction processes take place at the surface of working electrode, which significantly controls the sensitivity therefore; improvement of surface morphology of

working electrode is a subject of considerable attention. In many cases, the modification of surface of the working electrode markedly boosts the response of oxidation or reduction peaks in terms of enhance sensitivity and selective analysis of analytes and decreased detection limit. The common surface modification agents, carbon nanomaterials, metallic and metal oxide nanoparticles, enzymes, surfactants and conducting polymers also provide the desired functionalities for achieving useful properties to the sensing surface.

Electroanalytical techniques being the most versatile methods have attracted enormous importance in the research areas of analytical chemistry and are routinely employed for quantitative and qualitative analysis of various biologically important molecules, traces of pharmaceutical drugs and quality control of industrial materials in the last few decades. The electroanalytical methods confer a suitable approach for analyzing the redox chemistry of biomolecules that occur in biological and physicochemical processes and specified as bio-electrochemistry. Usually bio-electrochemistry manages the analysis of the processes of biological and electrical relevance, which is aftereffect of the electron transfer processes in the biological systems. Electrochemical and reactions in biological system (enzymatic reactions) have numerous similarities, such as both types of process normally occur at similar temperature of 37^{o}C, same physiological pH of 7.4 and similar ionic strength of the electrolytes. In the electrochemical processes the reaction take places at an electrode-solution interface, whereas the biological processes take place at the enzyme-solution interface. The heterogeneous electron transfer processes are essential in both biological and electrochemical reactions. These similarities undoubtedly permit the extensive studies of drugs and biomolecules in physiological fluids using electrochemical techniques [9-11].

The organic compounds, which are produced by the living organisms are of immense significance in various biological processes due to their metabolic and biological effects and are commonly termed as biomolecules. Biomolecules, such as neurotransmitters, vitamins, amino acids, proteins, genetic materials, small molecules and their metabolites are of extreme clinical importance. Any kind of damage in DNA leads the production of DNA metabolites and its oxidized products can be taken as a signature of carcinogenesis and mutagenesis even at early stage. As the biomolecules are directly involved in various biological actions and have proper functions in human systems, the minute alteration in their concentration in the body fluids causes physiological imbalance, several diseases and pathological disorders. **Fig 1.1** represents the reference concentration ranges of some clinically relevant biomolecules. As any alteration in this

concentration can cause physiological imbalance in the human system; therefore, the quantitative assessment of such biomolecules in human physiological fluids is highly desirable.

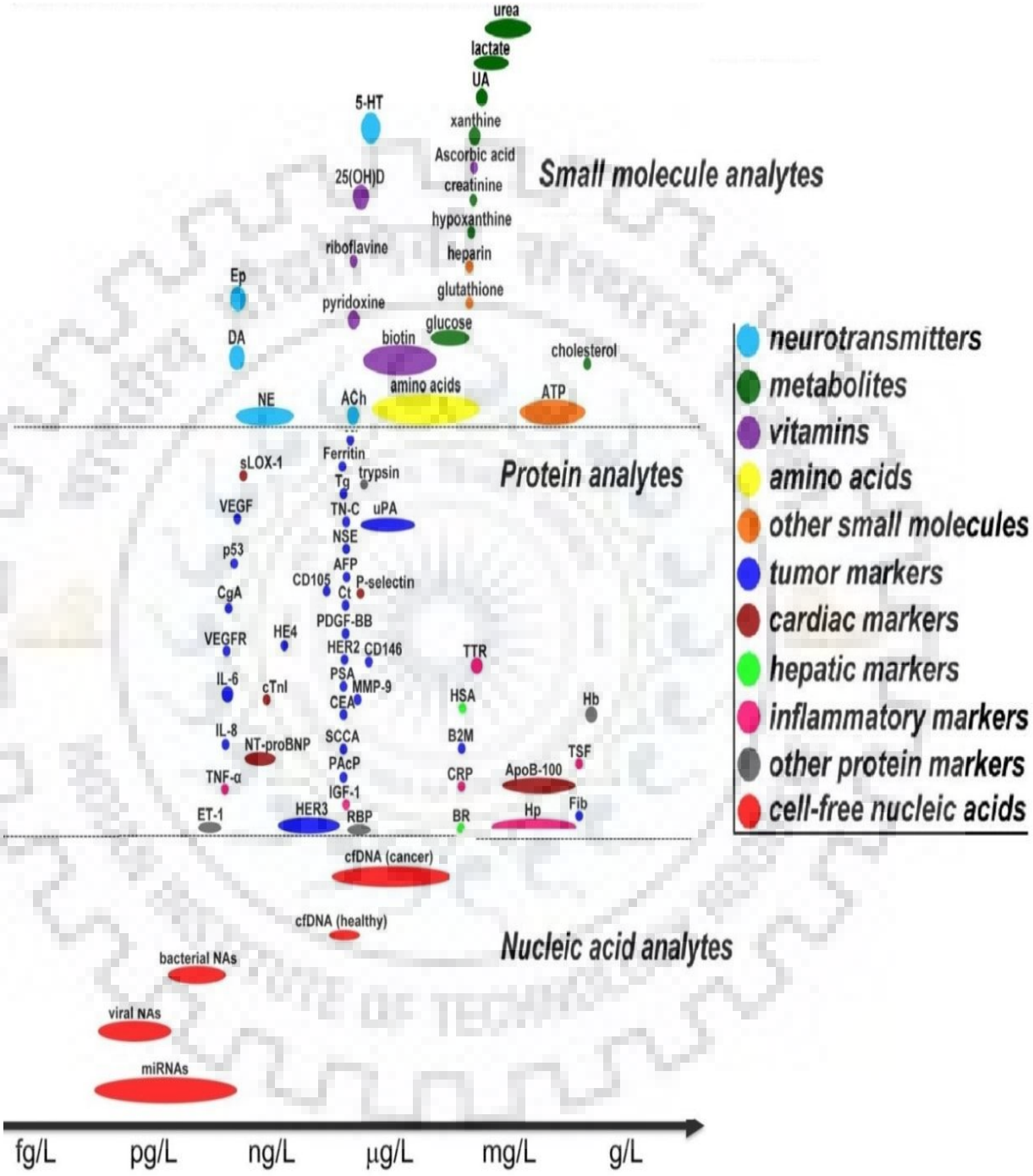

Fig. 1.1: Reference concentration ranges for some clinically relevant biomolecules.

Quantification of drugs is exceptionally essential for the pharmaceutical industries, biomedical research, to detect doping cases in competitive games etc. Doping agents are

performance enhancing drugs or substance (e.g. diuretics, stimulates, anti-estrogen), which are often used by the athletes in competitive games for enhancing physical performance, mental stamina and muscular strength. The World Anti-Doping Agency (WADA) has prohibited the large number of doping agents and established the maximum permissible limit for such substances in blood and urine [12-13]. Hence, it is highly desirable to develop a suitable method, which is capable to find out such biomolecules and drugs with low detection limit in human system. Thus, electrochemical sensing methods are used for the quantitative determination of biologically important molecules, pharmaceutical drugs and doping agents [14-15]. The research work presented in this dissertation basically deals with the fabrication and characterization of surface modified sensors and their application for the determination of biomolecules/pharmaceutical drugs. The upcoming sections are intended to furnish a concise description of the employed voltammetric methods and surface modifiers used in the development of voltammetric sensors.

1.2 METHODOLOGY AND MATERIALS USED FOR INVESTIGATIONS

A brief description about the techniques used in the present studies is presented in this section.

1.2.1 VOLTAMMETRIC TECHNIQUES

Voltammetric methods constitute a number of definite merits to an electroanalytical chemist, such as wide linear potential range, remarkable sensitivity, rapid and low cost analysis, accuracy and high selectivity, which make voltammetry a suitable choice for the routine analysis. In voltammetry, potential is applied at the electrode surface and the resulting current is measured as a function of that potential. The voltammetric studies are performed in an electrochemical cell having three electrode system to minimize the ohmic resistance as shown in **Fig. 1.2.**

.

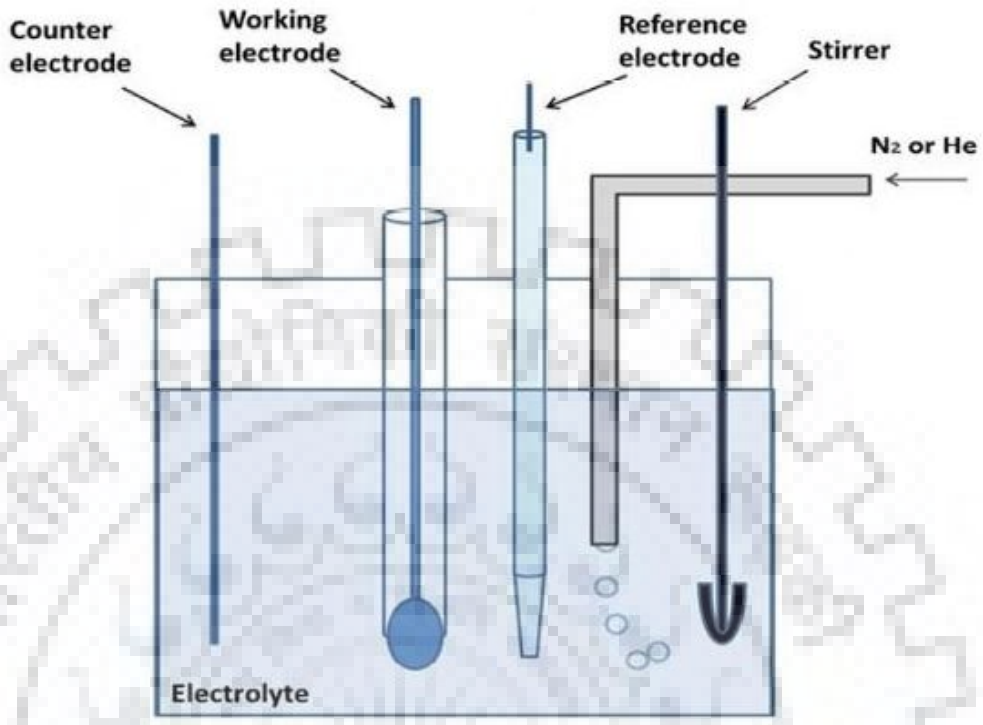

Fig. 1.2: Typical cell used in electrochemical investigations.

The potential of reference electrode is constant and taken as standard. Commonly used reference electrodes are Ag/AgCl (silver /silver chloride electrode, E^o = 0.22 V) or the saturated calomel electrode (SCE, E^o = 0.244 V). A platinum wire is used as a counter electrode or an auxiliary electrode through which 98% of the current flows in the circuit. The third electrode used is called as working electrode, at which oxidation or reduction reaction takes place. The current flowing between the counter electrode and the working electrode is measured. A supporting electrolyte is also added to the analyte solution to ensure the sufficient conductivity and reduce the migration current [16,17]. The voltammetric experiments in the present studies were carried out by using Bio-analytical system (BAS) electrochemical workstation; Epsilon as shown in the **Fig. 1.3**.

Fig. 1.3: Epsilon system used for the electrochemical investigations.

A brief discussion about the voltammetric techniques employed to perform electrochemical analysis is presented below:

1.2.1.1 Cyclic Voltammetry

Cyclic voltammetry (CV) is a modern, most functional and extensively used electrochemical technique, which is frequently employed to determine the redox couples of molecular species, kinetics and the mechanism of many redox systems [18,19]. According to the reported literature, several attempts have been made for sensing analytes based on CV from late 1970's. The performed studies were carried out for elucidating the mechanism of Cu(II) reduction, dopamine release regulation, NADH oxidation and study of metal-carbonyls and many more. However, CV is not used frequently in the quantitative analysis but it is appreciably used to demonstrate the electron transfer kinetics of the redox couple, nature and stability of the product in reaction and characterization of the reaction intermediates. CV is an electrochemical technique, which involves cycling the potential of a working electrode at a specific sweep rate and the current vs. time curve that develops in an electrochemical cell is a linear scan of potential with a triangular waveform as depicted in **Fig. 1.4 (A)**. The observed results from the redox reaction of

biomolecules and drugs provide thoughtful effects on understanding of their pharmaceutical activity and redox performance. CV comprises scanning the applied potential at the stationary working electrode in an unstirred solution from an initial potential (E_i) to final potential (E_f) in both forward and reverse directions at a constant sweep rate and the resulting current (i_P) is measured. Sweep rate or scan rate can be applied from few millivolts per seconds to hundreds of volts per second [6, 20-22].

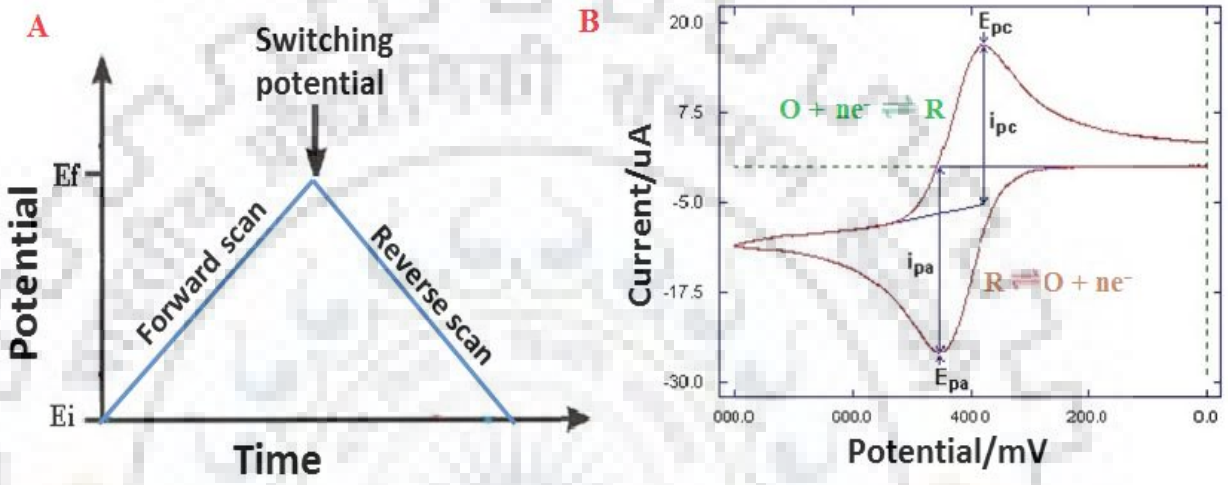

Fig. 1.4: (A) A triangular potential waveform in CV **(B)** Typical cyclic voltammogram for a reversible redox process.

The current measured during this process is assigned as current density, which is often normalized to the electrode surface area and plotted against the applied potential and the resultant curve obtained is referred as cyclic voltammogram as shown in **Fig. 1.4 (B)**, where i_{pa} and i_{pc} are the currents of anodic and cathodic peaks; E_{pa} and E_{pc} are the potentials of anodic and cathodic peaks, respectively. In the reversible redox reaction, the redox couple exchange electrons with the working electrode rapidly. The anodic and cathodic peak currents are expected to be equal for a reversible redox reaction and the ratio i_{pa}/i_{pc} is 1.0. The number of electrons involved in the reversible chemical process can be calculated using the cathodic and anodic potential according to the following relation:

$$\mathbf{\Delta E_p/V = 0.059/n = [E_{pa} - E_{pc}]}$$

The calculated difference between the two peaks should be close to 0.059 V involving one electron transfer for a reversible chemical reaction. This peak separation (ΔE_p) is usually larger for an irreversible process due to slow electron exchange. The current varies as a function of analyte concentration for a reversible reaction and is governed by Randles-Sevcik equation (at 25ºC):

$$I_p = (2.69\times10^5)\, n^{3/2}\, A\, C\, D^{1/2}\, \nu^{1/2}$$

where, I_p represents the peak current in ampere, A denotes the surface area of electrode in cm^2, C represents the concentration in $mol.cm^{-3}$, D is the diffusion coefficient in cm^2s^{-1} and ν represents the sweep rate in Vs^{-1}. The peak current is directly proportional to analyte concentration and increases with the square root of the sweep rate. At all sweep rates, the observed value of I_{pa}/I_{pc} should be unity for a reversible couple. In recent years, CV has also been extensively used for the qualitative analysis of redox reactions, since it provides a wide potential range for oxidizable and reducible species. However, for sensitive quantitative aspects, the pulse techniques, such as, square wave voltammetry, differential pulse voltammetry etc. are more advantageous as they provide better sensitivity due to lower charging current [23-26].

1.2.1.2 Square Wave Voltammetry

Square-wave Voltammetry (SWV), a form of linear potential sweep voltammetry, is originated from Barker square-wave polarography and Kalousek commutator and can be used for quantitative chemical analysis as well as to determine the kinetics, thermodynamic and mechanism of chemical reactions with enhanced sensitivity, low detection limits with lower background current. SWV technique provides excellent sensitivity due to the discrimination against charging current, hence, oxidation and reduction peaks are observed with respect to the faradic current. SWV is much faster technique than normal and differential pulse voltammetry since scan rates up to 1 V/sec can be used and voltammograms can be obtained in less than 10 ms. Voltammograms can be achieved by superimposing symmetrical square wave pulse of amplitude E_{sw} on the stair case wave, where the forward pulse (pulse direction same as the scan direction) goes along with the step of staircase as shown in **Fig 1.5 (A)**.

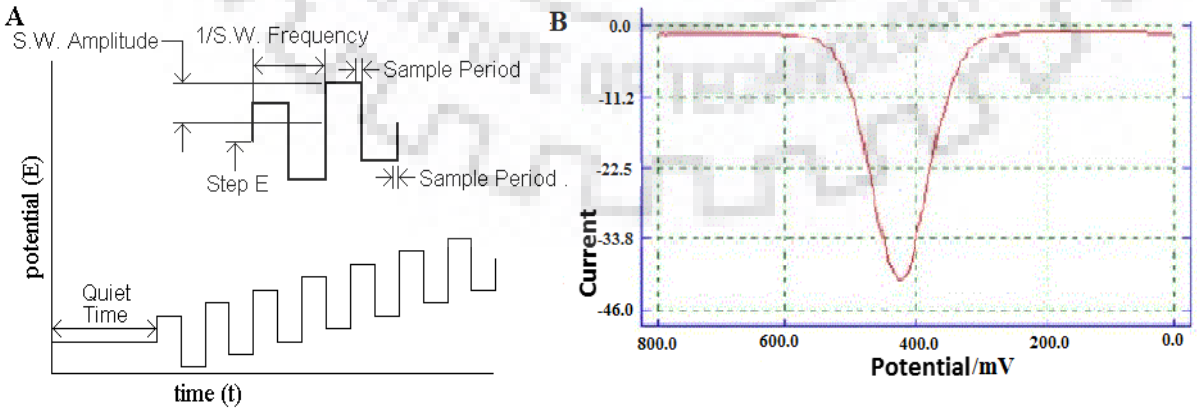

Fig. 1.5: (A) A typical potential waveform in SWV **(B)** A typical Square-wave voltammogram.

The charging current in the SWV can be minimized by subtracting the current at the beginning of pulse from the current at the end of pulse. The current of forward pulse (I_f) and the current of reverse pulse (I_r) provide cathodic current and anodic current, respectively, and the difference between them gives the net current (ΔI). This net current is proportional to the concentration of analyte and the potential at which peak centred is known as redox potential. The resulting net current or the differential current is plotted against potential as oxidation or reduction peak as shown in the Fig **1.5 (B)**. SWV has become widely used technique in recent year for the analysis of trace amount of biomolecules and pharmaceutical drugs in physiological fluids, since it provides increased sensitivity and lower limit of detection due to negligible charging current. The theory of SWV has been well presented in literature [27-29]. Santos et al. reported quantification of benzodiazepines up to 50–100 ng mL^{-1} in toxicological cases in blood and plasma samples by the use of SWV [30]. Saleh et al. determined antiviral drug valacyclovir up to pico-molar range by applying SW voltammetric procedure [31].

1.2.2. HIGH PERFORMANCE LIQUID CHROMATOGRAPHY

High-performance liquid chromatography (HPLC) is an analytical technique used for the identification, purification and separation of variety of compounds in the field of pharmacy, environment, food manufacturing, polymer industries, forensic and research laboratories etc. HPLC, an advanced method of column liquid chromatography was first developed in the late 1960's. HPLC has been employed in several applications, such as quality control, quantification and stability of drugs, determination of pollutants in drinking water, detection of preservatives, analysis of steroids, protein and biomolecules in bio-fluids samples and many more. HPLC is operated by injecting a small amount of liquid sample (2 to 5 μL) into a mobile phase that passes through a column packed with stationary phase. A detector of HPLC system detects the different component present in the liquid mobile phase and provides the results in the form of electric signal. Mainly four types of detectors used in this technique are the fluorescence detector, Ultraviolet-Visible (UV-Vis) detector, the refractive index detector and electrical conductivity detector. Most commonly used detector is UV-Vis detector, which can detect amounts lower than 10^{-10} g/mL. The detector in the investigation is selected according to the sample and purpose of analysis [32,33].

1.3 WORKING ELECTRODE

Working electrode plays the role of heart of the electrochemical analysis as it provides an ideal phase interface (i.e. electrode-electrolyte interface); at which charge transfer takes place for oxidation and reduction processes in electrochemical reaction and resulting current is monitored. The response of electrochemical reaction for any compound is significantly influenced by the nature of material of the electrode; hence, a suitable electrode material for construction of working electrode is essential to get precise and accurate results. The material of working electrode should be electro-chemically inert in the electrolyte solution to prevent the production of current due to applied potential in the experiment. Some other characteristics of an ideal working electrode material are as follows, which improve the sensitivity, selectivity, accuracy and reproducibility of an electrode:

- ✓ Easy handling and incorporating in the form of electrode
- ✓ Easy surface renewal to prevent toxicity
- ✓ Durability, low cost maintenance and ease of availability
- ✓ Rapid electron transfer rate without electrode fouling
- ✓ Long term technical and electrochemical stability
- ✓ Wide potential window for analyte and low background current

The common materials used for the construction of working electrode include carbon and carbon materials, platinum, silver, gold, mercury and semiconductors. Mercury electrodes are liquid working electrodes, which provide uniform and uncontaminated surface, are of several types and include mercury film rotating disc electrode, dropping mercury electrode (DME), mercury film electrode and hanging mercury drop electrode. Mercury electrodes have some traditional drawbacks such as anodic dissolution, toxicity and disposal of mercury, which makes them cornered for frequent use in the electrochemical analysis in laboratories [34,35].

The generally used solid stationary electrodes in the electrochemical analysis for obtaining current-voltage curves in the unstirred solutions are made up of carbon and metallic gold, palladium, copper, silver or platinum. The metallic electrodes provide wide anodic potential range, lower toxicity of mercury, remarkable conductivity with enhanced electron transfer rate and possess high affinity for the pharmaceutical drugs and biologically important molecules. Pt electrodes provide wide potential range, excellent conductivity and enhanced reaction kinetic for redox processes that make them prominent amidst a variety of feasible metals. The Au based electrodes are more inert than Pt and have been widely used in the trace detection of metal ions.

The metal electrodes have an extraordinary ability to interact with aromatic molecules and stabilize reactive intermediates, hence, carry a certain affinity towards biologically important molecules [36-39]. A wide variety of carbon electrodes; an inert material electrodes used for the voltammetric analysis include glassy carbon, pyrolytic graphite, carbon fibre, carbon paste, screen-printed and many more. Carbon based electrodes are generally preferred as they are less expensive and provide good electron transfer kinetics as well as they are biocompatible. The carbon electrodes provide surface functionalities, which are advantageous for the modification of surface of the sensor to increase sensing properties of electrode.

The graphene layers, bonding of one sp^2 hybridized carbon atom with other sp^2 hybridized carbon atom are adhered with each other by weak Vander Waals forces, which can be delocalized and hence, provide high electrical conductivity [40,41]. In this dissertation, pyrolytic graphite and screen printed carbon electrodes are mainly used as working electrodes for the voltammetric studies.

1.3.1 PYROLYTIC GRAPHITE

Pyrolytic graphite is profoundly familiarizing, pure and highly ordered form of graphite constructed by pyrolysis of hydrocarbons at high temperature (1900°C to 2500°C) followed by successive crystallization of graphitic crystals. Pyrolytic graphite displays several exceptional physical characteristics such as:

- ✓ Immensely resistant to gases and liquids
- ✓ Highly inert to chemical attack
- ✓ Remarkably free of metallic contaminant and entrapped gases
- ✓ Highly ordered layers of carbon crystallites

The pyrolytic graphite is anisotropic in nature and has a proper alignment of microcrystals of graphite with respect to each other, hence, consists of two different kinds of planes i.e. edge plane and basal plane as displayed in **Fig 1.6 A.**

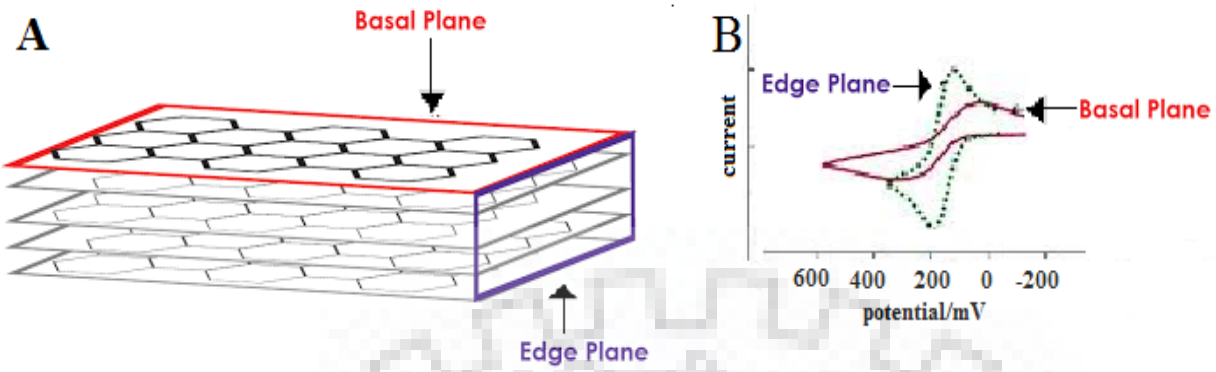

Fig. 1.6: (A) Representation of edge and basal planes of pyrolytic graphite **(B)** Typical cyclic voltammograms observed of an analyte from edge and basal planes of pyrolytic graphite.

Both the planes of pyrolytic graphite have different physical, chemical properties as well as different charge transfer kinetic in the electrochemical process as shown in **Fig 1.6 B**. Several investigators have studied the applicability of different planes of pyrolytic graphite in voltammetric sensing of biomolecules and drugs [42-46]. Salimi et al. prepared a biosensor by using the basal plane pyrolytic graphite electrode (BPPGE) [47] and used for the sensitive determination of glucose i.e. an important human biomarker because so many diseases can occur due to the minute alteration in its concentration in blood. Sims et al. also utilized the basal plane pyrolytic graphite electrodes for the electrochemical determination of nicotine in a wide linear range of concentration [48]. On the other hand, Banks and Compton fabricated an edge plane pyrolytic graphite electrode (EPPGE) and successfully used for NADH detection with high sensitivity [49]. A different approach based on unmodified edge plane pyrolytic graphite electrode has also been reported for the simultaneous determination of dopamine, serotonin and ascorbic acid and the electrode was successfully utilized in real samples with high sensitivity and selectivity [50].

1.3.2 SCREEN PRINTED CARBON ELECTRODE

Recently, the working electrodes have been produced by incorporating the chemical modifiers into the carbon ink and the resulting electrodes are known as screen printed electrodes (SPEs), which acquired massive importance in the field of electroanalysis. The conducting paste or filler of silver and carbon, a volatile solvent with a nonconducting binder are essential constituents of the printing ink used to prepare the screen printed electrodes. The carbon ink is applied to print working electrode and silver ink is used to arrange the conducting track of the electrode. The conductive inks of SPEs contain carbon with organic solvents, insulating polymers, mineral

binding paste and some other additives that improve functional characteristics as well as adhesion and dispersion onto the surface of substrate. These additional non-conductive substances may lead to sluggish electron transfer kinetics for electrochemical processes. SPEs works as inexpensive and portable sensing electrode for electrochemical analysis of trace amount of analytes in pharmaceutical formulations, physiological and environmental samples with high sensitivity and reproducibility. The screen printed carbon electrodes have complete three electrode system consisting of an auxiliary electrode, a reference electrode and the working electrode, which are printed on one substrate surface as witnessed in **Fig 1.7**.

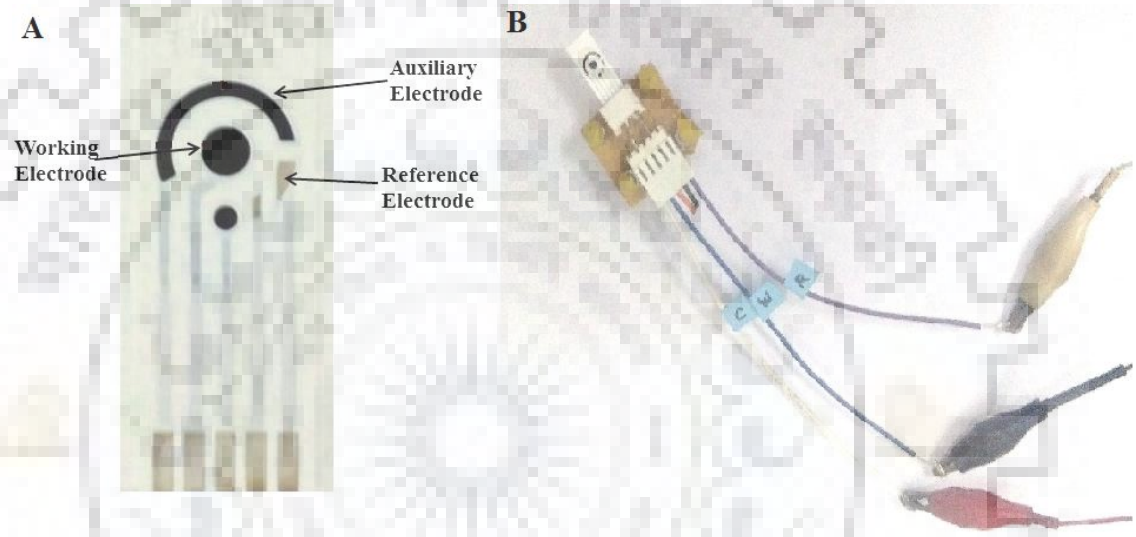

Fig. 1.7: (A) Enlarged view of screen printed electrode **(B)** A setup of screen printed electrode used in electrochemical investigations in the present studies.

Screen printed carbon electrodes have many advantages over other conventional solid electrodes, such as, low cost, portability, exponential reduction in required volume of sample for detection and no fouling (as electrode is changed after one or two runs). Therefore, these electrodes have gained significant attention in the field of electrochemical analysis of clinical samples, environmental samples (i.e. pesticides, heavy metals), food processing samples, biomolecules detection (glucose, protein, neurotransmitters, hormones, DNA damage) and pharmaceutical drugs analysis [51-55].

1.4 SURFACE MODIFIERS

In voltammetric studies modification of the electrode surface can significantly enhance peak response in terms of increased peak current, decreased oxidation or reduction potential and decreased limit of detection. Hence, recent interest of electrochemists and analytical

electrochemists is the development of new surface modifying materials. The surface modification of the electrode is an approach in which a reagent is placed onto the electrode surface to impart the behaviour of that reagent in terms of increased effective surface area and sensitivity. Recently, the area of surface modified sensors has received considerable attention, due to many applications, such as determination of pharmaceutical dosages forms, biological important molecules in physiological fluids, quality control of drugs and food and electrocatalytic reaction studies. The electrode surface modified with carbon nanomaterials, conducting polymers, metal nanoparticles and their different composites exhibit diminution of the over-potential as well as acceleration of electron transfer reactions, which imparts improved selectivity for different analytes, increased sensitivity and electrochemical stability. In this dissertation, the modification of the electrode surface is carried out with the use of conducting polymers and their composites with carbon nanomaterial, such as graphene, carbon nanotubes (CNTs) as well as metal nanoparticles of gold, silver and palladium. The prepared sensor is then used for the sensitive determination of different bio-molecules and drugs in human physiological fluids and pharmaceutical samples. A brief discussion of surface modifiers used in present studies and relevant review of research work carried out using these modifiers in the recent years is presented below.

1.4.1 CARBON BASED NANOMATERIAL

Carbon based nanomaterials, such as graphene, carbon nanotubes and their nanocomposites have attracted attention in electroanalysis due to their potential to prepare high-performance electrochemical sensors via their exceptional catalytic, mechanical, thermal and electronic properties. The high effective surface area, small size, better electrical conductivity and exceptional biocompatibility make them a potential candidate for electrochemical biosensors.

1.4.1.1 GRAPHENE

Graphene, a one atom thick two dimensional carbon allotrope exists in sp^2 hybridized carbon atoms arranged in six membered rings and form a packed honeycomb crystal lattice (**Fig. 1.8**). Graphene can be prepared by several methods i.e. chemical cleavage exfoliation, mechanical exfoliation, chemical vapour deposition, thermal and electrochemical reduction and provide different level of purity, size and crystallinity. The presence of delocalized π-electron system imparts the excellent electronic properties to the graphene due to accumulation of aromatic systems capable of chemically interacting with the graphene sheets via π-π interaction. Graphene has unique mechanical strength, large surface area, elasticity, good thermal and electrical

conductivity and potential biocompatibility. The presence of heavily oxygenated groups at the surface of graphene oxide make their functionalization much easier and gives better dispersion and compatibility for several other materials, such as metal based nanoparticles, solvents and conducting polymers. The biocompatibility of graphene makes it a potential material for the immobilization of biological recognition elements. Therefore, in last few decades numerous approaches have been reported for utilizing graphene and its derivatives in electrochemical sensing [56,57].

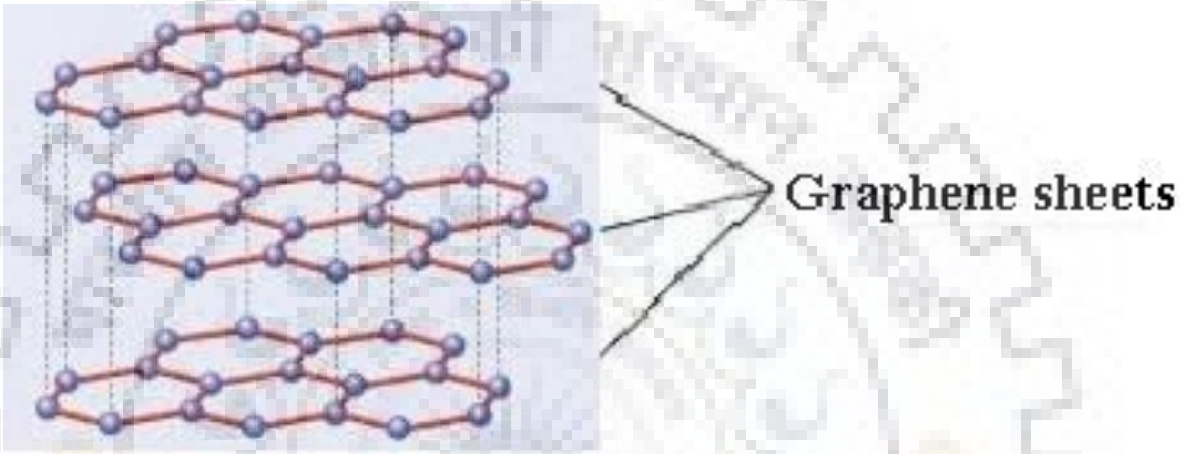

Fig.1.8 A typical representation of graphene sheets.

Kim et al. [58] reported an approach to construct graphene modified glassy carbon electrode, which was successfully used in the electrochemical detection of dopamine (DA) in the presence of ascorbic acid (AA). Mallesha et al. developed functionalized-graphene modified graphite electrode for the voltammetric detection of DA in presence of uric acid (UA) and AA in serum and pharmaceutical samples [59]. Rosy et al. utilized Graphene for the modification of palladium sensor to determine norepinephrine [60]. The developed sensor showed a dynamic linear range of 0.0005–0.5 mM in pH 7.2 phosphate buffer and limit of detection as 67.44 nM. The authors successfully employed the prepared sensor for the analysis of norepinephrine in biological fluids and pharmaceuticals formulation. A GCE modified with graphene nanosheets was prepared by Navaee and co-workers for the determination of three opiate drugs; heroine, morphine and noscapine [61]. The proposed method has advantages of high sensitivity, low cost, rapid response time and long term stability and was applied for the individual and simultaneous determinations of these three narcotic components at micro molar concentration without performing any pre-treatment and separation procedures. Du et al. reported a sensitive voltammetric sensor modified

with graphene to determine catechol (CC) and hydroquinone (HQ) [62]. The remarkable shifting of oxidation and reduction peaks was observed for both CC and HQ in pH 4.5 acetate buffer solution at the surface of prepared GR/GCE sensor, which provided a good separation of peaks for successful simultaneous determination. A facile electrochemical approach to prepare electrochemically reduced graphene oxide (ERGO) was also reported by Li et al. [63]. The ERGO modified GCE was applied to analyze the electrochemical behaviour of codeine and the detection limit was found very low due to outstanding electrical conductivity of graphene. The practically applicability of the sensor was successfully demonstrated by determining codeine in the urine and sample of cough syrups. Similarly, another method is also reported for the one step preparation and electro-deposition of ERGO on the surface of GCE [64]. The sensor was successfully used for the detection of acetaminophen with high sensitivity in pharmaceuticals to control drug quality and to determine hepatotoxicity. A sensitive simultaneous determination of biomolecules; dopamine (DA), ascorbic acid (AA) and uric acid (UA) at the ERGO/GCE sensor was also presented by Yang et al. [65]. The applicability and reliability of the proposed method was demonstrated by observed acceptable recoveries in human urine samples. Graphene sheets have a huge tendency to make irreversible aggregation and pileup through π-π stacking or vander-waal's interaction, hence, to prevent this agglomeration the composite of graphene can be prepared with conducting polymer, nanoparticles or other species. Yin et al. constructed an electrode based on graphene-chitosan composite sheets and used it for the determination of 4-aminophenol, which is a primary hydrolytic degradation product of an antipyretic and analgesic drug, paracetamol [66]. Graphene composite with chitosan showed good electrocatalytic activity towards oxidation of 4-aminophenol in terms of increased sensitivity and decreased oxidation potential. In order to check practical utility of the proposed method, sensor was employed in water samples and paracetamol tablet samples to determine 4-aminophenol, where the observed results revealed the effectiveness and reliability of the proposed method. A novel composite electrode based on graphene, [2,4-$C_{l2}C_6H_3C(O)CHPPh_3$] and 1-n-octylpyridinum hexa-fluoro phosphate was fabricated by Bagheri et al. [67]. Electrochemical sensing of Tl^+, Pb^{2+} and Hg^{2+} was carried out at this ionic liquid/graphene modified electrode with excellent selectivity and sensitivity without performing any separation steps prior to the analysis. To ensure the practical applicability, the developed sensor was applied in tap water; river water and soil sample collected from various polluted sites and was used to detect these trace ions with satisfactory results. A facile direct-precipitation method to immobilize iron sulfide (FeS) on reduced graphene oxide (rGO) nanosheets at GCE was fabricated by Liu et

al. [68]. The sensor displayed excellent electrocatalytic activity towards the individual and simultaneous oxidation of dopamine and acetaminophen without affecting the oxidation of electro-active potential interfering species such as AA and UA. Due to the good anti-interference ability to AA and UA, this method is quite promising for simultaneous analysis of dopamine and acetaminophen in actual physiological samples as well. In view of such advantages of graphene, PG sensor modified with graphene is used in the present dissertation for the determination of biomolecules.

1.4.1.2. CARBON NANOTUBES

Carbon nanotubes (CNT), a novel material for modification, first discovered and described by S. Injima in 1991, has drawn considerable research interests in the field of electrochemical sensors. CNTs offer the feasibility of fabricating sensitive voltammetric sensors due to their catalytic and electrical properties that facilitate the upgradation of analytical response. Moreover, CNTs modified voltammetric sensors furnish significant advantages, such as larger effective surface area, high chemical stability in both aqueous and non-aqueous solutions, wide potential window, exclusive mechanical strength, high sensitivity, increased stiffness and fast electron transfer. One or more number of flat graphene sheets contains carbon atoms in a honeycomb arrangement roll-up (**Fig. 1.9**) and form one or multi-layered tubulenes i.e. Single-Walled CNT and Multi-walled CNT (SWCNT and MWCNT).

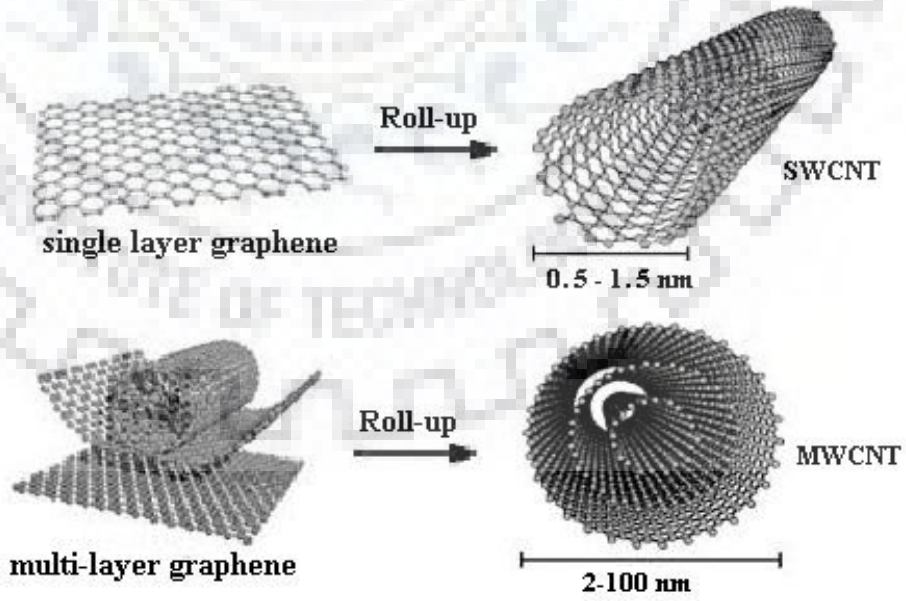

Fig. 1.9: Schematic representation of rolling up of graphene sheets to form SWCNT and MWCNT.

The surface of prepared CNTs is usually functionalized by the treatment of strong acids. The resultant CNTs have shorten length of nanotubes and carboxylic group, oxide groups may also be added to the defects site and ends of nanotubes. Moreover, these oxide groups can also be functionalized with amides, thiols and so on. The alteration on the surface of CNTs firmly influences solubility, which further enhances the ease of preparation of CNTs modified sensors [69-71]. In the last decade, the literature on voltammetric sensors modified with CNTs and their applications in the sensitive determination of biomolecules have been reported. Alothman et al. reported a GC electrode modified with acid functionalized multi-wall carbon nanotubes for the simultaneous determination of DA and acetaminophen (AP) [72]. The proposed sensor provided remarkable sensitivity, selectivity, long term stability and high recoveries in human serum and pharmaceutical formulations. A novel voltammetric glassy carbon senor based on MWNTs bridged meso-cellular graphene foam (MGF) nanocomposite was presented for simultaneous determination of AA, DA, UA and tryptophan (TRP) [73]. There was more space among sheets in the MGF, which tended to resolve the issues of conglomeration. MWNTs may bind to MGF via π-π interaction; lead to formation of porous and loose 3-D structures, which provide enhanced effective surface area and high electrical conductivity, therefore, sensors exhibited excellent selectivity and sensitivity towards the individual and simultaneous determination of AA, DA, UA and TRP. Mokhtari et al. reported a novel carbon paste electrode modified with vinyl ferrocene/multiwall carbon nanotubes for morphine and diclofenac determination in pharmaceutical and biological samples [74]. This work demonstrated that the vinyl ferrocene/vinyl ferricenium redox couple acted as a quasi-reversible system in the carbon nanotubes, therefore; the modified electrode was quite stable, which significantly shifted the peak potentials of the analytes and ease the oxidation of both the analytes with good sensitivity. To improve the properties of CNTs, MWCNTs and SnO_2–Zn_2SnO_4 nanocomposite modified voltammetric sensor was prepared by Taei and co-workers [75]. The electrochemical studies were carried out using DPV, CV and chrono-amperometry for the simultaneous determination of morphine and codeine. The developed sensor was capable to separate the peaks with a potential difference of about 550 mV and low detection limits were obtained. The presented approach was also applicable to determine the morphine and codeine in pharmaceutical and biological fluids samples with the satisfactory results. Functionalized MWCNT modified sensor has been used in the present studies for the determination of ATP metabolites.

1.4.2 METAL BASED NANOPARTICLES

Metal nanoparticles possess apparent physical and chemical features that make them potential candidate for the modification of electrochemical sensors. Various metal nanoparticles such as platinum, palladium, gold, silver etc. have been synthesized and extensively used for the modification of various sensors, like electrochemical sensors, gas sensors and biosensors for inorganic and organic molecules due to their large surface to volume ratio, high electron storing properties and surface energy. The nanoparticles have special ability to store large number of excess electrons, which can be applied to initiate any electrochemical reaction, thus, metal nanoparticles also act as a catalyst to catalyze the redox process of biomolecules.

Among the metal nanoparticles gold has been widely explored due to its ease of formation process, high stability, unique electronic properties, large surface-to-volume ratio and outstanding biocompatibility [76-79]. Saha et al. reviewed the different ways to synthesize gold nanoparticles having control over their size and shape and their applications in chemical and biological sensing. AuNPs also provide a stage for multi functionalization with a large number of organic ligands for the selective and sensitive analysis of small biological significant molecules [80]. Jiao et al. prepared gold nanoparticles composites with graphene to determine the electrocatalytic activity towards the oxidation of 4-nitrophenol. Fabricated sensor was successfully applied in wide linear range concentration of river water samples and detection limit was found as 10 nM [81]. Another approach having composite of gold nanoparticles with graphene oxide was reported by Karthik et al. to determine nilutamide, an anti-cancer drug [82]. The method showed excellent electrocatalytic activity even in the serum and pharmaceutical samples and a detection limit of 0.4 nM was reported. A facile electrochemical sensor was reported by Wang et al. based on Au nano-plates and reduced graphene oxide for the simultaneous determination of AA, UA and dopamine. The sensor exhibited good sensitivity in the wide linear range of concentration for all the analytes with excellent anti-interference ability, long-term stability and reproducibility [83]. Some other metal nanoparticles are also widely used for the fabrication of electrochemical sensors. Pt nanoparticles modified carbon paste electrode was fabricated by Ensafi and co-workers for the simultaneous determination of naturally occurring alkaloids; morphine and codeine. The presented method showed high sensitivity towards the oxidation of both morphine and codeine due to the synergetic interaction of PtNPs and ionic liquid and give low detection limits in biological fluids [84]. Hence, it was concluded that the spectacular electrocatalytic properties of the metallic nanoparticles offer a suitable platform for the surface modification of the sensor in the analysis of different catalyzing

processes, redox processes of biologically important molecules and pharmaceutical drugs, peroxide reduction, gas sensing and bio-sensing.

1.4.3 CONDUCTING POLYMERS

In recent years, conducting polymers (CPs) have been extensively used for the electrochemical applications of biomolecules because of their inherent charge transport properties and compelling biocompatibility [85]. The exceptional characteristics of conducting polymers are associated with the presence of conjugated delocalized π-electron system in the polymer backbone, due to which CPs interact with the other conjugated systems of aromatic molecules and exhibit catalytic applications. Conducting polymers have been widely used in electroanalytical techniques as signal-enhancing elements and have attracted significant importance in the last decade due to their unique electrical, mechanical and optical properties, inherent charge transport properties and biocompatibility in electroanalytical applications. The unique traits of conducting polymers and their applications in different fields are summarized in the **Fig: 1.10**.

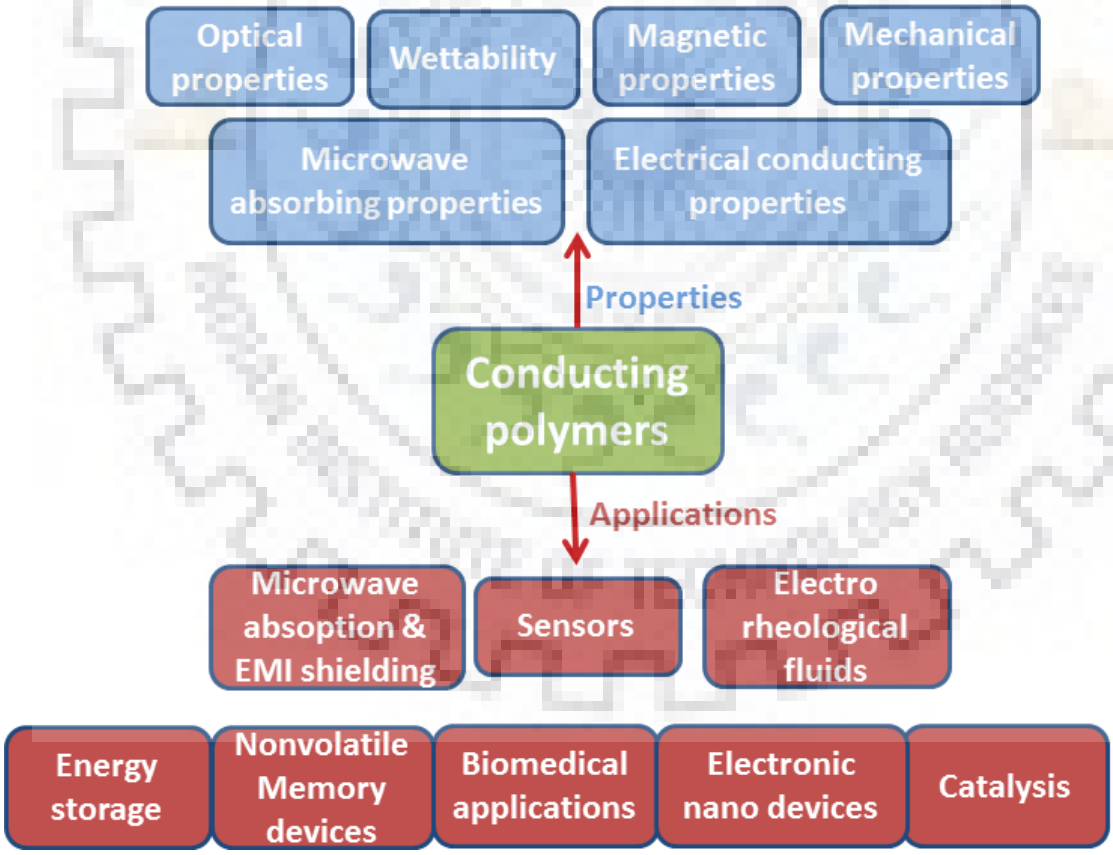

Fig. 1.10: Different properties and applications of conducting polymers.

CPs exhibit high electron transfer kinetics, enormous electrocatalytic ability and mechanical properties, which make them an attention seeker of the scientific community in the field of sensing. The fabrication of polymeric layer on the surface of the sensor can be easily achieved by electro-polymerization and controlled by altering the electro-polymerization parameters, such as applied potential window, sweep rate of scans and number of CV scans. Hence, the electro-polymerization method is quite simple and prevailing way, which can be used to design desired polymeric layer at the surface of the sensor for electrochemical sensing.

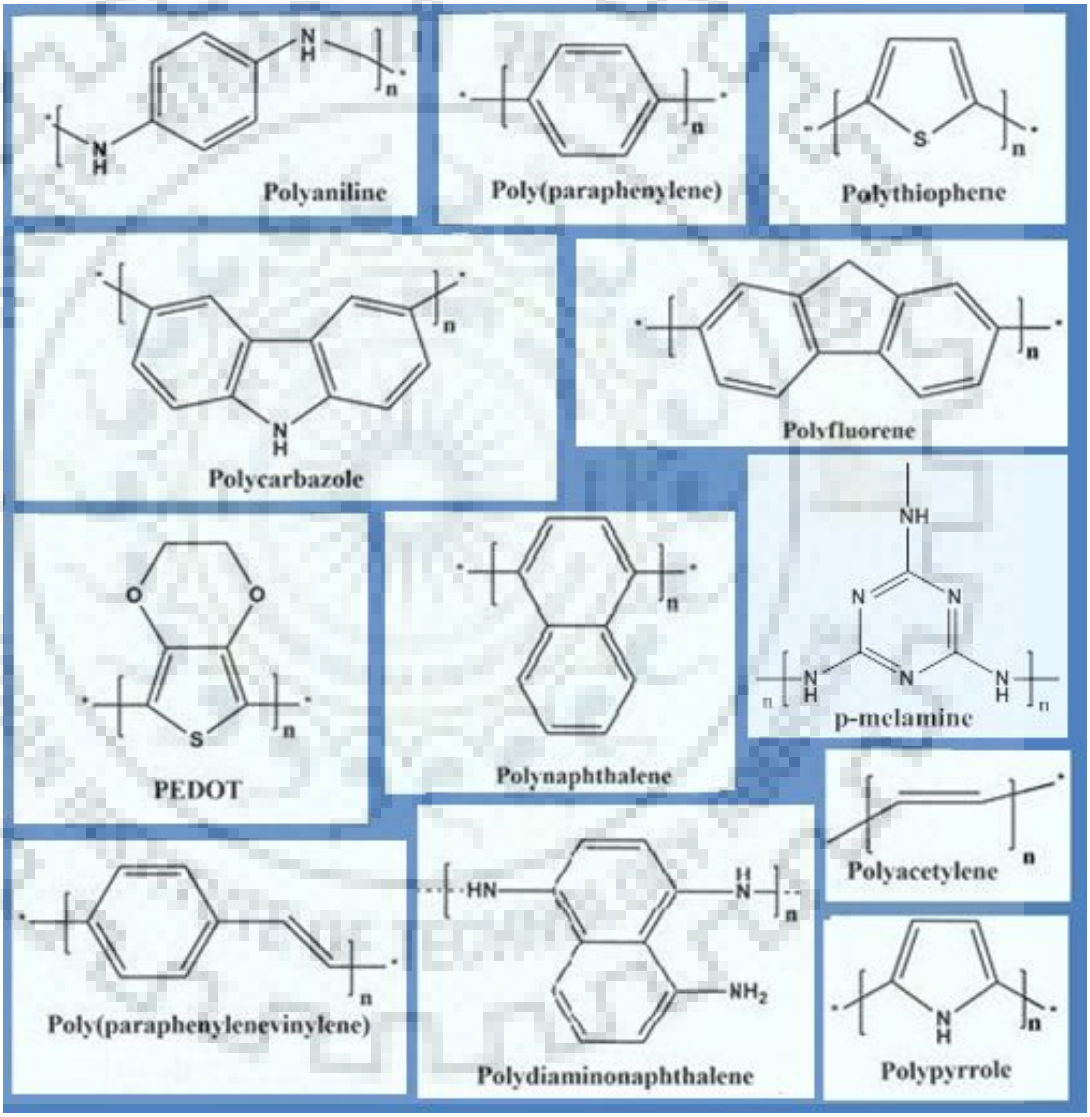

Fig. 1.11: Structure of some commonly used conducting polymers.

The organic conducting polymers commonly used in electroanalysis are polypyrrole, polyaniline, polythiophene, polyfluorine, poly(4-amino-3-hydroxy-1-naphthalene sulfonic acid), poly diamino napthalene, poly(p-phenylene vinylene), poly(3,4-ethylenedioxythiophene)

(PEDOT), polycarbazole, polynapthalene, polymelamine, polyazulene etc. The structures of these polymers are displayed in **Fig 1.11** [86-90].

A novel electrochemical sensor was fabricated by the use of poly (1,2-diamino anthraquinone) polymer for the determination of contamination of heavy metals, such as Cd^{2+}, Hg^{2+}, Cu^{2+} and Pb^{2+} in water samples. The sensor provided high sensitivity due to the presence of three aromatic rings and two amino groups, which on combination made a suitable material for electrochemical sensing [91]. A Number of polymer nanocomposites with other nanoparticles have also been reported in recent years, which provided more sensitivity due to the synergic interaction between nanocomposite materials and good compatibility with biomolecules. A polymer nanocomposite of poly-cyclodextrin with graphene and MWCNTs nanocomposite was fabricated by Zhang et al. [92]. The polymer nanocomposite (PNC) modified sensor was then used for the simultaneous determination of DA, AA and NO_2^- by incorporating polymeric layers. The aggregation between the graphene sheets was prevented and dispersibility was successfully improved, which exhibited a strong inter-layer attraction in the composite materials. Another approach based on conducting polymer PEDOT with Au and graphene nanocomposite was also reported for the voltammetric determination of paracetamol [93]. The PNC modified electrochemical sensor showed excellent sensitivity towards the oxidation of paracetamol over a wide linear range of 0.15 μM to 5.88 mM. The sensor exhibited detection limit as 41 nM and was capable in analyzing paracetamol in the real samples and pharmaceutical samples with good accuracy. A co-polymeric film of polyaniline and polystyrene was fabricated with the graphene for the determination of $Pb^{2+}$and Cd^{2+} as an alternative tool for heavy metal detection in environmental monitoring [94].

Thus, it is understandable that different modifications at the electrode surface provide enhanced sensitivity and selectivity for the electrochemical determination of analytes. In view of this, an attempt has been made in the present studies to apply surface modification by carbon materials, metal nanoparticles, carbon nanotubes, conducting polymers and their composites for the quantification of various biomolecules and pharmaceutical drugs.

1.5 COMPOUNDS OF INTEREST

Biologically important organic molecules are the foundation of the biological system and the living beings. Several physiological processes are regulated by these biomolecules in living system and any alteration in the concentration of these biomolecules can severely affect the proper

functioning of the biological processes and causes several abnormalities and disorders. These physical disorders and dysregulation in physiological processes can be prevented by the use of pharmaceutical drugs. Hence, the quantitative analysis of these biomolecules and drugs in bio-fluid samples and pharmaceutical formulations is of utmost relevance in the diagnosis and prevention of the diseases, doping cases, various abnormalities and to improve human health with quality of life.

1.5.1 DRUGS

Thioxanthines, piperidines, phenothiazines and butyrophenones have been explored in the treatment of Schizophrenia and psychotic disorders [95]. **2-Thioxanthine** (2-TX), a thio-modified nucleic acid base, works as an uncompetitive DNA inhibitor that binds to the enzyme/DNA complex outside the active site, 2-TX is widely used in the chemotherapy for cancer and inhibition of myeloperoxidase. It blocks oxidative stress associated with inflammation, alzheimer disease, pulmonary disease, chronic obstructive, Parkinson disease, rheumatoid arthritis and atherogenesis [96-98]. **Propranolol**, 1-[(1-methylethyl) amino]-3-(1-naphthylenyloxy)-propan-2-ol, a non-selective beta-adrenergic antagonist, shows little intrinsic sympathomimetic activity, which is used for the treatment of various cardio vascular disorders, like phaeochromocytoma, sinus tachycardia, hypertension, dysfunctional labor, cardiac arrhythmia, myocardial infarction, angina pectoris and migraine. Propranolol blocks the effect of adrenaline and inhibits the actions of norepinephrine; hence, it has also been extensively used in the treatment of thyrotoxicosis or anxiety and tremor [99-101]. These two compounds have been selected in the present studies because propranolol is used as a drug for the relief of side effects of antipsychotic drugs.

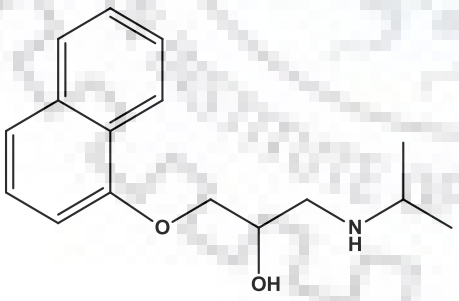

Propranolol

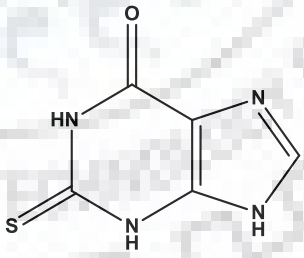

2-Thioxanthine

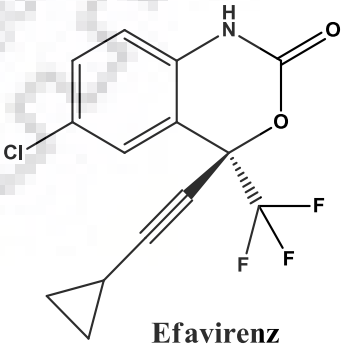

Efavirenz

Efavirenz (EFZ), chemically known as 6-chloro-4(cyclopropylethynyl)-1,4-dihydro-4-(trifluoromethyl)-2H-3,1benzoxazin-2-one is a first-generation non-nucleoside reverse transcriptase inhibitor (NNRTI) drug, efficiently used for the treatment of human immunodeficiency virus (HIV) type 1 infections [102]. The reverse transcriptase (RT) enzyme

plays an important role in the life-cycle of HIV as it converts the single stranded RNA (HIV genetic material) into a double-stranded DNA via polymerase and Ribo-nuclease H activities. The EFZ directly binds to the RT and disrupt the enzyme's catalytic site, which hinders the formation of viral double-stranded DNA from the single-stranded viral RNA genome [103,104]. EFZ is a first-line drug which is usually prescribed either in combination with protease inhibitor or nucleoside reverse-transcriptase inhibitor for the management of the disease [105]. In view of increasing cases of HIV type 1 infection in the last decade, the studies on the determination of this drug is taken up in the present dissertation.

1.5.2 BIOMOLECLUES

Dopamine [4-(2-aminoethyl) benzene-1,2-diol, DA], a catecholamine neuro-transmitter, is largely found in the mammalian brain tissues. In the mammalian system, DA works in the cardio-vascular function, vascular tone, catecholamine release, gastrointestinal motility, renal function, hormone secretion as well as in the significant physiological functions like voluntary movement, control, motivation and reward etc. [106-108]. Any alteration in the regulation of transmission of DA can cause various neurological disorders, such as, Tourette's syndrome, Schizophrenia, Parkinson's disease etc. [109,110]. **3,4-Dihydroxyphenylacetic acid** (DOPAC), is the main metabolite of dopamine (DA) which is formed in the central nervous system (CNS) by the action of the monoamine oxidase. In the case of increased Parkinson's overexpression, the DOPAC level in the cerebrospinal fluid (CSF) is greatly reduced from 9 ng/mL to 6 ng/mL. The low level of DOPAC in the plasma has also been witnessed in the cases of L-aromatic-amino acid decarboxylase deficiency and dihydropyridine reductase deficiency [111-114]. **Serotonin** (5-hydroxytryptamine, 5-HT), a biogenic monoamine neurotransmitter, occurs in the human brain, from where it significantly works to regulate and control several physiological functions, including muscle contraction, sleep, eating disorder, sexual activity and thermoregulation. It also plays an important role in psychopathological processes, like obsessive-compulsive disorder, infantile autism, liver regeneration, anxiety disorder, drug dependency and alcoholism [115-117]. 5-HT is involved in several gastro intestinal disorders including irritable bowel syndrome, secretion, food hypersensitivity and inflammatory bowel disease [118]. **5-Hydroxyindoleacetic acid** (5-HIAA), a main metabolite of serotonin (5-hydroxytryptamine, 5-HT), is excreted in the urine and regulates the homeostatic state of the human body with 5-HT. In CSF, the amount of 5-HIAA is remarkably altered by the stress, diet, alcohol exposure and 5-HT reuptake inhibitors. Suicide risk after

attempted suicide can be predicted by monitoring the level of 5-HIAA concentrations in the CSF. The low CSF 5-HIAA predicts the short-range suicide risk in the depressed suicide attempters and mood disorder in patients [119-122]. In view of such an importance of these biomolecules, their determination was considered highly desirable.

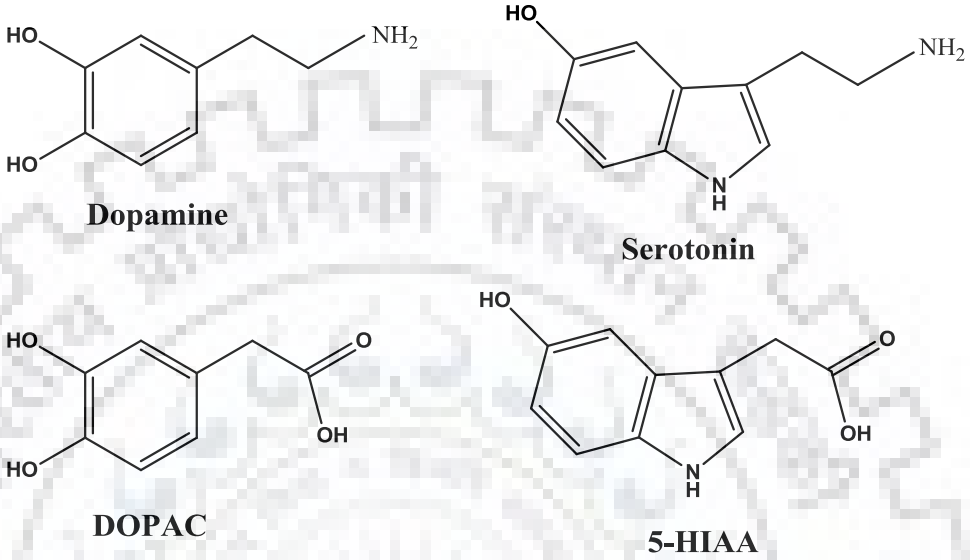

Inosine (INO), the major metabolite of ATP degradation, performs various important functions in the human body, such as, participation in tumor necrosis factor, which induces nitric oxide production in cultured sertoli cells, protection against myocardial damage, participation in receptor mediated signaling, having inflammatory and immune modulatory effects, reduction of LPS-induced acute lung injury and association with multiple sclerosis. **Hypoxanthine** (HX) is found in low concentration as 1.47-2.94 μM in blood plasma and is also a potential biomarker for acute cardiac ischemia (AMI), where the concentration of HX elevated in the bloodstream. Further conversion of HX to **Xanthine** (XT), which is found in the physiological fluids as 20 μg/dL is important to measure as the level of xanthine is required for the diagnosis and treatment of Gouty arthritis (gout), hyperuricaemia, and xanthinuria. The final metabolic product **Uric acid** (UA) is produced in liver, intestines and other tissues and is normally excreted via urine. The release of ATP-catabolites is less in new-born than in the adult's hearts during reperfusion, which coincides with lower xanthine oxidase activity. In the patients with acute myocardial infarction AMI, angina pectoris and other ischemic diseases, a significant rise in the intermediates and end products of purine metabolism i.e. INO, HX, XT, and UA can be an indicator of a heart attack [123-129]. The simultaneous determination of these four purine derivation is therefore taken in the present dissertation.

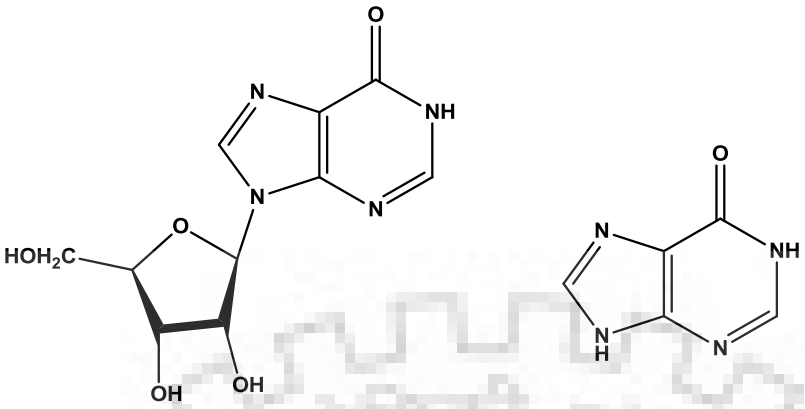

Inosine

Hypoxanthine

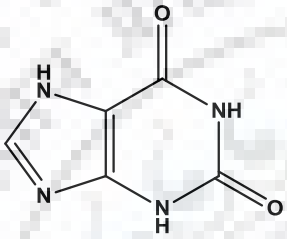

Xanthine

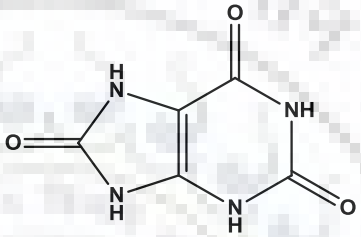

Uric acid

Estradiol, 1,3,5 (10)-estratrien-3, 17 β-diol (EST), a major female sex hormone is one of the most potent endogenous estrogen steroids. In human body estradiol is synthesized from cholesterol through different pathways. A common pathway includes the formation of testosterone by the aromatization of androstenedione, which can be converted into EST [130,131]. EST acts primarily as a growth hormone for the female reproductive organs. Secondary role, such as breast development, alteration of the body shape and maintenance of female reproductive tissues are also driven by estradiol [132]. **Caffeine**, 1,3,7-trimethylxanthine, (CAF) is a natural psychoactive drug, which stimulates central nervous system and cardiovascular system. This is one of the most widely consumed foods and supplements in the world, which is mainly found in common beverages, i.e. coffee, tea, soft drinks, numerous foods and drugs. CAF has some positive physiological effects, such as diuresis, increased metabolic rate, gastric acid secretion and lower risk of diabetes but it also produces many severe adverse effects on the human health [133-135]. In postmenopausal women, the risk of Parkinson's disease is reduced by CAF intake but an increased risk is associated among estrogen users and middle age females [136]. CAF consumption for the long time can influence the women's EST level and these variations in EST level over a long period of time may lead to many disorders, such as breast cancer, endometriosis, endometrial, ovarian cancers, increased blood pressure, plasma homocysteine concentrations, osteoporosis, serum total

and low-density lipoprotein cholesterol concentrations [137-140]. Hence, it was considered desirable to study the effect of CAF on EST in women of child bearing age.

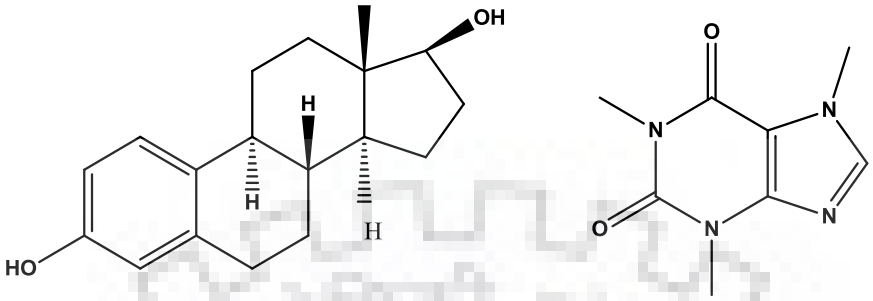

Estradiol **Caffeine**

1.6 THESIS LAYOUT

Analysis of biologically important molecules and drug in human physiological fluids is a significant task due to their minor concentration level in body fluids. The normal metabolism gets altered in the case of any pathophysiological dysfunction in human system, which leads to minute alteration in their concentration level. Monitoring the concentration level of biomolecules and pharmaceutical drugs in human urine, plasma and serum is considered as biomarker in the diagnosis of several diseases. Implementation of nanomaterial and nanocomposites modified sensors in electrochemical techniques in the analysis of biomolecules may provide rapid, effective, inexpensive and highly sensitive biomarker analysis. Hence, in the present thesis, several modified sensors have been fabricated by the use of carbon based nanomaterials, metal nanoparticles, polymers and their composite and sensitive detection of various biomolecules and pharmaceutical drugs in human physiological fluids has been carried out. The investigation has been systematically organized in six chapters in the thesis as follows:

Chapter 1: Introduction

Chapter 2: Determination of 2-Thioxanthine, an antipsychotic drug and Propranolol used to treat its side effect.

Chapter 3: PtNPs and ErGO based sensitive sensor for the determination of Efavirenz.

Chapter 4: Graphene based sensors for the determination of biomolecules.

Chapter 5: Functionalized SWCNTs based sensor for the determination of ATP metabolites.

Chapter 6: AgNPs and ErGO modified sensor for determining the effect of caffeine on the Estradiol release.

1.7 REFERENCES

[1] M.D. Ryan, J.Q. Chambers, "Dynamic electrochemistry: methodology and application", Anal. Chem. 64 (1992) 79R.

[2] G. Chen, "Electrochemical technologies in waste water treatment", Sep. Purif. Technol. 38 (2004) 11.

[3] J. Wang, "Analytical Electrochemistry", Wiley-VCH (A John Wiley & Sons, Inc.): New York, 2nd ed. (2000) p 45.

[4] S. Nesic, J. Postlethwaite, S. Olsen, "An electrochemical model for prediction of corrosion of mild steel in aqueous carbon dioxide solutions", Corros. Sci. 52 (1996) 280.

[5] E.R. Gonzalez, S. Srinivasan, "Electrochemistry of fuel cells for transportation applications", Int. J. Hydrogen Energy 9 (1984) 215.

[6] S. Suzen, B.T. Demircigil, E. Buyukbingol, S.A. Ozkan, "Electroanalytical evaluation and determination of 5-(3'-indolyl)-2-thiohydantoin derivatives by voltammetric studies: possible relevance to in vitro metabolism", New J. Chem. 27 (2003) 1007.

[7] J. Barek, J. Zima, "Eighty years of polarography-history and future", Electroanalysis 15 (2003) 467.

[8] R.S. Nicholson, I. Shain, "Theory of stationary electrode polarography: single scan and cyclic methods applied to reversible, irreversible and kinetic systems", Anal. Chem. 36 (1964) 706.

[9] J.G. Dick, "Electroanalytical techniques: principles and applications", Tech. Instr. Anal. Chem. 18 (1997) 267.

[10] A. Isaac, C. Livingstone, A.J. Wain, R.G. Compton, J. Davis, "Electroanalytical methods for the determination of sulfite in food and beverages", Trends Anal. Chem. 25 (2006) 589.

[11] B. Uslu, S.A. Ozkan, "Electroanalytical methods for the determination of pharmaceuticals: a review of recent trends and developments", Anal. Lett. 44 (2011) 2644.

[12] M. Labib, E.H. Sargent, S.O. Kelley, "Electrochemical methods for the analysis of clinically relevant biomolecules", Chem. Rev. 116 (2016) 9001.

[13] A.B. Cadwallader, X. Torre, A. Tieri, F. Botre, "The abuse of diuretics as performance-enhancing drugs and masking agents in sport doping: pharmacology, toxicology and analysis", Br J Pharmacol. 161 (2010) 1.

[14] M. Bijad, H.K. Maleh, M. Farsi, S.A. Shahidi, "An electrochemical-amplified-platform based on the nanostructure voltammetric sensor for the determination of carmoisine in the

presence of tartrazine in dried fruit and soft drink samples", J Food Meas Charact. 12 (2018) 634.

[15] O. Gurtova, L. Ye, F. Chmilenko, "Potentiometric propranolol-selective sensor based on molecularly imprinted polymer", Anal. Bioanal. Chem. 405 (2013) 287.

[16] V.V. Pavlishchuk, A.W. Addison, "Conversion constants for redox potentials measured versus different reference electrodes in acetonitrile solutions at 25°C", Inorg. Chim. Acta 298 (2000) 97.

[17] G. Gritzner, J. Kuta, "Recommendations on reporting electrode potentials in non-aqueous solvents", Pure & Appl. Chem. 56 (1984) 461.

[18] S.H. Duvall, R.L. Mccreery, "Control of catechol and hydroquinone electron-transfer kinetics on native and modified glassy carbon electrodes", Anal. Chem. 71 (1999) 4594.

[19] R.S. Nicholson, "Theory and application of cyclic voltammetry for measurement of electrode reaction kinetics", Anal. Chem. 37 (1965) 1351.

[20] J.L. Anderson, I. Shain, "Cyclic voltammetric studies of the pH dependence of Copper(ll) reduction in acidic aqueous nitrate and perchlorate solutions", Anal. Chem. 48 (1976) 1274.

[21] C. Degrand, L.L. Miller, "An electrode modified with polymer-bound dopamine which catalyzes NADH oxidation", J. Am. Chem. Soc. 102 (1980) 5728.

[22] G.A. Carriedo, "The use of cyclic voltammetry in the study of the chemistry of metal-carbonyls", J. Chem. Educ. 65 (1988) 1020.

[23] P.T. Kissinger, W.R. Heineman, "Cyclic Voltammetry", J. Chem. Educ. 60 (1983) 702.

[24] N. Elgrishi, K.J. Rountree, B.D. McCarthy, E.S. Rountree, T.T. Eisenhart, J.L. Dempsey, "A practical beginner's guide to cyclic voltammetry", J. Chem. Educ. 95 (2018) 197.

[25] C.B. McAuley, E. Katelhon, E.O. Barnes, R.G. Compton, E. Laborda, A. Molina, "Recent advances in voltammetry", Chemistry Open 4 (2015) 224.

[26] A.M. Bond, S.W. Feldberg, "Analysis of simulated reversible cyclic voltammetric responses for a charged redox species in the absence of added electrolyte", J. Phys. Chem. B 102 (1998) 9966.

[27] L. Ramaley, M.S. Krause, "Theory of Square Wave Voltammetry", Anal. Chem. 41 (1969) 1362.

[28] M. Lovric, S.K. Lovric, "Theory of square-wave voltammetry of two-electron reduction with the adsorption of intermediate", Int. J. Electrochem. 2012 (2012) 1.

[29] B. Yilmaz, S. Kaban, B.K. Akcay, "Anodic oxidation of etodolac and its linear sweep, square wave and differential pulse voltammetric determination in pharmaceuticals", Indian J. Pharm. Sci. 77 (2015) 413.

[30] M.M.C. Santos, V. Famila, M.L.S. Goncalves, "Square-wave voltammetric techniques for determination of psychoactive 1,4-benzodiazepine drugs", Anal Bioanal Chem 374 (2002) 1074.

[31] G.A. Saleh, H.F. Askal, I.H. Refaat, A.H. Naggar, F.A.M. Abdelaal, "Adsorptive square wave voltammetric determination of the antiviral drug valacyclovir on a novel sensor of copper micro particles–modified pencil graphite electrode", Arab. J. Chem. 9 (2016) 143.

[32] B. Prathap, A. Dey, G.H.S. Rao, P. Johnson, P. Arthanariswaran, "A Review- importance of RP-HPLC in analytical method development", Int. J. Novel Trends Pharm. Sci. 3 (2013) 15.

[33] M. Thammana, "A review on high performance liquid chromatography (HPLC)", J. Pharm. Anal. 5 (2016) 22.

[34] M. Fojta, E. Palecek, "Supercoiled DNA-modified mercury electrode: A highly sensitive tool for the detection of DNA damage", Anal. Chim. Acta 342 (1997) l.

[35] V.K. Gupta, S. Chandra, H. Lang, "A highly selective mercury electrode based on a diamine donor ligand", Talanta 66 (2005) 575.

[36] T. Stora, R. Hovius, Z. Dienes, M. Pachoud, H. Vogel, "Metal ion trace detection by a chelator-modified gold electrode: a comparison of surface to bulk affinity", Langmuir 13 (1997) 5211.

[37] B.M. Quinn, P. Liljeroth, V. Ruiz, T. Laaksonen, K. Kontturi, "Electrochemical resolution of 15 oxidation states for monolayer protected gold nanoparticles", J. Am. Chem. Soc. 125 (2003) 6644.

[38] A.V. Benedetti, P.T.A. Sumodjo, K. Nobe, P.L. Cabot, W.G. Proud, "Electrochemical studies of copper, copper-aluminium and copper-aluminium-silver alloys: impedance results in 0.5 M NaCl", Electrochim. Acta 40 (1995) 2657.

[39] R.F. Lane, A.T. Hubbard, "Differential double pulse voltammetry at chemically modified platinum electrodes for in vivo determination of catecholamines", Anal. Chem. 48 (1976) 1287.

[40] H.R. Zare, N. Rajabzadeh, N. Nasirizadeh, M.M. Ardakani, "Voltammetric studies of an oracet blue modified glassy carbon electrode and its application for the simultaneous

determination of dopamine, ascorbic acid and uric acid", J. Electroanal. Chem. 589 (2006) 60.

[41] R.L. McCreery, "Advanced carbon electrode materials for molecular electrochemistry", Chem. Rev. 108 (2008) 2646.

[42] F.J. Miller, H.E. Zittel, "Fabrication and use of pyrolytic graphite electrode for voltammetry in aqueous solutions", Anal. Chem. 35 (1963) 1866.

[43] C.E. Banks, R.G. Compton, "Edge plane pyrolytic graphite electrodes in electroanalysis: A review", Anal. Sci. 21 (2005) 1263.

[44] W. Zhang, S. Zhu, R. Luque, S. Han, L. Hu, G. Xu, "Recent development of carbon electrode materials and their bioanalytical and environmental applications", Chem. Soc. Rev. 45 (2016) 715.

[45] R.R. Moore, C.E. Banks, R.G. Compton, "Basal plane pyrolytic graphite modified electrodes: comparison of carbon nanotubes and graphite powder as electrocatalysts", Anal. Chem. 76 (2004) 2677.

[46] C.H.A. Wong, M. Pumera, "On reproducibility of preparation of basal plane pyrolytic graphite electrode surface", Electrochem. Commun. 13 (2011) 1054.

[47] A. Salimi, R.G. Compton, R. Hallaj, "Glucose biosensor prepared by glucose oxidase encapsulated sol-gel and carbon-nanotube-modified basal plane pyrolytic graphite electrode", Anal. Biochem. 333 (2004) 49.

[48] M.J. Sims, N.V. Rees, E.J.F. Dickinson, R.G. Compton, "Effects of thin-layer diffusion in the electrochemical detection of nicotine on basal plane pyrolytic graphite (BPPG) electrodes modified with layers of multi-walled carbon nanotubes (MWCNT-BPPG)", Sens. Actuators B 144 (2010) 153.

[49] C.E. Banks, R.G. Compton, "Exploring the electrocatalytic sites of carbon nanotubes for NADH detection: an edge plane pyrolytic graphite electrode study", Analyst 130 (2005) 1232.

[50] R.T. Kachoosangi, R.G. Compton, "A simple electroanalytical methodology for the simultaneous determination of dopamine, serotonin and ascorbic acid using an unmodified edge plane pyrolytic graphite electrode", Anal.Bioanal. Chem. 387 (2007) 2793.

[51] M.I.G. Sanchez, B.G. Monedero, J. Agrisuelas, J. Iniesta, E. Valero, "Highly activated screen-printed carbon electrodes by electrochemical treatment with hydrogen peroxide", Electrochem. Commun. 91 (2018) 36.

[52] X. Niu, C. Chen, H. Zhao, J. Tang, Y. Li, M. Lan, "Porous screen-printed carbon electrode", Electrochem. Commun. 22 (2012) 170.

[53] M. Hatada, W. Tsugawa, E. Kamio, N. Loew, D.C. Klonoff, K. Sode, "Development of a screen-printed carbon electrode based disposable enzyme sensors trip for the measurement of glycated albumin", Biosens. Bioelectron. 88 (2017) 167.

[54] Q. Gao, X. Cui, F. Yang, Y. Ma, X. Yang, "Preparation of poly (thionine) modified screen-printed carbon electrode and its application to determine NADH in flow injection analysis system", Biosens. Bioelectron.19 (2003) 277.

[55] J. Wang, B. Tian, V.B. Nascimento, L. Angnes, "Performance of screen-printed carbon electrodes fabricated from different carbon inks", Electrochim. Acta 43 (1998) 3459.

[56] Y. Shao, J. Wang, H. Wu, J. Liu, I.A. Aksay, Y. Lin, "Graphene Based Electrochemical Sensors and Biosensors: A Review", Electroanalysis 22 (2010) 1027.

[57] M.J. Allen, V.C. Tung, R.B. Kaner, "Honeycomb carbon: A review of graphene", Chem. Rev. 110 (2010) 132.

[58] Y.R. Kim, S. Bong, Y.J. Kang, Y. Yang, R.K. Mahajan, J.S. Kim, H. Kim, "Electrochemical detection of dopamine in the presence of ascorbic acid using graphene modified electrodes", Biosens. Bioelectron. 25 (2010) 2366.

[59] M. Mallesha, R. Manjunatha, C. Nethravathi, G.S. Suresh, M. Rajamathi, J.S. Melo, T.V. Venkatesha, "Functionalized-graphene modified graphite electrode for the selective determination of dopamine in presence of uric acid and ascorbic acid", Bioelectrochemistry 81 (2011) 104.

[60] Rosy, S.K. Yadav, B. Agrawal, M. Oyama, R.N. Goyal, "Graphene modified Palladium sensor for electrochemical analysis of norepinephrine in pharmaceuticals and biological fluids", Electrochim. Acta 125 (2014) 622.

[61] A. Navaee, A. Salimi, H. Teymourian, "Graphene nanosheets modified glassy carbon electrode for simultaneous detection of heroine, morphine and noscapine", Biosens. Bioelectron. 31 (2012) 205.

[62] H. Du, J. Ye, J. Zhang, X. Huang, C. Yu, "A voltammetric sensor based on graphene-modified electrode for simultaneous determination of catechol and hydroquinone", J. Electroanal. Chem. 650 (2011) 209.

[63] Y. Li, K. Li, G. Song, J. Liu, K. Zhang, B. Ye, "Electrochemical behaviour of codeine and its sensitive determination on graphene-based modified electrode", Sens. Actuators B 182 (2013) 401.

[64] B.R. Adhikari, M. Govindhan, A. Chen, "Sensitive detection of acetaminophen with graphene-based electrochemical sensor", Electrochim. Acta 162 (2015) 198.

[65] L. Yang, D. Liu, J. Huang, T. You, "Simultaneous determination of dopamine, ascorbic acid and uric acid at electrochemically reduced graphene oxide modified electrode", Sens. Actuators B 193 (2014) 166.

[66] H. Yin, Q. Ma, Y. Zhou, S. Ai, L. Zhu, "Electrochemical behavior and voltammetric determination of 4-aminophenol based on graphene–chitosan composite film modified glassy carbon electrode", Electrochim. Acta 55 (2010) 7102.

[67] H. Bagheri, A. Afkhami, H. Khoshsafar, M. Rezaei, S.J. Sabounchei, M. Sarlakifar, "Simultaneous electrochemical sensing of thallium, lead and mercury using a novel ionic liquid/graphene modified electrode", Anal. Chim. Acta 870 (2015) 56.

[68] X. Liu, E. Shangguan, J. Li, S. Ning, L. Guo, Q. Li, "A novel electrochemical sensor based on FeS anchored reduced graphene oxide nanosheets for simultaneous determination of dopamine and acetaminophen", Mater. Sci. Eng. C 70 (2017) 628.

[69] A.J.S. Ahammad, J.J. Lee, M.A. Rahman, "Electrochemical sensors based on carbon nanotubes", Sensors 9 (2009) 2289.

[70] S.K. Vashist, D. Zheng, K.A. Rubeaan, J.H.T. Luong, F.S. Sheu, "Advances in carbon nanotube based electrochemical sensors for bioanalytical applications", Biotechnol Adv 29 (2011) 169.

[71] A. Cernat, M. Tertis, R. Sandulescu, F. Bedioui, A. Cristea, C. Cristea, "Electrochemical sensors based on carbon nanomaterials for acetaminophen detection: A review", Anal. Chim. Acta 886 (2015) 16.

[72] Z.A. Alothman, N. Bukhari, S.M. Wabaidur, S. Haider, "Simultaneous electrochemical determination of dopamine and acetaminophen using multiwall carbon nanotubes modified glassy carbon electrode", Sens. Actuators B 146 (2010) 314.

[73] H. Li, Y. Wang, D. Ye, J. Luo, B. Su, S. Zhang, J. Kong, "An electrochemical sensor for simultaneous determination of ascorbic acid, dopamine, uric acid and tryptophan based on MWNTs bridged mesocellular graphene foam nanocomposite", Talanta 127 (2014) 255.

[74] A. Mokhtari, H.K. Maleh, A.A. Ensafi, H. Beitollahi, "Application of modified multiwall carbon nanotubes paste electrode for simultaneous voltammetric determination of morphine and diclofenac in biological and pharmaceutical samples", Sens. Actuators B 169 (2012) 96.

[75] M. Taei, F. Hasanpour, V. Hajhashemi, M. Movahedi, H. Baghlani, "Simultaneous detection of morphine and codeine in urine samples of heroin addicts using multi-walled carbon nanotubes modified SnO_2–Zn_2SnO_4nanocomposites paste electrode", Appl. Surf. Sci. 363 (2016) 490.

[76] K. Kerman, M. Saito, S. Yamamura, Y. Takamura, E. Tamiya, "Nanomaterial-based electrochemical biosensors for medical applications", Trends Anal. Chem 27 (2008) 585.

[77] E. Katz, I. Willner, J. Wang, "Electroanalytical and bioelectro analytical systems based on metal and semiconductor nanoparticles", Electroanalysis 16 (2004) 19.

[78] A. Chen, S. Chatterjee, "Nanomaterials based electrochemical sensors for biomedical applications", Chem. Soc. Rev. 42 (2013) 5425.

[79] J.M. Pingarron, P.Y. Sedeno, A.G. Cortes, "Gold nanoparticle-based electrochemical biosensors", Electrochim. Acta 53 (2008) 5848.

[80] K. Saha, S.S. Agasti, C. Kim, X. Li, V.M. Rotello, "Gold Nanoparticles in Chemical and Biological Sensing", Chem. Rev. 112 (2012) 2739.

[81] X.X. Jiao, H.Q. Luo, N.B. Li, "Fabrication of graphene–gold nanocomposites by electrochemical co-reduction and their electrocatalytic activity toward 4-nitrophenol oxidation", J. Electroanal. Chem. 691 (2013) 83.

[82] R. Karthik, N. Karikalan, S.M. Chen, P. Gnanaprakasam, C. Karuppiah, "Voltammetric determination of the anti-cancer drug nilutamide using a screen-printed carbon electrode modified with a composite prepared from β-cyclodextrin, gold nanoparticles and graphene oxide", Microchim. Acta 184 (2017) 507.

[83] C. Wang, J. Du, H. Wang, C. Zou, F. Jiang, P. Yang, Y. Du, "A facile electrochemical sensor based on reduced graphene oxide and Au nano-plates modified glassy carbon electrode for simultaneous detection of ascorbic acid, dopamine and uric acid", Sens. Actuators B 204 (2014) 302.

[84] A.A. Ensafi, M.M. Abarghoui, B. Rezaei, "Simultaneous determination of morphine and codeine using Pt nanoparticles supported on porous silicon flour modified ionic liquid carbon paste electrode", Sens. Actuators B 219 (2015) 1.

[85] M.M. Barsan, M.E. Ghica, C.M.A. Brett, "Electrochemical sensors and biosensors based on redox polymer/carbon nanotube modified electrodes: A review", Anal. Chim. Acta 881 (2015) 1.

[86] R. Zhang, G.D. Jin, D. Chen, X.Y. Hu, "Simultaneous electrochemical determination of dopamine, ascorbic acid and uric acid using poly(acid chrome blue K) modified glassy carbon electrode", Sens. Actuators B 138 (2009) 174.

[87] M. Gerard, A. Chaubey, B.D. Malhotra, "Application of conducting polymers to biosensors", Biosens. Bioelectron. 17 (2002) 345.

[88] J.M. Pernaut, J.R. Reynolds, "Use of conducting electro-active polymers for drug delivery and sensing of bioactive molecules. A redox chemistry approach", J. Phys. Chem. B 104 (2000) 4080.

[89] M. Trojanowicz, "Application of conducting polymers in chemical analysis", Microchim. Acta 143 (2003) 75.

[90] A. Ramanavicius, A. Ramanaviciene, A. Malinauskas, "Electrochemical sensors based on conducting polymer—polypyrrole", Electrochim. Acta 51 (2006) 6025.

[91] K.M. Hassan, S.E. Gaber, M.F. Altahan, M.A. Azzem, "Novel sensor based on poly (1,2-diaminoanthraquinone) for individual and simultaneous anodic stripping voltammetry of Cd^{2+}, Pb^{2+}, Cu^{2+} and Hg^{2+}", Electroanalysis 30 (2018) 1155.

[92] Y. Zhang, R. Yuan, Y. Chai, W. Li, X. Zhong, H. Zhong, "Simultaneous voltammetric determination for DA, AA and NO_2 based on graphene/poly-cyclodextrin/MWCNTs nanocomposite platform", Biosen. Bioelectron. 26 (2011) 3977.

[93] M. Li, W. Wang, Z. Chen, Z. Song, X. Luo, "Electrochemical determination of paracetamol based on Au@ graphene core-shell nanoparticles doped conducting polymer PEDOT nanocomposite", Sens. Actuators B 260 (2018) 778.

[94] N. Promphet, P. Rattanarat, R. Rangkupan, O. Chailapakul, N. Rodthongkum, "An electrochemical sensor based on graphene/polyaniline/polystyrene nano porous fibers modified electrode for simultaneous determination of lead and cadmium", Sens. Actuators B 207 (2015) 526.

[95] B.E. Leonard, "Antipsychotic Drugs and their Side-Effects-A volume in Neuroscience Perspectives; (Chapter 1 The pharmacology of the phenothiazines, butyrophenones, thioxanthines and diphenyl butylpiperidines)" Elsevier (1993) p 3-26.

[96] X. Yuan, Y. Wang, X. Wang, W. Chen, J.S. Fossey, N. Wong, "An initio and AIM investigation into the hydration of 2-thioxanthine", Chem. Cent. J. 4 (2010) 1.

[97] J. Ward, S.N. Spath, B. Pabst, P.A. Carpino, R.B. Ruggeri, G. Xing, A.E. Speers, B.F. Cravatt, K. Ahn, "Mechanistic characterization of a 2-thioxanthinemyeloperoxidase inhibitor and selectivity assessment utilizing click chemistry activity-based protein profiling", Biochemistry 52 (2013) 9187.

[98] A. Biela, F. Coste, F. Culard, M. Guerin, S. Goffinont, K. Gasteiger, J. Ciesla, A.Winczura, Z. Kazimierczuk, D. Gasparutto, T. Carell, B. Tudek, B. Castaing, "Zincfinger oxidation of Fpg/Nei DNA glycosylases by 2-thioxanthine: biochemical and X-ray structural characterization", Nucleic Acids Res. 42 (2014) 10748.

[99] W. Fischer, "Anticonvulsant profile and mechanism of action of propranolol and its two enantiomers", Seizure 11 (2002) 285.

[100] A.M. Barrett, V.A. Cullum, "The biological properties of the optical isomers of propranolol and their effects on cardiac arrhythmias", Br. J. Pharmac. 34 (1968) 43.

[101] P. Partani, Y. Modhave, S. Gurule, A. Khuroo, T. Monif, "Simultaneous determination of propranolol and 4-hydroxy propranolol in human by solid phase extraction and liquid chromatography/electrospray tandem mass spectrometry", J. Pharm. Biomed. Anal. 50 (2009) 966.

[102] M.M. Bastos, C. Costa, T.C. Bezerra, F. Silva, N. Boechat, "Efavirenz a non-nucleoside reverse transcriptase inhibitor of first-generation: Approaches based on its medicinal chemistry", Eur. J. Med. Chem. 108 (2016) 455.

[103] M. Wei, B. Kost, I. R. Muller, E. Wolf, I. Mylonas, A. Bruning, "Efavirenz Causes Oxidative Stress, Endoplasmic Reticulum Stress, and Autophagy in Endothelial Cells", Cardiovasc Toxicol 16 (2016) 90.

[104] M. Sadeghi, M. Bayat, S. Cheraghi, K. Yari, R. Heydari, S. Dehdashtian, M. Shamsipur, "Binding studies of the anti-retroviral drug, efavirenz to calf thymus DNA using spectroscopic and voltammetric techniques", Luminescence 31 (2016) 108.

[105] A.A. Castro, M. Souza, N. A. Rey, P. Farias, "Determination of Efavirenz in Diluted Alkaline Electrolyte by Cathodic Adsorptive Stripping Voltammetry at the Mercury Film Electrode", J. Braz. Chem. Soc. 22 (2011) 1662.

[106] T.M. Love, "Oxytocin, motivation and the role of dopamine", Pharmacol. Biochem. Behav. 119 (2014) 49.

[107] C. Missale, S.R. Nash, S.W. Robinson, M. Jaber, M.G. Caron, "Dopamine receptors: from structure to function", Physiol. Rev. 78 (1998) 189.

[108] P.A. Jose, G.M. Eisner, R.A. Felder, "Renal dopamine receptors in health and hypertension", Pharmacol. Ther. 80 (1998) 149.

[109] M.M. Ardakani, H. Rajabi, H. Beitollahi, B.B.F. Mirjalili, A. Akbari, N. Taghavinia, "Voltammetric determination of dopamine at the surface of TiO_2 nanoparticles modified carbon paste electrode", Int. J. Electrochem. Sci. 5 (2010) 147.

[110] R. Zanettini, A. Antonini, G. Gatto, R. Gentile, S. Tesei, G. Pezzoli, "Valvular heart disease and the use of dopamine agonists for Parkinson's disease", N. Engl. J. Med. 356 (2007) 39.

[111] A. Liu, I. Honma, H. Zhou, "Electrochemical biosensor based on protein–polysaccharide hybrid for selective detection of nanomolar dopamine metabolite of 3,4-dihydroxyphenylacetic acid (DOPAC)", Electrochem. Commun. 7 (2005) 233.

[112] G.E.D. Benedetto, D. Fico, A. Pennetta, C. Malitesta, G. Nicolardi, D.D. Lofrumento, F.D. Nuccio, V.L. Pesa, "A rapid and simple method for the determination of 3,4-dihydroxyphenylacetic acid, norepinephrine, dopamine, and serotonin in mouse brain homogenate by HPLC with fluorimetric detection", J Pharm Biomed Anal 98 (2014) 266.

[113] E. Watson, S. Wilk, "Assessment of Cerebrospinal Fluid Levels of Dopamine Metabolites by Gas Chromatography", Psycho. Pharmacologia. (Berl). 42 (1975) 57.

[114] D.S. Goldstein, G. Eisenhofer, I.J. Kopin, "Sources and Significance of Plasma Levels of Catechols and Their Metabolites in Humans", J. Pharmacol. Exp. Ther. 305 (2003) 800.

[115] L. Gyermek, "Pharmacology of serotonin as related to anesthesia", J. Clin. Anesth. 8 (1996) 402.

[116] K. Wu, J. Fei, S. Hu, "Simultaneous determination of dopamine and serotonin on a glassy carbon electrode coated with a film of carbon nanotubes", Anal. Biochem. 318 (2003) 100.

[117] R.N. Goyal, M. Oyama, V.K. Gupta, S.P. Singh, R.A. Sharma, "Sensors for 5-hydroxytryptamine and 5-hydroxyindole acetic acid based on nanomaterial modified electrodes", Sens. Actuators B 134 (2008) 816.

[118] K. Gregersen, J. Valeur, K. Lillestol, L. Froyland, P. Araujo, G.A. Lied, A. Berstad, "Subjective food hypersensitivity: assessment of enterochromaffin cellmarkers in blood and gut lavage fluid", Int. J. Gen. Med. 4 (2011) 555.

[119] Z. Zhou, A. Roy, R. Lipsky, K. Kuchipudi, G. Zhu, J. Taubman, M.A. Enoch, M. Virkkunen, D. Goldman, "Haplotype-Based Linkage of Tryptophan Hydroxylase 2 to Suicide Attempt, Major Depression, and Cerebrospinal Fluid 5-Hydroxyindoleacetic Acid in 4 Populations", Arch Gen Psychiatry 62 (2005) 1109.

[120] P. Kestell, L. Zhao, M.B. Jameson, M.R.L. Stratford, L.K. Folkes, B.C. Baguley, "Measurement of plasma 5-hydroxyindoleacetic acid as a possible clinical surrogate marker for the action of antivascular agents", Clin Chim Acta 314 (2001) 159.

[121] G.N. Pandey, Y. Dwivedi, "The Neurobiological Basis of Suicide-Chapter 20 Peripheral Biomarkers for Suicide", CRC Press/Taylor & Francis (2012) p20.1.

[122] P. Nordstrom, M. Samuelsson, M. Asberg, L.T. Bendz, A.A. Wistedt, C. Nordin, L. Bertilsson, "CSF 5-HIAA predicts suicide risk after attempted suicide", Suicide Life Threat. Behav. 24 (1994) 1.

[123] D.E. Farthing, C.A. Farthing, L. Xi, "Inosine and hypoxanthine as novel biomarkers for cardiac ischemia: From bench to point-of-care", Exp. Biol. Med. 240 (2015) 821.

[124] L.F. Souza, A.P. Horn, D.P. Gelain, F.R. Jardim, G. Lenz, E.A. Bernard, "Extracellular inosine modulates ERK 1/2 and p38 phosphorylation in cultured Sertoli cells: Possible participation in TNF-alpha modulation of ERK 1/2", Life Sci. 77 (2005) 3117.

[125] S. Buckley, L. Barsky, K. Weinbergand, D. Warburton, "In vivo inosine protects alveolar epithelial type 2 cells against hyperoxia-induced DNA damage through MAP kinase signaling", Am. J. Physiol. Lung Cell Mol. Physiol. 288 (2005) L569.

[126] S.B. Revin, S.A. John, "Selective determination of inosine in the presence of uric acidand hypoxanthine using modified electrode", Anal. Biochem. 421 (2012) 278.

[127] J.R. Docherty, A. Camba, E. Lendoiro, C. Cordeiro, I.M. Silva, M.S.R. Calvo, D.N. Vieira, J.I.M. Barus, "High variation in hypoxanthine determination after analytical treatment of vitreous humor samples", Forensic Sci. Med. Pathol. 10 (2014) 627.

[128] S.Z. Bas, H. Gulce, S. Yildiz, A. Gulce, "Amperometric biosensors based on deposition of gold and platinum nanoparticles on polyvinyl ferrocene modified electrode for xanthine detection", Talanta 87 (2011) 189.

[129] A.P.M Farias, A.A. Castro, "Determination of xanthine in the presence of hypoxanthine by adsorptive stripping voltammetry at the mercury film electrode", Anal. Chem. Insights 9 (2004) 49.

[130] K.J. Ryan, "Biochemistry of aromatase: significance to female reproductive physiology", Cancer Research 42 (1982) 3342s.

[131] J. Cui, Y. Shen, R. Li, "Estrogen synthesis and signaling pathways during ageing: from periphery to brain", Trends Mol Med. 19 (2013) 197.

[132] F. Kordi, H. Khazali, "The effect of ghrelin and estradiol on mean concentration of thyroid hormones", Int J Endocrinol Metab. 13 (2015) e17988.

[133] L. Svorc, P. Tomcik, J. Svitkova, M. Rievaj, D. Bustin, "Voltammetric determination of caffeine in beverage samples on bare boron-doped diamond electrode", Food Chem. 135 (2012) 1198.

[134] J.Y. Sun, K.J. Huang, S.Y. Wei, Z.W. Wu, F.P. Ren, "A graphene-based electrochemical sensor for sensitive determination of caffeine", Colloids Surf. B 84 (2011) 421.

[135] Y. Tadesse, A. Tadese, R.C. Saini, R. Pal, "Cyclic voltammetric investigation of caffeine at anthraquinone modified carbon paste electrode", Int. J. Electrochem. Sc. 2013 (2013) 1.

[136] A. Ascherio, M.G. Weisskopf, E.J. OReilly, M.L. McCullough, E.F. Calle, C. Rodriguez, M.J. Thun, "Coffee consumption, gender, and parkinson's disease mortality in the cancer prevention study ii cohort: the modifying effects of estrogen", Am J Epidemiol 160 (2004) 977.

[137] C. Nagata, M. Kabuto, H. Shimizu, "Association of coffee, green tea, and caffeine intakes with serum concentrations of estradiol and sex hormone-binding globulin in premenopausal japanese women", Nutr. Cancer 30 (1998) 21.

[138] K. Xu, Y. Xu, D.B. Jermyn, J.F. Chen, A. Ascherio, D.E. Dluzen, M.A. Schwarzschild, "Estrogen Prevents Neuroprotection by Caffeine in the Mouse 1-Methyl-4-Phenyl-1,2,3,6-Tetrahydropyridine Model of Parkinson's Disease", J. Neurosci. 26 (2006) 535.

[139] M. Fujimaki, S. Saiki, Y. Li, N. Kaga, H. Taka, T. Hatano, K.I. Ishikawa, Y. Oji, A. Mori, A. Okuzumi, T. Koinuma, S.I. Ueno, Y. Imamichi, T. Ueno, Y. Miura, M. Funayama, N. Hattori, "Serum caffeine and metabolites are reliable biomarkers of early Parkinson disease", Neurology 90 (2018) e404.

[140] D.R. Lee, J. Lee, M. Rota, J. Lee, H.S. Ahn, S.M. Park, D. Shin, "Coffee consumption and risk of fractures: A systematic review and dose–response meta-analysis", Bone 63 (2014) 20.

Chapter 2

Determination of 2-Thioxanthine, an antipsychotic drug and Propranolol used to treat its side effect

2.1 INTRODUCTION

In last decades, modification of the surface of electrode has been gaining much consideration in the field of electrochemical sensors. Conducting polymers have unique mechanical, optical and chemical properties, which accelerate the charge transfer kinetics and give enhanced sensitivity, reproducibility and biocompatibility in electrochemical analysis. The effective higher surface area and more reactivity provided by the conducting polymers can accommodate more molecules at the surface due to which they are used used in a variety of fields, such as electroanalysis, energy conversion, catalysis, storage, electrochemistry etc. A polymer modified electrode surface is usually achieved by electro-polymerization by applying the potential, whereas the thickness of the modified polymeric film can be controlled by varying the applied range of potential, number of scans and sweep rate.

This chapter deals with the fabrication of conducting polymer modified electrochemical sensors and their application in the voltammetric determination of antipsychotic drug; 2-Thioxanthine and a beta blocker; Propranolol used in the treatment of disorders caused by antipsychotic drugs. Antipsychotic drugs cause some under-recognized side effects and results into Drug-Induced Movement Disorders (DIMDs), which is also known as extrapyramidal symptoms (EPS). DIMDs include several clinically distinct movement disorders, such as dystonia, Parkinsonism, akathisia, tardive dyskinesia and so on. Propranolol has been effectively used in the treatment of such disorders and mainly for akathisia [1,2].

The voltammetric studies and observed results are categorized into two sections. The **first section** of this chapter deals with the fabrication of a co-polymeric film of poly-melamine (p-melamine) and p-glutamic acid at the surface of the edge plane pyrolytic graphite (EPPG) and its application for the sensitive determination of antipsychotic drug, 2-Thioxanthine. The **second section** of this chapter is devoted to the preparation, characterization of p-melamine modified EPPG sensor and its applicability in the sensitive estimation of a β-blocker drug, Propranolol used to treat medication-induced movement disorders caused by antipsychotic drugs.

2.2 SECTION A: Co-polymeric film of p-melamine and p-glutamic acid modified sensor to determine 2-Thioxanthine

The modification of the surface of a sensor by the conducting polymeric film is a novel and advanced area and receiving extensive interest these days in the area of electrochemical sensors

and biosensors [3]. Conducting polymers act as a potential candidate for the sensor modification due to their specific properties, such as high electron affinity, low ionization potential, sensitivity, greater number of active sites, homogeneity and porous with the extreme cohesion to the sensor surface [4-6]. These polymers have the combined characteristics of organic polymers and electronic properties of semiconductors and their 3-D molecular structure regulates the electronic properties and nanostructure shape. Furthermore, the physical, chemical and electrical properties of conducting polymers can be adjusted to the particular requirement of their application by incorporating biomolecules. Conducting polymers also show highly sensitive characteristics to minute disturbance and produce a remarkable increment in the electrocatalytic property and reaction kinetics [7-9]. Melamine (1,3,5-triazine-2,4,6-triamine) readily polymerizes to give polymelamine, a conducting polymer having many amino groups, which block aggregation. Melamine monomers electro-polymerize by the oxidation of amino groups and results the formation of polymer film by head to head coupling having NH-NH bonding [10-12]. Glutamic acid, an amino acid can also easily polymerize on the electrode surface and there is a repetition of glutamate units and free protonated carboxylic groups by linking α-amino and δ-carboxylic acid functional groups. In the combination of both monomers, COOH and NH_2 functional groups interact with each other and form a stable film at the electrode surface, which can be utilized for the sensitive detection of biomolecules [13-16].

Xanthine (a purine base) belongs to a class of clinically significant alkaloids used as stimulants and drugs for the treatment of obstructive pulmonary diseases and bronchial asthma. Thiopurines is a group of effective drugs to treat leukaemia and related neoplastic diseases [17,18]. In thioxanthines, the oxygen atom present in xanthines is replaced by sulphur atom, which initiates some alterations in the properties of the nucleo-bases and thus stabilizes the DNA, hence, increases the possibility of mutations that arise in DNA [19]. 2-Thioxanthine (2-TX) is a thio-modified nucleic acid base, a most efficient and uncompetitive inhibitor that binds to the enzyme/DNA complex outside the active site, hence works as a DNA inhibitor [20], and antipsychotic drug. 2-TX also plays a significant role in chemotherapy for cancer disease and inhibition of myeloperoxidase viz., it blocks oxidative stress associated with inflammation, chronic obstructive pulmonary disease, Parkinson disease, atherogenesis, rheumatoid arthritis and alzheimer disease [20-22]. 2-TX also exists in different tautomeric forms and the stability and the tautomerisation energies of these tautomeric forms impart knowledge of its biological activity and the molecular stability. In equilibrium, 2-TX has the ability to exist in various tautomeric structures and the

protropic tautomerism can be found in the pyrimidine ring as well as in the imidazole ring. In the aqueous phase, the most stable tautomeric form is suggested as oxothione tautomeric form i.e., containing hydrogen atom at the N9 position of the imidazolic ring [23] (**Scheme 1**).

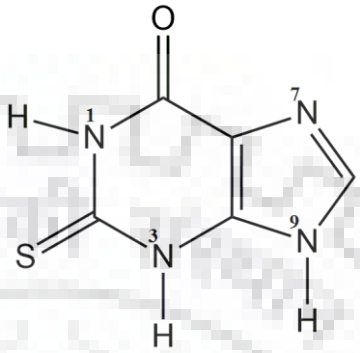

Scheme 1: Most stable tautomeric structure of 2-Thioxanthine proposed in aqueous solutions.

The investigation of 2-thioxanthine is considered of biological importance due to its potential as pharmacological agent in numerous diseases. The literature survey signifies that very scarce attempts have been made to understand the electrochemical behaviour of 2-TX. The electro-analysis and voltammetric behaviour of 2-TX have also not been much explored [24,25].

In the present section, for carrying out the sensitive determination of 2-TX, a rapid, single step polymerization method has been used to form a co-polymer film of melamine with glutamic acid at the surface of edge plane pyrolytic graphite sensor (EPPG). The electro polymerization of melamine with glutamic acid leads to a conducting polymer film that consists NH_2 and COOH groups on its backbone, which increases the bonding between both the monomers and causes a large net-stabilized structure. The prepared poly-(melamine)/poly-(glutamic acid) EPPG (p-Mel-Glu/EPPG) sensor exhibited good performance for the quantitative determination of 2-TX in human biological fluids with a low detection limit.

2.2.1 EXPERIMENTAL

2.2.1.1 Chemicals and Reagents

2-TX, L-glutamic acid and melamine were purchased from Sigma-Aldrich (USA). Phosphate buffers (PBS) of ionic strength (1.0 M) were prepared according to the reported method [26] and all the chemicals NaH_2PO_4, Na_2HPO_4 and NaOH used for the preparation of phosphate buffers were obtained from E. Merck (India) Ltd. Mumbai. Biological samples of human plasma and urine were collected from the Institute hospital, I.I.T. Roorkee, after the permission of Institute

Human Ethics Committee [IHEC-No: BIOTECH/IHEC/AP/15/1] of IIT Roorkee and were used after suitable dilution. All other chemicals and solvents used in the experiment were of analytical grade and double distilled water was used throughout the experiments.

2.2.1.2 Instruments

All voltammetric experiments were carried out using an electrochemical work station (BAS Epsilon-EC USB, ver. 2.00.71) equipped with three electrodes in a single compartment glass cell. Bare or Polymelamine modified edge plane pyrolytic graphite sensor (p-(melamine)/EPPG) was used as a working electrode, an Ag/AgCl (3 M NaCl) (BAS Model MF-2052 RB- 5B) and Pt wire were used as reference and counter electrodes, respectively. The pH measurement of the buffers was carried out using a Thermo Fisher Scientific, Singapore Digital pH meter (Eutech pH 700). The pyrolytic graphite pieces were acquired from Pfizer Inc. New York, USA as a gift. The characterization of the surface morphology of the bare and modified sensor was studied by using Horizontal Attenuated Total Reflectance-infrared spectroscopy (HATR-IR, PerkinElmer, Inc) and Field Emission Scanning Electron Microscopy (FE-SEM, model; Zeiss ultra plus 55). Electrochemical Impedance Spectroscopy (EIS) was performed using a galvanostat (model; Versastat 3, PAR).

2.2.1.3 Fabrication of polymeric film

To get the clean surface, EPPG was first manually rubbed on an emery paper (P-400) followed by rinsing with double distilled water and set aside to dry. The fabrication of co-polymer film of melamine with glutamic acid on the surface of EPPG was carried out in a solution containing 1:1 of 1 mM of melamine (prepared in 0.1 M H_2SO_4 solution) and 1 mM glutamic acid (prepared in pH 7.2 buffer, μ = 1.0 M) by scanning the potential between -200 mV to +1600 mV for optimized 15 scans at a sweep rate of 100 mVs^{-1}. In the first sweep, an anodic peak (a) at 435 mV was appeared, while in the reverse sweep, two cathodic peaks (c and c') were observed at 207 mV and −79 mV, respectively as shown in **Fig. 2.1**. In the successive cycles, all the peak potentials shifted to the more positive values (except the cathodic peak c') and the increment in the peak current for anodic as well as cathodic peaks was also observed, which signifies the consecutive growth of the polymer film on the EPPG sensor surface. In the last optimized scan, the anodic peak (a) was noticed at 564 mV and in the reverse sweep the cathodic peak (c) was observed at 408 mV. The fabricated sensor was then rinsed with distilled water to remove unreacted adsorbed molecules of both monomers from the surface of sensor.

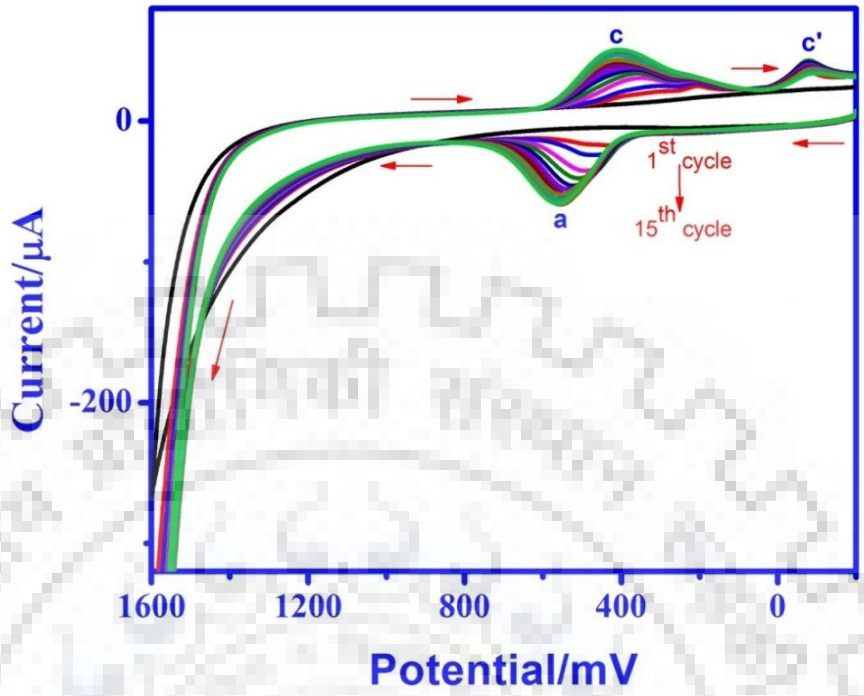

Fig. 2.1: A series of 15 consecutive cyclic voltammograms recorded between -200 mV and 1600 mV at a scan rate of 100 mVs^{-1} in the solution containing 1:1 of 1 mM of melamine (prepared in 0.1 M H_2SO_4 solution) and 1 mM of glutamic acid (prepared in pH 7.2 buffer, μ = 1.0 M) using EPPG.

After the polymerization, the stabilization of modified surface was carried out in pH 7.2 buffer (μ = 0.5 M) to get a steady cyclic voltammogram by scanning the potential between −1200 mV and +1200 mV. Finally, the fabricated sensor was allowed to dry. To get the maximum sensitivity of the sensor, the optimization studies were performed by varying the concentration of both glutamic acid and melamine monomers up to four times. It was clearly found that the highest peak current was attained of the fabricated co-polymeric film when the fabrication was carried out in the 1:1 concentration solution of both the monomers.

2.2.1.4 Procedure

For carrying out experimental studies, the stock solution of 2-TX (1 mM) was prepared by dissolving the required amount of the compound in the double distilled water. For recording the voltammograms, desired amount from the stock solution of 2-TX was taken to the electrochemical cell and 2 ml of pH 7.2 phosphate buffer was added and the solution was made 4 ml. The optimized parameters for cyclic voltammetry (CV) were sweep rate (ν): 100 mVs^{-1}, initial

potential (E_i): 300 mV, switching potential (E): 1200 mV and the final potential (E_f): 300 mV. The optimum conditions for square wave voltammetry (SWV) were SW frequency (f): 15 Hz, initial potential (E_i): 300 mV, final potential (E_f): 1200 mV, SW amplitude (E_{sw}): 25 mV and potential step (E): 4 mV. All the potentials are reported at an ambient temperature of 25 ± 2°C with respect to Ag/AgCl electrode. The controlled potential electrolysis was used to remove any adsorbed material to regenerate the sensing surface. For this purpose, after each voltammetric run, a constant potential of −600 mV was applied in the blank solution for 180 s.

2.2.1.5 Sample preparation for analysis by HATR-IR spectroscopy

First an aluminum sheet (0.6 × 0.6 cm^2) was rinsed with ethanol and double distilled water and allowed to dry in oven overnight. The co-polymeric film was deposited by scanning the potential between −200 mV to +1600 mV for optimized 15 scans at a sweep rate of 100 mVs^{-1} in the solution containing 1:1 of 1 mM of melamine (prepared in 0.1 M H_2SO_4 solution) and 1 mM glutamic acid (prepared in pH 7.2 buffer, μ = 1.0 M) and then prepared sample was used for HATR-IR spectroscopy analysis.

2.2.2 RESULTS AND DISCUSSION

2.2.2.1 Surface morphology of fabricated sensor

FE-SEM was employed to investigate the surface morphology of the unmodified, p-glutamic acid (p-Glu/EPPG) modified and p-Mel-Glu/EPPG modified sensors and typical obtained microscopic images are shown in **Fig. 2.2. Fig. 2.2 (A)** represented that the unmodified EPPG surface is flat and smooth. On the other hand, the p-Glu/EPPG surface has a layered structure of polymer on the electrode surface (**Fig. 2.2 B**), moreover the p-Mel/EPPG surface displayed a net of cubic structure of polymer on electrode surface as shown in **Fig. 2.2 C**. Furthermore, the p-Mel-Glu/EPPG surface (**Fig. 2.2 D**) exhibited crystalline herbs like clusters of p-Glu and p-Mel on the surface of sensor. Both polymer layers appeared to be interlinked with one another and provided constructive large surface area, which elevated the interaction between the modified surface and analyte.

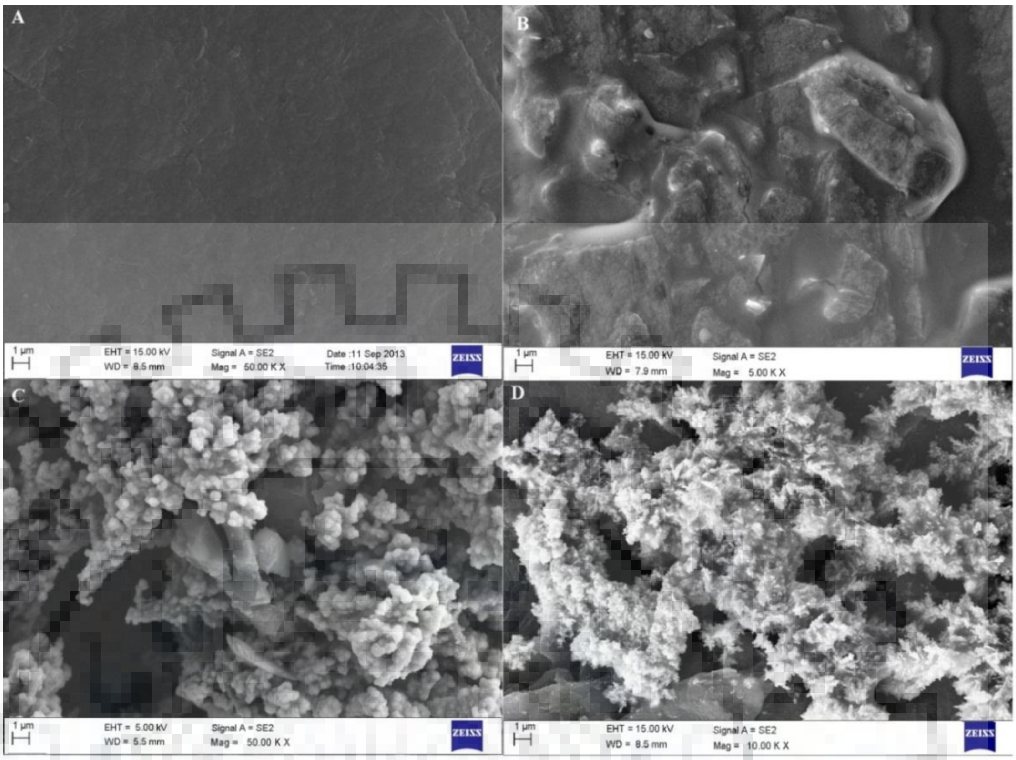

Fig. 2.2: Typical FE-SEM images observed for (**A**) unmodified EPPG (**B**) p-Glu/EPPG and (**C**) p-Mel/EPPG and (**D**) p-Mel-Glu/EPPG

The EIS measurements were used to explore the alteration on the sensor surface after the modification of p-Mel-Glu/EPPG in the form of charge transfer resistance. The working solution containing 1:1 mixture of 0.1 M KCl and 5 mM $K_3Fe(CN)_6$ was used for the experiments in the frequency range 0.1–100 kHz at a potential of 50 mV. **Fig. 2.3** presents the results observed for the perfect fit to a Randles equivalence circuit, where diameter of observed semicircle indicates the electron transfer resistance (R_{CT}) at a higher frequency, whereas the linear part displays the mass transfer effects at lower frequency. The electron transfer resistance (R_{CT}) values for the unmodified EPPG sensor is obtained as 1120 Ω (curve a), whereas the p-Glu/EPPG and p-melamine modified EPPG (p-Mel/EPPG) sensor showed the R_{CT} values as 580 Ω (curve b) and 350 Ω (curve c), respectively. The value of R_{CT} determined for the p-Mel-Glu/EPPG sensor was 175 Ω (curve d), which indicated its lowest resistance and highest electron transfer efficiency which facilitated the oxidation process of 2-TX.

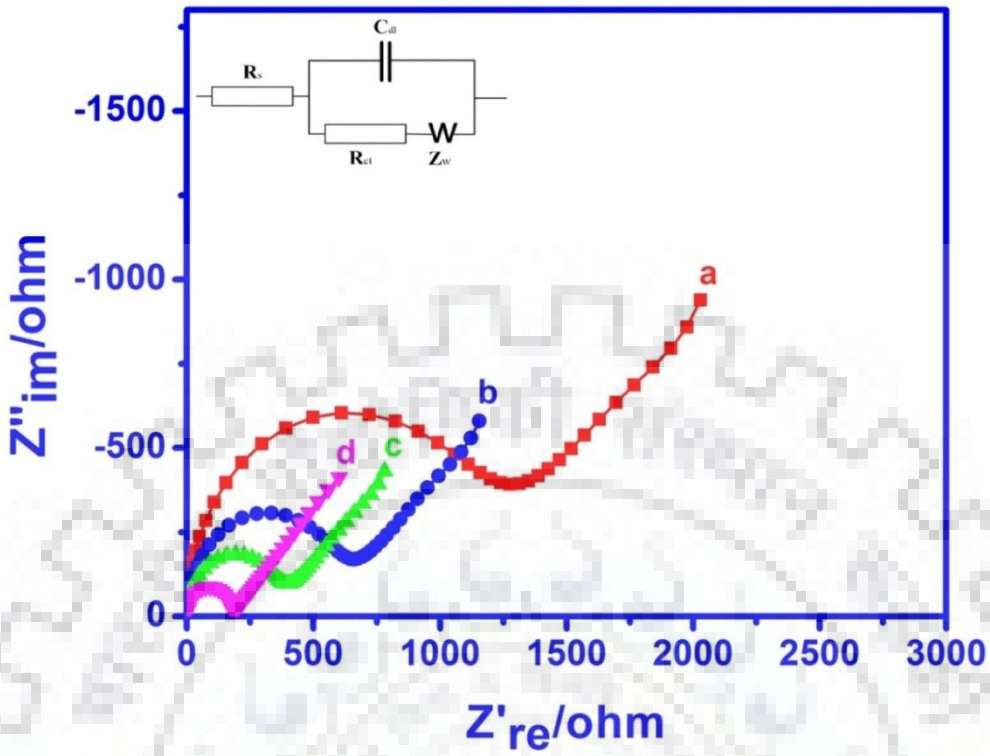

Fig. 2.3: Nyquist plots of EIS measurements of (a) unmodified EPPG, (b) p-Glu/EPPG (c) p-Mel/EPPG and (d) p-Mel-Glu/EPPG.

The HATR-IR spectrum (**Fig. 2.4**) of poly-(melamine)/poly-(glutamic acid) co-polymer shows a broad peak at 3324 cm^{-1} (N-H, O-H stretching vibrations), indicating that the primary amine and free OH groups are no longer present in the polymeric film. The sharp band at 2920 cm^{-1} is assigned to C-H stretching vibrations of sp^3 hybridized alkyl and another band at 2854 cm^{-1} is present due to C-C stretching vibrations. A strong amide absorption in poly-glutamic acid (**Fig. 2.4 A**) is observed at 1630 cm^{-1}, which shifted to 1652 cm^{-1} in co-polymer (**Fig. 2.4 B**) because of the attachment of the aromatic ring. Whereas, the peak of C-O stretching vibration at 1074 cm^{-1} observed in the case of poly glutamic acid shifted to 1104 cm^{-1} due to the ionic bonding in between the C-O and N-H groups of co-polymer as shown in the **Scheme 2.** Liu et al. [13] have reported the electro-polymerization of glutamic acid and from the IR data it was explained that the condensation occurred between the $-NH_2$ and -COOH groups and one carboxylic group still remained free in the polymer chain of glutamic acid. From the present IR studies it can be concluded that the free -COOH group of glutamic acid reacts with the amino group of melamine and form a co-polymer network.

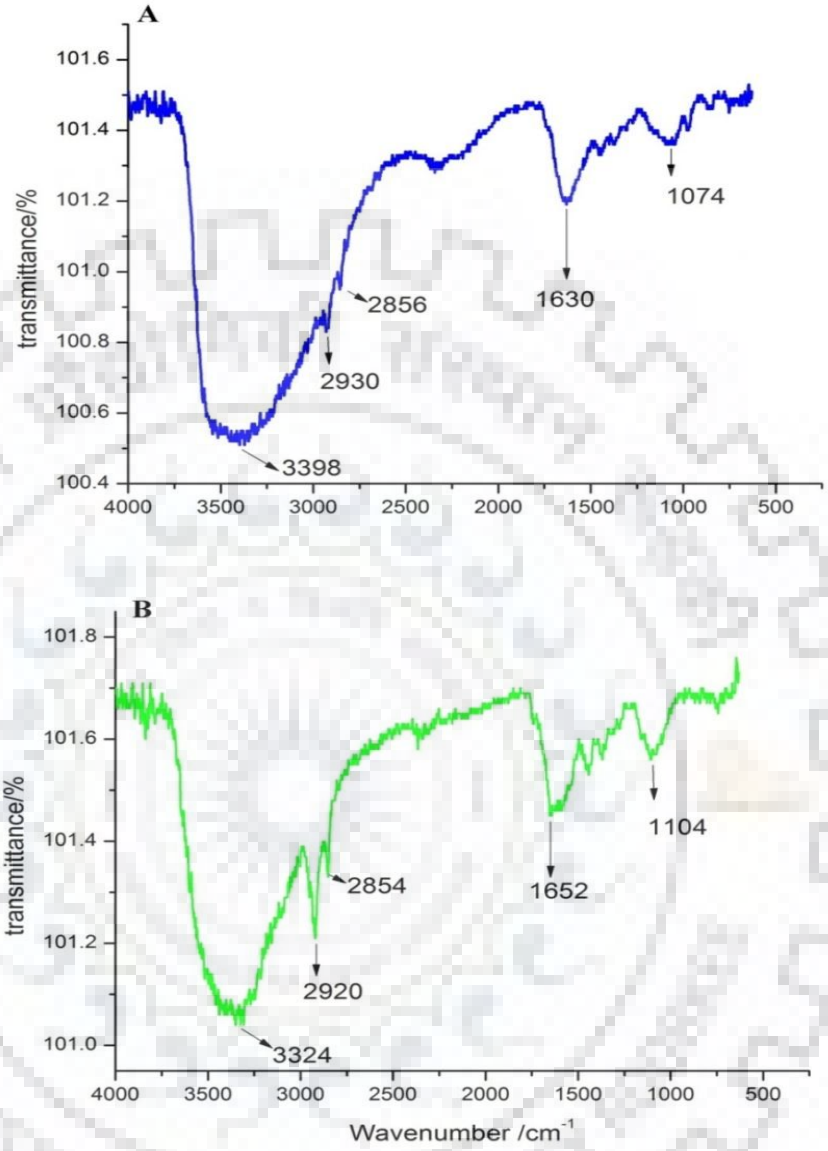

Fig. 2.4: HATR-IR spectrum observed for (**A**) poly glutamic acid, and (**B**) co-polymer poly-(melamine)/poly-(glutamic acid).

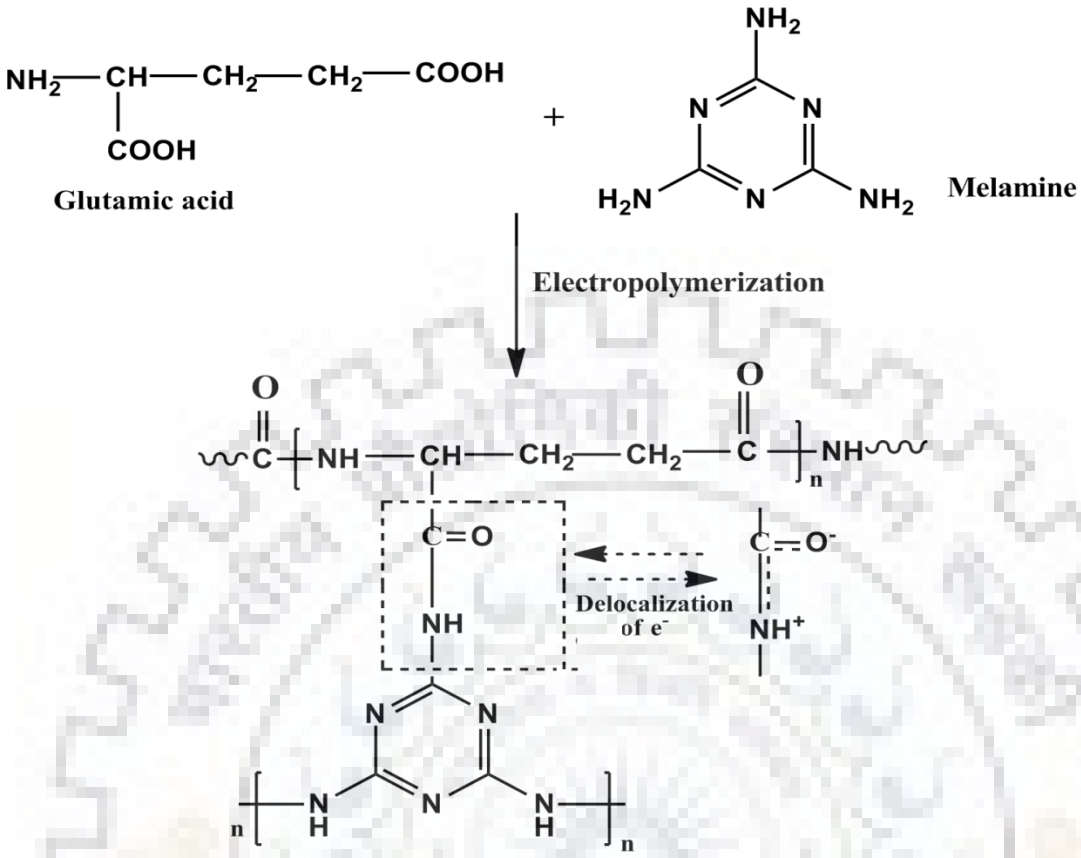

Scheme 2: Electropolymerization of glutamic acid and melamine.

To illustrate the potential of modification at the surface of presented sensor, the effective surface area of unmodified EPPG, p-Glu/EPPG, p-Mel/EPPG and p-Mel-Glu/EPPG sensors were calculated by using cyclic voltammograms, which were recorded for 2 mM $K_3Fe(CN)_6$ containing supporting electrolyte 0.1 M KCl at different sweep rates. The effective surface areas were calculated by the slop of i_p vs. $\nu^{1/2}$ plots according to Randle's Sevcik equation,

$$\mathbf{i_p = 0.4463\ (F^3/RT)^{1/2}\ An^{3/2}\ D_R{}^{1/2}\ C_0 \nu^{1/2}}$$

where i_p refers to the peak current (Ampere), R (8.314 J $K^{-1}mol^{-1}$) represents universal gas constant, F Faraday's constant (96,485 C mol^{-1}), T the absolute temperature (in present case 298 K), A surface area of electrode (cm^2), n = 1 for $K_3Fe(CN)_6$, ν sweep rate (Vs^{-1}), D_R the diffusion coefficient (7.6×10^{-6} cm^2s^{-1}) and C_0 refers to the concentration of $K_3Fe(CN)_6$ in $molL^{-1}$. The calculated surface areas for the unmodified EPPG, p-Glu/EPPG, p-Mel/EPPG and p-Mel-Glu/EPPG sensors were found to be 0.083 cm^2, 0.112 cm^2, 0.138 cm^2 and 0.410 cm^2, respectively. The results indicate that the p-Mel-Glu/EPPG sensor has a significant enhanced effective surface

area, which accelerates the charge transfer property and indicates the good performance of the modified sensor for the electrochemical detection.

2.2.2.2 Cyclic voltammetry

Fig. 2.5 shows a typical cyclic voltammogram obtained for 2-TX (30 µM) using unmodified EPPG, p-Mel/EPPG and p-Mel-Glu/EPPG sensors at phosphate buffer of pH 7.2 at a sweep rate of 100 mVs^{-1}. At unmodified EPPG, a small anodic peak was observed at 825 mV having peak current of 2.35 µA as shown by curve a in **Fig. 2.5**. At p-Glu/EPPG sensor surface the oxidation peak shifted to 805 mV (curve b) with peak current of 3.1 µA and at p-melamine/EPPG sensor an oxidation peak at 795 mV (curve c) with peak current of 4.3 µA was noticed, however as can be seen from the curve d in **Fig. 2.5** the highest peak current (10.6 µA) at E_p~786 mV, corresponding to the oxidation of 2-TX was observed at p-Mel-Glu/EPPG sensor. In the reverse scan, absence of any reduction peak at the sensors clearly revealed the irreversibility of oxidation process of 2-TX.

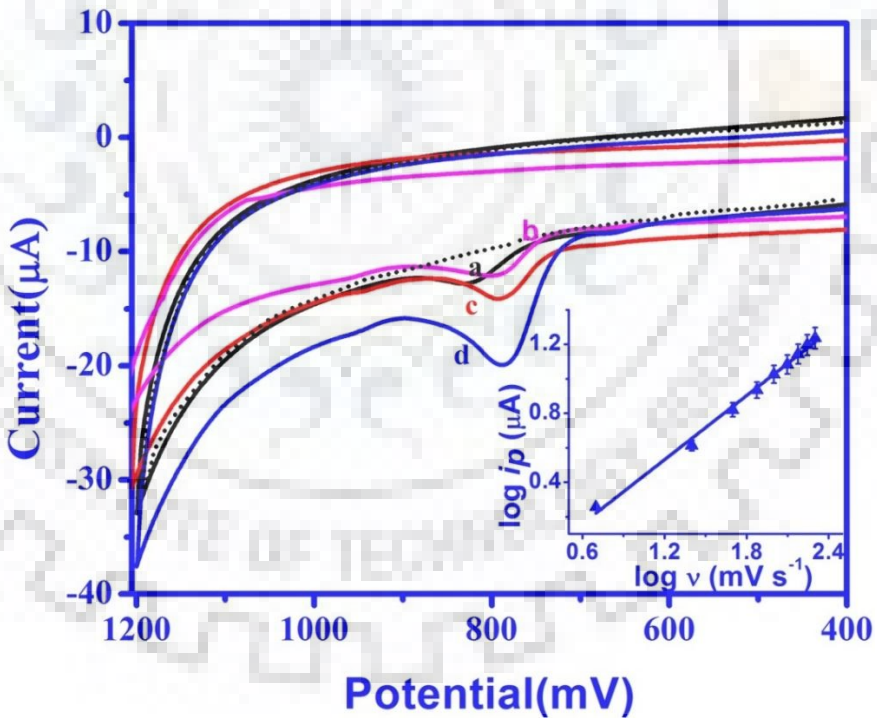

Fig. 2.5: A comparison of CVs observed at unmodified EPPG (curve a), p-Glu/EPPG (curve b), p-Mel/EPPG (curve c) and p-Mel-Glu/EPPG (curve d) sensors for 30 µM 2-TX in pH 7.2 phosphate buffer at a scan rate of 100 mVs^{-1}. The background is shown by dotted line.

The significant enhancement in the peak current with the shift of peak potential towards negative side demonstrated that the modification with p-Mel-Glu/EPPG enhanced the electron transfer characteristics and sensitivity of modified EPPG sensor surface, which promoted the oxidation of 2-TX.

To elucidate the nature of the electron transfer process involved in the electrochemical oxidation of 2-TX, sweep rate (ν) studies were carried out. For these studies, the peak current of 2-TX (30 µM) was measured with increasing scan rate in the range of 5–200 mVs^{-1} using p-Mel-Glu/EPPG sensor. It was found that the anodic peak current (i_p) linearly increased with increasing sweep rate (ν). The linear relation of i_p versus ν can be represented by the relation:

$$\mathbf{i_p / \mu A = 0.0772\ \nu + 2.2992 \qquad (R^2 = 0.991)}$$

where, i_p is the anodic peak current (µA) and ν is the sweep rate (mVs^{-1}). The linearity of i_p versus ν indicated that the oxidation of 2-TX was adsorption controlled process at the p-Mel-Glu/EPPG sensor, which was also validated by the linear plot between log i_p versus log ν. The linear relation between log i_p and log ν can be expressed as:

$$\mathbf{\log i_p = 0.6195 \log \nu - 0.2122}$$

having (R^2) 0.994 and slope value 0.6195. As the slope (d log i_p / d log ν) of the plot was > 0.5, it suggested that the electron transfer in the 2-TX oxidation involved adsorption controlled pathway [27].

2.2.2.3 Square Wave Voltammetry

For comprehensive electrochemical analysis of 2-TX, square wave voltammetry (SWV) is used as it exhibits lower background currents than the CV. SWV was employed using unmodified EPPG, p-Mel/EPPG and p-Mel-Glu/EPPG sensor for 30 µM 2-TX at phosphate buffer of pH 7.2 to manifest the electrocatalytic activity of the fabricated surface. At unmodified EPPG, a broad peak at 800 mV (curve a) with peak current of ~2.9 µA was observed as displayed in **Fig. 2.6.** The use of p-Mel on the EPPG surface also exhibited an increase in the peak current (~5.8 µA) with a slight negative shift of peak potential at 772 mV (curve b). The best result was observed for p-Mel-Glu/EPPG in terms of sensitivity as well as electrocatalytic activity for the oxidation of 2-TX with a well-defined peak at the 756 mV (curve c) with peak current of ~10.09 µA. Thus, p-Mel-Glu/EPPG was used as the final sensing surface for the quantification of 2-TX.

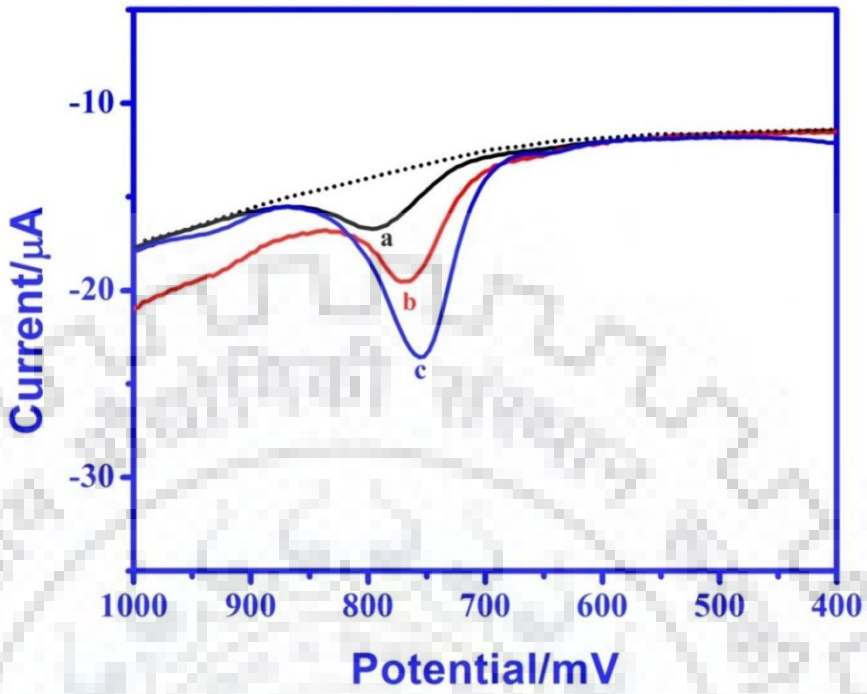

Fig. 2.6: A comparison of square wave voltammograms observed for 30 µM 2-TX at unmodified EPPG (curve a), p-Mel/EPPG (curve b) and p-Mel-Glu/EPPG sensors (curve c) at pH 7.2. The background is shown by dotted line.

2.2.2.3.1 Effect of pH

To demonstrate the effect of pH of the supporting electrolyte towards oxidation of 2-TX, the pH studies were performed in the range of 2.4–10.5 at a fix concentration (30 µM) of 2-TX using p-Mel-Glu/EPPG sensor. It was observed that with increasing the pH, the peak potential (E_p) of 2-TX shifted towards less positive potentials. The liner relation of the peak potential (E_p) with pH can be represented by the following equation:

$$\mathbf{E_p\ (pH\ 2.2\text{-}10) = -56.036\ pH + 1182.8\ mV\ vs.\ Ag/AgCl}$$

where, the value of the correlation coefficient was found as 0.969. The observed slope value (dE_p/dpH) of 56 mV/pH was close to the value of theoretical Nernstian value, which is 59 mV, and hence, indicated that in the oxidation of 2-TX the number of involved electrons and protons are equal. The number of electron involved in the oxidation is also calculated using the Laviron's equation:

$$\mathbf{E_p = E^0 + RT/\alpha nF - RT/\alpha nF\ ln\ \nu}$$

where, α is the electron transfer coefficient, T is the absolute temp (in present case 298 K), R (8.314 J $K^{-1}mol^{-1}$) represents universal gas constant, n is the no. of electron, F (96,485 C mol^{-1})

is the Faraday constant, E_p is the peak potential and ν is the sweep rate. The E_p of 2-TX was found to be dependent on sweep rate and the linearity between the peak potential E_p and log ν can be represented as:

$$\mathbf{E_p = 62.453 \log \nu + 641.75 \qquad (R^2 = 0.971)}$$

Using the Laviron's equation the number of electron involved in oxidation is found as 1.90, assuming α = 0.5 for totally irreversible systems [28]. Thus it was concluded that $2e^-$ were involved in the 2-TX oxidation. The $2e^-$, $2H^+$ oxidation of 2-TX gives corresponding diimine as shown in **Scheme 3**. A similar mechanism has also been proposed earlier for the oxidation of 2-TX [24].

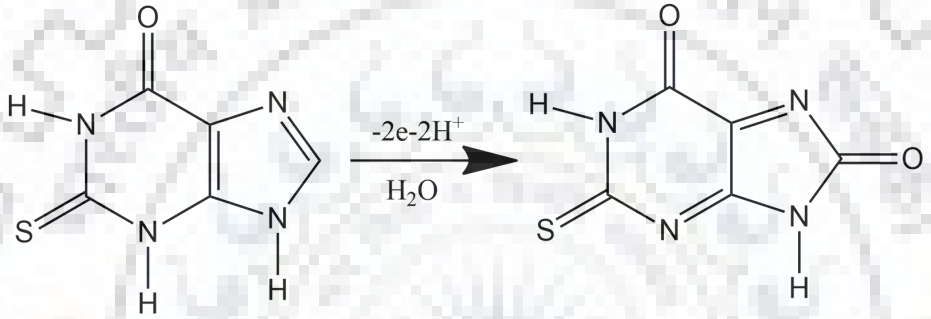

Scheme 3: Tentative mechanism suggested for the oxidation of 2-Thioxanthine.

2.2.2.3.2 Effect of square wave frequency

The effect of frequency on the oxidation peak current (i_p) of 2-TX was studied by changing the frequency from 5 to 40 Hz and recording the SWVs in phosphate buffer of pH 7.2 at p-Mel-Glu/EPPG sensor. It is observed that the peak current of 2-TX increases with increasing the frequency and a linear dependency of peak current with frequency is observed. The linear relation between peak current (i_p) and frequency (f) plot can be expressed as:

$$\mathbf{i_p / \mu A = 0.2897\ f + 2.7414 \qquad (R^2 = 0.996)}$$

where, i_p is the anodic peak current (μA), f is the square wave frequency (Hz) and R^2 is the correlation coefficient. The linear dependence of i_p versus f indicated an adsorption controlled oxidation of 2-TX at the p-Mel-Glu/EPPG sensor, which has also been checked by the log i_p versus log f plot. The linear dependence between log i_p versus log f can be expressed as:

$$\mathbf{\log i_p = 0.6276 \log f + 0.1332 \qquad (R^2 = 0.997)}$$

The slope of log (i_p) vs. log (f) plot was found to be > 0.5, which further confirmed the adsorption controlled oxidation of 2-TX.

2.2.2.3.3 Effect of concentration

The concentration study was performed for the quantification of 2-TX as well as to calculate the detection limit of the fabricated sensor. The typical SWVs recorded using p-Mel-Glu/EPPG sensor for the different concentrations of 2-TX at optimal SWV parameters at pH 7.2 are depicted in **Fig. 2.7**. The background current value was subtracted to calculate the peak current values; moreover the calibration curve was then plotted using an average of three repeated observations. In the calibration plot of the concentration range 0.5 µM–150 µM, the peak current versus concentration curve exhibited a break at around 15 µM. A linear increase in the oxidation peak current (i_p) of 2-TX was noticed with the increase in concentration of 2-TX in the range 0.5 µM–15 µM. However, in the higher concentration range of 2-TX i.e. 25 µM–150 µM a different linear relation was seen as presented in the inset of **Fig. 2.7**.

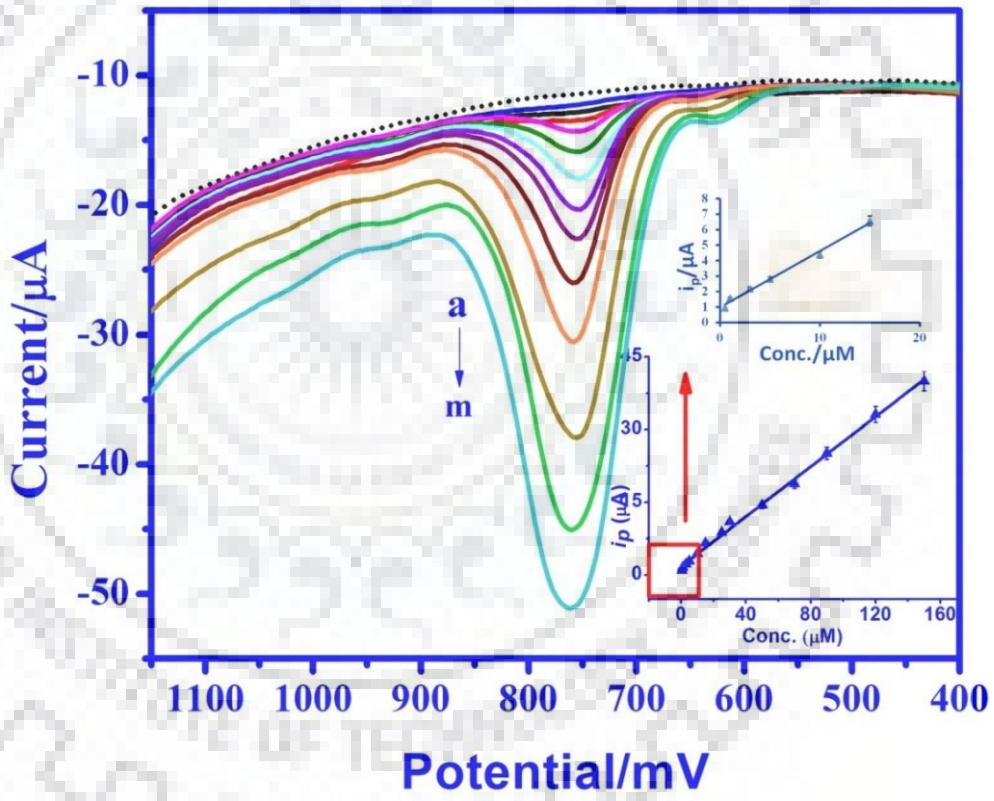

Fig. 2.7: Square wave voltammograms recorded for the increasing concentration of 2-TX at p-Mel-Glu/EPPG in the phosphate buffer of pH 7.2. Curves were recorded at (a) 0.5, (b) 1, (c) 3, (d) 5, (e) 10, (f) 15, (g) 25, (h) 30, (i) 50, (j) 70, (k) 90, (l) 120 and (m) 150 µM concentration of 2-TX; inset is the calibration plot.

The dependence of the i_p with 2-TX concentration can be represented as:

$$\mathbf{i_p/\mu A = 0.3634\,[C,\,0.5-15\,\mu M] + 0.9832,\quad R^2 = 0.991}$$

$$\mathbf{i_p/\mu A = 0.2507\,[C,\,25-150\,\mu M] + 2.4078,\quad R^2 = 0.996}$$

The i_p (peak current) is in µA and C (concentration) is in µM. The limit of detection (L.O.D.) and limit of quantification (L.O.Q.) for 2-TX were calculated by using LOD = 3 σ/b and LOQ = 10 σ/b, where σ (standard deviation of the blank signals), b (slope of the linear calibration graph). The L.O.D. and L.O.Q. for the 2-TX at the p-Mel-Glu/EPPG sensor were determined as 1.0 nM and 3.4 nM, respectively. This detection limit of 2-TX is nearly 50 times lower in comparison to the reported earlier [25].

2.2.2.4 Effect of interferents

To evaluate the selectivity of p-Mel-Glu/EPPG sensor, an investigation of the interference of various commonly present biomolecules in human urine and blood, such as ascorbic acid (AA), uric acid (UA), xanthine (XT) and hypoxanthine (HX) was carried out. Since the biological fluids consist of high concentration of these biomolecules (UA 4–8 mg/dL; AA 0.5–1.2 mg/dL; XT ~ 20 µg/dL and HX ~ 40µg/dL), they can cause variations in the response of the fabricated p-Mel-Glu/EPPG sensor, therefore influence the selective determination of 2-TX [29,30]. Under the optimized experimental conditions, the SWVs were recorded for 2-TX at the fixed concentration (30 µM) and changing the interferents concentration up to AA (1 mM), UA (2 mM), XT (500 µM), HX (500 µM). The well-defined oxidation peaks were found at −0.009 mV (AA), 308 mV (UA), 651 mV (XT) and 976 mV (HX) along with the oxidation peaks of 2-TX at 756 mV. **Fig. 2.8** clearly indicates that even high concentration of interferents do not affect the peak current response of 2-TX. Moreover, the analytes having almost similar chemical structures i.e. XT and HX with 2-TX, were showing the oxidation potential sufficiently apart from the oxidation peaks of 2-TX and did not interfere. Thus, the co-polymer based p-Mel-Glu/EPPG sensor exhibited strong synergistic electrocatalytic effects towards the oxidation of 2-TX. From the observed results, it was inferred that the proposed method can be successfully used for the analysis of 2-TX in the biological fluids, even in the presence of the high concentration of similar interfering molecules.

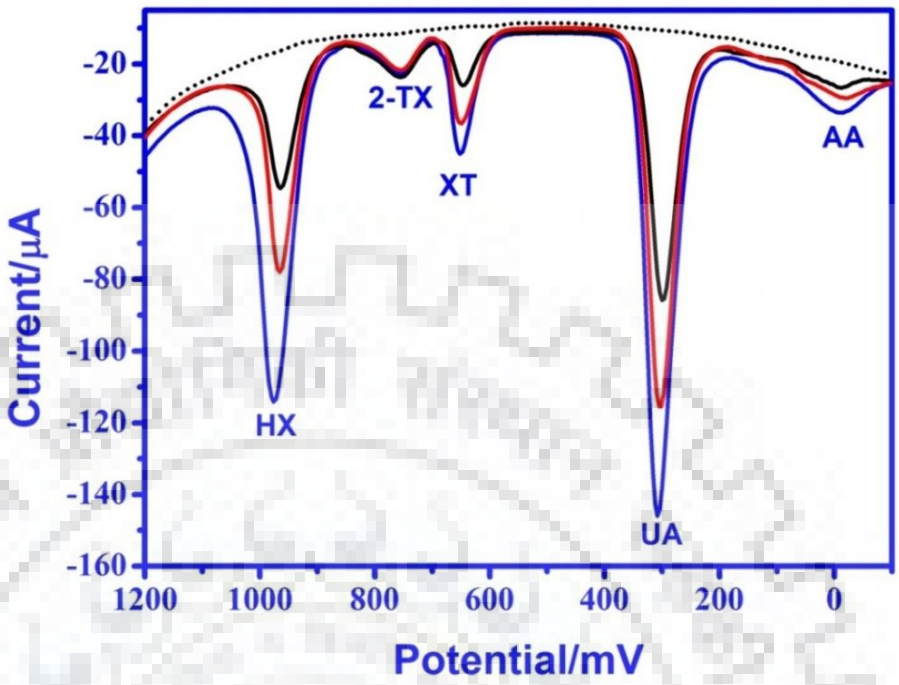

Fig. 2.8: SWVs recorded for 30 μM 2-TX in the presence of ascorbic acid (AA), uric acid (UA), xanthine (XT) and hypoxanthine (HX) at the surface of p-Mel-Glu/EPPG sensor. The background is represented by the dotted line.

2.2.2.5 Stability and reproducibility study

The electrochemical performance of p-Mel-Glu/EPPG sensor at a fixed concentration of 30 μM 2-TX in the pH 7.2 phosphate buffer over a period of 30 days was monitored for determining its stability. The fabricated sensor was employed each day for recording voltammograms and stored under the ambient conditions. The observed results reveal that a slight drop in the peak current < 3% is observed during the first 15 days, however, up to 5.5% decrement in the peak current is observed in the next 15 days. Thus, the fabricated sensor was sufficiently stable for at least 15 days. To determine the intraday reproducibility, five replicated voltammograms were recorded in the blank solution as well as in 30 μM 2-TX solution at an interval of 1 h during the same day and R.S.D. for replicative voltammograms was determined. The calculated value of R.S.D. was found to be ± 0.92% for the repetitive measurements (n = 5) and ± 1.52% for intraday measurements (n=5). Thus, it was concluded that the fabricated p-Mel-Glu/EPPG sensor maintains significant stability, excellent reproducibility and repeatability.

2.2.2.6 Spiked sample assay

Fabricated p-Mel-Glu/EPPG sensor was applied in the complex matrix like human urine sample for analysing 2-TX to manifest the practical applicability of the proposed method. As we could not get urine sample from the patients undergoing treatment with 2-TX in spite of our best efforts, it was decided to carry out spiked sample analysis in the urine sample of healthy volunteers. The urine samples of healthy volunteers were diluted three times with pH 7.2 phosphate buffer. The known volume of 2-TX was spiked in the diluted urine samples and SWVs were recorded. The results obtained are shown in **Table 1.** The recoveries of 2-TX were found in the range of 98.64–101.4%. The excellent recoveries with good RSD values indicate the great potential of p-Mel-Glu/EPPG sensor for the sensitive determination of 2-TX in bio-fluids.

Table 1: Recovery results observed for 2-TX in human urine samples at p-Mel-Glu/EPPG sensor.

S.No.	Spiked amount (µM)	Detected amount (µM)	Recovery* %	Error %
Sample 1				
1.	5	4.96	99.20	-0.80
2.	10	9.97	99.70	-0.3
3.	15	15.21	101.40	1.4
Sample 2				
1.	20	20.12	100.60	0.6
2.	30	30.20	100.66	0.66
3.	40	39.86	99.65	-0.35
Sample 3				
1.	25	24.95	99.80	-0.20
2.	50	50.63	101.26	1.26
3.	75	73.98	98.64	-1.36

*The R.S.D. value for the determination was 1.28% for n=3.

2.2.3 CONCLUSION

The studies reported in this section demonstrate fabrication of a novel and extremely sensitive p-Mel-Glu/EPPG sensor for the determination of 2-TX. The surface modification of the sensor illustrated the interlinked polymer layers of p-Glu and p-Mel with each other and imparts higher effective surface area of sensor. The fabricated active surface of the sensor enhances the interaction with analyte and facilitate the electrocatalytic effect towards the oxidation of 2-TX. The

modified sensor exhibited linear dependency of the oxidation peak current on the concentration of 2-TX in the range of 0.5–150 μM with a remarkable sensitivity in terms of low detection limit and quantification limit of 1.0 nM and 3.4 nM, respectively. The proposed sensor has excellent properties for analytical determination of 2-TX, even in the presence of various potential interfering electro-active biomolecules. The presented modified sensor was also favourably employed in the monitoring of 2-TX in human urine samples with acceptable range of recoveries. The significant stability and considerable reproducibility make the present method a promising approach for the sensitive quantification of 2-TX in pharmaceutical laboratories.

2.3 SECTION B: Poly- melamine modified sensor for the determination of Propranolol

Propranolol, 1-[(1-methylethyl) amino]-3-(1-naphthylenyloxy)- propan-2-ol, is a non-selective beta-adrenergic antagonist, which has little intrinsic sympathomimetic activity, used for the treatment of various cardio vascular disorders such as cardiac arrhythmia, hypertension, phaeochromocytoma, sinus tachycardia, angina pectoris, myocardial infarction, migraine and dysfunctional labour [31-33]. It has been used for the treatment of anxiety or thyrotoxicosis, sweating and tremor because it blocks the effect of adrenaline and also inhibits the actions of norepinephrine, a neurotransmitter that increases memory consolidation [34]. Propranolol is investigated for the potential treatment of PTSD (post-traumatic stress disorder) [35]. However, the overdose of propranolol shows adverse effects such as dizziness, fainting, bradycardia and disturbed heartbeat. It causes the alteration in transmission of nerve impulses from brain to the particular part of the body, which decreases the rate of heart beat by dilation of the blood vessel in turn lowering the blood pressure. It affects blood circulation by reducing cardiac frequency, coronary flow, myocardial contractility, contraction force, and secretion of rennin with decreasing the level of angiotensin II, which contributes to the hyper-tensive action of this drug [32,36,37].

In the last few years, propranolol has also been misused in many sports to reduce coronary flow, cardiac frequency contraction force, and controlling stage fright. Therefore the International Olympic Committee has considered propranolol as a doping material and included it in the category of forbidden substances. World Anti-Doping Agency (WADA) assigned the maximum amount of this drug in urine to be 0.5 μg/mL at the time of performance [38,39]. The accurate and rapid determination of the level of propranolol is necessary in commercial formulations as well as in biological fluids to control the cases of doping in the competitive games. Propranolol has an additive effect when used with other drugs which decrease blood pressure, or decrease cardiac contractility or conductivity. Due to its therapeutic and pharmacological relevance, determination of propranolol has been carried out in pharmaceutical preparations and biological fluids by different techniques, such as chemiluminescence [38,40–42], fluorometry [43,44], high performance liquid chromatography [33,45,46], spectrophotometry [47,48] and Infrared Spectrometry [49]. However, these methods have limitations, such as less sensitivity, long analysis time and requirement of expensive instrumentation due to which there is need of a rapid, accurate and more sensitive technique. Electrochemical techniques are feasible alternatives for

determination of electroactive compounds due to some important advantages such as accuracy, low-cost apparatus, sensitivity, reproducibility, less time consumption, simplicity, and negligible pre-treatment of samples. In addition, these techniques are also considered as eco-friendly [50].

For the determination of propranolol, various sensors have been constructed by using nano-composite films and metal oxides [51-54]. The modification with conductive polymer films for the determination of biomolecules has been receiving extensive interest due to their wide applications in the fields of chemical sensors and biosensors. Conducting polymers have unique properties such as good electrical conductivity, better chemical stability [7], magnetic property [28], high electronic affinities, low ionization potential and optical properties [3]. These are electro-chemical properties of conducting polymer are because of the extended π-electron conjugation in their backbone [4]. Conducting polymers have combined properties of organic polymer and electronic properties of semiconductor. Its molecular structure controls the electronic properties and maintains nanostructure shape (nanowires, films, nanoparticles). In view of these properties conducting polymers are widely used for the surface modification of sensors for the determination of electroactive compounds because they can significantly increase the electrocatalytic property, decrease over-potential, thereby increase the rate of reaction [55]. Conducting polymer modified sensors have an additional advantage that they are very sensitive to small perturbations [56]. Conducting polymer of melamine (1,3,5-triazine-2,4,6-triamine) possesses considerable nitrogen and amine groups, which are beneficial to prevent aggregation and provide biocompatibility, thus are gradually applied in the electrode surface modifications. The nitrogen functionalized matrix of electroactive poly-melamine film with π-electrons cloud is supposed to interact with the delocalized π-electrons of benzene ring and -OH and -NH functional groups present in the propranolol backbone. Melamine monomers electro-polymerize through the two oxidized amino groups and leads to the formation of polymer film. Thus, the polymer film was generated on the electrode surface by head-to head coupling with NH–NH bonding between melamine molecules. As the p-(melamine) has the characteristic properties of organic polymers such as large surface area and excellent conductivity, which causes an electrocatalytic activity, leads to the sensing of propranolol with very low detection limit in pharmaceutical samples [10,57,58]. Modification of the surface of electrode can be carried out by several methods, however, as compared to other methods the electropolymerization has been considered simple and has more advantages such as reproducibility, simplicity [8] and thickness of film can be controlled by regulating the

electrochemical parameters i.e. potential and current. Therefore, characteristics such as thickness of the film, charge transfer and permeation can be well defined in the case of conducting polymer modified surfaces [9].

Carbon materials have been widely used as the electrode substrates to make various electrodes. Due to the soft properties of carbon, these electrodes surface can be easily renewed for electron exchange. Carbon materials also have broad potential window, low background current, rich surface chemistry and comparative chemical inertness. The cost of carbon materials is also very low. In EPPG the graphite particles are randomly arranged inside the non-conducting matrix and exhibit microelectrode array behavior, thereby, giving EPPG a remarkable advantage above other conventional electrodes like GCE. The composite structure of PGE has high level of porosity, which gives better intrinsic characteristics as compared to the GCE. The advantage of PGE over the existing GCE and other electrodes like gold, Platinum, Palladium is its high electrochemical reactivity, excellent reproducibility along with high stability, commercial availability, good mechanical rigidity and low cost [59-61]. In the proposed method, we have demonstrated the fabrication and characterization of a sensitive electrochemical sensor for the determination of propranolol by using edge plane pyrolytic graphite sensor (EPPG) modified with polymelamine film. In the voltammetric analysis, EPPG has been widely used due to its unique characteristics such as large potential range, high sensitivity and selectivity, low background current, long term stability and reproducibility [55,62]. Melamine monomer has been used for the modification because of its commercially availability, high catalytic current, low cost, excellent polymeric film stability and better sensitivity. The prepared sensor has been used for the determination of propranolol in biological samples and pharmacological formulations.

2.3.1 EXPERIMENTAL

2.3.1.1 Chemicals and Reagents

Propranolol hydrochloride was purchased from Sigma-Aldrich (USA). Phosphate buffer solutions of ionic strength (1.0 M) in the pH range 2.4–10.0 were used. Considering the physiological pH, the phosphate buffer of pH 7.4 was used for recording the blank and experimental voltammograms. Biological samples of human plasma and urine were collected from the Institute hospital, I.I.T. Roorkee, as reported in the previous section of this chapter. All other chemicals and solvents used in the experiment were of analytical grade and double distilled water was used throughout the experiments.

2.3.1.2 Instruments

The equipment used for electrochemical observations and characterization techniques were essentially similar to that reported in the section A of this chapter.

2.3.1.3 Experimental procedure

The stock solution of propranolol (1 mM) was prepared by dissolving the necessary amount in the double distilled water. The required amount of this solution was added to the cell containing 2 ml of the phosphate buffer and total volume was made to 4 ml using double distilled water. Solutions were purged with high purity nitrogen for 10–12 min to remove oxygen before recording each voltammogram. Phosphate buffer of pH 7.4 was used as supporting electrolyte during the experiments. The optimized operating conditions for square wave voltammetry (SWV) were initial potential (E): 100 mV, final potential (E): 1400 mV, square wave frequency (f): 15 Hz, square wave amplitude (E_{sw}): 25 mV and potential step (E): 4mV. All the potentials reported are with respect to Ag/AgCl electrode at an ambient temperature of 25 ± 2°C.

The human urine and plasma samples of patients undergoing pharmacological treatment with propranolol were obtained from the Institute Hospital after the permission of Ethical Clearance Committee of IIT Roorkee. The anthropometric data of the patients were sample (1): Male, 52 years, 78 kg; (2): Male, 66 years, 76 kg. All the patients were on oral medication of propranolol (2 tablets of 80 mg/day). Urine and plasma samples were diluted two times with phosphate buffer of pH 7.2 prior to analysis.

2.3.1.4 Fabrication of polymeric film

Poly (melamine) modified EPPG was prepared as reported earlier [63]. Briefly, The EPPG was rubbed on an emery paper (P-400) and then rinsed with double distilled water and dried. The polymer film was then deposited on the cleaned surface of EPPG by electropolymerization of 1.0×10^{-3} mol L^{-1} melamine in 0.1 mol L^{-1} H_2SO_4 solution. The electropolymerization was carried out using cyclic voltammetry by scanning the potential from 0.1 to 1.6 V for 20 cycles at 0.1 Vs^{-1}. During the first cycle, one oxidative and one reductive peak appeared at about +0.61, and −0.51 V respectively. In the consecutive scans, the peak current increased and finally stabilized after 20 scans as shown in **Fig. 2.9**. In the stable voltammograms, well-defined anodic and cathodic peaks are observed at about 0.66 V and −0.56 V, respectively. The increase in the peak current with the increase in number of potential scans indicates the subsequent growth of the polymer film on the

EPPG. The modified electrode was then rinsed with distilled water to remove physically adsorbed and unreacted molecules of melamine from the electrode surface. Subsequently, the modified electrode was stabilized in pH 7.4 buffer (0.5 M) by scanning the potential between -1.2 and +1.2 V until a steady cyclic voltammogram was obtained. Finally, the modified electrode was dried in air and was ready for use.

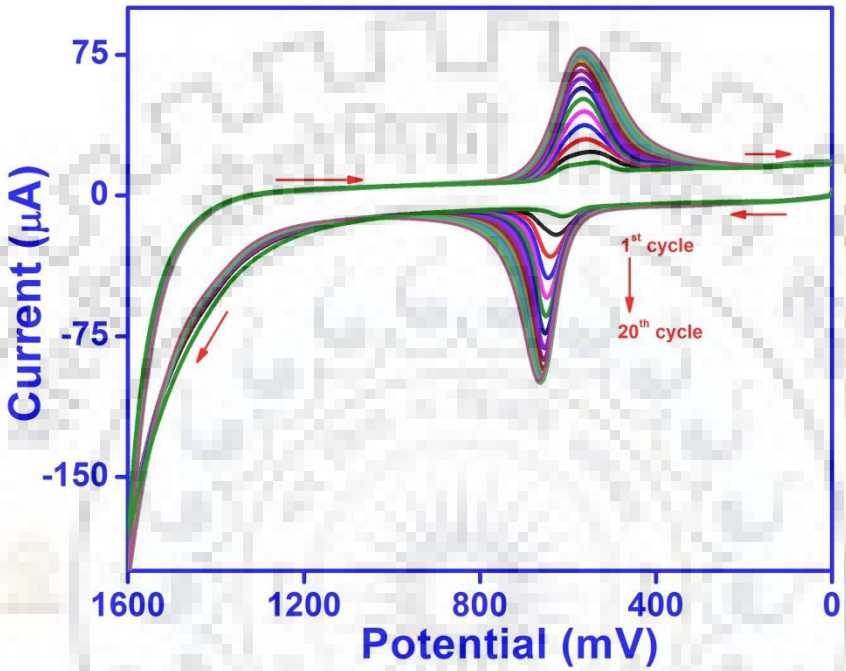

Fig. 2.9: A series of 20 consecutive cyclic voltammograms recorded between 0 and 1600 mV in 0.1 M H_2SO_4 solution containing1 mM melamine monomer at a scan rate 100 mVs^{-1} using EPPG.

For surface characterization by IR spectroscopy, an aluminum sheet (0.8 × 0.8 cm^2) was used. The electropolymerization of p-(melamine) film on the surface of aluminum sheet was carried out with the same procedure. The HATR-IR spectrum of melamine monomer showed the peak of N-H torsional vibration at 1020 cm^{-1}, C = N stretching vibration at 1555 cm^{-1}, N-H bending vibration at 1650 cm^{-1}, N-H asymmetric stretching vibration at 3465 cm^{-1} and 3418 cm^{-1} indicating the existence of primary amine in the melamine monomer. The HATR-IR spectra of p-(melamine) displayed some variations. The fine peaks, which were observed in the melamine monomer IR curve at 3465 cm^{-1} and 3418 cm^{-1}, were disappeared and a single peak at 3446 cm^{-1} suggested the formation of tertiary amine and confirmed the formation of p-(melamine). Finally, the peak of N-H torsional vibration at 1080 cm^{-1} in p-(melamine) curve in contrast to 1020 cm^{-1} in the monomer proved that the nitrogen atom was still attached to the hydrogen atom in the structure

of p-(melamine). The results of HATR-IR were essentially similar as reported in the literature earlier [11,63].

2.3.2 RESULT AND DISCUSSION

2.3.2.1 Surface morphology of melamine modified EPPG

The surface morphology of melamine/EPPG sensor was studied by FE-SEM as shown in **Fig. 2.10**. From **Figs. 2.10A**, **2.10B** and **2.10C**, it can be seen that the blank EPPG surface is smooth and flat before the deposition of polymer film, but becomes uneven after the deposition indicating that the polymerization on the surface of EPPG is successful. As seen from **Fig. 2.10B**, the melamine monomers bonded with each other after polymerization and formed a porous, crystalline three dimensional network with cubic structures. The polymeric layers have been distributed uniformly and homogenously by layer to layer deposition all over the electrode surface. For electropolymerization, optimal scan number of 20 is used. If more number of scans is used for the polymerization, then the agglomeration of melamine molecules occurs and a dense layer is observed (**Fig. 2.10C**) which is less sensitive toward the electron transfer and electrochemical sensing of the analyte.

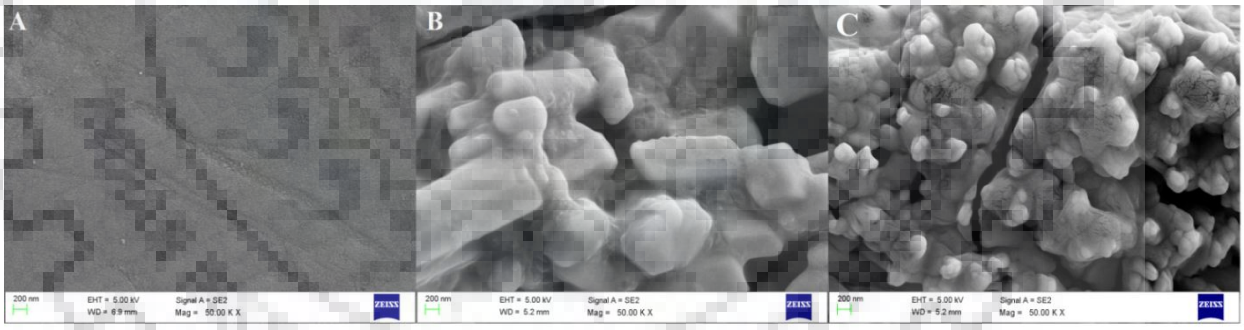

Fig. 2.10: Typical FE-SEM images observed for bare EPPG (**A**), p-(melamine)/EPPG after 20 scans (**B**) and 30 scans of polymerization (**C**).

Fig. 2.11 depicts the results of impedance studies carried out to determine the charge transfer resistance at bare EPPG and p-(melamine)/EPPG surfaces in 1: 1 solution of 5 mM $K_3Fe(CN)_6$ and 0.1 M KCl in the frequency range of 0.1 to 100 kHz at a potential of 0.05 V. The results were found to fit best to a simple Randles equivalence circuit. The electron transfer resistance (R_{CT}) values for bare EPPG and p-(melamine)/EPPG are determined as 1105 Ω (curve a)

and 356 Ω (curve b), respectively. The lower value of R_{CT} of the p-(melamine)/EPPG indicated its low resistance and high electron transfer efficiency.

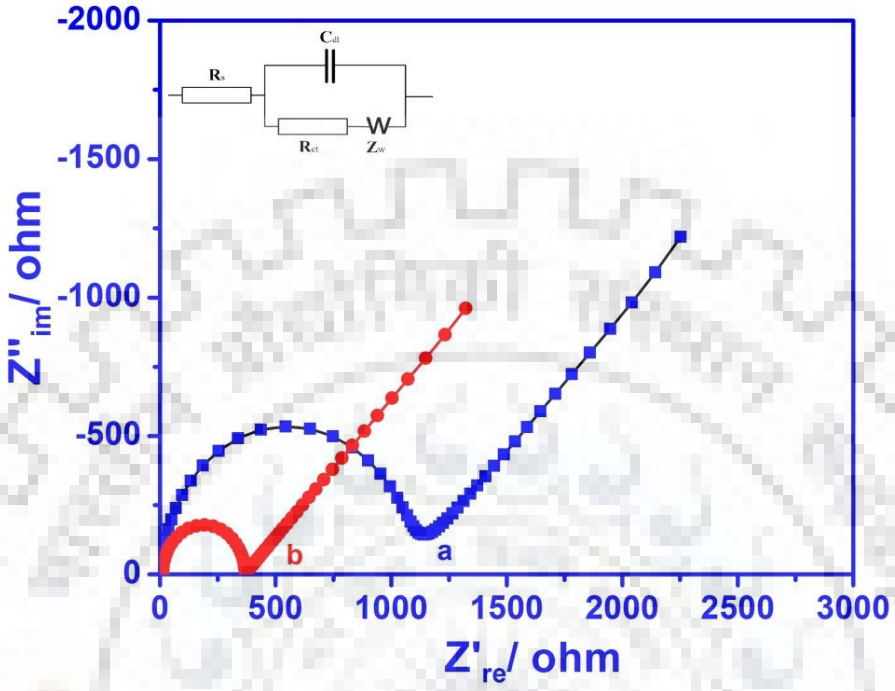

Fig. 2.11: Observed Nyquist-diagram showing variation in the charge transfer resistance corresponding to (a) bare and (b) p-(melamine)/EPPG Surfaces. The inset represents Randles equivalent circuit.

After electrochemical polymerization of poly-melamine film onto the EPPG surface, the efficacy of the p-(melamine)/EPPG surface was examined. For this purpose, surface area of the bare and modified EPPG were calculated by using cyclic voltammograms, which were recorded for 1 mM $K_3Fe(CN)_6$ at different scan rates using 0.1 M KCl as the supporting electrolyte. Well defined redox couple (E_{pa}; E_{pc}) was observed due to the presence of Fe^{+3}/Fe^{+2} at both the electrodes. However, the peak currents for the redox couple increased for the p-(melamine)/EPPG and lesser value of ΔE_p were observed showing more reversible nature of the redox couple at the modified surface. The effective surface areas were calculated from the slop of i_p vs. $v^{1/2}$ plots using the Randles-Sevcik equation and found as 0.34 cm^2 and 0.88 cm^2 for bare and p-(melamine)/EPPG, respectively. Experimental results indicated that the modified sensor exhibited significant improvement in the surface area and electropolymerization of melamine causes increase in the effective surface area by ~2 times. The increased effective surface area accelerates the

charge transfer, which is good for the electrochemical detection performance of the modified surface. The increase in the current may also be related to the activation of the graphite substrate after modification of the surface.

2.3.2.2 Cyclic voltammetry

Cyclic voltammograms (CVs) obtained for the oxidation of propranolol at the bare EPPG and p-(melamine)/EPPG at pH 7.4 are shown in **Fig. 2.12**. A broad, weak irreversible oxidation peak at ~1120 mV was observed at bare EPPG (curve a). The enhanced peak current response along with a simultaneous negative shift was observed at ~945 mV on the surface of p-(melamine)/EPPG. The increase in the oxidation peak current and shift in E_p to less positive potentials indicate that the p-(melamine) film forms a better electron conducting pathway and accelerates the rate of electron transfer at the electrode surface.

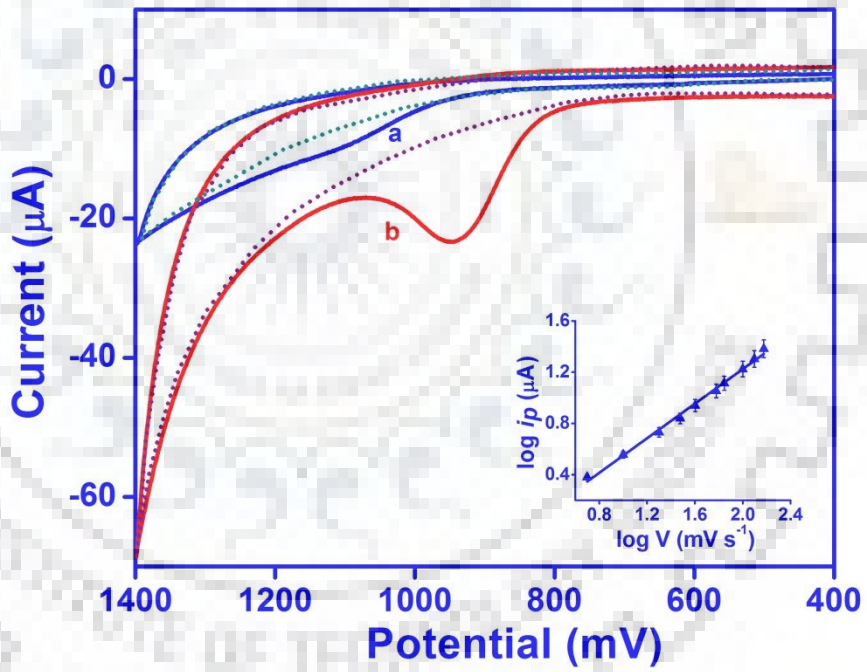

Fig. 2.12: Comparative cyclic voltammograms of 100 µM propranolol at (a) bare and (b) p-(melamine)/EPPG in phosphate buffer of pH 7.4 at a scan rate of 100 mVs^{-1}. The inset shows the plot of dependence of log i_p and log v. The background is shown by the dotted line.

To determine the nature of the electron transfer process, scan rate studies were performed in the range of 5–150 mVs^{-1}. The analyte peak current was found to increase with increasing sweep rates and dependence of the peak current on the scan rate can be expressed by the relation:

$$\mathbf{i_p/\mu A = 0.1451\ [v] + 2.3745}$$

with a correlation coefficient of 0.997, where ν is the scan rate in mVs^{-1} and i_p is the peak current in μA. The linearity of i_p versus scan rate plot indicated that oxidation of propranolol at p-(melamine)/EPPG is adsorption controlled, which was further confirmed by linearity of log i_p vs. log ν plot. The linear relation can be expressed by the following equation:

$$\log i_p = 0.674 \log \nu - 0.1256$$

with a correlation coefficient 0.994. The slope value (> 0.5) of log i_p vs. log ν plot (inset of **Fig. 2.12**) further confirmed that oxidation of propranolol involved by adsorption process [63,64].

2.3.2.3. Square Wave Voltammetry

Square wave voltammetry is used for the determination of propranolol as it has several advantages including excellent sensitivity and low background currents. The electrochemical behavior of 100 μM propranolol at bare EPPG and p-(melamine)/EPPG was investigated at physiological pH 7.4 using SWV (**Fig. 2.13**).

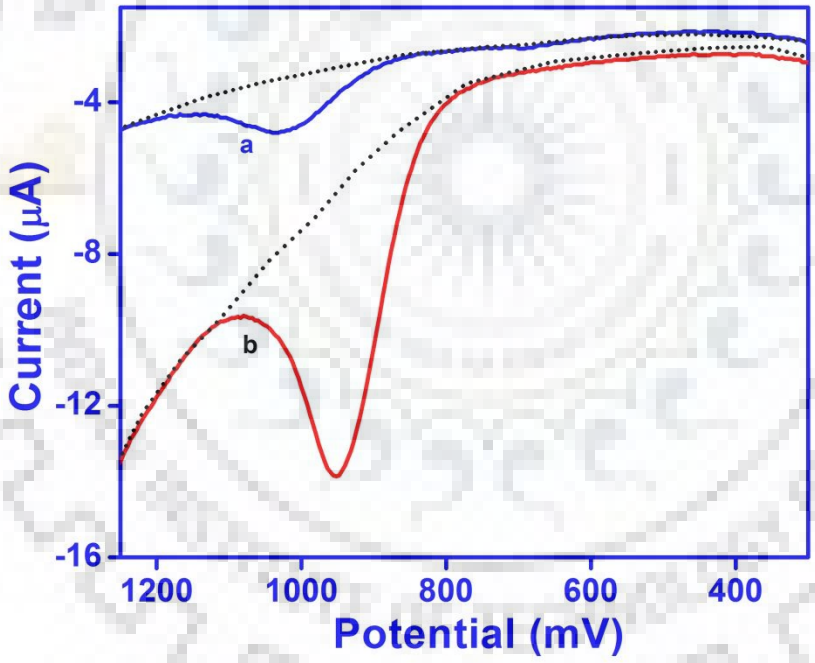

Fig. 2.13: Comparison of SWVs observed for 100 μM propranolol at (a) bare EPPG and (b) p-(melamine)/EPPG at pH 7.4. The background is shown by the dotted line.

At bare EPPG, a poorly defined oxidation peak was observed at 1035 mV corresponding to the propranolol oxidation. In the case of p-(melamine)/EPPG, a sharp with manifold improvement of the anodic peak response was observed and the peak potential shifted to less positive potential (~950 mV). This behavior can be attributed to the increased surface area of the modified surface

with (-NH_2) functional groups and improved conductivity provided by the p-(melamine) film leading to a significant rate increase in the electron transfer. However, the propranolol adsorption on the surface implies a change in the oxidation mechanism which also contributes to the electrocatalytic effect.

2.3.2.3.1 Effect of pH

The pH of the supporting electrolyte has a significant effect on the oxidation of propranolol at p-(melamine)/EPPG. Effect of pH of PBS was studied in the range of 2.4–10.5 using p-(melamine)/EPPG. It was found that the peak potential of propranolol displayed a negative shift with increasing pH. A linear relationship was observed between E_p and pH, which was expressed by the equation:

$$\mathbf{E_p/mV\ (pH\ 2.4 - 10.5) = - 59.85\ pH + 1368}$$

with a correlation coefficient of 0.995. The dEp/dpH value of ~59 mV/pH suggests that equal number of protons and electrons participate in the electro-oxidation of the propranolol. The oxidation in propranolol is likely to occur at the secondary alcoholic group, involving two electrons and two protons to produce a ketone as shown in **Scheme 4**. Similar mechanism for the oxidation of propranolol has been suggested earlier [36,37].

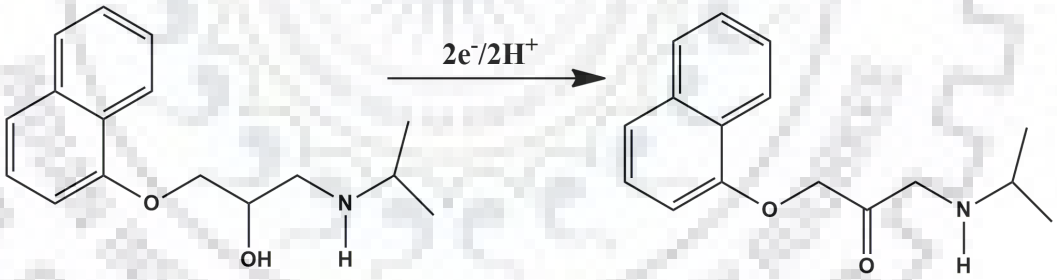

Scheme 4. Tentative mechanism suggested for the oxidation of propranolol.

2.3.2.3.2 Effect of square wave frequency

The dependence of peak current (i_p) of propranolol on the square wave frequency (f) was carried out in the range 5–80 Hz. The peak current showed a linear variation with the square wave frequency indicating adsorption controlled nature [63] of the electron transfer process at the p-(melamine)/EPPG and the linear relation between i_p and f can be expressed by the relation:

$$\mathbf{i_p\ /\mu A = 0.5983\ [\ \mathit{f}\ ] + 2.334 \qquad (R^2 = 0.995)}$$

Where, i_p is the peak current in μA and [*f*] is the square wave frequency in Hz.

2.3.2.3.3 Effect of concentration

The **Fig. 2.14** displays the SWVs of propranolol under the optimal experimental conditions. The oxidation peak current was found to increase with the increasing concentration of propranolol and have a linear relationship with propranolol concentration in the range 0.1 to 800 µM (**Fig. 2.14**). The linear regression equation is expressed as:

$$\mathbf{i_p/\mu A = 0.0513\,[C,\ 0.1 - 800\ \mu M] + 2.1738}$$

with a correlation coefficient of 0.998, and where C is the concentration of propranolol in µM. The values of limits of detection (L.O.D.) and quantification (L.O.Q.) for propranolol were obtained by utilizing L.O.D .= 3σ/b and L.O.Q .= 10σ/b, where σ is the standard deviation of the blank signals and b is the slope of the linear calibration graph. The L.O.D. and L.O.Q. for the determination of propranolol were calculated as 9 nM and 30 nM respectively. Thus, with the wide linear range and low detection limit, the proposed method is useful for the determination of propranolol in pharmaceutical formulations and biological fluids.

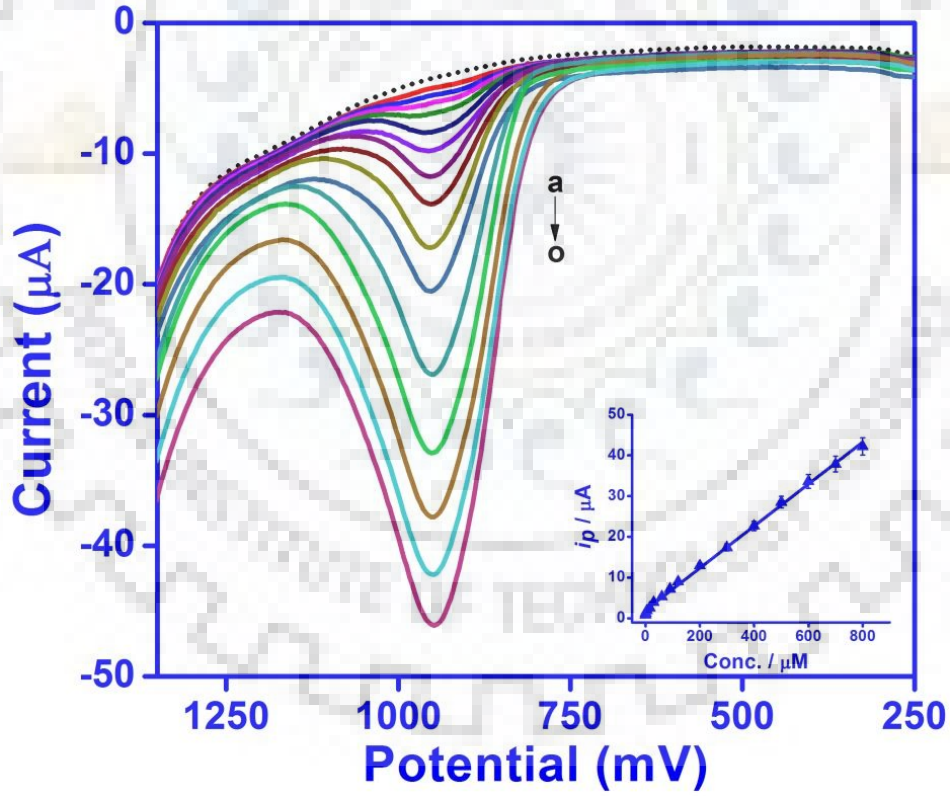

Fig. 2.14: Square wave voltammograms recorded at (a) 0.1; (b) 1; (c) 5; (d) 15; (e) 30; (f) 50; (g) 80; (h) 100; (i) 200; (j) 300; (k) 400; (l) 500; (m) 600; (n) 700 and (o) 800 µM concentration of propranolol using p-(melamine)/EPPGS in phosphate buffer of pH 7.4. Inset is the observed calibration plot between [C] and i_p. The background curve is shown by dotted line.

2.3.2.4 Interference study

In order to demonstrate the specificity of the developed sensor, the influence of some common interfering species (present in the biological fluids) on the determination of 30 µM propranolol in pH 7.4 buffers was investigated. The tolerance limit for the interferents was considered as the maximum concentration causing relative error of less than ± 5.0% in the oxidation peak current of the drug. The square wave voltammograms observed for the mixture of AA, UA, XT and propranolol are presented in **Fig. 2.15**. It was found that upto 100 fold concentration of each of the interferents have no influence on the peak current response of propranolol because these compounds oxidize at significant less potential than propranolol. The observed results suggested that the proposed method had appreciable selectivity and free from the interferents of most common metabolite presents in biological samples such as urine and plasma.

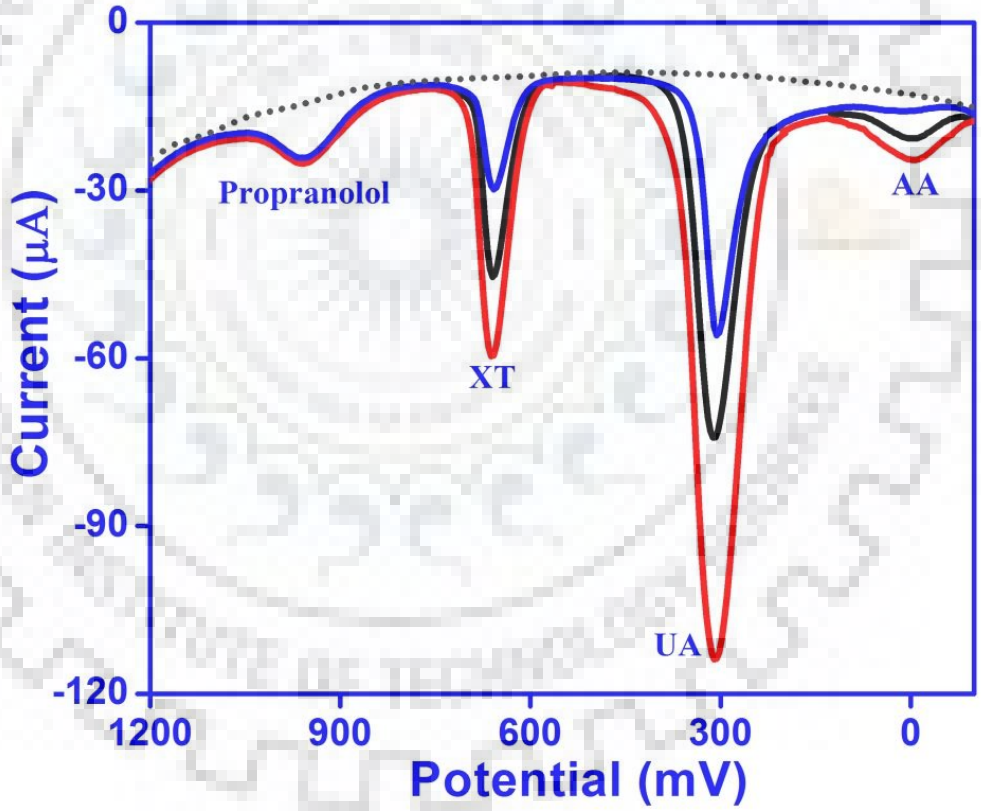

Fig. 2.15: Square wave voltammograms showing interference of ascorbic acid (AA), uric acid (UA) and xanthine (XT) at fixed propranolol concentration (30 µM); dotted line shows background current of phosphate buffer.

2.3.2.5 Stability and reproducibility study

The stability of the p-(melamine)/EPPG was investigated by measuring the oxidation peak current response for a fixed concentration of 20 μM propranolol in the phosphate buffer of pH 7.4 over a period of 30 days. The sensor was used daily and kept under ambient conditions. The results demonstrated that a slight decrease in the peak current was observed with a relative standard deviation (R.S.D.) of 2.1%. After 15 days the current started decreasing and R.S.D. increased to ~ 4.9% till 30 days, thus it is recommended that after 30 days a new sensor should be prepared. In order to measure intraday reproducibility, five measurements were carried out for 20 μM propranolol solution at an interval of 1 h in same day. Voltammetric responses were obtained with R.S.D. of 0.89% for propranolol. Thus, it is concluded that the modified sensor possesses significant stability, reproducibility and repeatability.

2.3.2.6 Analytical applicability

2.3.2.6.1 Pharmaceutical samples

In order to evaluate the practical utility of the fabricated sensor in drugs, three commercial pharmaceutical samples, Ciplar (40 mg), Betacap (20 mg) and propranolol (10 mg) tablets were purchased from the local market of Roorkee. Prior to the determination of propranolol, tablets were powdered and dissolved in double distilled water and suitably diluted so that the concentration of the drug was in the working concentration range. SWVs were then recorded under the similar conditions that were used during concentration study. The results were found to be highly reproducible and in good agreement with the labeled amount stated by the manufacturer (as demonstrated in **Table 2**). Thus, the proposed method presented good accuracy and precision for the determination of propranolol in pharmaceutical preparations.

Table 2: Determination of propranolol in pharmaceutical samples using p-(melamine)/EPPG.

Tablet	Stated content (mg)	Observed content (mg)	Error %
Ciplar	40	39.42	1.42
Betacap	20	19.87	0.65
Propranolol	10	9.89	1.10

2.3.2.6.2 Real samples

To illustrate the feasibility of the p-(melamine)/EPPG for routine real sample analysis, the electrode was applied to determine the propranolol concentration in urine and human plasma samples which were obtained from the patients, who were undergoing treatment with propranolol (80 mg; 2 tablets/day) for more than 5 days. As half-life of propranolol is ~3–4 h, the samples were collected after 3 h of oral administration of propranolol. All the samples were properly diluted with pH 7.4 buffers to reduce the matrix effect. Square wave voltammograms were recorded and it was found that a peak at E_p (950 mV) was observed corresponding to the oxidation of propranolol which was further confirmed by the spiking of exogenous propranolol in the same solution. By using standard addition plot the concentration of propranolol in urine and plasma samples were calculated. The absolute value of the x-intercept represents the concentration of propranolol in the urine and plasma sample which was detected as 142 μM and 0.27 μM. The main advantage of the standard addition method is that the matrix remains unchanged. The method is suitable for cases in which the matrix is complex or is difficult to reproduce. The analytical results observed are shown in **Tables 3** and **4**. As observed, the recoveries were in the range of 98.55–101.62% with a RSD (n = 5) of less than 2.13%. Hence, it is clear that p-(melamine)/EPPG has great potential for the determination of propranolol in human body fluids.

Table 3: Analysis results observed for propranolol in human urine sample after 3 hrs of propranolol administration at p-(melamine)/EPPG.

Sample	Spiked(μM)	Observed[a](μM)	Actual[b](μM)	Recovery *(%)
1.	0	142.32	142.32	--
	100	242.87	142.87	100.38
	200	343.92	143.92	101.12
	400	540.27	140.27	98.55
2.	0	139.56	139.56	--
	150	290.23	140.23	100.48
	250	388.37	138.37	99.14
	400	541.26	141.26	101.21

*The R.S.D. value for the determination was less than 2.14% for n=3.

[a]The observed values are sum of propranolol present + spiked amount

[b]The actual amount is observed –spiked amount

Table 4: Analysis results observed for propranolol in human plasma sample at p-(melamine)/EPPG.

Sample 1			Sample 2		
Spiked (µM)	**detected[a] (µM)**	**Recovery* (%)**	**Spiked (µM)**	**detected[a] (µM)**	**Recovery * (%)**
0	0.27	--	0	0.23	--
1	1.29	101.57	0.5	0.72	98.63
1.5	1.78	100.56	1	1.25	101.62
2	2.26	99.55	2	2.24	100.44

[a]Detected amount is "propranolol present + spiked amount"

*The R.S.D. value for the determination was less than 1.73% for n=3.

2.3.3 CONCLUSION

In conclusion, a novel p-(melamine)/EPPG prepared by electro-polymerization has excellent electrocatalytic activity for analytical determination of propranolol. The proposed method displayed fast, inexpensive and selective quantification of propranolol with high sensitivity and low L.O.D of ~9 nM. The approach demonstrates the excellent electrocatalytic activity toward the oxidation of propranolol in terms of, increase in peak current and the shift of the oxidation potential to less positive values. This effect can be attributed to the combined effects of the high surface area and conductivity of poly-melamine film as compared to the unmodified EPPG. The modified sensor was successfully applied in determining the propranolol in presence of potential interfering substances. The modified sensor was also successfully used for the determination of propranolol in pharmaceutical and human biological samples. The importance of the present protocol is also demonstrated by comparing the present method with those reported recently in the literature for the determination of propranolol and is tabulated in **Table 5**.

Table 5: Comparison of the detection limits and working range performed at p-(melamine)/EPPG with recently reported electroanalytical methods.

S. No.	Electrode Type	Linear range (µM)	Detection Limit (µM)	Real sample	Reference
1.	γ-CD–CNT/CPE	0.14-47.6	0.04	Yes	[36]
2.	GR/PDAN/EPPGE	0.1–750	0.02	Yes	[37]
3.	HPC-8/MWCNT	0.3-54	0.135	No	[39]
4.	PtNPs/MWCNTs/GCE	0.2-50	0.15	Yes	[51]
5.	MWCNTs–PAH/GCE	0.074-1	0.026	No	[52]
6.	PtNPs/MWCNTs	0.67-38	0.0845	No	[53]
7.	n-MCPE	10-104	2.91	Yes	[54]
8.	n-MIP-CP	0.1–10	0.08	No	[65]
9.	boron-doped diamond electrode	0.20-9.0	0.18	No	[66]
10.	MWCNT/SR	5.4-7	0.078	No	[67]
11.	n-ITIES	2-10	0.8	No	[68]
12.	microneedle-µITIES	0.05-0.2	0.05	No	[69]
13.	ta-C:N electrode	0.9-9.8	0.75	Yes	[70]
14.	p-(melamine)/EPPG	0.1-800	0.009	Yes	[present work]

γ -CD–CNT: γ -cyclodextrin–carbon nanotube, **CPE** : carbon paste electrode, **GR/PDAN:** graphene and (poly-1,5-diaminonaphthalene), **HPC-8/MWCNT:** multi-walled carbon nanotubes (MWCNT) and 8-hydroxy-8-propoxycalix[8] arene, **PAH**: poly (allylamine hydrochloride), **SR:** silicone-rubber, **n-MCPE:** CuO nanoparticles modified electrode, **PtNPs** platinum nanoparticle, **n-ITIES:** nanoscale interfaces between two immiscible electrolyte solutions, **ta-C:N:** nitrogen-containing tetra hedralamorphous carbon electrode.

It was interesting to observe that the simple modification with p-(melamine) leads to essentially similar sensitivity and L.O.D. in contrast to the complicated modification carried out by using graphene and other conducting polymer (**Table 5**). The method also provides an ecofriendly procedure for applying the detrimental compound (melamine) of life in the electrode modification for the detection of life substances.

2.4 REFERENCES

[1] J.J. Chen, "Drug-Induced Movement Disorders: A Primer", US Pharm. 32 (2007) HS16.

[2] T. Fischel, H. Hermesh, D. Aizenberg, Z. Zemishlany, H. Munitz, Y. Benjamini, A. Weizman, "Cyproheptadine versus propranolol for the treatment of acute neuroleptic-induced akathisia: a comparative double-blind study", J Clin Psychopharmacol. 21 (2001) 612.

[3] T. Ahuja, I.A. Mir, D. Kumar, Rajesh, "Biomolecular immobilization on conducting polymers for biosensing applications", Biomaterials 28 (2007) 791.

[4] M. Gerard, A. Chaubey, B.D. Malhotra, "Application of conducting polymers to biosensors", Biosens. Bioelectron. 17 (2002) 345.

[5] R. Balint, N.J. Cassidy, S.H. Cartmell, "Conductive polymers: towards a smart biomaterial for tissue engineering", Acta Biomater. 10 (2014) 2341.

[6] M. Amare, S. Admassie, "Differential pulse voltammetric determination of the ophylline at poly (4-amino-3-hydroxynaphthalene sulfonic acid) modified glassy carbon electrode", Bull. Chem. Soc. Ethiop. 26 (2012) 73.

[7] G. Inzelt, M. Pineri, J.W. Schultze, M.A. Vorotyntsev, "Electron and proton conducting polymers: recent developments and prospects", Electrochim. Acta 45 (2000) 2403.

[8] G.G. Wallace, M. Smyth, H. Zhao, "Conducting electro-active polymer-based biosensors", Anal. Chem. 18 (1999) 245.

[9] A. Ramanavicius, A. Ramanavicien, A. Malinauskas, "Electrochemical sensors based on conducting polymer—polypyrrole", Electrochim. Acta 51 (2006) 6025.

[10] S. Baskar, C.W. Liao, J. L. Chang, J. M. Zen, " Electrochemical synthesis of electroactive poly(melamine) with mechanistic explanation and its applicability to functionalize carbon surface to prepare nanotube–nanoparticles hybrid", Electrochim. Acta 88 (2013) 1.

[11] X. Liu, L. Luo, Y. Ding, Q. Wu, Y. Wei, D. Ye, "A highly sensitive method for determination of guanine, adenine and epinephrine using poly-melamine film modified glassy carbon electrode", J. Electroanal. Chem 675 (2012) 47.

[12] M. Raj, P. Gupta, R.N. Goyal, "Poly-melamine film modified sensor for the sensitive and selective determination of propranolol, a β-blocker in biological fluids", J. Electrochem. Soc. 163 (2016) H388.

[13] X. Liu, L. Luo, Y. Ding, Ye Daixin, "Poly-glutamic acid modified carbon nanotube-doped carbon paste electrode for sensitive detection of L-tryptophan", Bioelectrochemistry 82 (2011) 38.

[14] D.P. Santos, M.F. Bergamini, A.G. Fogg, M.V.B. Zanoni, "Application of a glassy carbon electrode modified with poly (glutamic acid) in caffeic acid determination, Microchim. Acta 151 (2005) 127.

[15] A. Yu, H. Chen, "Electrocatalytic oxidation and determination of ascorbic acid at poly (glutamic acid) chemically modified electrode", Anal. Chim. Acta 344 (1997) 181.

[16] A. Yu, H. Chen, "Electrocatalytic oxidation of hydrazine at the poly (glutamic acid) chemically modified electrode and its amperometric determination", Anal. lett. 30 (1997) 599.

[17] K. Miyamoto, Y. Yamamoto, M. Kurita, R. Sakai, K. Konno, F. Sanae, T. Ohshima, K. Takagi, T. Hasegawa, N. Iwasaki, M. Kakiuchi, H. Katos, "Bronchodilator activity of xanthine derivatives substituted with functional groups at the 1- or 7-position", J. Med. Chem. 36 (1993) 1380.

[18] K. Yasui, A. Komiyama, "New clinical applications of xanthine derivatives: modulatory actions on leukocyte survival and function", Int. J. Hematol. 73 (2001) 87.

[19] S.E. kalyoubi, F. Agili, S. Youssif, "Novel 2-Thioxanthine and dipyrimido pyridine derivatives: synthesis and antimicrobial activity", Molecules 20 (2015) 19263.

[20] X. Yuan, Y. Wang, X. Wang, W. Chen, J.S. Fossey, N. Wong, "An ab initio and AIM investigation into the hydration of 2-thioxanthine", Chem. Cent. J. 4 (2010) 1.

[21] J. Ward, S.N. Spath, B. Pabst, P.A. Carpino, R.B. Ruggeri, G. Xing, A.E. Speers, B.F. Cravatt, K. Ahn, "Mechanistic characterization of a 2-thioxanthinemyeloperoxidase inhibitor and selectivity assessment utilizing click chemistry activity-based protein profiling", Biochemistry 52 (2013) 9187.

[22] A. Biela, F. Coste, F. Culard, M. Guerin, S. Goffinont, K. Gasteiger, J. Ciesla, A. Winczura, Z. Kazimierczuk, D. Gasparutto, T. Carell, B. Tudek, B. Castaing, "Zinc finger oxidation of Fpg/Nei DNA glycosylases by 2-thioxanthine: biochemical and X-ray structural characterization", Nucleic Acids Res. (2014) 1.

[23] P.U. Civcir, "Tautomerism of 2-thioxanthine in the gas and aqueous phase using AM1 and PM3 method", J. Mol. Struc. Theochem. 546 (2001) 163.

[24] W.U. Malik, R.N. Goyal, M. Rajeshwari, "Electrochemical oxidation of 2-thioxanthine", Bull. Chem. Soc. France (1988) 39.

[25] B. Zeng, W.C. Purdy, "Infuence of cetyltrimethyl ammonium bromide on the voltammetric behaviour of thiopurines at a silver electrode", Electroanalysis 11 (1999) 879.

[26] G.D. Christian, W.C. Purdy, "The residual current in orthophosphate medium", J. Electroanal. Chem 3 (1962) 363.

[27] M. Raj, P. Gupta, N. Thapliyal, R.N. Goyal, "A novel hybrid nano-composite grafted electrochemically reduced graphene oxide based sensor for sensitive determination of efavirenz", Electroanalysis 28 (2016) 1.

[28] J.R. Retama, D. Mecerreyes, B.L. Ruiz, E.L. Cabarcos, "Synthesis & characterization of semi conducting polypyrrole/polyacrylamide micro particles with GOx for biosensor application", Colloids Surf. A 270 (2005) 239.

[29] R. Boulieu, C. Bory, P. Baltassat, C. Gonnet, "Hypoxanthine and xanthine levels determined by high-performance liquid chromatography in plasma, erythrocyte, and urine samples from healthy subjects: the problem of hypoxanthine level evolution as a function of time", Anal. Biochem. 129 (1983) 398.

[30] S.A. Margolis, D.L. Duewer, "Measurement of ascorbic acid in human plasma and serum: stability, intra laboratory repeatability, and inter laboratory reproducibility", Clin. Chem. 42 (1996) 1257.

[31] W. Fischer, "Anticonvulsant profile and mechanism of action of propranolol and its two enantiomers", Seizure 11 (2002) 285.

[32] A.M. Barrett, V.A. Cullum, "The biological properties of the optical isomers of propranolol and their effects on cardiac arrhythmias", Br. J. Pharmac. 34 (1968) 43.

[33] P. Partani, Y. Modhave, S. Gurule, A. Khuroo, T. Monif, "Simultaneous determination of propranolol and 4-hydroxy propranolol in human plasma by solid phase extraction and liquid chromatography/electrospray tandem mass spectrometry", J. Pharm. Biomed. Anal. 50 (2009) 966.

[34] S.M. Southwick, J.D. Bremner, A. Rasmusson, C. A. Morgan III, A. Arnsten, D.S. Charney, "Role of norepinephrine in the pathophysiology and treatment of posttraumatic stress disorder", Biol. Psychiatry 46 (1999) 1192.

[35] A. Brunet, S.P. Orr, J. Tremblay, K. Robertson, K. Nader, R.K. Pitman, "Effect of post-retrieval propranolol on psycho physiologic responding during subsequent script-driven traumatic imagery in post-traumatic stress disorder", J. Psychiatr. Res. 42 (2008) 503.

[36] R.R. Gaichore, A.K. Srivastava, "Electrocatalytic determination of propranolol hydrochloride at carbon paste electrode based on multi-walled carbon-nanotubes and c-cyclodextrin", J. Incl Phenom Macro 78 (2014) 195.

[37] P. Gupta, S.K. Yadav, B. Agrawal, R.N. Goyal, "A novel graphene and conductive polymer modified pyrolytic graphite sensor for determination of propranolol in biological fluids", Sens. Actuators B 204 (2014) 791.

[38] Y. Qi, F. R. Xiu, "Sensitive and rapid chemiluminescence detection of propranolol based on effect of surface charge of gold nanoparticles", J. Lumin. 171 (2016) 238.

[39] Z. Kun, Y. Shuai, T. Dongmei, Z. Yuyang, "Electrochemical behavior of propranolol hydrochloride in neutral solution on calixarene/multi-walled carbon nanotubes modified glassy carbon electrode", J. Electroanal. Chem. 709 (2013) 99.

[40] A. Townshend, J.A.M. Pulgarin, M.T.A. Pardo, "Flow injection-chemiluminescence determination of propranolol in pharmaceutical preparations", Anal. Chim. Acta 488 (2003) 81.

[41] H. Qi, C. Wang, R. Zou, L. Li, "Electro-generated chemiluminescence sensor for the determination of propranolol hydrochloride", Anal. Methods 3 (2011) 446.

[42] K.L. Marques, J.L.M. Santos, J.L.F.C. Lima, "Chemiluminometric determination of propranolol in an automated multicommutated flow system", J. Pharm. Biomed. Anal. 39 (2005) 886.

[43] P. Valderrama, R.J. Poppi, "Determination of propranolol enantiomers in plasma and urine by spectro-fluorimetry and second-order standard addition method", Anal. Chim. Acta 651 (2009) 31.

[44] T. Madrakian, A. Afkhami, M. Mohammadnejad, "Simultaneous spectrofluorimetric determination of levodopa and propranolol in urine using feed-forward neural networks assisted by principal component analysis", Talanta 78 (2009) 1051.

[45] M.E. Hitscherich, E.M. Rydberg, D.C. Tsilifonis, R. E. Daly, "Simultaneous determination of hydrochlorothiazide and propranolol hydrochloride in tablets by high performance liquid chromatography," J. Liq. Chromatogr. 10 (1987) 1011.

[46] S.S. Imam, A. Ahad, M. Aqil, Y. Sultana, A. Ali, "A validated RP-HPLC method for simultaneous determination of propranolol and valsartan in bulk drug and gel formulation", J. Pharm Bioallied Sci. 5 (2013) 61.

[47] M.A.E. Ries, F.M.A. Attia, S.A. Ibrahim, "AAS and spectrophotometric determination of propranolol HCl and metoprolol tartrate," J. Pharm. Biomed. Anal. 24 (2000) 179.

[48] A.M.E. Didamony, "A sensitive spectrophotometric method for the determination of propranolol HCl based on oxidation bromination reactions," Drug Test Anal 2 (2010) 122.

[49] J.M.M. Junior, A.L.H. Muller, E.L. Foletto, A.B. Costa, C.A. Bizzi, E.I. Muller, "Determination of Propranolol Hydrochloride in Pharmaceutical Preparations Using Near Infrared Spectrometry with Fiber Optic Probe and Multivariate Calibration Methods", J Anal Methods Chem 2015 (2015) 1.

[50] Rosy, S.K. Yadav, B. Agrawal, M. Oyama, R.N. Goyal, "Graphene modified Palladium sensor for electrochemical analysis of norepinephrine in pharmaceuticals and biological fluids", Electrochim. Acta 125 (2014) 622.

[51] Z. Kun, C. Hongtao, Y. Yue, B. Zhihong, L. Fangzheng, L. Sanming, "Platinum nanoparticle-doped multiwalled carbon-nanotube-modified glassy carbon electrode as a sensor for simultaneous determination of atenolol and propranolol in neutral solution", Ionics 21 (2015) 1129.

[52] G.G. Oliveira, D.C. Azzi, F.C. Vicentini, E.R. Sartori, O.F. Filho, "Voltammetric determination of verapamil and propranolol using a glassy carbon electrode modified with functionalized multiwalled carbon nanotubes within a poly (allylamine hydrochloride) film", J. Electroanal. Chem 708 (2013) 73.

[53] Z. Kun, H. Yi, Z. Chengyun, Y. Yue, Z. Shuliang, Z. Yuyang, "Electrochemical behavior of propranolol hydrochloride in neutral solution on platinum nanoparticles doped multi-walled carbon nanotubes modified glassy carbon electrode", Electrochim. Acta 80 (2012) 405.

[54] N. Shadjou, M. Hasanzadeh, L. Saghatforoush, R. Mehdizadeh, A. Jouyban, "Electrochemical behavior of atenolol, carvedilol and propranolol on copper-oxide nanoparticles", Electrochim. Acta 58 (2011) 336.

[55] P. Gupta, R.N. Goyal, "Polymelamine modified edge plane pyrolytic graphite sensor for the electrochemical assay of serotonin", Talanta 120 (2014) 17.

[56] P. Gupta, R.N. Goyal, "Sensitive determination of domperidone in biological fluids using a conductive polymer modified glassy carbon electrode", Electrochim. Acta 151 (2015) 1.

[57] S. He, Z. Chen, Y. Yu, L. Shi, "A novel non-enzymatic hydrogen peroxide sensor based on poly-melamine film modified with platinum nanoparticles", RSC Adv. 4 (2014) 45185.

[58] Rosy, R.N. Goyal, "Gold nanoparticles decorated poly-melamine modified glassy carbon sensor for the voltammetric estimation of domperidone in pharmaceuticals and biological fluids", Talanta 141 (2015) 53.

[59] G. Li, P. Miao, "Electrochemical analysis of proteins. in: electrochemical analysis of proteins and cells", Springer Briefs in Molecular Science (2013) 19.

[60] H.M. Elqudaby, H.A.M. Hendawy, E.R. Souaya, G.G. Mohamed, G.M.G. Eldin, "Utility of activated glassy carbon and pencil graphite electrodes for voltammetric determination of nalbuphine hydrochloride in pharmaceutical and biological fluids", Int. J. Electrochem. 2016 (2015) 9.

[61] A. Erdem, P. Papakonstantinou, H. Murphy, "Direct DNA hybridization at disposable graphite electrodes modified with carbon nanotubes", Anal. Chem. 78 (2006) 6659.

[62] R.N. Goyal, S. Bishnoi, B. Agrawal, "Electrochemical sensor for the simultaneous determination of caffeine and aspirin in human urine samples", J. Electroanal. Chem 655 (2011) 97.

[63] P. Gupta, S.K. Yadav, R.N. Goyal, "A sensitive polymelamine modified sensor for the determination of lomefloxacin in biological fluids", J. Electrochem. Soc. 162 (2015) H86.

[64] E. Laviron, "General expression of the linear potential sweep voltammogram in the case of diffusionless electrochemical systems", J. Electroanal. Chem. 101 (1979) 19.

[65] T. Alizadeh, L. Allahyari, "Highly-selective determination of carcinogenic derivative of propranolol by using a carbon paste electrode incorporated with nano-sized propranolol-imprinted polymer", Electrochim. Acta 111 (2013) 663.

[66] E.R. Sartori, R.A. Medeiros, R.C.R. Filho, O.F. Filho, "Square-wave voltammetric determination of propranolol and atenolol in pharmaceuticals using a boron-doped diamond electrode", Talanta 81 (2010) 1481.

[67] S.X. Santos, E.T.G. Cavalheiro, C.M.A. Brett, "Analytical Potentialities of Carbon Nanotube/Silicone Rubber Composite Electrodes: Determination of Propranolol", Electroanalysis 22 (2010) 2776.

[68] Y. Liu, J. Strutwolf, D.W.M. Arrigan, "Ion-transfer voltammetric behavior of propranolol at nanoscale liquid–liquid interface arrays", Anal. Chem. 87 (2015) 4487.

[69] P. Vazquez, G. Herzog, C. Mahony, J. Brien, J. Scully, A. Blake, C. Mathuna, P. Galvin, "Microscopic gel–liquid interfaces supported by hollow micro needle array for voltammetric drug detection", Sens. Actuators B 201 (2014) 572.

[70] B.C. Lourencao, T.A. Silva, O.F. Filho, G.M. Swain, "Voltammetric studies of propranolol and hydrochlorothiazide oxidation in standard and synthetic biological fluids using a nitrogen-containing tetrahedral amorphous carbon (ta-C:N) electrode", Electrochim. Acta 143 (2014) 398.

Chapter 3

PtNPs and ErGO based sensitive sensor for the determination of Efavirenz

3.1 INTRODUCTION

Efavirenz (EFZ), chemically known as 6-chloro-4(cyclopropylethynyl)-1,4-dihydro-4-(trifluoromethyl)-2H-3,1benzoxazin-2-one (**Scheme 1**) is a first-generation non-nucleoside reverse transcriptase inhibitor (NNRTI) drug, used in the treatment of human immunodeficiency virus (HIV) type 1 infections [1]. The reverse transcriptase (RT) enzyme plays an important role in the life-cycle of HIV as it converts the single stranded RNA (HIV genetic material) into a double-stranded DNA via polymerase and Ribonuclease H activities. The EFZ directly binds to the RT that causes a disruption of the enzyme's catalytic site, which hinders the formation of viral double-stranded DNA from the single-stranded viral RNA genome [2,3]. EFZ is a first-line drug and it is usually prescribed either in combination with protease inhibitor or nucleoside reverse-transcriptase inhibitor for the management of the disease [4]. EFZ is metabolized in human system into hydroxylated compounds by cytochrome P450 (CPY) with CYP2B6 and CYP2A4 being the major isozymes responsible for the biotransformation and excreted through the urine and feces. The peak plasma concentration of EFZ was observed ~5 h after single or multiple doses of the drug. Efavirenz has a relatively long terminal half-life of 40 to 76 h showing large variation, which basically depends upon the conditions of the drug administration [5-8]. Approximately 1% of the administered drug dose is recovered in the urine as unchanged EFZ. High inter-individual variability in plasma concentrations of EFZ drug in the patients leads to the treatment failure and a variety of side effects in the central nervous system (CNS). The CNS side effects include dizziness to hallucination, insomnia, abnormal dreams, light headedness, impaired concentration, depression, aggressive behavior, anxiety and paranoid and such side effects reflect varying EFZ plasma concentrations [8-10]. Thus, the quantitative analysis of EFZ is essential for optimizing the therapeutic concentration of EFZ to minimize the risk of virological failure, for pharmaceutical quality control and clinical diagnosis. Several analytical methods such as chromatographic, spectrophotometric and spectrometric have been attempted to quantify the EFZ [11-17]. However, an expensive instrumentation is required in these techniques with sophisticated process, tedious extraction procedures and number of separation steps, which result in high detection times as compared to the electroanalytical methods. Electrochemical techniques have been explored to overcome these difficulties as they are advantageous and provide high selectivity, sensitivity, convenient tool with fast response, reproducibility and the analysis can be carried out without complicated sample pretreatment [18,19]. However to the best of our knowledge, very scarce attempts have been made for the determination of EFZ by electrochemical methods [4, 20-22]. In

these methods dsDNA or NiO nanoparticle modified glassy carbon electrodes were used and a very low linear dynamic range was observed. In addition, the surface modification procedure was tedious, time consuming and analysis is reported in pharmaceutical samples and human biological samples are rarely analyzed. In the previously reported method for EFZ [21], the preparation of nanoparticles-mixture of NiO and ZrO_2 was very time consuming and required high energy mechanical milling for a time period of ~10 h. In addition, the ball to mass ratio during milling also affected nature of NiO-ZrO nanoparticles. To overcome this problem, we developed a one pot synthesis method, which required only few minutes for the modification of the sensor surface and almost similar detection limit for EFZ was observed [21].

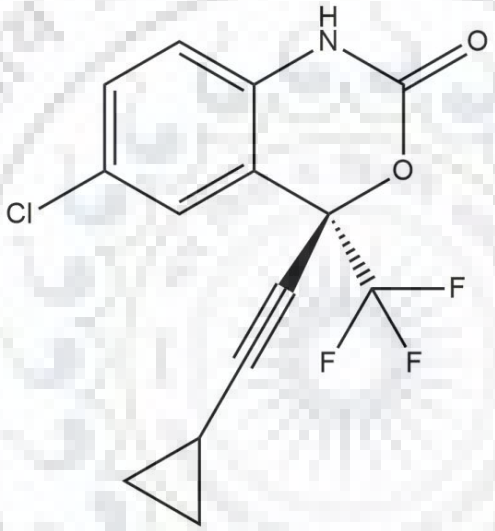

Scheme 1: Chemical structure of EFZ.

Graphene, a single-atom thick, two dimensional, extensively conjugated carbonaceous nano-material has gained enormous interest during the last decade due to its excellent and distinct properties, such as high mechanical strength, good thermal conductivity, tunable band gap, large specific surface area, impressive mobility of charge carriers, superior biocompatibility and electrical conductivity [23-27]. The unique nanostructure and properties of graphene provide potential applications in many technological fields like nanocomposite synthesis [28], fabrication of electrical devices such as batteries [29], supercapacitors [30], field-effect transistors [31], electro-mechanical resonators [32] and so on. Nowadays, researches have manifested that graphene also carries excellent electrochemical catalytic activity, therefore should be a unique material for the modification of the surface with exceptional performance [33,34]. The electrochemical reduction of graphene oxide is a simple, efficient, rapid, inexpensive and eco-

friendly technique over other methods for synthesizing pure, high quality and little aggregated electrochemically reduced graphene oxide (ErGO). ErGO has a tendency to form a stable film on the surface of electrode without any additional treatment [35]. Another advantage to perform the electrochemical reduction method is to control the thickness of film via changing experimental parameters i.e. potential, scan rate and to overcome the structural defects on the electrode surface [36]. ErGO offers more approachable planes and edge sites in comparison to the graphene [37]. The grafting of the nano-materials or their composites on to the ErGO sheets can also be used to reduce the aggregation between the graphene sheets [38]. The incorporation of noble metal nanoparticles (NPs) in conducting matrix materials such as reduced graphene is another efficient procedure to improve the electrocatalytic activity and stability [39]. Such types of nanoparticles have large surface area and high surface energy, which show high oxidation current and also catalyze the reaction kinetics at the electrode surface [40]. To acquire better dispersions of the ErGO, addition of dispersant, which can bind tightly onto ErGO sheets is required. Nafion, a proton exchange perfluoro sulfonate ionomer is used. Due to the perfluoro alkyl backbone, Nafion has higher hydrophobicity and strongly interacts with graphene in comparison to the traditional hydrocarbon-based surfactants such as poly(sodium 4-styrenesulfonate), DNA and SDBS (sodium dodecyl benzene sulphonate) [41]. Nafion plays an important role in the prevention of aggregation of ErGO and for organic molecules as a modifying agent with some extraordinary properties such as chemically inertness, good antifouling capacity and high permeability to proton [42]. The electrochemically reduced graphene oxide (ErGO) has the tendency to aggregate or reconvert into the graphite, thus, the nafion has been used to increase the dispersion of graphene sheets, while incorporation of PtNPs increases the spacing between adjacent carbon sheets by blocking the vander Waals interaction. Thus, PtNPs act as nanoscale spacers on the surface of ErGO, thereby making both the faces of ErGO accessible and hence, leads to the enhancement in the active surface area [43]. In the present work, an electrochemical sensor has been fabricated by the electrochemical deposition of GO in combination with PtNPs and Nafion hybrid nano-composite for the sensitive and selective determination of EFZ in biological and pharmaceutical samples. An edge plane pyrolytic graphite (EPPG) has been used as a substrate for the surface modification due to its wide potential range, high sensitivity and good conductivity. ErGO grafted with hybrid nano-composite has been used to minimize the aggregation of the graphene layers on the EPPG surface. The sensor has been successfully applied to the determination of EFZ in the biological samples and in the commercial pharmaceutical formulations with good reproducibility and stability.

3.2. EXPERIMENTAL

3.2.1 Reagents and materials

EFZ, Potassium tetrachloroplatinate (II), Nafion (5 wt.% in low aliphatic alcohols), uric acid (UA) and xanthine (XT) were purchased from Sigma Aldrich. The graphite powder (< 20 mm), hydrazine, perchloric acid, sulphuric acid, potassium chloride and potassium ferricyanide were also obtained from E. Merck, Mumbai. The plasma and urine samples were obtained from the Institute hospital of I.I.T. Roorkee as reported in the section A of the chapter 2.

3.2.2 Instruments

Bruker D8-advance X-ray powder diffractometer (XRD) was used for the Powder X-ray diffraction measurements of the sample. Raman spectroscopic measurements were carried out using Renishaw Invia Raman microscopy. All other characterization techniques and electrochemical observations techniques were essentially similar to that reported in the section A of the chapter 2.

3.2.3 Fabrication of ErGO-Pt/Nafion/EPPG Sensor

3.2.3.1 Preparation of GO-Nafion/Pt Nano-composite

The GO was obtained from the graphite in the laboratory using the improved Hummers method [44]. Briefly, graphite powder (1.5 g) was mixed in H_3PO_4 and H_2SO_4 (20:180) mixture. 9 g of $KMnO_4$ was added into the reaction vessel and the solution was heated to 50^oC under continuous stirring for 12 h, after which a dark brown material was observed. Subsequently, the mixture was cooled to room temperature and diluted with 100 mL of distilled water under continuous stirring for another 15 min. 1.5 mL of H_2O_2 (30%) was then added to the reaction mixture drop-wise, which turned the color of the solution to yellow. To separate out the exfoliated graphite, the reaction mixture was centrifuged. The obtained residue material was washed with plenty of water followed 100 mL of HCl (30%). Finally the residue was washed with ethanol and water and dried in the vacuum to obtain GO powder. The XRD and Raman spectra of the GO powder obtained were essentially similar as reported in the literature [45,46].

A homogeneous mixture of GO-nano-hybrid composite material was prepared by exfoliating 2 mg GO in 2 mL water. A uniform dispersion was observed after 20 min of ultra-sonication. Now 2 mL of each 1 mM K_2PtCl_4 and Nafion solution (0.5 wt% in water and ethanol

mixture of 1 :1 vol/vol) were mixed with GO suspension and sonicated for 15 min to achieve homogeneous mixture.

3.2.3.2 Preparation of Modified Sensor

Initially, the surface of the edge plane pyrolytic graphite (area 4 mm^2) was cleaned by rubbing on an emery paper (P-400) and then washed with the double distilled water to remove carbon particles and dried. Now, 15 µL of GO nano-hybrid composite was drop casted (volume was optimized) on EPPG and then dried at an ambient temperature. The GO-nano-composite modified EPPG was then electrochemically reduced by scanning 8 cycles with in a range of -1.7 to +0.2 V at 100 mVs^{-1} in N_2-saturated buffer solution of pH 7.2 [47]. After the electrochemical treatment the sensor is termed as ErGO-Pt/Nafion/EPPG.

3.2.4 Voltammetric procedure

The stock solution of EFZ (100 ppm) was prepared in methanol, rapped in black paper and kept in the refrigerator. The working solutions for recording the voltammogram were prepared by the appropriate dilution of the known volume of the stock solution with 2 mL of buffer solution and total volume was made to 4 mL with double distilled water. The voltammograms were recorded after bubbling high purity nitrogen for 10–12 min to remove oxygen. For square wave voltammetric studies optimized parameters used were: initial potential (E): 400 mV, final potential: 1400 mV, square wave amplitude (E_{sw}): 25 mV, potential step (E): 4 mV and square wave frequency (f): 15 Hz. Optimum conditions for cyclic voltammetry (CV) were initial (E): 400 mV, switching potential (E): 1400 mV, final (E): 400 mV and scan rate (ν): 100 mV/s. All the potentials are reported with respect to Ag/AgCl electrode at an ambient temperature of 25±2^oC. The surface of the modified sensor was cleaned after each run by applying a potential of -800 mV for 120 s using time base technique in the blank solution.

3.2.5 Sample preparation

To investigate pharmaceutical samples, the commercially available EFZ tablets were obtained from the local market of Delhi, India. The tablets were powdered to a homogeneous fine powder and the required amount of the powder was weighed and diluted with methanol to prepare 1 mM stock solution.

The plasma and urine samples were obtained from two healthy volunteers (Female, age 28 and Male, age 21). Samples were then diluted 2 and 10 times, respectively with phosphate buffer

of pH 7.2 to reduce the matrix complexity and then square wave voltammograms were recorded to quantify the drug in the spiked human plasma and urine samples.

3.3 RESULT AND DISCUSSION

3.3.1 Electrochemical characterization of ErGO-Pt/Nafion nanocomposite modified EPPG

The surface morphology of unmodified EPPG and at different steps of the modification was characterized with the help of FE-SEM and the observed microscopic images are shown in **Fig. 3.1**.

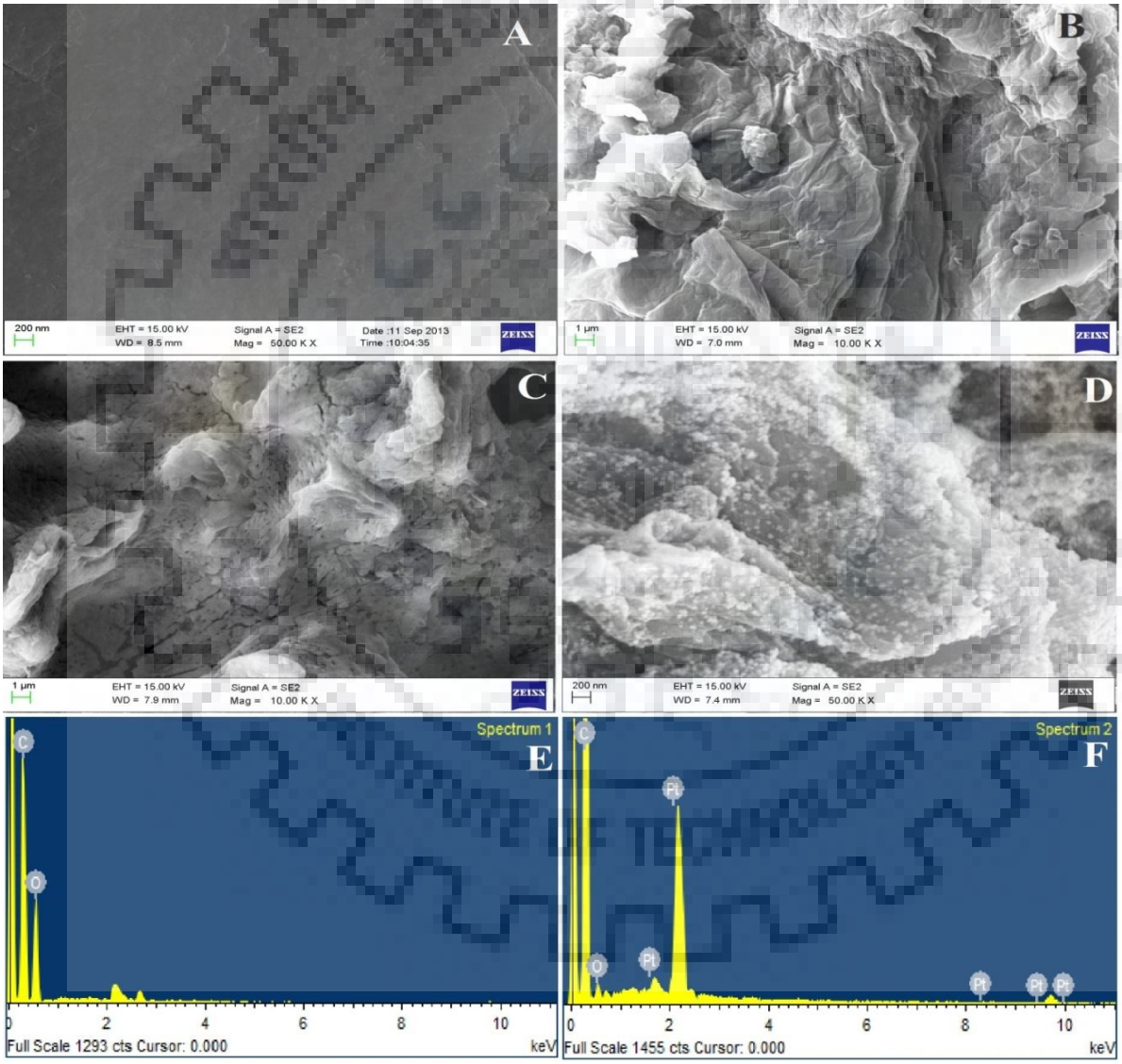

Fig. 3.1: Typical FE-SEM image observed for unmodified EPPG (**A**), GO modified EPPG (**B**), ErGO modified EPPG (**C**), and ErGO-Pt/Nafion modified EPPG (**D**). EDX spectra of GO (**E**) and ErGO/ PtNPs (**F**).

As displayed in **Fig. 3.1B**, morphology of GO consists of wrinkled, thin stacked flakes and has a model multilayer structure, which is fairly smooth. The prepared electrochemically reduced grapheme oxide film has a comparatively rougher surface than GO and appeared to have some cracks and pinhole structures (**Fig. 3.1C**). **Fig. 3.1D** shows the deposition of highly dispersed PtNPs on the surface of homogeneous microstructural film of Nafion and ErGO sheets and observed exfoliated layered structure exhibits nano-scale texture indicative of much more roughness. In order to investigate the element constituents, EDX spectra of GO (**Fig. 3.1E**) and ErGO/PtNPs (**Fig. 3.1F**) were recorded, respectively. The comparison of the spectra shows that a small number of O elements in ErGO/PtNPs are from the oxygen-containing functional groups of ErGO, confirming the electrochemical reduction of GO. The peaks of PtNPs were found in the EDX spectra as thin layers of nanoparticle are deposited on ErGO/EPPG.

The interfacial properties of the EPPG, ErGO/EPPG and ErGO-Pt/Nafion/EPPG surfaces and characteristics of the nanocomposite film, the electrochemical impedance spectroscopy was employed. The charge transfer resistance (R_{CT}) of the electrode provides vital insight into the nature of the interface. The experiment was carried out in 5 mM $K_3Fe(CN)_6$ and 0.1 M KCl (1 :1) solution in the frequency range of 0.1–100 kHz at a potential of 0.05 V. The value of the charge transfer resistance (R_{CT}) was determined using Randles equivalent circuit. The diameter of the semicircle represents R_{CT} and the linear response at low frequency represented the mass transfer diffusion of analyte molecules from the bulk of the electrolyte to the interface and represents Warburg resistance (Z_W). The observed results were found to fit best with Randles equivalence circuit. **Fig. 3.2** represents a comparison of Nyquist plots observed for the EPPG, ErGO/EPPG and ErGO-Pt/Nafion/EPPG sensors and in all cases a semicircular pattern followed by a linear portion was observed. The charge-transfer resistance (R_{CT}) for $Fe[CN]_6^{3-/4-}$ redox process at bare EPPG was determined to be 1014 Ω (**curve a**). However, for ErGO/EPPG and ErGO-Pt/Nafion/EPPG, the value of R_{CT} decreased significantly to about 480Ω and 140Ω (**curve b and c**), respectively. The results indicated that the grafting of the hybrid nanocomposite with ErGO increased the charge transfer rate and showed a very good conductivity with negligible charge transfer resistance.

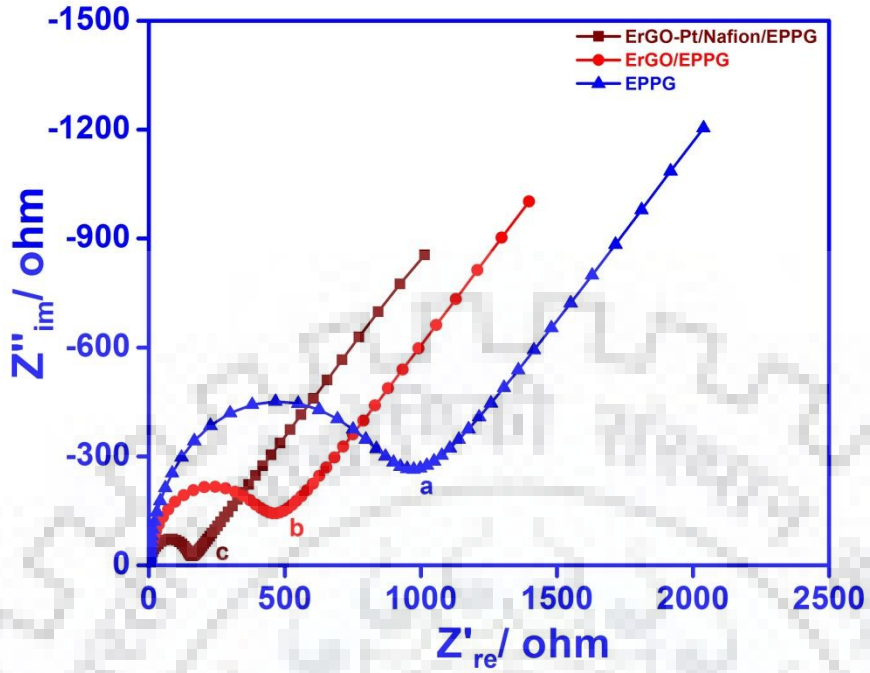

Fig. 3.2: EIS spectra observed for (a) unmodified EPPG, (b) ErGO/EPPG and (c) ErGO-Pt/Nafion/EPPG. The inset displays Randles equivalent circuit.

The effective electro-active surface area of the unmodified and modified sensors was calculated by the electrochemical method to evaluate the effect of modification. For this purpose, cyclic voltammograms of 2 mM $K_3[Fe(CN)_6]$ were recorded in 0.1 M KCl at different scan rates. The surface area was calculated from the slopes of i_p vs. $\nu^{1/2}$ plots using Randles-Sevcik equation and found as 0.087, 0.158 and 0.261 cm^2 for bare EPPG, ErGO/EPPG and ErGO-Pt/Nafion/EPPG surfaces, respectively. From the observed results it was concluded that the surface area of ErGO/EPPG and ErGO-Pt/Nafion/EPPG increased nearly 2 and 3 times more than that of the bare EPPG. Thus, the deposition of electrochemically reduced graphene oxide and grafting of the hybrid nanomaterial with ErGO on the surface of EPPG increased the active surface area.

3.3.2 Cyclic Voltammetry

Cyclic voltammograms of EFZ were recorded at bare EPPG, ErGO/EPPG and ErGO-Pt/Nafion/EPPG sensors in phosphate buffer of pH 7.2 using a scan rate of 100 mVs^{-1}. At bare EPPG, a weak irreversible anodic peak was noticed at 1234 mV, while in the case of ErGO/EPPG, a well-defined oxidation peak was observed at 1160 mV. However, after incorporation of the hybrid composite of platinum nano-particles and Nafion, the peak current of EFZ increased and shifted to less positive potentials. In the reverse scan, absence of reduction peak indicated that the

nature of oxidation process of EFZ is irreversible. From the cyclic voltammograms, it was observed that the ErGO-Pt/Nafion/EPPG exhibited better response in the terms of increase in the anodic peak current with a negative shift in the peak potential as compared to the bare and ErGO/EPPG. The result indicates that the hybrid nanocomposite grafted ErGO shows electrocatalytic activity towards the electrochemical oxidation of EFZ. The less aggregate or high surface area of ErGO, anchors the nano-particles composite and accelerates the kinetics of the electron transfer. As Nafion works as a conductive polymer and platinum nano particles as a nano-scale spacer; the grafting of metal nano particles and polymer increases the interlayer spacing between graphene sheets and conductivity of the composite material increases.

The nature of the electrode reaction has been ascertained by carrying out scan rate studies in the range of 10-200 mVs^{-1}. The peak of EFZ increased with the increase in the sweep rate. The linearity of i_p versus ν can be expressed by the relation:

$$\mathbf{i_p\ (\mu A) = 0.0983\ \nu - 0.8271} \qquad \mathbf{(R^2 = 0.991)}$$

In the relation, ν is the scan rate in mVs^{-1} and i_p the peak current in μA. The linearity of i_p versus scan rate (ν) plot indicated the adsorption controlled oxidation of EFZ at the ErGO-Pt/Nafion/EPPG which has further been confirmed by the linear plot obtained for log i_p vs. log ν. The linear dependence of log i_p on log ν as:

$$\mathbf{\log i_p = 1.0037 \log \nu - 1.0746}$$

having R^2 as 0.987 and slope value (> 0.5) further confirmed the adsorption controlled oxidation of EFZ [45,48].

3.3.3 Square Wave Voltammetry

To demonstrate the electrocatalytic activity of the modified sensor, the square wave voltammograms (SWV) were recorded at EPPG, ErGO/EPPG and ErGO-Pt/Nafion/EPPG in phosphate buffer of pH 7.2 containing 50 mM EFZ. At ErGO-Pt/Nafion/EPPG a well-defined peak at ~1106 mV was observed (**Fig. 3.3 c**), and can be assigned to the oxidation of nitrogen atom of the secondary amine of EFZ to give a free radical species as reported in the literature [21]. Under similar conditions, very small anodic peaks were observed at potential 1148 mV and 1120 mV at EPPG, ErGO/EPPG, respectively (**Fig. 3.3 a and b**). This behavior indicates that ErGO/EPPG also catalyzes the oxidation of EFZ, however, the extent of catalysis is lesser than that observed in the case of ErGO-Pt/Nafion/EPPG. The similar voltammetric response was observed for the PtNPs/EPPG and ErGO/EPPG while in the case of ErGO/Nafion/EPPG the increase in the peak

current was noticed but the increase was lesser than the one observed for ErGO-Pt/Nafion composite. Thus, it was observed that apart from increasing the effective surface area the hybrid nano composite also has strong electrocatalytic effect towards the oxidation EFZ. Therefore, the ErGO-Pt/Nafion modified EPPG sensor is used for the quantification of EFZ.

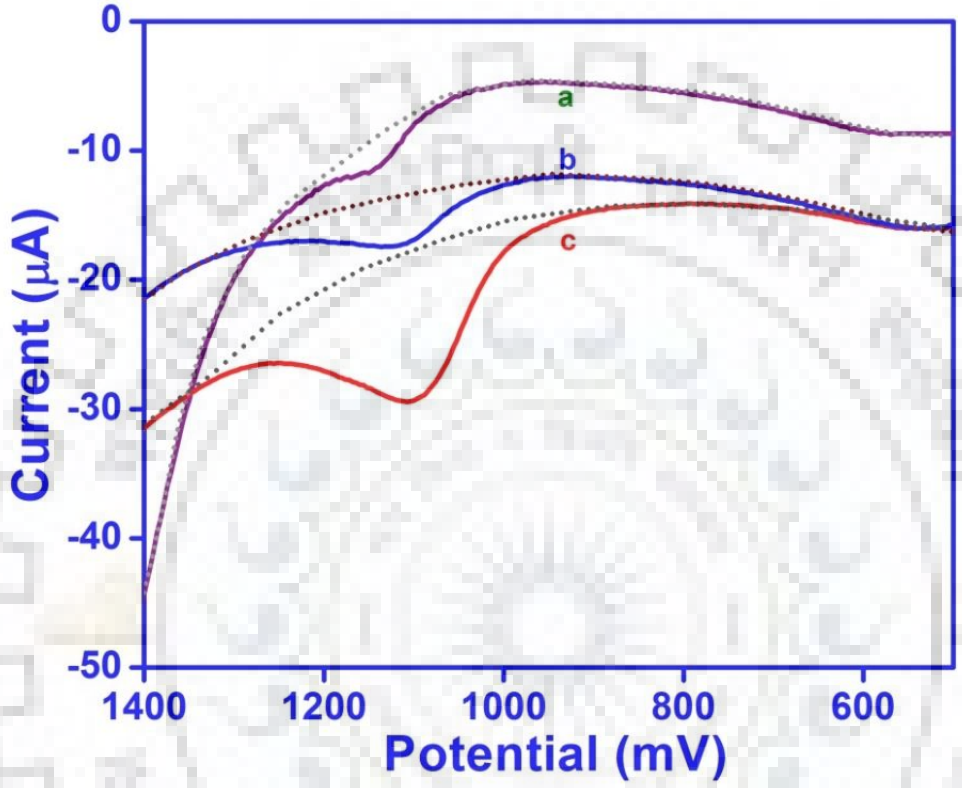

Fig. 3.3: Comparative Square wave voltammograms observed for 50 µM EFZ at (a) bare EPPG and (b) ErGO/EPPG (c) ErGO-Pt/Nafion/EPPG in phosphate buffer of pH 7.2. The background is represented by the dotted line.

3.3.3.1 Effect of pH

The influence of the pH on the peak current of EFZ was studied in the range 2.4-10.5 using ErGO-Pt/Nafion/EPPG sensor. It is observed that the E_p of EFZ shifts towards less positive potentials with an increase in the pH. The plot of E_p vs. pH was linear and the dependence of the peak potential on pH can be expressed as:

E_p (pH 2.4 – 10.5) = -58.386 pH + 1579.4 mV vs. Ag/AgCl (R^2 = 0.993)

The value of dE_p/pH observed was close to the Nernst value ~59 mV/pH, which clearly indicated the involvement of equal number of electrons and protons in the oxidation of EFZ.

3.3.3.2 Effect of square wave frequency

The effect of square wave frequency (f) on the peak current (i_p) of EFZ was examined in the range of 5-50 Hz using ErGO-Pt/Nafion/EPPG at pH 7.2. The peak current was found to linearly increase with increase in frequency in the range 5-50 Hz. The relation between the peak current and square wave frequency can be expressed by the relation:

$$\mathbf{i_p/\mu A = 0.384\ f + 1.6529 \qquad (R^2 = 0.994)}$$

where i_p and [f] are peak current in μA and square wave frequency in Hz, respectively. The linear dependence of the peak current on frequency suggested the adsorption controlled oxidation of EFZ, which was further confirmed by drawing a plot between log (i_p) and log (f). The linear relation between log (i_p) vs. log (f):

$$\mathbf{\log i_p = 0.8363 \log f\ - 0.1073 \qquad (R^2 = 0.998)}$$

The slope value of log (i_p) vs. log (f) was found to be > 0.5 and further confirmed that an adsorption controlled oxidation of EFZ.

3.3.3.3 Effect of concentration

The quantitative determination of EFZ was carried out at ErGO-Pt/Nafion/EPPG in phosphate buffer of pH 7.2 keeping methanol concentration constant. The square wave voltammograms were recorded in the concentration range 0.05-150 μM. The current values were calculated by subtracting the background current and an average of at least three replicate determinations was used to plot the calibration curve. The peak current increased with increase in the concentration of EFZ (**Fig. 3.4**).

The plot of i_p vs. [C] was linear and the dependence can be expressed by the relation:

$$\mathbf{i_p\ (\mu A) = 0.215\ [C\ 0.05 - 150\ \mu M] + 2.0103 \qquad (R^2 = 0.997)}$$

where, i_p is the peak current and C is the concentration (μM). The sensitivity of the proposed method is found to be 0.215 $\mu A \mu M^{-1}$. The limit of detection (L.O.D.) and limit of quantification (L.O.Q.) were calculated by using the formula 3 σ/b and 10 σ/b, where σ represents the standard deviation of the blank solution and b slope of the calibration curve. The values of L.O.D. and L.O.Q. were found to be 1.8 nM and 6.0 nM, respectively. The validation characteristics of the proposed method are shown in the **Table 1**. Due to the low detection limit of EFZ at ErGO-Pt/Nafion/EPPG the proposed sensor can be successfully used for the determination of EFZ in pharmaceutical formulations as well as in biological fluids [49].

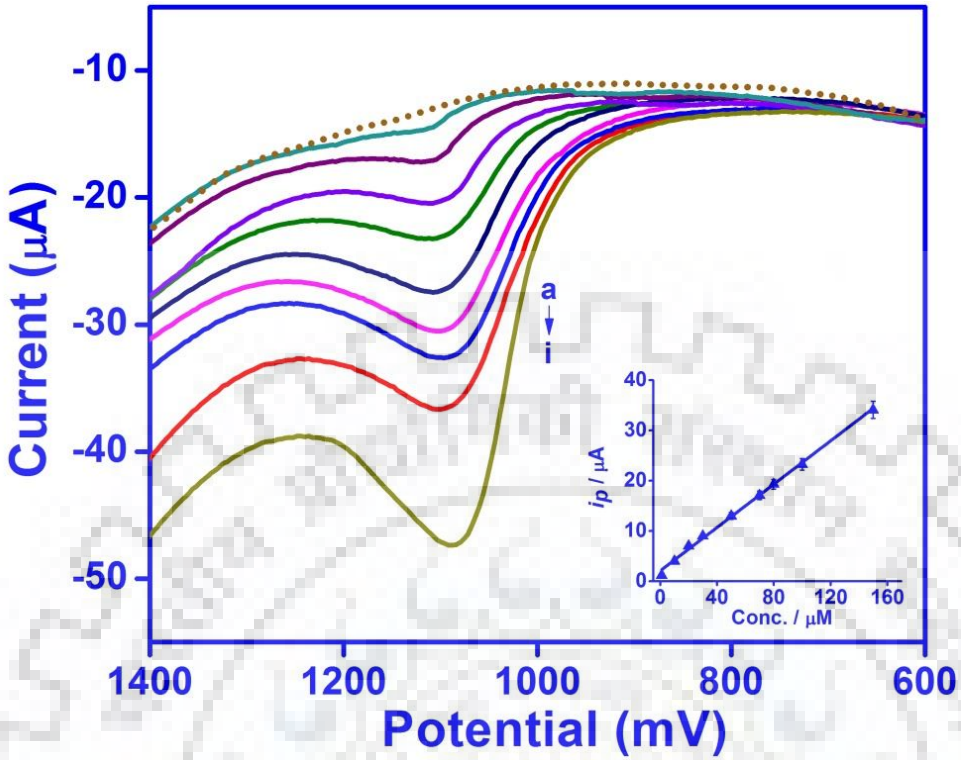

Fig. 3.4: Square wave voltammograms observed for (a)1; (b) 10; (c) 20; (d) 30; (e) 50; (f) 70; (g) 80; (h) 100 and (i) 150 μM EFZ. Inset is the linear calibration plot observed for EFZ at ErGO-Pt/Nafion/EPPG. The background is represented by the dotted line.

Table 1: Validation characteristics of ErGO-Pt/Nafion/EPPG sensor for the determination of EFZ.

S.No.	Validation Parameters	ErGO-Pt/Nafion/EPPG
1	**Concentration range (μM)**	0.05–150 μM
2	**Correlation coefficient (R^2)**	0.997
3	**Detection limit (nM)**	1.8
4	**Limit of quantification (nM)**	6.0
5	**Bias% of peak current**	0.00179%
6	**Sensitivity (μA/μM)**	0.215
7	**Standard error of slope (α, 0.05)**	±0.00543
8	**Standard error of intercept (α, 0.05)**	±0.39528

3.3.4 Analytical utility

3.3.4.1 Interference study

To evaluate the selectivity of the proposed method in biological fluids, the influence of potentially interfering substances such as ascorbic acid (AA), uric acid (UA) and xanthine (XT) on the determination of EFZ was investigated. The tolerance limit for the interferents was considered as the maximum concentration that gave a relative error less than ±5.0% in the oxidation peak current of the drug. The interference study was carried out for EFZ fixed at 10 µM at pH 7.2 and the concentration of interferents up to 100-fold excess was varied. **Fig. 3.5** presents the effect of high concentration of potential interfering substances (AA, UA and XT) on the voltammograms of EFZ. It can be seen that EFZ exhibited an anodic peak at 1106 mV and well defined and separate peaks at ~ 54, 306, 692 mV corresponding to the oxidation of interferents AA, UA and XT. From the results, it was observed that up to 100 fold concentrations of the major interfering biological metabolites, no substantial change in the anodic peak response of EFZ was noticed. This proved that the ErGO-Pt/Nafion/EPPG sensor can be successfully applied for the determination of EFZ in biological fluids without any complexity.

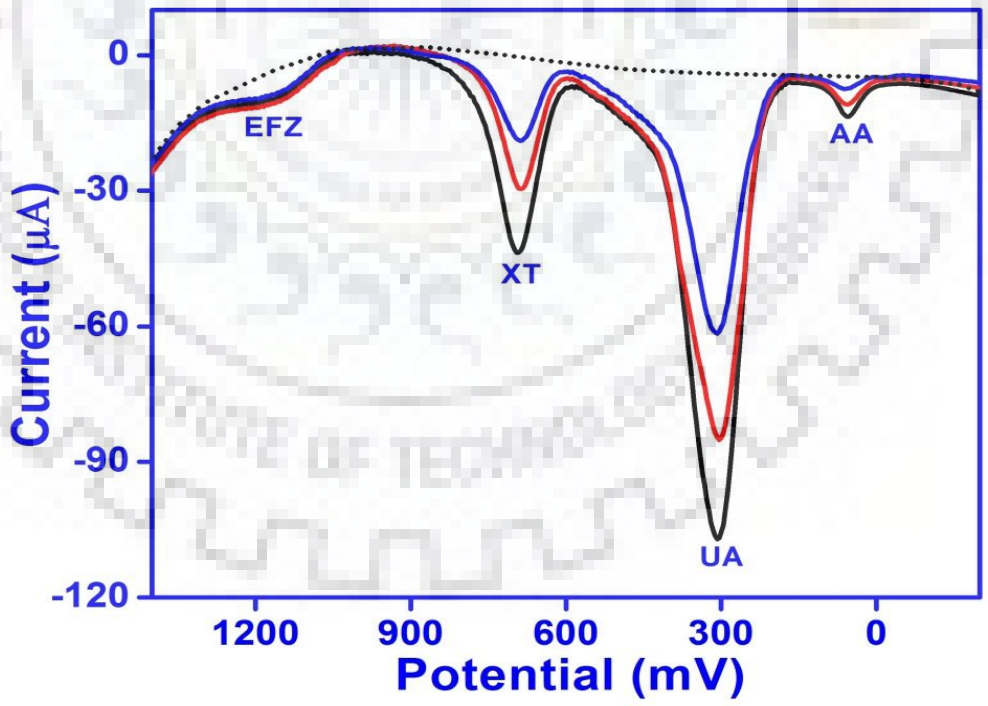

Fig. 3.5: SWVs recorded for 10 µM EFZ in presence of xanthine (XT), uric acid (UA) and ascorbic acid (AA). The background is represented by the dotted line.

3.3.4.2 Stability and reproducibility of ErGO-Pt/Nafion/EPPG sensor

The development of a sensor having long term stability, excellent sensitivity and reproducibility is the need of routine clinical and industrial applications in view of the growing demand of anti HIV compounds. The long term stability of ErGO-Pt/Nafion/EPPG was investigated by determining the current response for EFZ (10 μM) at pH 7.2 for a period of 30 days. The sensor was stored at the room temperature of 22 ± 2 ºC and used daily for recording voltammogram. It is observed that for the first 25 days the peak current values do not show significant variation and a R.S.D. of 1.85% is observed. However, after 25 days, the current values showed a significant decrease and the R.S.D. increased to >5%. This clearly indicates that the modified sensor is sufficiently stable for at least 25 days.

The intraday reproducibility of ErGO-Pt/Nafion/EPPG was examined by recording six voltammograms in the solution containing 10 μM EFZ at an interval of 1 h in same day. The observed results indicate practically very little variation in the i_p. The R.S.D was ± 1.08% for the repetitive measurements (n=4) and ± 1.78% for intraday measurements (n=5). Thus, it is concluded that the ErGO-Pt/Nafion/EPPG exhibit excellent stability, reproducibility and repeatability for EFZ detection.

3.3.4.3 Pharmaceutical analysis

To test the applicability of the proposed method in anti HIV drugs, quantitative analysis of EFZ in three commercially available pharmaceutical formulations viz. Efavir-600 mg (Cipla limited), Efcure-200 mg (Emcure pharmaceutical Ltd.) and Efferven-200 mg (Ranbaxy Laboratories Ltd.) was carried out using ErGO-Pt/Nafion/EPPG sensor. The prepared methanolic solution of the tablet was diluted with buffer (pH 7.2) so that the concentration of the drug lies in the range of working concentration range. SWVs were then recorded under optimized parameters and the concentration of the drug in the corresponding tablets was analyzed, keeping the dilution factor into consideration. As demonstrated in **Table 2**, it can be seen that the calculated results were in good agreement with the labelled amount stated by the manufacturers. The EFZ content for all the pharmaceutical samples were within an error range of ~0.2% to 0.8% and demonstrated good accuracy and precision of the proposed method.

Table 2: Determination of EFZ in pharmaceutical samples using ErGO-Pt/Nafion/EPPG sensor.

Sample	Stated content (mg)	Determined content (mg)	Error %	Bias %
Efavir	600	598.73	0.21	0.214
Efcure	200	199.17	0.41	0.413
Efferven	200	198.39	0.82	0.821

*The R.S.D. value for EFZ determination was less than 2.13% for n =3.

3.3.4.4 Spiked sample assay

The presence of EFZ drug in patient's biological fluid for a long time has been assigned to the treatment failure and central nervous system (CNS) side effects, which are associated with the low and high EFZ plasma levels [8]. It has also been reported that the virological failure observed in the patients having low EFZ levels (< 1000 µg/l), while CNS toxicity was almost three times more frequent in patients with high EFZ levels (> 4000 µg/l) as compared to the patients with 1000 ± 4000 µg/l [8,10]. Hence, for the dose adjustment and to optimize the treatment, it is worthwhile to analysis the EFZ concentration in the patient plasma and urine samples. However, we could not get samples of plasma and urine of the patients undergoing treatment with EFZ. Hence, an attempt to study the recovery experiments was performed in plasma and urine sample of healthy volunteers.

Prior to analysis, the urine and plasma samples were diluted 10 times and 2 times respectively, with phosphate buffer (pH 7.2) to decrease the matrix complexity. Diluted samples were then spiked with the known concentration of EFZ and square wave voltammograms were recorded using optimized parameters. In all the cases a well-defined peak was observed having E_p~1106 mV corresponding to the oxidation of EFZ. In the case of urine samples, uric acid peak was also observed at 350 mV, but the presence of this biological substance in the urine did not interfere in the determination of the drug as the E_p of EFZ was well separated. Similarly AA and HT did not show any interference with the peak of EFZ. The concentration of EFZ was calculated using regression equation of the calibration plot for ErGO-Pt/Nafion/EPPG and observed results are summarized in **Tables 3** and **4**. The recovery of the spiked samples is varied in the range 98.80% to 101.0% in the case of plasma and from 98.0% to 102.0% in the case of urine. The results indicated that the proposed sensor can be utilized successfully for the determination of EFZ in the human body fluids with adequate accuracy**.**

Table 3: Results observed for EFZ in human plasma sample at ErGO-Pt/Nafion/EPPG sensor.

Sample 1			Sample 2		
Spiked (µM)	**detected (µM)**	**Recovery* (%)**	**Spiked (µM)**	**detected (µM)**	**Recovery * (%)**
1.0	1.01	101.00	10	9.93	99.30
2.5	2.47	98.80	15	14.88	99.20
5.0	4.98	99.60	25	25.17	100.68

*The R.S.D. value for the determination was less than 1.17% for n=3.

Table 4: Results observed for EFZ in human urine sample at ErGO-Pt/Nafion/EPPG sensor.

Sample 1			Sample 2		
Spiked (µM)	**detected (µM)**	**Recovery* (%)**	**Spiked (µM)**	**detected (µM)**	**Recovery * (%)**
0.5	0.49	98.00	1	0.99	99.00
1.5	1.53	102.00	5	4.97	99.40
2.5	2.48	99.20	10	10.13	101.30

*The R.S.D. value for the determination was less than 1.58% for n=3.

3.4 CONCLUSION

In this work, an electrochemically reduced graphene oxide grafted with hybrid nano-composite of PtNPs and Nafion modified EPPG based sensor has been fabricated for the ultra-sensitive determination of EFZ. Morphological studies of the prepared sensor illustrated that Nafion, acts as a dispersant, strongly adsorbed by the hydrophobic interaction on to the surface of ErGO followed by a uniform distribution of Pt nanoparticles. This increases the spacing between the neighbouring ErGO sheets and results a more available active surface for the adsorption. The grafting of the hybrid nano-composite with ErGO electro-catalyse the kinetics of the reaction and a significant enhanced current response and reduced the anodic peak potential of EFZ. The present sensor was efficient to detect nano-concentration of EFZ, even in the presence of potential electro-active interferents with good recovery limits for the direct determination in the biological fluids and pharmaceutical formulations. A sufficiently wide linear relationship between the EFZ concentration and the current response was obtained at ErGO-Pt/Nafion/EPPG sensor with excellent reproducibility and a low detection limit of 1.8 nM. The fabricated sensor exhibited good

stability, high sensitivity, reproducibility and the fabrication procedure was simple. A comparison of the presented sensor with recently reported in the literature is shown in **Table. 5**.

Table: 5. Comparison of the linear range and detection limit of EFZ at proposed ErGO-Pt/Nafion/EPPG with reported analytical methods.

S. No	Electrode	Method used	Concentration range (µM)	LOD (nM)	Analytical Sample	Reference
1	TFME	DPASV	0.03-0.79	3	No	4
2	PGE	DPASV	0.05- 8.11	13.3	Pharmaceutical	20
	dsDNA/PGE	DPV	6.33-7.60	1900	Pharmaceutical	20
3	NiO-ZrO_2 /GCE	CV	0.01-10	1.4	Pharmaceutical, urine	21
4	ErGO-Pt/Nafion/EPPG	SWV	0.05-150	1.8	Pharmaceutical, urine, plasma	Present work

* DPASV- Differential pulse adsorptive stripping voltammetry, DPV- Differential pulse voltammetry, CV- cyclic voltammetry, SWV- square wave voltammetry.

It can be clearly seen that the proposed sensor provides an excellent platform for EFZ oxidation and detection. It is believed that the developed sensor will provide high level of quality control of these drugs in pharmaceutical industries.

3.11 REFERENCES

[1] M.M. Bastos, C. Costa, T.C. Bezerra, F. Silva, N. Boechat, "Efavirenz a nonnucleoside reverse transcriptase inhibitor of first-generation: Approaches based on its medicinal chemistry", Eur. J. Med. Chem. 108 (2016) 455.

[2] M. Sadeghi, M. Bayat, S. Cheraghi, K. Yari, R. Heydari, S. Dehdashtian, M. Shamsipur, "Binding studies of the anti-retroviral drug, efavirenz to calf thymus DNA using spectroscopic and voltammetric techniques", Luminescence 31 (2016) 108.

[3] M. Wei, B. Kost, I.R. Muller, E. Wolf, I. Mylonas, A. Bruning, "Efavirenz Causes Oxidative Stress, Endoplasmic Reticulum Stress, and Autophagy in Endothelial Cells", Cardiovasc Toxicol 16 (2016) 90.

[4] A.A. Castro, M. Souza, N.A. Rey, P. Farias, "Determination of Efavirenz in Diluted Alkaline Electrolyte by Cathodic Adsorptive Stripping Voltammetry at the Mercury Film Electrode", J. Braz. Chem. Soc. 22 (2011) 1662.

[5] D.W. Haas, H.J. Ribaudo, R.B. Kim, C. Tierney, G.R. Wilkinson, R.M. Gulick, D.B. Clifford, T. Hulgan, C. Marzolini, E.P. Acosta, "Pharmacogenetics of efavirenz and central nervous system side effects: an Adult AIDS Clinical Trials Group study", AIDS 18 (2004) 2391.

[6] A.I. Veldkamp, M. Harris, J. Montaner, G. Moyle, B. Gazzard, M. Youle, M. Johnson, M.O. Kwakkelstein, H. Carlier, R.V. Leeuwen, J.H. Beijnen, J. Lange, P. Reiss, R. Hoetelmans, "The Steady-State Pharmacokinetics of Efavirenz and Nevirapine When Used in Combination in Human Immunodeficiency Virus Type 1-Infected Persons", J. Infect. Dis. 184 (2001) 37.

[7] D.Y. Cho, E.T. Ogburn, D. Jones, Z. Desta, "Contribution of N-Glucuronidation to Efavirenz Elimination In Vivo in the Basal and Rifampin-Induced Metabolism of Efavirenz", Antimicrob. Agents Chemother. 55 (2011) 1504.

[8] C. Marzolini, A. Telenti, L.A. Decosterd, G. Greub, J. Biollaz, T. Buclin, "Efavirenz plasma levels can predict treatment failure and central nervous system side effects in HIV-1-infected patients", AIDS 15 (2001) 71.

[9] A. Carr, D.A Cooper, "Adverse effects of antiretroviral therapy", The Lancet 356 (2000) 1423.

[10] A. Abdissa, L. Wiesner, H. McIlleron, H. Friis, A.B. Andersen, P. Kaestel, "Evaluation of an immunoassay for determination of plasma efavirenz concentrations in resource-limited settings", J. Int. AIDS Soc. 17 (2014) 1.

[11] B. Prathap, A. Dey, G.S. Rao, S. Vennela, S. Hussain, "Method Development and Validation of Efavirenz in Bulk and Pharmaceutical Dosage Form by UV Spectrophotometer", Int. J. Innovative Phar. Research 4 (2013) 269.

[12] N.P. Reddy, Y. Padmavathi, P. Mounika, A. Anjali, "FTIR spectroscopy for estimation of efavirenz in raw material and tablet dosage form", Int. Curr. Pharm. J. 395 (2015) 390.

[13] G. Ramachandran, A.K.H. Kumar, S. Swaminathan, P. Venkatesana, V. Kumaraswami, D.J. Greenblatt, "Simple and rapid liquid chromatography method for determination of efavirenz in plasma", J. Chromatogr. B 835 (2006) 131.

[14] A. Theron, D. Cromarty, M. Rheeders, M. Viljoen, "Determination of salivary efavirenz by liquid chromatography coupled with tandem mass spectrometry", J. Chromatogr. B 878 (2010) 2886.

[15] A. Behera, D.G. Sankar, S.K. Moitra, S.C. Si, "Development and validation of a rplc method for dissolution test of efavirenz tablets and its application to drug quality control studies", Asian J. Pharm Clin Res 6 (2013) 180.

[16] P. Srivastava, G.S. Moorthy, R. Gross, J.S. Barrett, "A Sensitive and Selective Liquid Chromatography/ Tandem Mass Spectrometry Method for Quantitative Analysis of Efavirenz in Human Plasma", Plos One 8 (2013) 1.

[17] P. Srilatha, N.K. Sathish, B.P. Kumar, "Quantitative determination of Efavirenz in bulk drug and formulation by colorimetry", Adv. App. Sci. Research 5 (2014) 176.

[18] M. Satyanarayana, K.Y. Goud, K.K. Reddy, K.V. Gobi, "Biopolymer Stabilized Nanogold Particles on Carbon Nanotube Support as Sensing Platform for Electrochemical Detection of 5-Fluorouracil invitro", Electrochim. Acta 178 (2015) 608.

[19] P. Gupta, S.K. Yadav, B. Agrawal, R.N. Goyal, "A novel graphene and conductive polymer modified pyrolytic graphite sensor for determination of propranolol in biological fluids", Sens. Actuator B 204 (2014) 791.

[20] B.D. Topal, B. Uslu, S.A. Ozkan, "Voltammetric studies on the HIV-1 inhibitory drug Efavirenz: The interaction between dsDNA and drug using electrochemical DNA biosensor and adsorptive stripping voltammetric determination on disposable pencil graphite electrode", Biosens. Bioelectron 24 (2009) 2358.

[21] N. Thapliyal, N.S.E. Osman, H. Patel, R. Karpoormath, R.N. Goyal, T. Moyo, R. Patel, "NiO–ZrO_2 nanocomposite modified electrode for the sensitive and selective determination of efavirenz, an anti-HIV drug", RSC Adv. 5 (2015) 40057.

[22] B. Bozal, B. Uslu, S.A. Ozkan, "A Review of Electroanalytical Techniques for Determination of Anti-HIV Drugs", Int. J. Electrochem. 2011 (2011) 1.

[23] H.I. Rasool, C. Ophus, W.S. Klug, A.Z.K. Gimzewski, "Measurement of the intrinsic strength of crystalline and polycrystalline graphene", Nat. Commun. 4 (2013) 1.

[24] M.Y. Han, B.O. Zyilmaz, Y. Zhang, P. Kim, "Energy Band-Gap Engineering of Graphene Nanoribbons", Phys. Rev. Lett. 98 (2007) 1.

[25] C. Lee, X. Wei, J.W. Kysar, J. Hone, "Measurement of the Elastic Properties and Intrinsic Strength of Monolayer Graphene", Science 321 (2008) 385.

[26] T. Gan, S. Hu, "Electrochemical sensors based on graphene materials", Microchim Acta 175 (2011) 1.

[27] J. Liu, J. Tanga, J.J. Gooding, "Strategies for chemical modification of graphene and applications of chemically modified graphene", J. Mater. Chem. 22 (2012) 12435.

[28] Y.Xu, H. Bai, G. Lu, C. Li, G. Shi, "Flexible Graphene Films via the Filtration of Water-Soluble Noncovalent Functionalized Graphene Sheets", J. Am. Chem. Soc. 130 (2008) 5856.

[29] T. Cassagneau, J.H. Fendler, "High Density Rechargeable Lithium-Ion Batteries Self-Assembled from Graphite Oxide Nanoplatelets and Polyelectrolytes", Adv. Mater. 10 (1998) 877.

[30] A. Valipour, N. Hamnabard, Y. Ahn, "Performance evaluation of highly conductive graphene (RGOHI–AcOH) and graphene/metal nanoparticle composites (RGO/Ni) coated on carbon cloth for super-capacitor applications", RSC Adv. 5 (2015) 92970.

[31] S. Gilje, S. Han, M. Wang, K.L. Wang, R.B. Kaner, "A Chemical Route to Graphene for Device Applications", Nano Lett. 7 (2007) 3394.

[32] A.M. Zande, R.A. Barton, J.S. Alden, C.S. Vargas, W.S. Whitney, P.H.Q. Pham, J. Park, J.M. Parpia, H.G. Craighead, P.L. McEuen, "Large-Scale Arrays of Single-Layer Graphene Resonators", Nano Lett. 10 (2010) 4869.

[33] K. Chen, Z. Zhang, Y. Liang, W. Liu, "A Graphene-Based Electrochemical Sensor for Rapid Determination of Phenols in Water", Sensors 13 (2013) 6204.

[34] C. Shan, H. Yang, D. Hana, Q. Zhang, A. Ivaskab, L. Niu, "Graphene/AuNPs/chitosan nanocomposite film for glucose biosensing", Biosens. Bioelectron 25 (2010) 1070.

[35] J. Ping, Y. Wang, Y. Ying, J. Wu, "Application of Electrochemically Reduced Graphene Oxide on Screen-Printed Ion-Selective Electrode", Anal. Chem. 84 (2012) 3473.

[36] K. Pokpas, S. Zbeda, N. Jahed, N. Mohamed, P.G. Baker, E.I. Iwuoha, "Electrochemically reduced graphene oxide pencil-graphite in situ plated bismuth-film electrode for the determination of trace metals by anodic stripping voltammetry", Int. J. Electrochem. Sci. 9 (2014) 736.

[37] L. Liu, Y. Gou, X. Gao, P. Zhang, W. Chen, S. Feng, F. Hu, Y. Li, "Electrochemically reduced graphene oxide-based electrochemical sensor for the sensitive determination of ferulic acid in A. sinensis and biological samples", Mater. Sci. Eng. C 42 (2014) 227.

[38] S. Stankovich, D.A. Dikin, G.H.B. Dommett, K.M. Kohlhaas, E.J. Zimney, E.A. Stach, R.D. Piner, S.T. Nguyen, R.S. Ruoff, "Graphene-based composite materials", Nature 442 (2006) 282.

[39] M. Li, X. Bo, Z. Mu, Y. Zhang, L. Guo, "Electro-deposition of nickel oxide and platinum nanoparticles on electrochemically reduced graphene oxide film as a nonenzymatic glucose sensor", Sens. Actuator B 192 (2014) 261.

[40] Z.L. Zhou, T.F. Kang, Y. Zhang, S.Y. Cheng, "Electrochemical sensor for formaldehyde based on Pt–Pd nanoparticles and a Nafion-modified glassy carbon electrode", Microchim Acta 164 (2009) 133.

[41] Y. Liu, L. Gao, J. Sun, Y. Wang, J. Zhang, "Stable Nafion-functionalized graphene dispersions for transparent conducting films", Nanotechnology 20 (2009) 465605.

[42] E. Er, H. Celikkan, N. Erk, M.L. Aksu, "A new generation electrochemical sensor based on Graphene nanosheets/Gold nanoparticles/Nafion nanocomposite for determination of Silodosin", Electrochim. Acta 157 (2015) 252.

[43] Y. Si, E.T. Samulski, "Exfoliated Graphene Separated by Platinum Nanoparticles", Chem. Mater. 20 (2008) 6792.

[44] D.C. Marcano, D.V. Kosynkin, J.M. Berlin, A. Sinitskii, Z. Sun, A. Slesarev, L.B. Alemany, W. Lu, J.M. Tour, "Improved Synthesis of Graphene Oxide", ACS-Nano 4 (2010) 4806.

[45] P. Gupta, R.N. Goyal, "Graphene and Co-polymer composite based molecularly imprinted sensor for ultratrace determination of melatonin in human biological fluids", RSC Adv. 5 (2015) 40444.

[46] Rosy, S.K. Yadav, B. Agrawal, M. Oyama, R.N. Goyal, "Graphene modified Palladium sensor for electrochemical analysis of norepinephrine in pharmaceuticals and biological fluids", Electrochim. Acta 125 (2014) 622.

[47] W. Liao, C. Guo, L. Sun, Z. Li, L. Tian, J. He, J. Li, J. Zheng, Z. Ma, Z. Luo, C. Chen, "The Electrochemical behavior of nafion/reduced graphene oxide modified carbon electrode surface and its application to ascorbic acid determination", Int. J. Electrochem. Sci. 10 (2015) 5747.

[48] M. Purushotham, P. Gupta, R.N. Goyal, "Graphene modified glassy carbon sensor for the determination of aspirin metabolites in human biological samples", Talanta 143 (2015) 328.

[49] "Validation of Analytical Methods: Definitions and Terminology", (1995) 1. CPMP/ICH/381/95,http://www.ema.europa.eu/docs/en_GB/document_library/Scientific_guideline/2009/09/WC500002662.pdf.

Chapter 4

Graphene based sensors for the determination of biomolecules

4.1 INTRODUCTION

In the last decade, nano-materials have attracted considerable attention due to their outstanding features, such as elasticity, mechanical strength, good thermal and electrical conductivity, large surface area and biocompatibility [1,2]. Graphene (GR), a carbon based nanomaterial gives better dispersion and compatibility with several other materials, such as conducting polymers, metal based nanoparticles and solvents, hence, provide increased biocompatibility with biological recognition elements, which significantly helps in the quantitative analysis of biomolecules. Conducting polymers (CP) also have unique electrochemical and electrical conductivity. The properties of conducting polymers can be strongly improved by combining some other dopants or nano-materials in the polymer matrix and the resulting material is known as polymer nanocomposite (PNC). The present chapter describes the synthesis, characterization and application of two different types of polymer nanocomposites based on graphene and graphene nanoribbons. On the combination of graphene with the conducting polymer, the aggregation of graphene sheets can be overcome and π-π stacking interaction significantly increases, hence, enhanced sensitivity and stability is witnessed [3,4]. The chapter has been divided into two sections: In the **first section,** the synergistic interaction between graphene and poly-4-amino-3-hydroxy-1-naphthalenesulfonic acid (AHNSA) at the screen printed surface has been exploited for simultaneous analysis of dopamine and serotonin. The **second section** describes the preparation of graphene nanoribbons coated with polymer of bromocresol green at the pyrolytic graphite surface for the simultaneous determination of the metabolites of dopamine and serotonin viz. 3,4-Dihydroxyphenylacetic acid and 5-Hydroxyindoleacetic acid.

4.2 SECTION A: Graphene based sensor for the simultaneous determination of dopamine and serotonin.

Nano-materials have attracted tremendous attention in recent years due to their unique physical, structural and electronic properties. GR, is a single-atom thick, extensively conjugated two dimensional carbonaceous nano-material with sp^2 hybridized carbon atoms attached in a six membered arrangement through weak π-π interactions [3,4]. In addition, the application of conducting polymers for modification of the surface of the electrode has been found to increase electrical conductivity, great chemical stability, better magnetic property, high electronic affinities, optical properties and low ionization potential [5]. Conducting polymer of 4-amino-3- hydroxy-1-naphthalenesulfonic acid (AHNSA) has been used with GR to overcome the aggregation of

graphene sheets and enhance stability and sensitivity [6]. The use of conducting polymer for the surface modification on one hand increases the conductivity of the surface, whereas, on the other hand the synergistic interaction between AHNSA polymer and graphene via π-π stacking interaction causes a large net stabilized structure, shorter ion diffusion paths and π-π interaction that encourages the electron transport [6,7].

Screen-printed carbon sensors (SPCs) have attracted enormous attention of researchers in the recent years due to their superiority over the common sensors as they are field-based size, portable, simple in fabrication and cost effective. As SPCs are less expensive they can be easily replaced after each run. SPCs have a very small working area which is highly suitable for the trace volume of determining species. SPCs are simple to operate, reliable and provide high sensitivity, better selectivity and good reproducibility [8,9].

Dopamine [4-(2-aminoethyl) benzene-1,2-diol, DA, **Scheme 1**] is the predominant catecholamine neuro-transmitter and has been extensively found in the tissues of mammalian brain and plays a significant role as a modulator of hormone secretion, cardio-vascular function, renal function, catecholamine release, vascular tone and gastrointestinal motility in mammals. Some other physiological functions, such as, motivation and reward, control of the movement of information in the brain, voluntary movement are also regulated by this catecholamine [10–12]. Dysregulation of dopaminergic transmission has been associated with neurological disorders like Parkinson's disease, Schizophrenia, Tourette's syndrome and many more [13,14]. DA also performs as a biochemical precursor of other catecholamine neurotransmitters norepinephrine and epinephrine [15]. The determination of DA has been considered useful in the diagnosis of several diseases and hence, makes it the choice of biologically and pharmacologically oriented research.

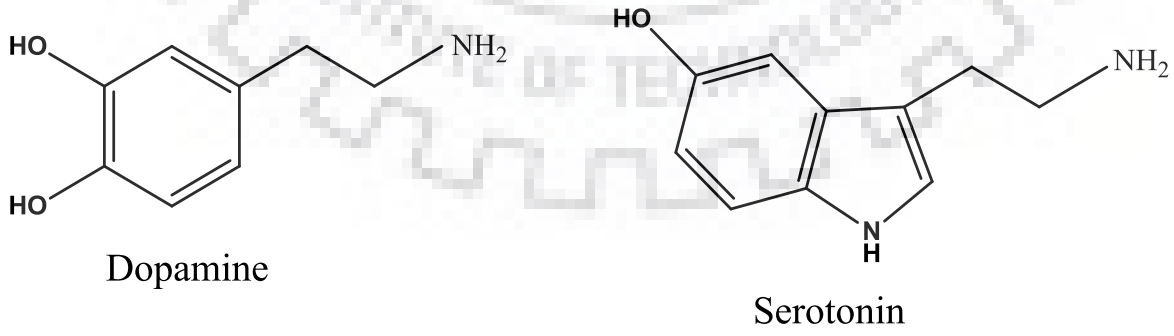

Scheme 1: Chemical structure of Dopamine and Serotonin.

Serotonin (5-hydroxytryptamine, 5-HT, **Scheme 1**), is a biogenic monoamine neurotransmitter and neuromodulator [16] found in the human brain [17], which plays a pivotal role to control and regulate various physiological functions such as eating disorder, sleep, muscle contraction, sexual activity and thermoregulation as well as in psychopathological processes such as anxiety disorder, liver regeneration, infantile autism, alcoholism, obsessive-compulsive disorder and drug dependency [5,18].

5-HT is synthesized in human system from an essential amino acid tryptophan by the enzyme tryptophan hydroxylase − I (TpH-1) and widely distributed in the central and peripheral nervous systems, smooth muscles, and platelets in the body. The large amount is localized in the enterochromaffin (EC) cells of gastrointestinal tract; (~90% of the whole 5-HT content of the body), whereas, platelets contain (~8%), and the rest amount is located in brain (central nervous system ~1%) [19]. 5-HT is involved in several gastrointestinal disorders including secretion, irritable bowel syndrome, food hypersensitivity and inflammatory bowel disease [20].

Research demonstrates that the respective release of DA and 5-HT influence each other [21]. Thus, simultaneous determination of DA and 5-HT is of considerable importance, since both coexists in the biological systems. Several analytical methodologies have been developed for the simultaneous determination of DA and 5-HT in the pharmaceutical and biological samples including HPLC [22], liquid chromatography [23], capillary electrophoresis [24], reverse-phase ion-pair HPLC with electrochemical detection [25], TLC [26] and mass spectrometry [27]. DA has also been studied at conducting polymer modified surfaces, whereas, little attention has been paid to 5-HT [28,29]. However, these methods have various limitations, such as poor selectivity and sensitivity, large analysis time and requirement of expensive instrumentation, thus there is need of a rapid, accurate and more sensitive technique. Electrochemical techniques are feasible for the estimation of electroactive compounds due to the advantages such as high sensitivity, better selectivity, low-cost apparatus, accuracy, ease of instrument, rapid response, simplicity and remarkable reproducibility [30,31]. The simultaneous measurement of these neurotransmitters is remained a challenge due to the inability of most of the electrodes to separate the oxidation potentials of these two species significantly enough to allow their accurate determination.

In this section, the simultaneous determination of DA and 5-HT is reported in human biological fluids and pharmacological formulations by using graphene and p-AHNSA composite

modified Screen-printed carbon sensor (SPCs). The fabricated sensor was able to sense and separate the two analytes from the common interfering electro-active species present in biological samples. The proposed method is simple and has low detection limits, which indicate the superiority of this technique over the methods reported in the recent years.

4.2.1 EXPERIMENTAL

4.2.1.1 Instrumentation

Screen printed carbon (SPCs) sensor having all in one electrode was used for the electrochemical experiments. For the screen printing of the SPCs, carbon and silver inks (Jujo Chemical, Japan) were used. The polystyrene-based film was used to print the working electrode (area = 0.07 cm^2) by using BANDO Industrial, Korea, screen printer. The SPCs were fabricated in the chemistry laboratory of Pusan National University, South Korea and were received as a gift. The working electrode of SPCs were modified with GR/p-AHNSA, an Ag/AgCl as a reference and carbon was used as a counter electrode. The instrument used for voltammetric studies and characterization techniques were essentially similar to that described in the section A of the chapter 2.

4.2.1.2 Chemicals and Reagents

Dopamine (DA), 5-hydroxytryptamine (5-HT), tryptophan (Trp), 4-amino-3-hydroxy-1-naphthalene sulfonic acid, ascorbic acid (AA), uric acid (UA) and graphite powder (< 20 nm) were purchased from Sigma-Aldrich (USA).

4.2.1.3 Preparation of GR/p-AHNSA modified SPCs

The improved Hummers method was used to synthesize GR from the graphite [32]. Powder XRD and Raman spectroscopic were applied for the characterization the GR and the results were obtained as reported earlier [30,33]. Before using the SPCs for recording the voltammograms, a drop of 0.1 M $FeCl_3$ solution was touched at the reference electrode. This procedure oxidized Ag into Ag/AgCl to avoid any interference of Ag particles in the experimental studies. Now cyclic voltammetry was used to scan the electrode between the potential ranges of −200 mV to +600 mV in 0.1 M HNO_3, where no peak was observed which confirmed the absence of Ag particle at SPCs. The suspension of the graphene at a concentration of 0.7 $mgmL^{-1}$ was prepared in a mixture of double distilled water and DMF (1:9). The optimum amount of graphene (6 µL) was dropped onto

the surface of the working electrode of SPCs and then SPCs were kept in an oven at 50–60 °C for 30 min to dry. The GR modified SPCs was dipped in a solution containing 2 mM of AHNSA in 0.1 M nitric acid solution and the polymeric layer was grown by scanning the potentials three times from −0.8 V to +2.0 V at a scan rate of 100 mVs^{-1}. The obtained polymer modified surface was rinsed with double distilled water and was characterized with the help of FE-SEM.

4.2.1.4 Voltammetric procedure and sample preparation

Stock solutions of 1 mM of DA and 5-HT were prepared in required amount of double distilled water. For the preparation of the standard concentration of analytes, desired volume of the analyte solution was added to the electrochemical cell containing 2 mL of phosphate buffer (pH = 7.2) as a supporting electrolyte. Double distilled water was used to make the final volume of 4 mL. The square wave voltammetric parameters were optimized as follows: initial potential (E): 0 mV, final potential (E): 800 mV, square wave amplitude (E_{SW}): 25 mV, potential step (E): 4 mV and square wave frequency (f): 15 Hz. All the potentials are reported with respect to the Ag/AgCl electrode at an ambient temperature of 25 ± 2 °C. After each run the SCE was discarded and a new electrode was taken.

The commercially available DA tablets obtained from the medical store of Roorkee were grounded into fine powder using pestle and mortar. Then 200 mg of the pharmaceutical formulations was suitably diluted with water and buffer solution of pH 7.2, so that the concentrations of analytes reached in the working concentration range. The proposed technique was used to determine the drug in the respective pharmaceutical formulations under similar conditions, which were used to obtain the concentration graph. The human biological samples (urine and blood) of the healthy volunteers were received from the hospital of IIT Roorkee. The plasma was separated from the blood samples by centrifugation at 2000 rpm for 5 min at 4°C using EDTA as the anticoagulant. The yellowish part (plasma) was used to analyze the concentration of DA and 5-HT. Urine and plasma samples were suitably diluted with phosphate buffer to minimize matrix complexity. The standard addition method was applied to calculate the concentration of both analytes DA and 5-HT.

4.2.2. RESULTS AND DISCUSSION

4.2.2.1 Characterization of GR/p-AHNSA/SPCs

The characterization of the surface of unmodified, graphene modified and GR/p-AHNSA nanocomposite modified SPCs was done using FE-SEM and obtained microscopic images are presented in **Fig. 4.1.** In the unmodified SPCs, only a film of the carbon used in the construction of the working electrode was noticed, whereas, deposition of the GR as flakes on SPCs surface was clearly noticed in the case of graphene modified SPCs as shown in **Fig. 4.1A** and **B**, respectively. The microscopic image of the GR-polymer nanocomposite film (**Fig. 4.1C**) showed that the p-(AHNSA) was amassed on the SPCs surface with nano-rod shape particles interwined with GR and formed a porous, crystalline and etched surface. It can be seen that the nanocomposite network was constructed uniformly throughout the surface, and provided a larger electroactive surface area in comparison to the unmodified sensor and promoted a facile electron transfer across the film efficiently.

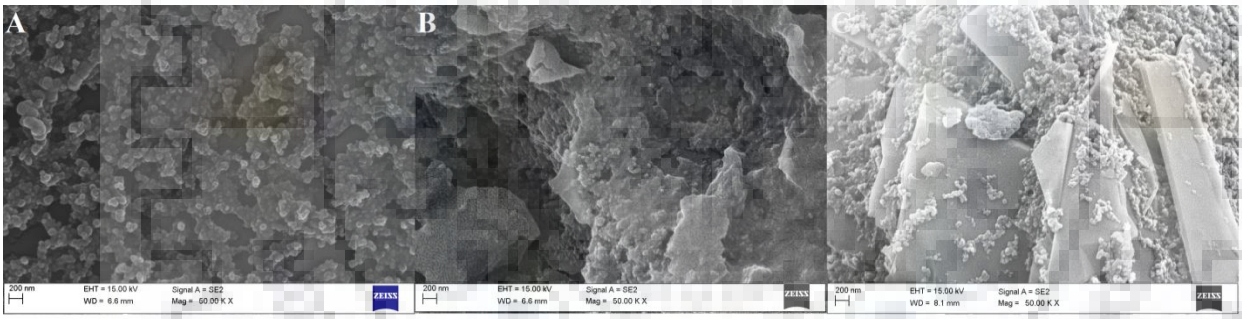

Fig. 4.1: Typical FE-SEM images observed for (**A**) unmodified SPCs (**B**) GR/SPCs and (**C**) GR/p-AHNSA/SPCs.

The electron-transfer resistance (R_{CT}) corresponding to unmodified, graphene modified and GR/p-AHNSA nanocomposite modified SPCs surfaces was calculated by using EIS. The experiment was carried out in 1:1 mixture of 0.1 M KCl and 5 mM $K_3Fe(CN)_6$ solution over the frequency range 100 kHz to 10 mHz at a potential of 0.05 V. The resulting Nyquist plots observed for the unmodified, graphene modified SPCs and GR/p-AHNSA/SPCs are shown in **Fig. 4.2**. After modification of the SPCs surface with GR and GR/p-AHNSA film, the R_{CT} values decreased in comparison to the unmodified surface of SPCs. As shown, the diameter of semicircle gets reduced for GR/p-AHNSA/SPCs, implying a facile electron transfer at the redox probes in the electrolyte solution. Whereas, at unmodified SPCs, the resistance to charge transport value increases

substantially and restrained the pathways for electron transfer. The value of R_{CT} for the redox process was calculated by fitting the Randles circuit (**inset of Fig. 4.2**) and was found to be 2790 Ω, 860Ω and 260Ω for the unmodified SPCs, GR/SPCs and GR/p-AHNSA/SPCs, respectively.

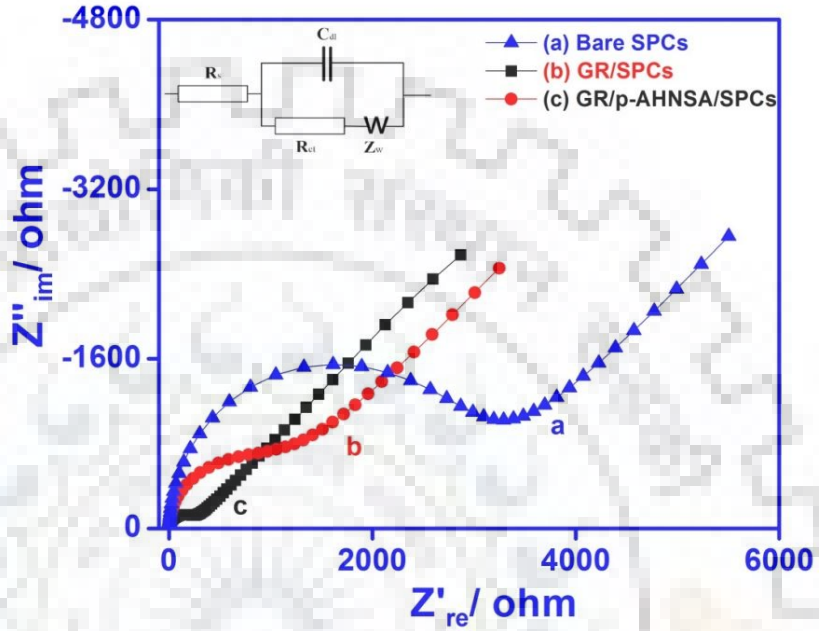

Fig. 4.2: Nyquist plots of EIS measurements of (a) unmodified SPCs (b) GR/SPCs and (c) GR/p-AHNSA/SPCs. The inset represents the Randles equivalent circuit used for data fitting.

4.2.2.2 Cyclic voltammetry

Cyclic voltammograms for a mixture of 50 μM DA and 5-HT in pH 7.2 phosphate buffer at unmodified SPCs, GR/SPCs and GR/p-AHNSA/SPCs are recorded at a scan rate of 100 mVs^{-1} and are shown in **Fig. 4.3.** The voltammogram of the mixture of DA and 5-HT shows broad and overlapped indefinable peaks (**curve a**) at an unmodified electrode as shown in **Fig. 4.3**. While at the surface of GR/SPCs, two well-defined voltammetric peaks (**curve b**) at about ~180 mV (I_a) and ~378 mV (II_b) corresponding to the oxidation of DA and 5-HT were observed, respectively. However, at the GR/p-AHNSA/SPCs, the peak current has greatly increased with negative shift in the peak current at ~146 mV (I'_a) and ~342 mV (II'_b) for the oxidation of DA and 5-HT, respectively. The oxidation peak of DA also formed a quasi-reversible couple with peak at ~90 mV (I_a) at GR/SPCs and at ~48 mV (I'_a) at GR/p-AHNSA/SPCs. The oxidation peaks (I_a and I'_a) were observed due to the oxidation of DA to o-dopaminequinone and the cathodic peak (I_b and I'_b) pointing the reduction of dopaminequinone back to dopamine as reported earlier [34]. The

enhanced peaks current with negative shift in the peak potential indicated that the composite of GR and p-AHNSA film accelerates the kinetics of the electrochemical oxidation of both DA and 5-HT.

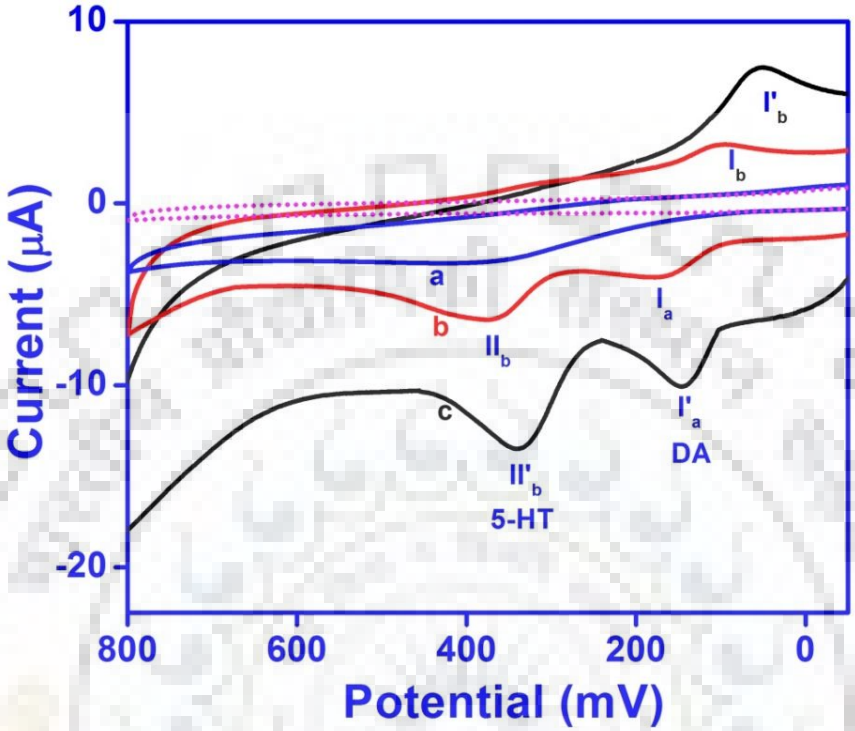

Fig. 4.3: A comparison of cyclic voltammograms recorded at unmodified SPCs (curve a), GR/SPCs (curve b) and GR/p-AHNSA/SPCs (curve c) for both DA and 5-HT in phosphate buffer of pH 7.2 at a scan rate of 100 mVs^{-1}. The background is shown by dotted line.

To clarify the nature of the electrode transfer process, scan rate (ν) studies were carried out. The anodic peak current was found to increase with increasing scan rate and the linearity of i_p versus ν and i_p versus log (ν) for DA and 5-HT are obtained in the scan rate range of 5–150 mVs^{-1} can be expressed by the relation:

For DA:

$$\mathbf{i_p\ (\mu A) = 0.1353\ \nu + 1.2968} \qquad \mathbf{(R^2 = 0.995)}$$

$$\mathbf{\log i_p = 0.7485 \log \nu - 0.3261} \qquad \mathbf{(R^2 = 0.993)}$$

For 5-HT:

$$\mathbf{i_p\ (\mu A) = 0.5262\ \nu - 0.0586} \qquad \mathbf{(R^2 = 0.986)}$$

$$\mathbf{\log i_p = 1.1196 \log \nu - 1.1443} \qquad \mathbf{(R^2 = 0.980)}$$

The linearity of i_p versus ν and log i_p versus log ν (slope > 0.5) reveals the adsorption controlled oxidation for both the compounds [33].

4.2.2.3. Square wave voltammetry

Fig. 4.4 compares the square wave voltammograms (SWVs) of a mixture of 50 µM DA and 5-HT in pH 7.2 phosphate buffer using unmodified SPCs, GR/SPCs and GR/p-AHNSA/SPCs. At unmodified SPCs, the oxidation peak current of DA and 5-HT get overlapped and a broad, poor response at a peak potential of ~338 mV (curve a) was observed. The obtained result cannot be assigned to DA or 5-HT. While in the case of p-AHNSA or GR modified SPCs, two peaks for DA and 5-HT at 160 mV and 365 mV or 150 mV and 340 mV were observed, respectively. GR modified SPCs displays higher peak current with negative shift of peak potential, which indicates the electrocatalytic effect of GR to the oxidation of analytes (curve b). There was virtually little difference in the peak height and peak current of DA and 5-HT at these sensors. The use of GR/p-AHNSA composite SPCs showed two well defined and separated oxidation peaks at around ~136 mV and ~325 mV corresponding to the oxidation of DA and 5-HT respectively. The use of GR or AHNSA also leads to the enhancement in the peak currents as well as shift in the peak potential, but the remarkable anodic peak current with shifting of more negative potential was observed for the GR/p-AHNSA composite based SPCs (curve c). The obtained results support the fact that the synergic effect of GR and conducting polymer (p-AHNSA) accelerate the rate of electron transfer and improves the sensitivity of detection [35].

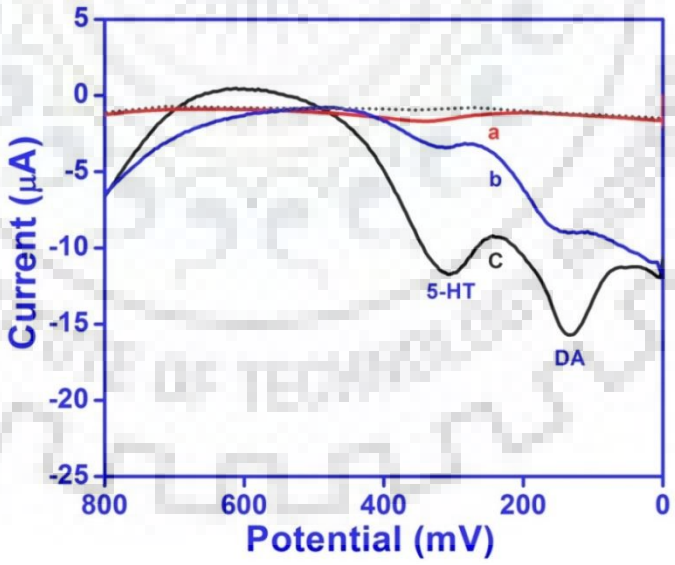

Fig. 4.4 A comparison of SWVs observed for 50 µM DA and 5-HT at unmodified SPCs (curve a), GR/SPCs (curve b) and GR/p-AHNSA/SPCs (curve c) at pH 7.2. The background is shown by dotted line.

4.2.2.3.1 Electrochemical investigations of DA

The square wave voltammograms of DA in the range 0.05–100 µM were recorded using the GR/p-AHNSA/SPCs at pH 7.2 at the optimal SWV parameters. The results showed that the anodic peak current (i_p) increased linearly with the increasing concentration of DA as shown in **Fig. 4.5**. The anodic current values are reported as an average of at least three replicate determinations. The dependence of i_p on concentration can be expressed by the equation:

$$\mathbf{i_p\ (\mu A) = 0.0997\ [C,\ 0.05 - 100\ \mu M] + 0.1815}$$

having correlation coefficients of 0.998, where [C] is the concentration of DA in µM. The limit of detection was calculated by using 3σ/b, where σ is the standard deviation of "n", number of blank voltammograms and b is the slope of calibration plot and was found to be 2 nM.

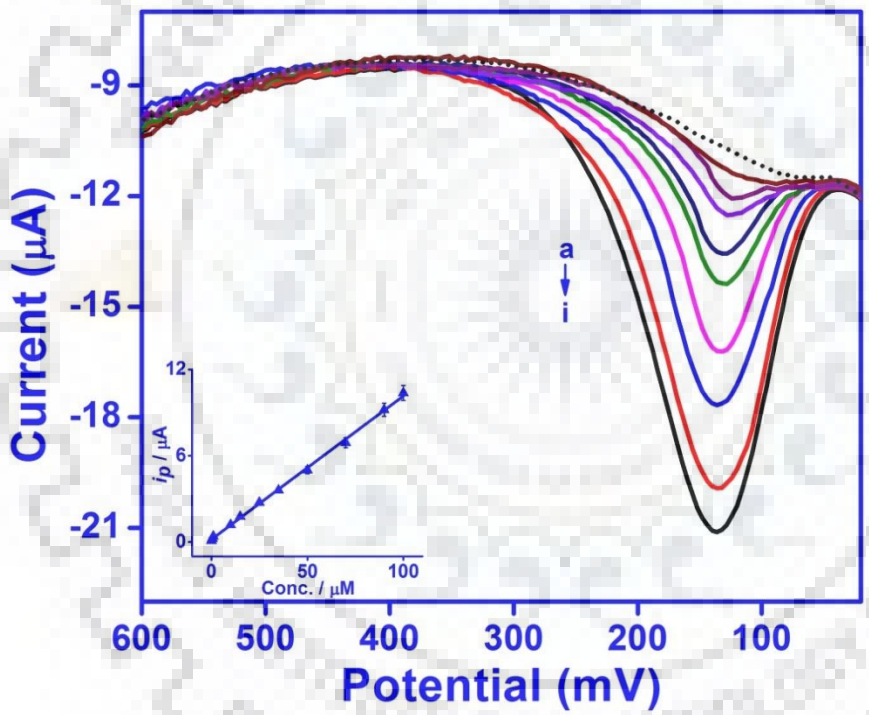

Fig. 4.5: Square wave voltammograms observed for the increasing concentration of DA using GR/p-AHNSA/SPCs in phosphate buffer of pH 7.2. Curves were recorded at (a) 0.05; (b) 10; (c) 15; (d) 25; (e) 35; (f) 50; (g) 70; (h) 90 and (i) 100 µM concentration of DA; inset is the calibration plot.

The electrochemical response of DA was analyzed at different pH of the supporting electrolytes at GR/p-AHNSA/SPCs. The pH of the supporting electrolytes influences the oxidation signal of DA. It was observed that at physiological pH 7.2, the highest peak current was observed

(**Fig. 4.6 A**) and with the increasing pH (2.4-10.0), the peak potential (E_p) gradually shifted to the less positive potentials and a linear relation was observed between anodic peak potential (E_p) and pH, which can be represented by the equation.

$$\mathbf{E_p\ (pH\ 2.2\text{-}10) = -55.421\ pH + 551.09\quad mV\ vs.\ Ag/AgCl}$$

having correlation coefficient of 0.985. The slope of the (dE_p/dpH) plot was 0.055 V and was close to the theoretical Nernstian value of 0.059 V and clearly demonstrated that the equal number of electrons and protons were transferred in the electrochemical oxidation process of DA [30].

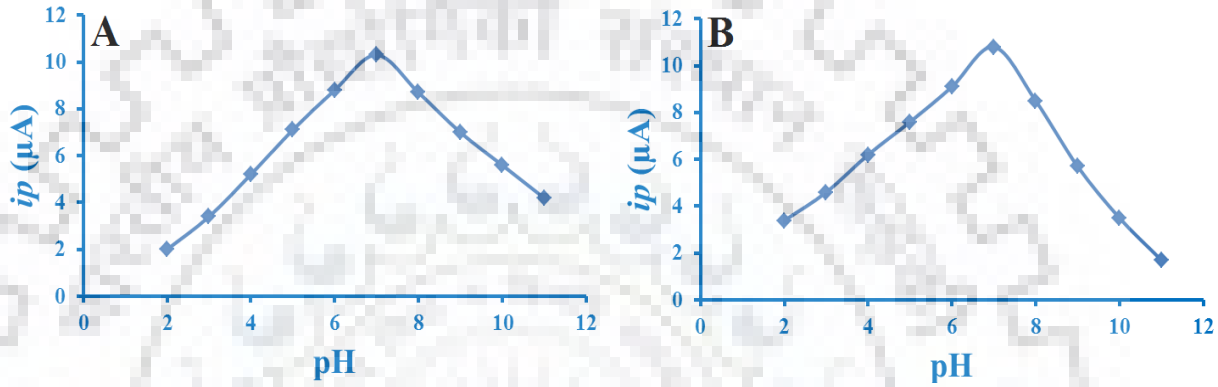

Fig. 4.6: Effect of the supporting electrolyte pH on the peak current of (**A**) DA and (**B**) 5-HT at GR/p-AHNSA/SPCs.

Further, the SWVs for DA were also recorded at different square wave frequency using GR/p-AHNSA/SPCs. The observed slope (0.998) of log i_p vs. log f plot, which was greater than 0.5, suggested the involvement of adsorption controlled electrode reaction.

4.2.2.3.2 Electrochemical investigations of 5-HT

The effect of supporting electrolyte pH on the electro-oxidation of 5-HT at GR/p-AHNSA/SPCs was investigated in the pH range 2.4–10.0. It was observed that the E_p shifted to more negative potentials with the increase in the pH. Also, the maximum peak current was observed at pH 7.2 (**Fig. 4.6B**). A linear relationship was observed between E_p and pH, which can be expressed by the equation:

$$\mathbf{E_p\ (pH\ 2.2\text{-}10.5) = -39.29\ pH + 615.83\quad mV\ vs.\ Ag/AgCl}$$

with a correlation coefficient of 0.988. The obtained slope of the E_p vs pH plot (0.039 V/pH), was nearly half to the theoretical Nernstian value and indicated that number of protons and electrons involved in the electrode oxidation of 5-HT were unequal. The involvement of one proton and two electron is well reported during the oxidation of 5-HT [5].

The effect of square wave frequency (f) on the voltammetric response of 5-HT was examined in the frequency range 5–40 Hz at GR/p-AHNSA/SPC sensor. The observed slope value of log i_p vs. log f plot (>0.5) further confirmed the involvement of adsorption complications in 5-HT oxidation.

The square wave voltammograms of 5-HT at different concentrations were similarly recorded at GR/p-AHNSA/SPCs. The peak current (i_p) of the anodic peak (after correction of background current) increased with the increase in the concentration of 5-HT at pH 7.2 as depicted in **Fig. 4.7**.

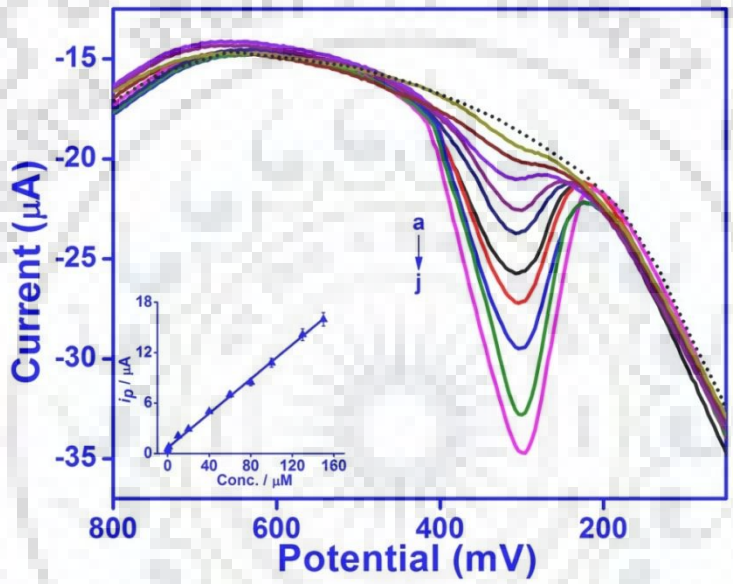

Fig. 4.7: Square wave voltammograms recorded at (a) 0.5; (b) 1; (c) 10; (d) 20; (e) 40; (f) 60; (g) 80; (h) 100; (i) 130; (j) 150 µM concentrations of 5-HT using GR/p-AHNSA/SPCs in phosphate buffer of pH 7.2; inset is the calibration plot.

The i_p vs. conc. plot was linear in the range 0.05–150 µM with a correlation coefficient of 0.998. The dependence of i_p on concentration can be presented as:

$$\mathbf{i_p\,(\mu A) = 0.1001\,[C\ 0.05\text{-}150\ \mu M] + 0.9119}$$

where C is the concentration of 5-HT in µM. The limit of detection (LOD) and limit of quantification (LOQ) for the determination of 5-HT were calculated to be 3 nM and 10 nM respectively. As the 5-HT concentration in healthy human beings is reported in the range of 0.5-1.4 µM [36], the proposed method with lower detection-limit can be applied for the analysis of 5-HT in the biological samples.

4.2.2.3.3 Simultaneous determination of DA and 5-HT

To investigate the simultaneous electrochemical responses of DA and 5-HT at the surface of GR/p-AHNSA/SPCs, experiment was executed in two steps. In the first set of experiment, the square wave voltammograms were recorded for the different concentrations of DA while the concentration of 5-HT was kept constant (20 µM) as shown in **Fig. 4.8 A**. It was observed that the oxidation peak current response of DA increases with the increase in its concentration without affecting the 5-HT signal. Similarly, **Fig. 4.8 B** shows square wave voltammograms obtained by varying the concentration of 5-HT keeping the concentration DA constant (10 µM). It was found that the anodic peak current of 5-HT increased linearly, while the voltammetric peak of DA was practically unchanged without affecting the peak current and peak shape. Thus, it is concluded that both compounds can be determined in presence of each other without affecting the oxidation peak current and peak shape. The dependence of the peak current for DA and 5-HT with concentration in the mixture solutions is identical to that observed during their individual voltammetric study.

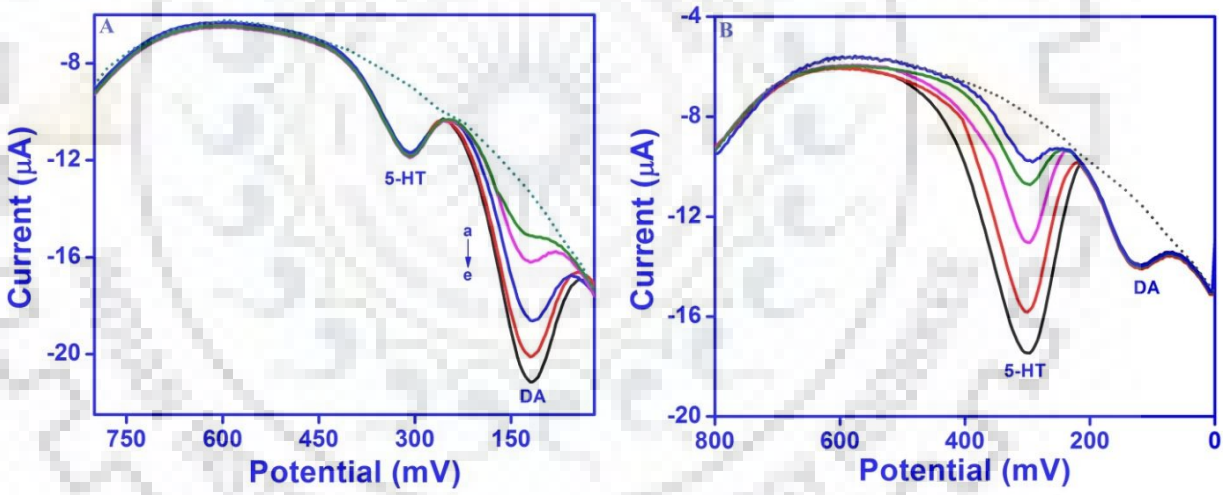

Fig. 4.8: Square wave voltammograms of a mixture of DA and 5-HT recorded at GR/p-AHNSA/SPCs in phosphate buffer of pH 7.2. (**A**) Concentration of DA was changed to (a) 15; (b) 25; (c) 50; (d) 65 and (e) 80 µM, keeping the concentration of 5-HT constant (20 µM). (**B**) 5-HT concentrations (a) 5; (b) 15; (c) 40; (d) 70 and (e) 90 µM at fixed concentration of DA (20 µM).

4.2.2.4 Interference study

Selectivity is an important indicator for the practical measurement due to the presence of various interfering substances in the biological fluids. The high concentration of common metabolites such as uric acid, ascorbic acid, xanthine etc. present in biological fluids may interfere

with the electrochemical signal of DA and 5-HT and consequently affect the selectivity. In these studies, it can be seen that the DA and 5-HT will not interfere with each other at GR/p-AHNSA/SPCs surface as the oxidation potentials of DA and 5-HT are about 400 mV apart. The interference with major electroactive biological components such as ascorbic acid (AA) and uric acid (UA), which commonly oxidize at potentials similar to DA and 5-HT, has been studied by recording the voltammograms at GR/p-AHNSA/SPCs using SWV. Initially, at the fix concentration of DA (20 µM) and 5-HT (10 µM) and with the increasing concentration of AA SWVs were recorded. It was found that the AA did not interfere upto 1 mM concentration in the determination of DA and 5-HT as the oxidation potential of AA was close to zero volt.

In another experiment, the effect of UA was examined on 20 µM DA. **Fig. 4.9** presents the SWVs corresponding to the oxidation of 20 µM DA with increasing concentration of UA (**Fig. 4.9 A**). Two well separate oxidation peaks at the potential of ~115 mV and ~440 mV were observed for DA and UA, respectively. Upto 2 mM concentration UA did not show any substantial changes in oxidation peak current of DA, indicating thereby that the oxidation of DA was free from the interference of UA. Similarly the SWVs were also recorded to investigate the interference effect of UA on 10 µM 5-HT. The result indicate that upto 50 µM, UA did not affect the oxidation signal of 5-HT, however, at higher concentrations of UA, the 5-HT oxidation peak became broaden. Thus, it was concluded that UA was tolerated upto five times concentration of 5-HT. When interference of UA was examined in the mixture of DA and 5-HT, again it was noticed that DA remained unaffected upto 2 mM concentration of UA, whereas the 5- HT peak tolerated only upto 50 µM UA, after which serious interference was observed.

The concentration of 5-HT in mammalian brain is fairly related to tryptophan (Trp) concentration because Trp is the key ingredient in making 5-HT. At a simplistic level, it could be thought of as a parent-child relationship, with tryptophan being the parent. Thus, due to their close relation and importance in human physiology, the electrochemical study of both analytes has also been carried out. **Fig. 4.9 B** shows the SWVs at GR/p-AHNSA/SPCs in the mixture of 10 µM of 5-HT and different concentrations of Trp at pH 7.2. From the results, it was observed that Trp did not influence the oxidation signal of 5-HT and a well-defined peak separation was also observed. Hence, it was concluded that the proposed electrochemical sensor provide the selective method, which can be used effectively for the determination of DA and 5-HT in human biological fluids having various possible interferents.

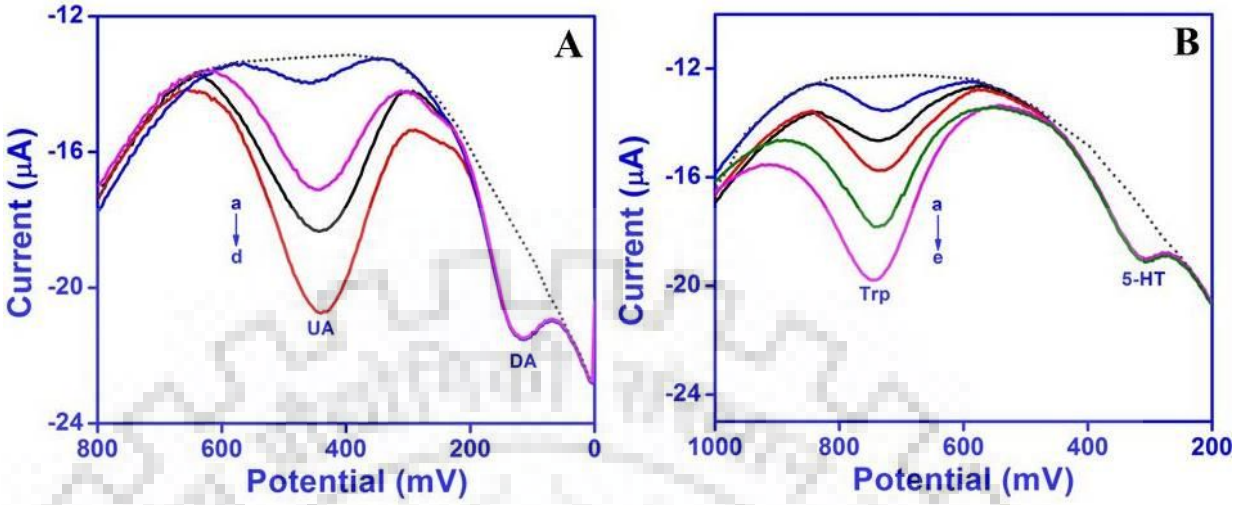

Fig. 4.9: (**A**) SWVs observed for various concentrations of UA at GR/p-AHNSA/SPCs in pH 7.2 phosphate buffer solution containing 20 µM DA and [UA]: (a) 100 (b) 800 (c) 1000 and (d) 1500 µM.

(**B**) Effect of different concentration of Trp (a) 50 (b) 100 (c) 150 (d) 200 and (e) 250 µM observed at GR/p-AHNSA/SPCs in pH 7.2 phosphate buffer solution containing 20 µM 5-HT. The background curve is shown by the dash line.

4.2.2.5 Stability and reproducibility of GR/p-AHNSA/SPCs

The studies on long term stability were not possible because SPCs were used only for one run and then was changed. However, sensor to sensor variation was monitored for eight GR/p-AHNSA/SPCs. The electrochemical experiment was executed in a solution having, DA (20 µM) and 5-HT (50 µM) at pH 7.2. The experimental results demonstrated that at all the modified SPCs a negligible variation in the oxidation current response was observed, From the calculations, relative standard deviation (RSD) were found to be 2.12% and 2.47% for DA and 5-HT, respectively. The results concluded that the sensor to sensor variation bear appreciable reproducibility. After 2–3 scans, a significant decrease in the oxidation peak current of analytes was observed at the surface of GR/p-AHNSA/SPCs. Hence, to get the reproducible results the modified SPCs was changed after each run.

4.2.2.6 Analytical applicability

4.2.2.6.1 Pharmaceutical analysis

The practical applicability of the developed sensor was evaluated for the determination of DA in three commercial pharmaceutical samples. The required amounts of pharmaceutical samples were suitably powdered and diluted with pH 7.2 buffer to bring the concentration of the drug in the working range. The SWVs were then recorded at GR/p-AHNSA/SPCs and with help of calibration plot DA content in the various pharmaceutical preparations was then ascertained. From the results, it can be observed that the calculated results were found to be in good agreement with the labeled amount. The obtained results suggesting that determination of DA in pharmaceutical preparations using proposed method is precise and convenient (**Table 1)**.

Table 1: Determination of DA in different pharmaceutical formulations at GR/p-AHNSA/SPCs.

Sample	Stated Content	DA determined	Error%
Dopalim	200 mg	198.92 mg	-0.54
Dopacef	50 mg	49.17 mg	-1.66
Dopamine	40 mg	39.23 mg	-1.92

*The R.S.D. value for DA determination was less than 2.38% for n = 3

4.2.2.6.2 Real sample assay

The accuracy of the present methodology was also investigated by applying it for the detection of DA and 5-HT in biological fluids, like plasma and urine. The samples were prepared following the procedure as discussed in section 4.2.1.4. Two times diluted plasma sample was used to record the SWVs, and a bump at E_p (300 mV) corresponding to the oxidation of 5-HT was observed. Now the further studies in the same solution were performed by spiking the exogenous 5-HT and then SWVs were recorded. The standard addition plot (**Fig. 4.10**) was used to calculate the concentration of 5-HT in the plasma sample and was detected as 1.6 µM (**Table 2**). The negative intercept on X-axis is insignificant. The % recovery value observed in the range of 98.1–101.2% is summarized in **Table 2**.

Table 2: Recovery data for 5-HT determination in plasma sample at GR/p-AHNSA/SPCs.

Sample	Spiked (µM)	Observed[a] (µM)	Actual[b] (µM)	Recovery [*] (%)
1.	0	1.60	1.60	--
2.	5.0	6.48	1.48	98.18
3.	10.0	11.49	1.49	99.05
4.	20.0	21.87	1.87	101.25

*The R.S.D. value for the determination was less than 2.08% for n=3.

[a]The observed values are sum of 5-HT present + spiked amount.

[b]The actual amount is observed –spiked amount

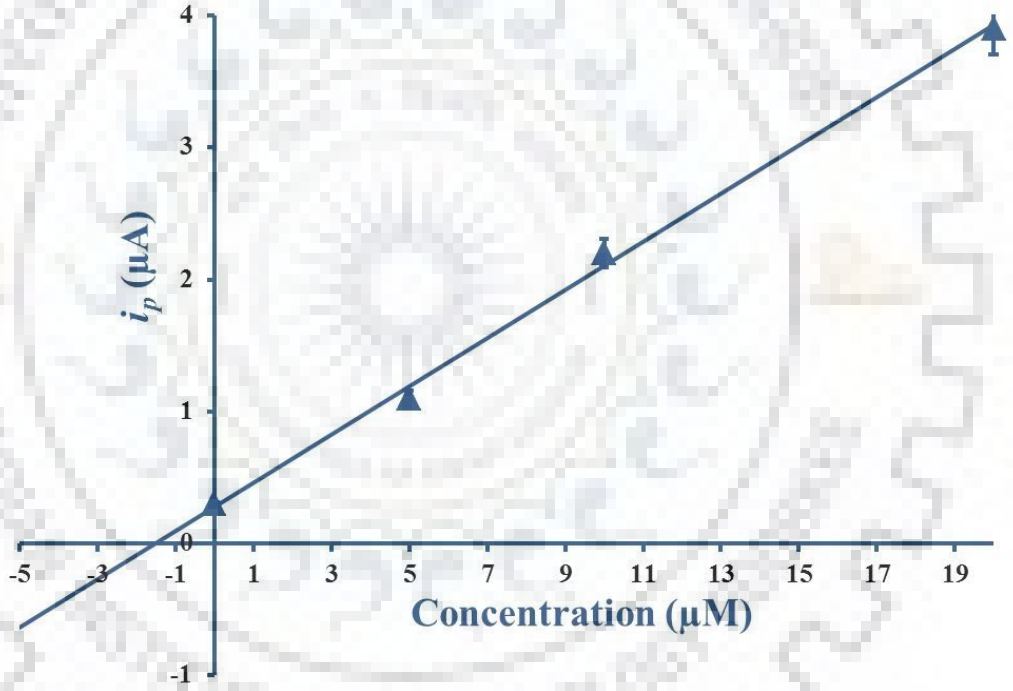

Fig. 4.10: The standard addition plot observed for the 5-HT concentration in patient plasma sample.

An attempt to determine DA in the plasma sample of normal person was then made, however, no peak for DA was observed in 2 times diluted plasma samples, as the discharged concentration of DA in a normal person is reported in the range of 10^{-10} to 10^{-12} M. Therefore, the recovery experiments were carried out by spiking the known DA in plasma samples. The concentrations of DA were then calculated by using regression equation and the results are summarized in **Table 3.**

Table 3: Determination of DA in different pharmaceutical formulations at GR/p-AHNSA/SPCs.

Sample 1			Sample 2		
Amount added (µM)	**Amount detected (µM)**	**Recovery (%)**	**Amount added (µM)**	**Amount detected (µM)**	**Recovery (%)**
1	0.99	99.00	5	4.97	99.40
2	1.97	98.50	10	10.11	101.10
3	3.05	101.66	15	14.93	99.53

*****The R.S.D. value for determination was less than 2.46% for urine respectively for n = 3.

The concentrations of both analytes were also analysed in obtained urine samples of healthy volunteers using GR/p-AHNSA/SPCs. To reduce the matrix complexity, the filtered urine samples were diluted 10 times with pH 7.2 buffer. Now the diluted samples were spiked with different concentrations of both the analytes and then SWVs were recorded. The obtained peak current values were used to calculate the concentration of DA and 5-HT by using the regression equation. The observed values for DA and 5-HT in the urine samples are summarized in **Table 4** showing recovery in the range of 98.6-100.38% with R.S.D of ± 2.17% (n=3). The catecholamines and 5-HT concentration have been found to increase in the patients suffering from carcinoid syndrome, Parkinson and hypertension. The detection limits of the proposed method is in nM level, hence, both the compounds can be easily determined at GR/p-AHNSA/SPCs in such patients without any interference from the metabolites present in the blood and urine.

Table 4: Recovery analysis of DA and 5-HT in human urine sample at the GR/p-AHNSA/SPCs.

		DA		5-HT	
Sample	**Amount added (µM)**	**Amount detected (µM)**	**Recovery (%)**	**Amount detected (µM)**	**Recovery (%)**
Urine	1	0.981	98.10	0.986	98.60
	5	4.961	99.22	5.019	100.38
	10	10.13	101.30	9.931	99.31

*****The R.S.D. value for determination was less than 2.17 for urine respectively for n = 3.

To validate the results observed for 5-HT in plasma by using GR/p-AHNSA/SPCs with some standard method, UV spectrum of 5-HT was recorded at pH 7.2. A well−defined absorption peak at 275 nm was observed. Using the standard addition method, the concentration of 5-HT in plasma sample was found to be 1.56 μM. The significant results observed by the two different techniques were also confirmed by the paired t-test. The calculated and tabulated t-test values were −1.671 and 4.303 observed, respectively, which are under a confidence limit of 95%. The insignificant difference between the investigated data by the two methods proves the validity of the proposed technique.

4.2.3. CONCLUSION

The proposed protocol deals with the fabrication of a novel electrochemical sensor for simultaneous determination of DA and 5-HT based on graphene and p-AHNSA disposable SPCs. The proposed method provides a simple, sensitive, selective, rapid and inexpensive detection of DA and 5-HT in human biological samples. In the developed sensor, the functional groups rich polymer film and the synergistic interaction between p-AHNSA and graphene via π-π stacking interaction encourages the electron transfer and showed a remarkable electrocatalytic activity toward neurotransmitters, DA and 5-HT. For both the analytes an increase in the peak current and shift of oxidation potentials to less positive values was observed. A low detection limit and high sensitivity of the proposed technique in comparison to the recently reported literatures (**Table 5 and Table 6**) demonstrating the ability of the polymer nanocomposite to catalyze the DA and 5-HT electro-oxidation.

Table 5: A comparison of the observed linear range and detection limit of DA with recently reported sensors.

S.No.	Electrode	Method	Conc. range (μM)	LOD (nM)	Real sample	Ref.
1.	MWNTs-SiO_2-chitosan/SPE	SWV	1-20	200	No	37
2.	CNTs/graphite	DPV	0.5-10	100	No	38
3.	DNA-PPyox/CFE	DPV	0.3-10	50	serum	39
4.	CNTs-IL/GCE	DPV	0.1-12	60	serum	40
5.	ACh/GCE	DPV,CV	0.7-5	300	No	41
6.	ERGO-P/GCE	DPV,CV	0.1-300	35	No	42
7.	5-HTP/GCE	DPV	0.5-35	300	No	43
8.	Nafion/$Ni(OH)_2$/MWNT/GCE	DPV,CV	0.05-25	15	serum	44
9.	CNFs electrode	DPV	0.1-10	50	No	45
10.	Au/NPSS	CV	3-2000	70	Urine,serum	46
		DPV	1.0-80	20	Urine,serum	46
11.	AuNPs-β-CD-Gra/GCE	SWV	0.5-150	150	Urine	47
12.	MBIP	DPV	0.02-7	6	Urine, plasma, pharmaceutical	48
13.	$NiFe_2O_3$-MWCNT/GCE	DPV	0.05-100	20	Urine,serum	49
14.	ZnO-NR/3,4-AA/CPE	SWV	0.01-0.3	56	Urine, serum	50
15.	MC-CNPEs	DPV	0.08-10	76	Urine,serum, pharmaceutical	51
16.	GR/p-AHNSA/SPCs	SWV	0.05-100	2	Urine, plasma, pharmaceutical	Present work

*SWV- square wave voltammetry, DPV- Differential pulse voltammetry, CV- cyclic voltammetry, CA-chronoamperometry, CNTs-IL/GCE- carbon nanotubes-ionic liquid composite modified glassy carbon electrode, ACh/GCE-acetate/choline/glass carbon electrode, 5-HTP- 5-Hydroxytryptophan, CNFs- carbon nanofibers, Au/NPSS-nanoporous stainless steel with nanostructured gold, AuNPs–β-CD–Gra/GCE - AuNPs and β-cyclodextrin (β-CD) on Graphene/GCE.

Table 6: A comparison of the observed linear range and detection limit of 5-HT with recently reported sensors.

S.No.	Electrode	Method	Conc. range (µM)	LOD (nM)	Real sample	Ref.
1.	MWNTs-SiO_2-chitosan/SPE	SWV	0.1-2	10	No	37
2.	CNTs/graphite	DPV	1-15	200	No	38
3.	DNA-PPyox/CFE	DPV	0.01-1	7	serum	39
4.	CNTs-IL/GCE	DPV	0.02-7	8	serum	40
5.	ACh/GCE	DPV,CV	1-30	500	No	41
6.	ERGO-P/GCE	DPV,CV	0.1-300	4.9	No	42
7.	5-HTP/GCE	DPV	5-35	1700	No	43
8.	Nafion/$Ni(OH)_2$/MWNT/GCE	DPV,CV	0.008-10	3	serum	44
9.	CNFs electrode	DPV	0.25-10	250	No	45
10.	GR/p-AHNSA/SPCs	SWV	0.05-150	3	Urine, plasma, pharmaceutical	Present work

SWV- square wave voltammetry, DPV- Differential pulse voltammetry, CV- cyclic voltammetry, CA- chronoamperometry, CNTs-IL/GCE- carbon nanotubes-ionic liquid composite modified glassy carbon electrode, ACh/GCE- acetate/choline/glass carbon electrode, 5-HTP- 5-Hydroxytryptophan, CNFs- carbon nanofibers.

The detection limits for DA and 5-HT with the linear dynamic range 0.05–100 µM and 0.05–150 µM observed at GR/p-AHNSA/SPCs were 2 nM and 3 nM respectively. The utility of this promising biosensor has been successfully demonstrated by the determination of 5-HT and DA levels in pharmaceutical preparations, human urine and plasma samples. Therefore, the proposed technique provided a good approach for the detection of DA and 5-HT with high sensitivity, selectivity and with good reproducibility. Moreover, the GR/p-AHNSA/SPC sensing platform confers an alternative choice for analytical determination of biological importance molecules in pharmaceutical and clinical analysis.

4.3 SECTION B: Graphene nanoribbons based sensor for the simultaneous determination of DOPAC and 5-HIAA

The detection and monitoring of neurotransmitters and their metabolites in plasma and urine are found helpful in the detection of variety of diseases, such as neuroblastoma, pheochromocytoma, hypertension or hypotension etc. [50-53]. 3,4-Dihydroxyphenylacetic acid (DOPAC, **Scheme 2**), the main metabolite of dopamine (DA), is formed in the central nervous system (CNS) by the action of the monoamine oxidase [54]. The amount of DOPAC is greatly reduced as a result of increased Parkinson's overexpression. The DOPAC level of 9 ng/mL in the cerebrospinal fluid (CSF) decrease to 6 ng/mL in Parkinson's patients [55,56]. In patients with dihydropyridine reductase deficiency and deficiency of L-aromatic-amino acid decarboxylase results in low plasma DOPAC levels [57,58]. 5-Hydroxyindoleacetic acid (5-HIAA, **Scheme2**), a main metabolite of serotonin (5-hydroxytryptamine, 5-HT), is excreted in the urine and regulates the homeostatic state of the human body with 5-HT.

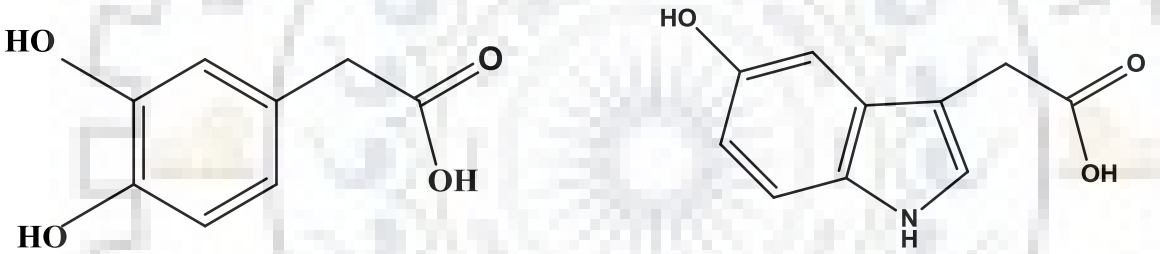

DOPAC 5-HIAA

Scheme 2: Chemical structure of DOPAC and 5-HIAA.

The level of 5-HIAA in CSF is significantly affected by the diet, stress and 5-HT reuptake inhibitors and alcohol exposure [59,60]. Suicide risk after attempted suicide can be predicted by monitoring the level of 5-HIAA concentrations in the CSF. The low CSF 5-HIAA predicts the short-range suicide risk in the depressed suicide attempters and mood disorder in patients [61,62]. 5-HIAA levels in the CSF are also decreased in SIDS infants (sudden infant death syndrome i.e. sudden death of an infant less than 12 months of age) as compared to the controls dying of known causes [63,64]. The increased ratio of 5-HIAA/5-HT in human system has been found to initiate natural aging. Plasma 5-HIAA may serve as a biomarker for the patients with appendices and cancer, such as intestinal cancers, where the amount of plasma 5-HIAA increased to 8.87 ± 1.25 µg/L as compared to 1.90 ± 0.09 µg/L in the healthy persons [65]. The low level of 5-HIAA in the CSF is indicative of aggressive behavior, while high level of 5-HIAA is suggested as the main

performer in depression, violent suicide attempts, autistic spectrum disorders and the originator of carcinoid tumors [65]. The carcinoid tumors can alter the urinary level and plasma levels, thus the monitoring of the levels of DOPAC and 5-HIAA act as a marker of the starting stage of these tumors and diagnosis of carcinoid tumors [18,66]. The monitoring of 5-HIAA and DOPAC has been considered to reflect the overall turnover of the neurotransmitters within the CNS. Patients with vascular dementia of the Binswanger type show significant increase in DA concentration and decrease in 5-HIAA concentration [67]. The synthesis, action and metabolism of neurotransmitters cause changes in the concentration of metabolites. The change is normally significant in the case of disorders in human system and particular pattern provides information about the necessity and outcome of the treatment [68]. Hence, the simultaneous determination of these two metabolites has been preferred.

Several methods, like fluorometry, spectrophotometry, capillary electrophoresis, high-performance liquid chromatography, capillary column gas chromatography, fluorescent spectrometry, mass spectrometry, infra-red spectroscopy have been used for the determination of DOPAC and 5-HIAA [69-75]. To our knowledge no attempt has been made in the last decade to determine these two metabolites simultaneously. However, most of the reported methods used for individual determination have limitations, such as long analysis time, less sensitivity and selectivity, requirement of costly instruments, complex sample preparation etc. Hence, a simple, rapid, sensitive and selective method for the simultaneous monitoring of the two compounds is highly needed. The electrochemical methods are important alternatives due to the advantages such as simple, less time consuming, ecofriendly, cost effective, sensitive and reproducible with significant accuracy [6,31]. Graphene nanoribbons (GNRs), a one-dimensional form of graphene strip with a high length-to-width ratio, intrinsic energy band gaps and straight edges attracted considerable attention in the last few years [76,77]. The electron confinement in GNRs results electronic properties and transforms semi-metallic to semiconducting properties. On decreasing the width, tunable electrical properties through dimension confinement can be achieved [78,79]. The polymeric bromocresol green (p-BG) has high-electron-density hydroxyl groups and negatively charged surface-functional groups [80-82], which can interact with GNRs to provide good biocompatibility, chemical stability, high electron efficiency and excellent electrocatalytic activity. In the proposed approach GNRs casted at the surface of pyrolytic graphite (EPPG) were coated with polymer of BG. The resulting sensor has been used for the simultaneous determination of DOPAC and 5-HIAA. The fabricated sensor (p-BG/GNRs/EPPG) showed large surface area and

good conductivity, which helped in the simultaneous determination of the target analytes with low detection limits.

4.3.1 EXPERIMENTAL

4.3.1.1 Reagents and materials

3,4-Dihydroxyphenylacetic acid (DOPAC), 5-hydroxyindoleacetic acid (5-HIAA), bromocresol green (BG) and multi-walled carbon nanotubes (MWCNT; code 773840 Sigma) were purchased from Sigma-Aldrich (USA). Considering the physiological pH, the phosphate buffer of pH 7.4 was used for detailed experimental studies.

4.3.1.2 Instruments

The voltammetric measurements and characterization techniques were similar to previously described in the Chapter 2 (section A). Raman Spectroscopy was performed using Renishaw invia Raman microscopy at 540 nm.

4.3.1.3 Preparation of graphene nanoribbons (GNRs)

The formation of graphene nanoribbons has been carried out via longitudinal unzipping of MWCNTs as previously reported [83]. Briefly, first MWCNTs were suspended in concentrated sulfuric acid for the duration of 9–10 h and then treated with $KMnO_4$ solution. The solution was stirred for 1–2 h at room temperature. After this, the solution was heated at 70^{o}C for another 2 h. The H_2SO_4 helps to flake off the structure of carbon nanotubes and graphene. The quenching of the reaction was performed by streaming the reaction mixture on the ice containing a solution of hydrogen peroxide and the reaction mixture was filtered. The obtained powder was washed with dilute HCl followed by ethanol/ether for five times and dried overnight.

4.3.1.4 Preparation of nanocomposite modified p-BG/GNRs/EPPG sensor

Initially the edge plane of pyrolytic graphite piece embedded in the glass tube [84] was cleaned by rubbing on an emery paper (P-400) then thoroughly washed with double distilled water and allowed to dry at room temperature. In the first step of modification, the optimized volume of 15 µL of prepared GNRs solution was casted on the dried surface of EPPG sensor and set aside to dry in an oven overnight. In the next step, electropolymerization of p-BG at the prepared GNRs/EPPG sensor was carried out by scanning the potential from −400 mV to 1800 mV for optimized 20 scans at a sweep rate of 100 mV/s in 1 mM BG solution prepared in 0.1 M NaOH.

The fabricated sensor was taken out after completion of 20 scans (optimized) and carefully rinsed with double distilled water to remove the suspended and unreacted adsorbed molecules of the BG monomer. Afterwards, the modified sensor was stabilized in the NaOH solution (0.1 M) by applying the potential between 400 mV and −1100 mV at the sweep rate of 100 mV/s for 10 scans (optimized) to get a steady cyclic voltammogram. The finally modified sensor was allowed to dry and referred as p-BG/GNRs/EPPG sensor.

In another approach, polymerization of BG was achieved followed by the drop casting of GNRs. However, in this case broad peaks with low currents were noticed for both the analytes. Hence, it was decided to use GNRs followed by the polymerization of BG, which provided good conductivity.

4.3.1.5 Voltammetric procedure

The required amount of the DOPAC or 5-HIAA was dissolved in the double distilled water to prepare 1 mM solutions. For recording voltammograms 2 ml of pH 7.4 phosphate buffer and desired amount of the stock solution of the analyte were added. The total volume was made to 4.0 mL by adding double distilled water and nitrogen was bubbled for 5 min at slow rate. The cyclic voltammetric studies were performed using optimized parameters as initial potential (E_i): 0 mV, switching potential (E): 600 mV, final potential (E_f): 0 mV with the sweep rate (ν):100 mV s^{-1}, whereas square wave voltammetric measurements have been carried out using optimized parameters, initial potential (E_i) as 0 mV, final potential (E_f) as 600 mV, potential step (E) as 4 mV, SW amplitude (E_{sw}) as 25 mV with the square wave frequency (f) of 15 Hz. All the potentials reported are with respect to Ag/AgCl electrode at an ambient temperature of 25 ± 2^{o}C. After each scan a constant potential of −600 mV was applied for 120 s in the blank solution to regenerate the sensing surface by removing the adsorbed material.

The urine samples of three healthy volunteers (anthropometric data; sample 1, male 26 yrs; sample 2, female 28 yrs; sample 3, male 52 yrs) were obtained from I.I.T. hospital. The blood samples obtained from the healthy volunteers were centrifuged for 15 min at 1000 r.p.m using Remi microcentrifuge (Model RMI 2C), Remi Motors, Mumbai and the plasma was collected.

4.3.2 RESULT AND DISCUSSION

4.3.2.1 Characterization of prepared GNRs and p-BG/GNRs/EPPG sensor

A comparison of Raman spectroscopic data for the GNRs formed and the starting material (MWCNTs) is presented in **Fig. 4.11**. The G band at 1597 cm^{-1}, which is characteristic peak of sp^2 symmetry and crystallinity of the MWCNTs was clearly observed (**curve a**) [85]. The band broadens and a new D band at 1358 cm^{-1} appeared after the formation GNRs (**curve b**), due to the increased edge effects of ribbons as compared to the MWCNTs. The positions of peaks were in good agreement with those reported by Amanda et al [32]. The D band showed the high intensity than G band due to the high distribution of edges and nipples within the graphene nanoribbons. The behaviour is similar to that reported for GNRs and MWCNTs earlier [78,86]. Thus, it is concluded that formation of GNRs from the MWCNTs has been achieved.

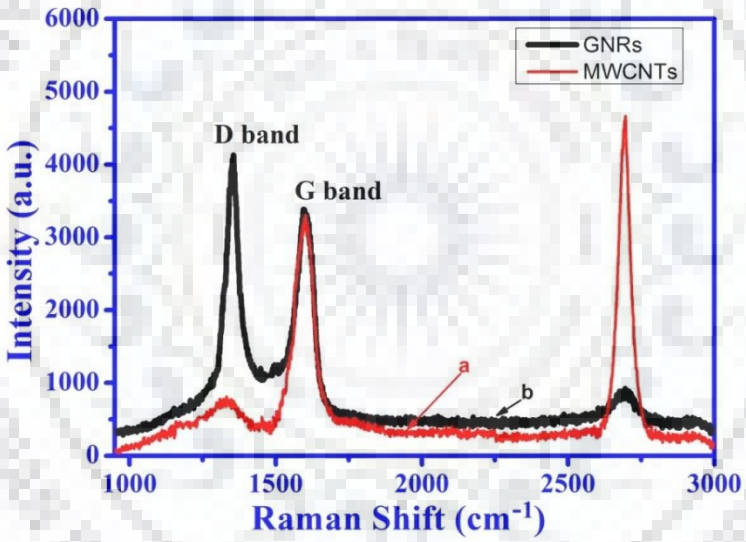

Fig. 4.11: A comparison of Raman spectra observed for MWCNTs (curve a) and GNRs (curve b).

The X-ray diffraction analysis has also been carried out to investigate the structure of the graphene nanoribbons formed by unzipping of MWCNTs. It was found that the XRD pattern of the prepared graphene nanoribbons exhibited crystalline structure having strong diffraction peaks at $2\theta=25.4^{\circ}$ (corresponding to (002) crystal plane), one at $2\theta=42.8^{\circ}$ (corresponding to (100) crystal plane) and other small peaks for (101), (004), (110) planes as shown in **Fig. 4.12**. The peak of 002 crystal plane appeared with the larger d-spacing (according to Bragg's equation) compared to MWCNTs which clearly indicated the presence of residual oxygen-containing functional groups or other structural defects in the nanoribbons. The presence of the remaining oxygen functionalities

and disorder improves accessibility to electrolyte ions and increase the layer space accordingly [85,87].

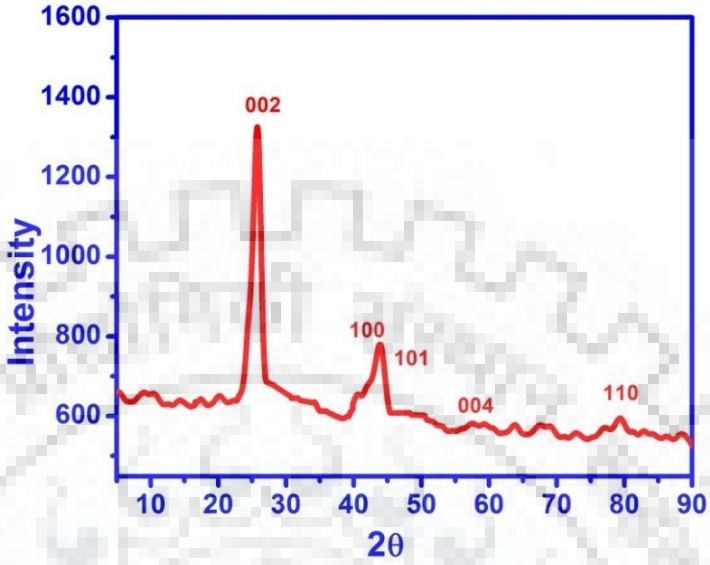

Fig. 4.12: XRD pattern observed for the GNRs.

To investigate the nanoscale variation in the surface morphology of each step used in the modification approach, the FE-SEM was employed and recorded micrographs are presented in **Fig. 4.13**. The unmodified EPPG surface was smooth and flat, as presented in **Fig. 4.13 (A)**. **Fig. 4.13 (B)** presents the EPPG surface after drop casting of GNRs and demonstrates the deposition of graphene nanoribbons. **Fig. 4.13 (C)** is the micrograph of the p-BG coated GNRs surface, where polymer appears to wet the GNRs surface and a strong interface formation takes place. This furnished more effective surface area and hence, the interaction of the modified surface with the analytes was more likely.

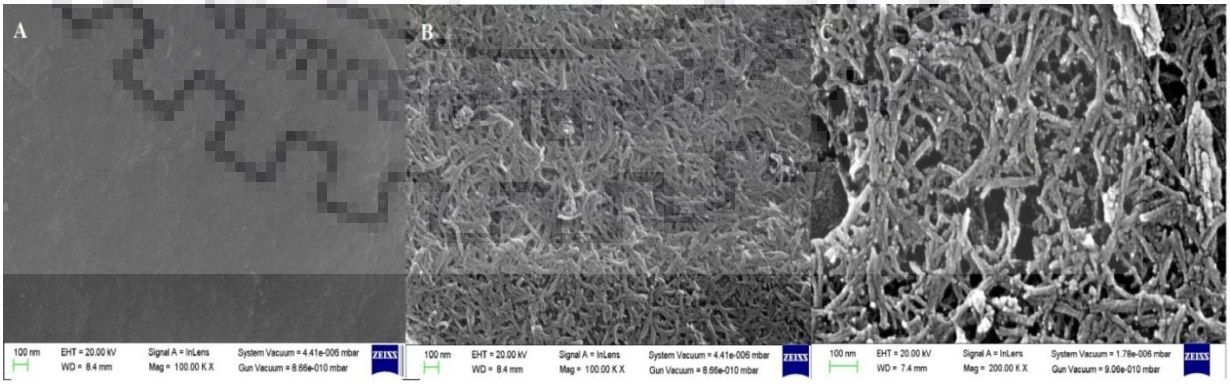

Fig. 4.13: FE-SEM micrographs observed for unmodified EPPG (**A**), GNRs/EPPG (**B**) and p-BG/GNRs/EPPG (**C**).

The value of the electron-transfer resistance (R_{CT}) of unmodified EPPG, GNRs/EPPG and p-BG/GNRs/EPPG sensor was determined in the solution of 1:1 KCl of 0.1 M and $K_3Fe(CN)_6$ of 5 mM at the frequency varying between 0.1 Hz and 100 kHz with an applied potential of 0.05 V and a comparison of the observed results is presented in **Fig. 4.14**. The EIS curves exhibited a semicircle followed by the linear portion. The diameter of the semicircle indicated the value of the charge transfer resistance (R_{CT}) and the linear portion of the curve indicated the mass transfer effects (at the lower frequency). The inset of the Figure exhibits the Randles equivalent circuit model, which is applied for simulating the experimental data. In the Randles equivalent circuit the electrolyte resistance is represented as R_s, charge transfer resistance is shown as R_{CT} and the double layer capacitance and Warburg impedance are denoted by C_{dl} and Z_w respectively. At the unmodified EPPG surface the R_{CT} value i.e. electron transfer resistance for the $Fe[CN]_6^{3-/4-}$ redox process was found as 1180 Ω (**curve a**), whereas for GNRs/EPPG sensor, the R_{CT} value was found as 540 Ω. The smallest semicircle was observed for the p-BG/GNRs/EPPG sensor, where the R_{CT} value was noticed as 220 Ω (**curve c**) and demonstrated the lowest resistance. Thus, in the case of p-BG/GNRs/EPPG sensor, maximum electron transfer efficiency is expected, which would facilitate the oxidation of DOPAC and 5-HIAA.

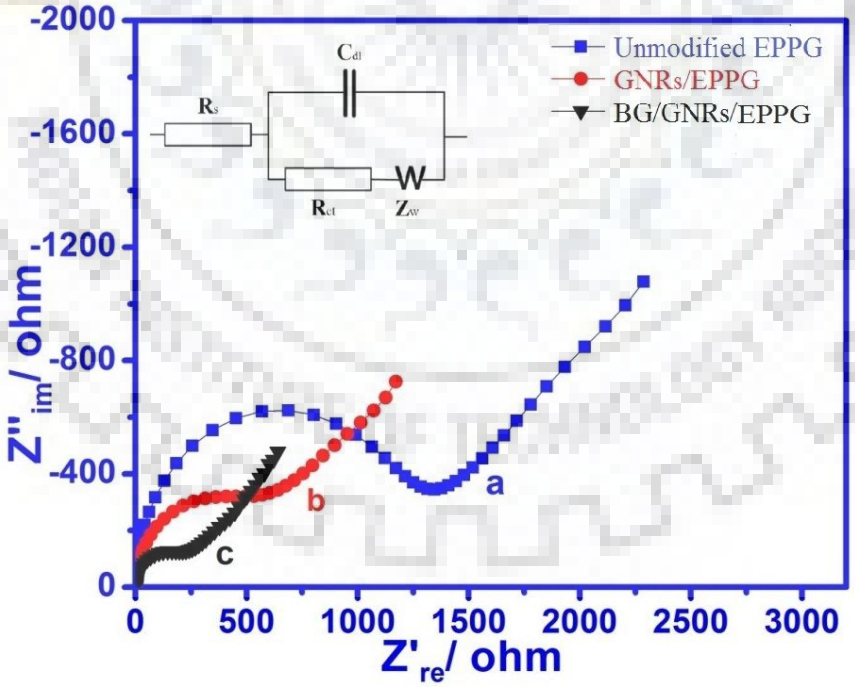

Fig. 4.14: Nyquist plots observed for unmodified EPPG (a), GNRs/EPPG (b) and p-BG/GNRs/EPPG (c). The inset represents the Randles equivalent circuit used for the simulation of the EIS data.

The effective surface areas of the unmodified EPPG, GNRs/EPPG and p-BG/GNRs/EPPG sensors were also calculated. The voltammograms were recorded at different sweep rates for 1 mM $K_3Fe(CN)_6$ containing 0.1 M KCl as supporting electrolyte. The slope of the i_p vs. $\nu^{1/2}$ polts was used to calculate effective surface areas using Randles-Sevcik equation:

$$\mathbf{i_p = 0.4463\ (F^3/RT)^{1/2}\ A.\ n^{3/2}\ D_R^{1/2}\ C_o.\ \nu^{1/2}}$$

here i_p (peak current) is in Ampere, F (Faraday's constant) is 96,485C mol^{-1}, R (universal gas constant) is 8.314 $JK^{-1}mol^{-1}$, T (absolute temperature) is taken as 298 K, n is the number of electron (1 in this case), A (surface area of electrode) in cm^2, D_R (diffusion coefficient) 7.6×10^{-6} cm^2s^{-1}, C_o is concentration in mol L^{-1} and ν (sweep rate) in Vs^{-1}. The effective surface areas were calculated as 0.082 cm^2, 3.954 cm^2 and 5.178 cm^2 for the unmodified EPPG, GNRs/EPPG and p-BG/GNRs/EPPG sensors, respectively. The observed results demonstrated that the proposed p-BG/GNRs/EPPG sensor displayed remarkable increment in the surface area, which facilitated the charge transfer kinetics for the electro-oxidation of the analytes.

4.3.2.2 Cyclic voltammetry

The cyclic voltammograms of 30 μM DOPAC or 5-HIAA exhibited a single well-defined peak at 154 mV and 319 mV at pH 7.4 at p-BG/GNRs/EPPG surface. The electrochemical responses observed for a mixture of DOPAC (30 μM) and 5-HIAA (30 μM) at the unmodified EPPG, GNRs/EPPG and p-BG/GNRs/EPPG sensors is presented in **Fig. 4.15**. At unmodified EPPG, a broad peak at 307 mV (**curve a**) with peak current of ~1.2 μA was observed. At the GNRs/EPPG surface two anodic peaks were clearly observed (**curve b**). The peak at 190 mV (peak b_1) with the peak current of ~1.52 μA was assigned to DOPAC and formed a quasi-reversible couple with the reduction peak observed in the reverse sweep at 154 mV (peak b_1'). The peak at 380 mV was assigned to 5-HIAA having peak current ~1.64 μA (peak b_2). At p-BG/ GNRs/EPPG sensor surface, 5-HIAA peak was observed at 319 mV. The peak at 154 mV (DOPAC) also formed a quasi-reversible couple with the peak observed in the reverse sweep (peak c_1').

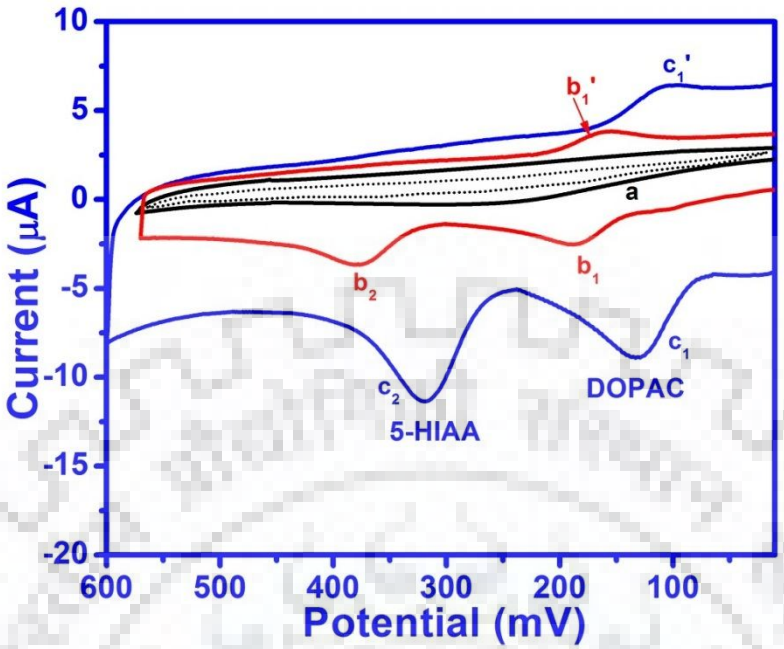

Fig. 4.15: Comparison of cyclic voltammograms observed at unmodified EPPG (curve a), GNRs/EPPG (curve b) and p-BG/GNRs/EPPG (curve c) sensors for a mixture of DOPAC and 5-HIAA (30 μM each) at a scan rate of 100 mVs^{-1} in phosphate buffer of pH 7.4. The background is denoted by the dotted line.

The nature of the electron transfer process at p-BG/GNRs/EPPG sensor was studied by monitoring the effect of sweep rate. The sweep rate studies were performed by recording the cyclic voltammograms at the fixed concentration of 30 μM of each analyte in the sweep range 5 mVs^{-1} to 250 mVs^{-1}. The peak current (i_p) increased linearly for both the analytes with increasing sweep rate and the linearity of i_p versus ν plots can be expressed as:

For DOPAC $\quad i_p\ (\mu A) = 0.0237\ \nu + 0.9636 \quad (R^2 = 0.991)$

$\log i_p = 0.5581 \log \nu - 0.5574 \quad (R^2 = 0.991)$

For 5-HIAA $\quad i_p\ (\mu A) = 0.0236\ \nu + 0.8317 \quad (R^2 = 0.985)$

$\log i_p = 0.6469 \log \nu - 0.7577 \quad (R^2 = 0.997)$

The linearity for i_p versus ν plots for both DOPAC and 5-HIAA revealed the adsorption controlled pathway for the oxidation of both the compounds, which was further confirmed by the slope of log i_p versus log ν plots. The slope values for DOPAC and 5-HIAA were 0.558 and 0.646,

respectively. As the slope for DOPAC was slightly greater than 0.5, hence it was difficult to decide whether the reaction was diffusion controlled or adsorption controlled, whereas, for 5-HIAA the slope was sufficiently higher than 0.5 and indicted adsorption controlled oxidation. Hence, further studies using square wave were carried out to establish the nature of electrode reaction for DOPAC and 5-HIAA [31].

4.3.2.3 Square wave voltammetry

Square wave voltammograms of a mixture of DOPAC and 5-HIAA (35 μM each) were also recorded at unmodified EPPG, GNRs/EPPG and p-BG/GNRs/EPPG sensors at pH 7.4. A comparison of the results observed at various surfaces is shown in **Fig. 4.16.** At the surface of unmodified EPPG, a single peak (E_p = 307 mV) was observed (**curve a**), while at the GNRs/EPPG sensor two peaks at 185 mV and 330 mV were observed with the peak currents ~2.14 μA and ~2.5 μA for DOPAC and 5-HIAA, respectively (**curve b**). The curve c of **Fig. 4.16** was recorded at p-BG/GNRs/EPPG sensor and clearly exhibited two well-defined anodic peaks. It was found that p-BG/GNRs/EPPG sensor gives excellent results for the simultaneous determination of DOPAC and 5-HIAA in terms of peak separation and sensitivity. Hence, detailed studies were carried out using p-BG/GNRs/EPPG sensor.

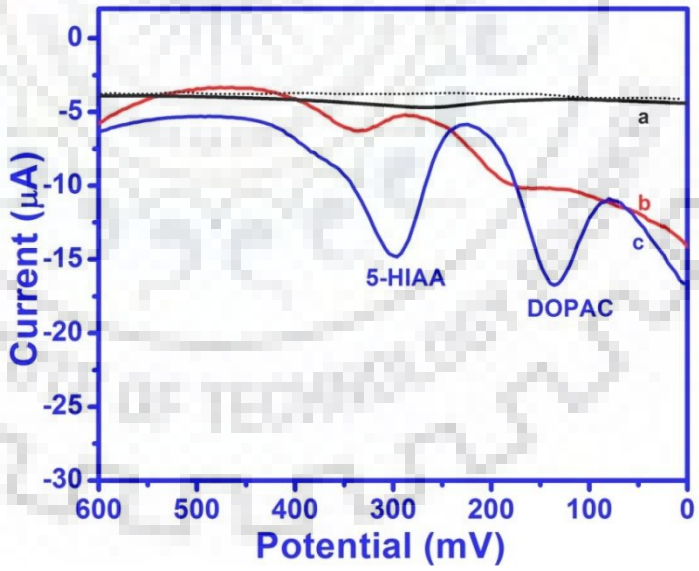

Fig. 4.16: A comparison of SWVs observed for 35 μM DOPAC and 5-HIAA at unmodified EPPG (curve a), GNRs/EPPG (curve b) and p-BG/GNRs/EPPG (curve c) at pH 7.4. The background current is represented by the dotted line.

4.3.2.3.1 Electrochemical investigations of DOPAC

The modified p-BG/GNRs/EPPG sensor was initially used for the quantification of DOPAC by using SWV. **Fig. 4.17 (A)** shows the effect of concentration in the range 0.05 to 180 μM on the SWV response in terms of the oxidation peak current of DOPAC at pH 7.4. The background current was subtracted for calculating the peak current and the reported value is an average of minimum three replicate voltammograms. Under the optimal conditions, the peak current remarkably increased with the increasing concentration of DOPAC and exhibited a linear relation over the concentration range of 0.05 to 180 μM. The linear dependence can be represented as:

$$\mathbf{i_p\ (\mu A) = 0.2093\ [C\ 0.05 - 180\ \mu M] + 2.1048}$$

having a determination coefficient 0.999. The i_p is the peak current of DOPAC in μA and C is the concentration in μM. The detection limit (LOD) and quantitation limit (LOQ) for DOPAC were calculated using the relation 3 σ/b and 10 σ/b, respectively, where σ represents the standard deviation of the blank signals and b represents the slope of the calibration curve and were found as 1.2 nM and 4.8 nM, respectively. The results demonstrate that the modified sensor is highly sensitive towards the electrochemical oxidation of DOPAC.

To study the effect of pH on the electrochemical oxidation of DOPAC, voltammograms were recorded in the phosphate buffers in the pH range 2.4-11.0 for 25 μM of analyte concentration. The peak potential of DOPAC shifted to the less positive values with the increase in pH. The E_p versus pH plot was linear and the dependence of E_P on pH can be represented as:

$$\mathbf{E_p\ (pH\ 2.4 - 11.0) = -52.40\ pH + 522.09\ mV\ \ vs.\ Ag/AgCl \qquad (R^2 = 0.998)}$$

where R^2 denotes the determination coefficient. The slope of 52.40 mV/pH was close to the theoretical value expected from the Nernst equation, and suggested that the equal number of electrons and protons were involved in the oxidation of DOPAC at the p-BG/ GNRs/EPPG surface.

The effect of the square wave frequency on the anodic peak current was also investigated by recording the voltammogram of DOPAC (25 μM) over the frequency range 5-40 Hz. The plot of peak current (i_p) vs. frequency (f) was linear and the dependence can be represented as:

$$\mathbf{i_p/\mu A = 0.3522\ f + 2.2975 \qquad (R^2 = 0.997)}$$

where, the peak current (i_p) is in µA and f is in Hz. The linearity of the above relation suggested that the process of oxidation of DOPAC was adsorption-controlled, which was further confirmed by the linear relation of log i_p versus log f:

$$\log i_p = 0.7042 \log f + 0.0704 \qquad (R^2 = 0.997)$$

As the value of d logf /d log i_p was sufficiently > 0.5, hence, it was established that the oxidation of DOPAC was adsorption controlled [31].

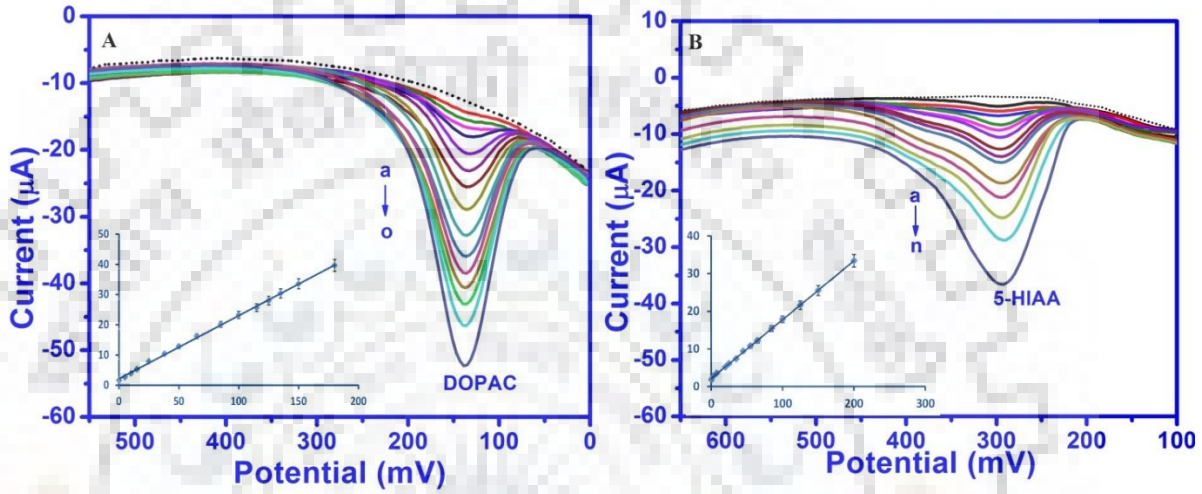

Fig. 4.17: (A) SWVs observed for the increasing concentration of DOPAC at p-BG/GNRs/EPPG sensor at pH 7.4. Curves were recorded at (a) 0.05, (b) 5, (c) 10, (d) 15, (e) 25, (f) 38, (g) 50, (h) 65, (i) 85, (j) 100, (k) 115, (l) 125, (m) 135, (n) 150 and (o) 180 µM concentration of DOPAC; inset is the calibration plot.

(B) SWVs observed for the increasing concentration of 5-HIAA at p-BG/GNRs/EPPG sensor at pH 7.4 at (a) 0.5, (b) 3, (c) 8, (d) 20, (e) 25, (f) 35, (g) 45, (h) 55, (i) 65, (j) 85, (k) 100, (l) 125, (m) 150 and (n) 200 µM; inset represents the calibration plot.

4.3.2.3.2 Electrochemical investigations of 5-HIAA

To investigate the effect of concentration of 5-HIAA on the peak current at the modified sensor, square wave voltammograms were recorded at different concentrations. At optimized conditions, the reported values of anodic peak currents are an average of at least three replicate runs after subtracting the background current. The peak currents of 5-HIAA increased with increasing concentration of 5-HIAA in the range 0.5–200 µM. The plot of i_p versus concentration was linear with a determination coefficient of 0.999 as shown in **Fig. 4.17 (B).** The linear relation can be represented as:

$$i_p\ (\mu A) = 0.1565\ [C,\ 0.5 - 200\ \mu M] + 2.1043$$

where, C is the concentration of 5-HIAA in μM. The limit of detection (LOD) and limit of quantification (LOQ) were found as 3 nM and 5.6 nM, respectively. A comparison of the detection limits of the present method with reported in recent years at other surfaces is tabulated in **Table 7.** It can be clearly seen that the LOD observed using p-BG/GNRs/EPPG is much lower.

Table 7: A comparison of analysis results of DOPAC and 5-HIAA at p-BG/GNRs/EPPG sensor with recently reported sensors.

S.No.	Method/Electrode	Conc. range (μM)	LOD (nM)	Real sample	Ref.
	DOPAC				
1.	Tyrosinase-chitosan/GCE	0.006-200	3	No	[89]
2.	SWNTs/GCE	1-120	400	No	[90]
3.	NSTP/AuE	0.2-10	90	No	[91]
4.	PPBA/MWCNTs/GCE	8.4-1500	3000	Yes	[92]
5.	Functionalized thiol SAM/AuE	1.6-130	1600	No	[93]
6.	p-BG/GNRs/EPPG	0.05-180	1.2	Yes	This work
	5-HIAA				
1.	NTGC	0.1-100	56	Yes	[18]
2.	NGITO	0.1-100	27	Yes	[18]
3.	Poly(sulphosalicylic acid)/CF	0.5-10	250	No	[66]
4.	AuNPs/SPCs	0.5-200	22	Yes	[88]
5.	OGCE	1.56-58.6	917	No	[94]
6.	AuNPs-SEPPGE	0.1-120	5.7	Yes	[95]
7.	GCE	0.2-20	80	Yes	[96]
8.	MWNT-Nafion/GCE	0.09-7.98	2.5	No	[97]
9.	p-BG/GNRs/EPPG	0.5-200	3	Yes	This work

NSTP/AuE:N-Succinimidyl-3-Thiopropionate-Functionalized Gold Electrodes, **PPBA/MWCNTs/GCE:** Poly(pyridine-3-boronic acid)/multi walled carbon nanotubes composite modified glassy carbon electrode, **Functionalized thiol SAM/AuE**: Functionalized thiol self-assembled monolayer mmobilized gold electrode, **NTGC**: single-walled carbon nanotube modified glassy carbon electrode, **NGITO:** gold nanoparticles modified indium tin oxide electrode, **AuNPs-SEPPGE**:gold nanoparticle modified screen-printed graphite electrode, **OGCE**: oxidized glassy carbon electrode, **SPCs**: screen printed carbon sensor.

The effect of pH of the supporting electrolytes on the peak potential of 5-HIAA was investigated in the pH range 2.4–11.0. In the entire pH range a single well-defined peak was noticed. It was observed that the E_p shifted to less positive potentials with increasing pH. The dependence of E_p on pH was linear and can be documented by the relation:

$$\mathbf{E_p\ (pH\ 2.4 - 11.0) = -52.98\ pH + 672.93\ mV\ vs.\ Ag/AgCl}$$

having determination coefficient (R^2) as 0.998. The slope of 52.98 mV/pH, is close to the theoretical Nernstian value, which clearly demonstrates that an equal number of protons and electrons are involved in the oxidation of 5-HIAA [88].

To investigate the effect of square wave frequency on the anodic peak current (i_p) of 5-HIAA, the square wave voltammograms were recorded by changing the frequency from 5 to 40 Hz at pH 7.4. It can be clearly seen from the results that the oxidation peak current is increased as the square wave frequency increases. The linear dependence of the anodic peak current (i_p) on the frequency (f) observed the relation:

$$\mathbf{i_p/\mu A = 0.3935\ f - 0.083 \qquad (R^2 = 0.995)}$$

where i_p is the peak current in μA and f is square wave frequency in Hz. Dependence of the log i_p on log f was also linear and relation can be represented as:

$$\mathbf{\log i_p = 0.9834 \log f - 0.3875 \qquad (R^2 = 0.996)}$$

The observed slope of d log i_p/d log f was found > 0.5, which confirmed the adsorption controlled pathway for the oxidation of 5-HIAA.

4.3.2.3.3 Simultaneous determination of DOPAC and 5-HIAA

The simultaneous analysis of DOPAC and 5-HIAA was then carried out at pH 7.4. In the first step, the experiments were performed by keeping the concentration of DOPAC constant (15 μM) and the concentration of 5-HIAA was varied from 10 μM to 70 μM. The observed results are displayed in **Fig. 4.18 (A)**, which clearly exhibit two peaks at 136 mV and 296 mV for DOPAC and 5-HIAA, respectively. On increasing the concentration of 5-HIAA, the peak current of 5-HIAA increases linearly, without affecting the peak current and peak potential of DOPAC. In the second set of experiments, the voltammograms were recorded for DOPAC in the concentration range 10 μM−70 μM by keeping the concentration of 5-HIAA constant (15 μM). The observed results are presented in **Fig. 4.18 (B)**, and clearly demonstrate that the peak current of DOPAC increased linearly with increasing concentrations, whereas no effect on the peak current or peak

potential was observed for 5-HIAA. Thus, it is concluded that simultaneous determination of the two analytes is possible using p-BG/GNRs/EPPG sensor.

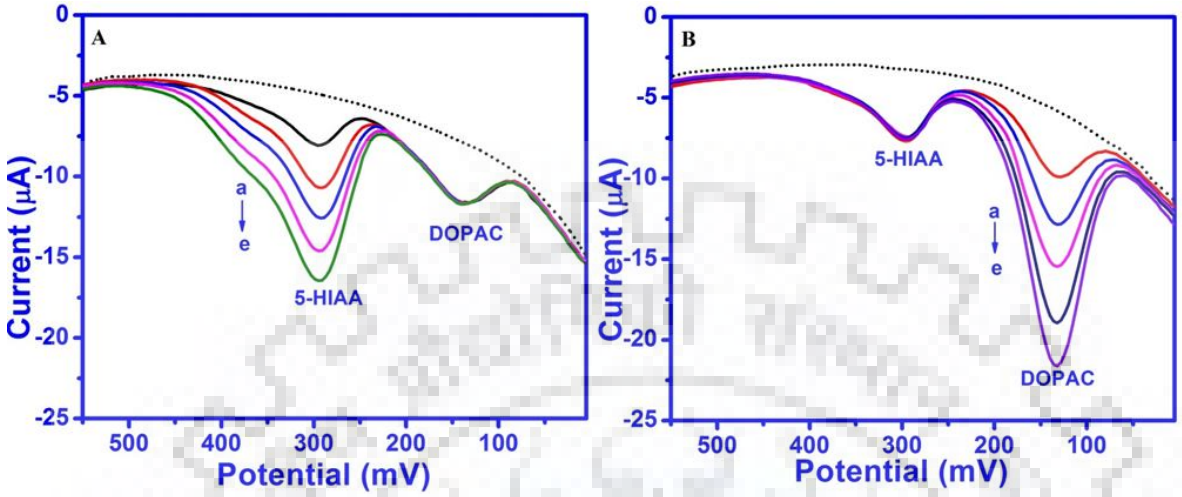

Fig. 4.18: (**A**) Square wave voltammograms of a mixture of DOPAC and 5-HIAA at p BG/GNRs/EPPG sensor at pH 7.4. at concentration of 5-HIAA (a) 10; (b) 25; (c) 35; (d) 50 and (e) 70 μM. The concentration of DOPAC was constant (15 μM). The background is shown by the dotted line.

(**B**) SWVs recorded for of a mixture of DOPAC and 5-HIAA recorded at p-BG/GNRs/EPPG sensor at pH 7.4, with concentration of DOPAC (a) 10; (b) 25; (c) 40; (d) 55 and (e) 70 μM, keeping the concentration of HIAA constant (15 μM). The dotted line represents the background.

4.3.2.4 Analytical utility

4.3.2.4.1 Interference study

As hypoxanthine (HX), xanthine (XT), uric acid (UA) and ascorbic acid (AA) are usually found in the biological fluids, i.e. human blood and urine, hence, it was considered desirable to check their interference. These biomolecules are found in high concentration, like HX as ~ 40 μg/dL, XT as ~ 20 μg/dL, UA as ~ 4–8 mg/dL and AA as ~ 0.5–1.2 mg/dL in the physiological fluids, hence, they may interfere in the response of the targeted analyte. Hence, voltammograms of DOPAC and 5-HIAA mixture were recorded in the presence of various concentrations of these interfering species under the optimized conditions. **Fig. 4.19 (A)** presents a typical voltammogram for a mixture of DOPAC (40 μM) and 5-HIAA (25 μM) in the presence of increasing concentration of HX, XT and AA at the p-BG/GNRs/EPPG sensor. It can be clearly seen that these

biomolecules do not interfere with the oxidation of DOPAC and 5-HIAA using proposed approach upto 1 mM concentration.

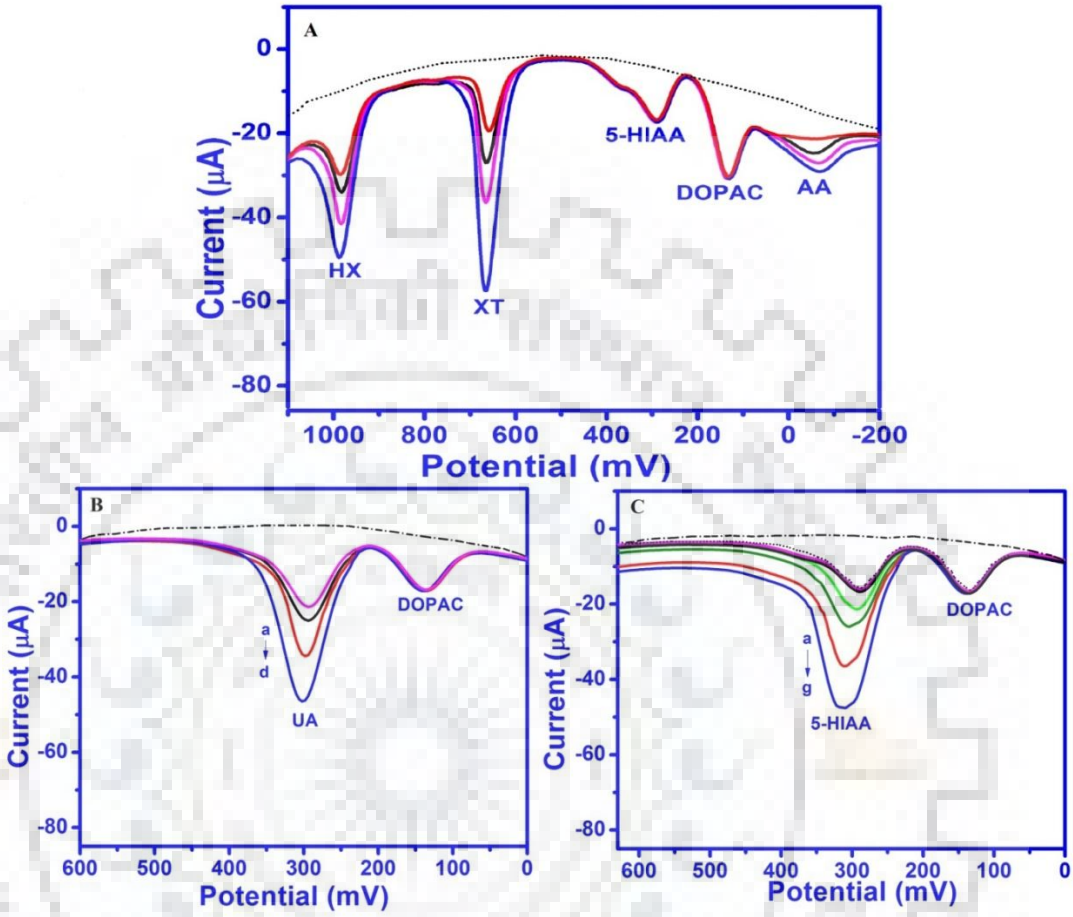

Fig. 4.19: (**A**) SWVs recorded for 40 μM DOPAC and 25 μM 5-HIAA in the presence of ascorbic acid (AA), xanthine (XT) and hypoxanthine (HX) at the p-BG/GNRs/EPPG sensor at pH 7.4. The background is displayed by the dotted line.

(**B**) SWVs observed for 25 μM DOPAC at different concentrations of UA (a) 100 μM (b) 400 μM (c) 700 μM, and (d) 1000 μM at the p-BG/GNRs/EPPG sensor. The background is displayed by the dash-dotted line.

(**C**) SWVs observed for 25 μM DOPAC and 25 μM 5-HIAA at different concentrations of UA (a) 0 μM {dotted line}, (b) 25 μM (c) 75 μM, (d) 100 μM, (e) 400 μM, (f) 700 μM and (g) 1000 μM at the p-BG/GNRs/EPPG sensor. The background is displayed by the dash-dotted line.

The effect of UA and its tolerance limit on the simultaneous determination of DOPAC and 5-HIAA was investigated up to 1 mM concentration of UA. It was observed that the peak of DOPAC remains unaffected upto 1 mM UA **(Fig. 4.19 B).** However, the presence of UA affected

the peak response of 5-HIAA at concentration >75 μM as shown in **Fig. 4.19 (C)**. The peak shape of 5-HIAA became broad on the addition of more than 75 μM UA. Thus, it is concluded that determination of DOPAC has no influence of AA, UA, XT and HX, whereas 5-HIAA is free from interferences of AA, XT and HX upto 1 mM and UA was tolerated only up to the three times concentration of 5-HIAA.

4.3.2.4.2 Stability and reproducibility of p-BG/GNRs/EPPG sensor

The stability of p-BG/GNRs/EPPG sensor was examined at the fixed concentration of DOPAC and 5-HIAA (25 μM each) at pH 7.4 over a period of 30 days. For recording voltammograms, the proposed sensor was used every day and kept under the ambient conditions. The results demonstrated a variation in the peak current of DOPAC and 5-HIAA with relative standard deviation (R.S.D) as ± 2.08% and ± 2.69% during the first 15 days for DOPAC and 5-HIAA, respectively. After 15 days, the current response exhibited a variation of ± 5.12% and ± 5.86 %. Hence, the p-BG/GNRs/EPPG sensor has sufficient stability for 15 days and can be employed for the simultaneous determination of DOPAC and 5-HIAA, after which a deviation was noticed.

To elucidate the intraday reproducibility of the proposed sensor, the sensor was employed for recording at least eight replicate voltammograms in the blank solution as well as in the mixture of DOPAC and 5-HIAA (25 μM each) during same day at an interval of 1 h. The calculated R.S.D. for replicate voltammograms (n = 4) was found to be ± 0.78% and ± 1.36% for DOPAC and 5-HIAA, respectively. The low R.S.D. values demonstrate the significant accuracy and good reproducibility of the proposed approach.

4.3.2.4.3 Recovery in human urine and plasma samples

The practical applicability of the modified sensor for the simultaneous determination of DOPAC and 5-HIAA was studied in the human urine samples by carrying out recovery studies. A known amount of the two analytes in the urine sample of healthy volunteers, after diluting the sample (three times) with phosphate buffer of pH 7.4, was added and the voltammograms were recorded. The observed results are documented in **Table 8**. The recoveries were found in the range 99.6–100.8% for DOPAC and 98.6–100.5% for 5-HIAA. The plasma samples were also spiked with exogenous DOPAC and 5-HIAA and the voltammograms were recorded. The recovery values were determined in the range 99.4–100.6% for DOPAC and 99.6–100.73% for 5-HIAA as shown by results which are summarized in **Table 9**. The recoveries observed from the results were in an

acceptable range, which showed that the developed method can be efficiently used for the selective determination of DOPAC and 5-HIAA in physiological samples.

Table 8: Recovery analysis of DOPAC and 5-HIAA at the modified p-BG/GNRs/EPPG sensor in the human urine samples.

	DOPAC			5-HIAA	
	Amount added (µM)	**Amount detected (µM)**	**Recovery*%**	**Amount detected (µM)**	**Recovery*%**
Sample 1					
	5	4.98	99.64	4.93	98.6
	10	10.01	100.1	9.96	99.60
	15	15.12	100.8	15.08	100.53
Sample 2					
	20	19.97	99.85	20.05	100.25
	30	30.04	100.13	29.92	99.70
	40	39.96	99.90	40.09	100.22
Sample 3					
	25	24.99	99.96	25.04	100.16
	50	50.03	100.06	50.07	100.14
	75	74.97	99.96	74.94	99.92

*The R.S.D. value for determination was less than 2.04 for n = 3.

Table 9: Recovery analysis of DOPAC and 5-HIAA at the modified p-BG/GNRs/EPPG sensor in the human plasma samples of healthy volunteers.

		DOPAC		5-HIAA	
S. No.	**Amount added (µM)**	**Amount detected (µM)**	**Recovery*%**	**Amount detected (µM)**	**Recovery*%**
1.	1	0.994	99.4	0.996	99.6
2.	2	2.012	100.6	1.988	99.4
3.	3	2.989	99.63	3.022	100.73

*The R.S.D. value for determination was less than 2.86 for n = 3.

4.3.3 CONCLUSION

The fabrication of a novel and intensely sensitive p-BG/GNRs/EPPG sensor is presented in this manuscript using graphene nanoribbons and polymeric bromocresol green. The modification approach by carrying out polymerization of BG after drop casting of GNRs was found useful in the fabrication of the sensor. The modified sensor has been successfully used for the simultaneous detection of DOPAC and 5-HIAA with excellent sensitivity and selectivity. The GNRs effectively interlinked with the polymeric layer of BG and provided large active surface area. The linear relation of the peak current with the increasing concentration was noticed in the range 0.05 – 180 µM for DOPAC and 0.5 – 200 µM for 5-HIAA and limit of detections were found as 1.2 nM and 3 nM for DOPAC and 5-HIAA, respectively. The common interfering agents such as AA, UA, XT and HX did not interfere at their physiologically relevant concentrations. UA was tolerated only upto three times concentration as it interfered with the peak of 5-HIAA. The presented sensor can be effectively applied to determine DOPAC and 5-HIAA in human urine samples. The method is simple, rapid, sensitive, highly reproducible, sufficient selective and the sensor is remarkably stable, which makes it a potential candidate for the clinical analysis of DOPAC and 5-HIAA in human physiological samples.

4.4 REFERENCES

[1] M.R. Nasarabadi, F. Ahmadi, S. Hamdi, N. Eslami, K. Didehban, M.R. Ganjali, "Preparation of nanosized chromium carbonate and chromium oxide green pigment through direct carbonation and precursor thermal decomposition", J. Mol. Liq. 216 (2016) 814.

[2] R. Bavandpour, H.K. Maleh, M. Asif, N. Atar, M. Abbasghorbani, "Liquid phase determination of adrenaline uses a voltammetric sensor employing $CuFe_2O_4$ nanoparticles and room temperature ionic liquids", J. Mol. Liq. 213 (2016) 369.

[3] C. Lee, X. Wei, J.W. Kysar, J. Hone, "Measurement of the elastic properties and intrinsic strength of monolayer graphene", Science 321 (2008) 385.

[4] J. Liu, J. Tanga, J.J. Gooding, "Strategies for chemical modification of graphene and applications of chemically modified graphene", J. Mater. Chem. 22 (2012) 12435.

[5] P. Gupta, R.N. Goyal, "Polymelamine modified edge plane pyrolytic graphite sensor for the electrochemical assay of serotonin", Talanta 120 (2014) 17.

[6] Rosy, M. Raj, R.N. Goyal, "A facile method to anchor reduced graphene oxide polymer nanocomposite on the glassy carbon surface and its application in the voltammetric estimation of tryptophan in presence of 5-hydroxytryptamine", Sens. Actuators B 233 (2016) 445.

[7] M. Amare, S. Admassie, "Differential pulse voltammetric determination of theophylline at poly (4-amino-3-hydroxynaphthalene sulfonic acid) modified glassy carbon electrode", Bull. Chem. Soc. Ethiop. 26 (2012) 73.

[8] P. Gupta, R.N. Goyal, Y.B. Shim, "Simultaneous analysis of dopamine and 5-hydroxyindoleacetic acid at nanogold modified screen printed carbon electrodes", Sens. Actuators B 213 (2015) 72.

[9] F.Y. Kong, S.X. Gu, W.W. Li, T.T. Chen, Q. Xu, W. Wang, "A paper disk equipped with graphene/polyaniline/aunanoparticles/glucose oxidase bio composite modified screen-printed electrode: toward whole blood glucose determination", Biosens. Bioelectron. 56 (2014) 77.

[10] P.A. Jose, G.M. Eisner, R.A. Felder, "Renal dopamine receptors in health and hypertension", Pharmacol. Ther. 80 (1998) 149.

[11] C. Missale, S.R. Nash, S.W. Robinson, M. Jaber, M.G. Caron, "Dopamine receptors: from structure to function", Physiol. Rev. 78 (1998) 189.

[12] T.M. Love, "Oxytocin, motivation and the role of dopamine", Pharmacol. Biochem. Behav. 119 (2014) 49.

[13] M.M. Ardakani, H. Rajabi, H. Beitollahi, B.B.F. Mirjalili, A. Akbari, N. Taghavinia, "Voltammetric determination of dopamine at the surface of TiO_2 nanoparticles modified carbon paste electrode", Int. J. Electrochem. Sci. 5 (2010) 147.

[14] R. Zanettini, A. Antonini, G. Gatto, R. Gentile, S. Tesei, G. Pezzoli, "Valvular heart disease and the use of dopamine agonists for Parkinson's disease", N. Engl. J. Med. 356 (2007) 39.

[15] T. Nagatsu, M. Sawada, "L-dopa therapy for Parkinson's disease: past, present, and future", Parkinsonism Rel. Disord. 15 (2009) S3.

[16] L. Gyermek, "Pharmacology of serotonin as related to anesthesia", J. Clin. Anesth. 8 (1996) 402.

[17] K. Wu, J. Fei, S. Hu, "Simultaneous determination of dopamine and serotonin on a glassy carbon electrode coated with a film of carbon nanotubes", Anal. Biochem. 318 (2003) 100.

[18] R.N. Goyal, M. Oyama, V.K. Gupta, S.P. Singh, R.A. Sharma, "Sensors for 5-hydroxytryptamine and 5-hydroxyindole acetic acid based on nanomaterial modified electrodes", Sens. Actuators B 134 (2008) 816.

[19] A. Sikander, S.V. Rana, K.K. Prasad, "Role of serotonin in gastrointestinal motility and irritable bowel syndrome", Clin. Chim. Acta 403 (2009) 47.

[20] K. Gregersen, J. Valeur, K. Lillestol, L. Froyland, P. Araujo, G.A. Lied, A. Berstad, "Subjective food hypersensitivity: assessment of enterochromaffin cell markers in blood and gut lavage fluid", Int. J. Gen. Med. 4 (2011) 555.

[21] M. Shirane, K. Nakamura, "Aniracetam enhances cortical dopamine and serotonin release via cholinergic and glutamatergic mechanisms in SHRSP", Brain Res. 916 (2001) 211.

[22] V. Carrera, E. Sabater, E. Vilanova, M.A. Sogorb, "A simple and rapid HPLC–MS method for the simultaneous determination of epinephrine, norepinephrine, dopamine and 5-hydroxytryptamine: application to the secretion of bovine chromaffin cell cultures", J. Chromatogr. B 847 (2007) 88.

[23] F.C. Cheng, Y. Shih, Y.J. Liang, L.L. Yang, C.S. Yang, "New dual electrochemical detector for microbore liquid chromatography determination of dopamine and serotonin in rat striatum dialysates", J. Chromatogr. B 682 (1996) 195.

[24] I.T. Kuo, Y.F. Huang, H.T. Chang, "Silica nanoparticles for separation of biologically active amines by capillary electrophoresis with laser-induced native fluorescence detection", Electrophoresis 26 (2005) 2643.

[25] S. Sasa, C.L. Blank, "Determination of serotonin and dopamine in mouse brain tissue by high performance liquid chromatography with electrochemical detection", Anal. Chem. 49 (1977) 354.

[26] I. Baranowska, M. Zydron, "Liquid chromatography in the analysis of neurotransmitters and alkaloids", J. Chromatogr. Sci. 40 (2002) 224.

[27] J.Y. Park, S.W. Myung, I.S. Kim, D.K. Choi, S.J. Kwon, S.H. Yoon, "Simultaneous measurement of serotonin, dopamine and their metabolites in mouse brain extracts by high-performance liquid chromatography with mass spectrometry following derivatization with ethyl chloroformate", Biol. Pharm. Bull. 36 (2013) 252.

[28] A.A. Abdelwahab, Y.B. Shim, "Simultaneous determination of ascorbic acid, dopamine, uric acid andfolic acid based on activated graphene/MWCNT nanocomposite loaded Au nanoclusters", Sens. Actuators B 221 (2015) 659.

[29] A.A. Abdelwahab, H.M. Lee, Y.B. Shim, "Selective determination of dopamine with a cibacron blue/poly-1,5-diaminonaphthalene composite film", Anal. Chim. Acta 650 (2009) 247.

[30] Rosy, S.K. Yadav, B. Agrawal, M. Oyama, R.N. Goyal, "Graphene modified Palladium sensor for electrochemical analysis ofnorepinephrine in pharmaceuticals and biological fluids", Electrochim. Acta 125 (2014) 622.

[31] M. Raj, P. Gupta, R.N. Goyal, "Poly-melamine film modified sensor for the sensitive and selective determination of propranolol, a -blocker in biological fluids", J. Electrochem. Soc. 163 (2016) H388.

[32] D.C. Marcano, D.V. Kosynkin, J.M. Berlin, A. Sinitskii, Z. Sun, A. Slesarev, L.B. Alemany, W. Lu, J.M. Tour, "Improved synthesis of graphene oxide", ACS nano 4 (2010) 4806.

[33] P. Gupta, R.N. Goyal, "Graphene and co-polymer composite based molecularly imprinted sensor for ultratrace determination of melatonin in human biological fluids", RSC Adv. 5 (2015) 40444.

[34] V.K. Ponnusamy, V. Mani, S.M. Chen, W.T. Huang, J.F. Jen, "Rapid microwave assisted synthesis of graphene nanosheets/polyethyleneimine/gold nanoparticle composite and its

application to the selective electrochemical determination of dopamine", Talanta 120 (2014) 148.

[35] M. Satyanarayana, K.K. Reddy, K.V. Gobi, "Nanobiocomposite based electrochemical sensor for sensitive determination of serotonin in presence of dopamine, ascorbic Acid and uric acid in vitro", Electroanal 26 (2014) 2365.

[36] P. Gupta, S.K. Yadav, B. Agrawal, R.N. Goyal, "A novel graphene and conductive polymer modified pyrolytic graphite sensor for determination of propranolol in biological fluids", Sens. Actuators B 204 (2014) 791.

[37] S. Wang, Y. Wang, Q. Min, T. Shu, X. Zhu, A. Peng, H. Ding, "Simultaneous electrochemical determination of dopamine and serotonin in rat cerebrospinal fluid using screen-printed electrode modified with mwnts-sio_2-chitosan composites", Int. J. Electrochem. Sci. 11 (2016) 2360.

[38] Z.H. Wang, Q.L. Liang, Y.M. Wang, G.A. Luo, "Carbon nanotube-intercalated graphite electrodes for simultaneous determination of dopamine and serotonin in the presence of ascorbic acid", J. Electroanal. Chem. 540 (2003) 129.

[39] X. Jiang, X. Lin, "Overoxidized polypyrrole film directed DNA immobilization for construction of electrochemical micro-biosensors and simultaneous determination of serotonin and dopamine", Anal. Chim. Acta 537 (2005) 145.

[40] Y. Sun, J. Fei, J. Hou, Q. Zhang, Y. Liu, B. Hu, "Simultaneous determination of dopamine and serotonin using a carbon nanotubes-ionic liquid gel modified glassy carbon electrode", Microchim. Acta 165 (2009) 373.

[41] G.P. Jin, X.Q. Lin, J.M. Gong, "Novel choline and acetylcholine modified glassy carbon electrodes for simultaneous determination of dopamine, serotonin and ascorbic acid", J. Electroanal. Chem. 569 (2004) 135.

[42] H.S. Han, H.K. Lee, J.M. You, H. Jeong, S. Jeon, "Electrochemical biosensor for simultaneous determination of dopamine and serotonin based on electrochemically reduced GO-porphyrin", Sens. Actuators B 190 (2014) 886.

[43] Y. Li, X. Huang, Y. Chen, L. Wang, X. Lin, "Simultaneous determination of dopamine and serotonin by use of covalent modification of 5-hydroxytryptophan on glassy carbon electrode", Microchim. Acta 164 (2009) 107.

[44] A. Babaeia, A.R. Taheri, "Nafion/$Ni(OH)_2$ nanoparticles-carbon nanotube composite modified glassy carbon electrode as a sensor for simultaneous determination of dopamine and serotonin in the presence of ascorbic acid", Sens. Actuators B 176 (2013) 543.

[45] E. Rand, A. Periyakaruppan, Z. Tanaka, D.A. Zhang, M.P. Marsh, R.J. Andrews, K.H. Lee, B. Chen, M. Meyyappan, J.E. Koehne, "A carbon nanofiber based biosensor for simultaneous detection of dopamine and serotonin in the presence of ascorbic acid", Biosens. Bioelectron. 42 (2013) 434.

[46] B. Rezaei, E. Havakeshian, A.A. Ensafi, "Decoration of nanoporous stainless steel with nanostructured gold via galvanic replacement reaction and its application for electrochemical determination of dopamine", Sens. Actuators B 213 (2015) 484.

[47] X. Tian, C. Cheng, H. Yuan, J. Du, D. Xiao, S. Xiec, M.M.F. Choi, "Simultaneous determination of l-ascorbic acid, dopamine and uric acid with gold nanoparticles–cyclodextrin-graphene-modified electrode by square wave voltammetry", Talanta 93 (2012) 79.

[48] E. Molaakbari, A. Mostafavi, H. Beitollahi, "Simultaneous electrochemical determination of dopamine, melatonin, methionine and caffeine", Sens. Actuators B 208 (2015) 195.

[49] H. Beitollahi, I. Sheikhshoai, "Novel nanostructure-based electrochemical sensor for simultaneous determination of dopamine and acetaminophen", Mater. Sci. Eng. C 32 (2012) 375.

[50] K. Hyland, "Clinical Utility of Monoamine Neurotransmitter Metabolite Analysis in Cerebrospinal Fluid", Clin. Chem. 54 (2008) 633.

[51] M. Monsaingeon, Y. Perel, G. Simonnet, J.B. Corcuff, "Comparative values of catecholamines and metabolites for the diagnosis of neuroblastoma", Eur J Pediatr 162 (2003) 397.

[52] J. Jokinen, A.L. Nordstrom, P. Nordstrom, "The relationship between CSF HVA/5-HIAA ratio and suicide intent in suicide attempters", Arch. Suicide Res. 11 (2007) 187.

[53] K. Hyland, "Neurochemistry and defects of biogenic amine neurotransmitter metabolism", J. Inherit. Metab. Dis. 22 (1999) 353.

[54] A. Liu, I. Honma, H. Zhou, "Electrochemical biosensor based on protein–polysaccharide hybrid for selective detection of nanomolar dopamine metabolite of 3,4-dihydroxyphenylacetic acid (DOPAC)", Electrochem Commun 7 (2005) 233.

[55] G.E.D. Benedetto, D. Fico, A. Pennetta, C. Malitesta, G. Nicolardi, D.D. Lofrumento, F.D. Nuccio, V.L. Pesa, "A rapid and simple method for the determination of 3,4-dihydroxyphenylacetic acid, norepinephrine, dopamine, and serotonin in mouse brain homogenate by HPLC with fluorimetric detection", J Pharm Biomed Anal 98 (2014) 266.

[56] E. Watson, S. Wilk, "Assessment of Cerebrospinal Fluid Levels of Dopamine Metabolites by Gas Chromatography", Psychopharmacologia (Berl.) 42 (1975) 57.

[57] D.S. Goldstein, G. Eisenhofer, I.J. Kopin,"Sources and Significance of Plasma Levels of Catechols and Their Metabolites in Humans", J. Pharmacol. Exp. Ther. 305 (2003) 800.

[58] K.S. Zafar, D. Siegel, D. Ross, "A Potential Role for Cyclized Quinones Derived from Dopamine, DOPA, and 3,4-Dihydroxyphenylacetic Acid in Proteasomal Inhibition", Mol. Pharmacol. 70 (2006) 1079.

[59] Z. Zhou, A. Roy, R. Lipsky, K. Kuchipudi, G. Zhu, J. Taubman, M.A. Enoch, M. Virkkunen, D. Goldman, "Haplotype-Based Linkage of Tryptophan Hydroxylase 2 to Suicide Attempt, Major Depression, and Cerebrospinal Fluid 5-Hydroxyindoleacetic Acid in 4 Populations", Arch Gen Psychiatry 62 (2005) 1109.

[60] P. Kestell, L. Zhao, M.B. Jameson, M.R.L. Stratford, L.K. Folkes, B.C. Baguley, "Measurement of plasma 5-hydroxyindoleacetic acid as a possible clinical surrogate marker for the action of antivascular agents", Clin Chim Acta 314 (2001) 159.

[61] G.N. Pandey, Y. Dwivedi, "The Neurobiological Basis of Suicide", CRC Press/Taylor & Francis publication (2012) 20.1.

[62] P. Nordstrom, M. Samuelsson, M. Asberg, L.T.Bendz, A.A.Wistedt, C. Nordin, L. Bertilsson, "CSF 5-HIAA predicts suicide risk after attempted suicide", Suicide Life-Threat. Behav. 24 (1994) 1.

[63] I.J. Rognum, H. Tran, E.A. Haas, K. Hyland, D.S. Paterson, R.L. Haynes, K.G. Broadbelt, B.J. Harty, O. Mena, H.F. Krous, H.C. Kinney, "Serotonin Metabolites in the Cerebrospinal Fluid in the Sudden Infant Death Syndrome: In Search of a Biomarker of Risk", J Neuropathol Exp Neurol. 73 (2014) 115.

[64] A. Makrlikova, E. Ktena, A. Economou, J. Fischer, T. Navratil, J. Barek, V. Vyskocil, "Voltammetric Determination of Tumor Biomarkers for Neuroblastoma (Homovanillic Acid, Vanillylmandelic Acid, and 5-Hydroxyindole-3-acetic Acid) at Screen printed Carbon Electrodes", Electroanalysis 29 (2017) 146.

[65] H. Xu, W. Zhang, D. Wang, W. Zhu, L. Jin, "Simultaneous determination of 5-hydroxyindoleacetic acid and 5-hydroxytryptamine in urine samples from patients with acute appendicitis by liquid chromatography using poly(bromophenol blue) film modified electrode", J. Chromatogr. B 846 (2007) 14.

[66] W. Zhang, X. Cao, Y.Z. Xian, Q. Xu, S. Zhang, L.T. Jin, "New microdialysis-electrochemical device for simultaneous determination of ascorbic acid and 5-hydroxyindole-3-acetic acid in rat striatum", Anal. Chim. Acta 458 (2002) 337.

[67] P. Wester, U. Bergstrom, A. Eriksson, C. Gezelius, J. Hardy, B. Winblad, "Ventricular cerebrospinal fluid monoamine transmitter and metabolite concentrations reflect human brain neurochemistry in autopsy cases", J Neurochem 54 (1990) 1148.

[68] K. Hyland, "The lumbar puncture for diagnosis of pediatric neurotransmitter diseases", Ann Neurol 54 (2003) S13.

[69] A.M. Kumar, J.B. Fernandez, N. Schneiderman, K. Goodkin, C. Eisdorfer, M. Kumar, "Simultaneous determination of 5-hydroxytryptamine, 5-hydroxytryptophan, 5-hydroxyindoleacetic acid, dopamine, and homovanillic acid in whole blood, using isocratic hplc with electrochemical detection", J. Liq. Chromatogr. Related Technol 22 (1999) 2211.

[70] H. Yokoo, H. Kojima, S. Yamada, T. Tsutsumi, N. Anno, S. Anraku, S. Nishi, K. Inanaga, "Simultaneous Determination of Dopamine, Serotonin, 3, 4-Dihydroxyphenyl- Acetic Acid, Homovanillic Acid, 3-Methoxytyramine and 5-Hydroxyindole- 3-Acetic Acid by High Performance Liquid Chromatography with Electrochemical Detection", Kurume Med J 32 (1985) 75.

[71] M. Tsunoda, C. Aoyama, H. Nomura, T. Toyoda, N. Matsuki, T. Funatsu, "Simultaneous determination of dopamine and 3,4-dihydroxyphenylacetic acid in mouse striatum using mixed-mode reversed-phase and cation-exchange high-performance liquid chromatography", J Pharm Biomed Anal 51 (2010) 712.

[72] J.D. Chi, J. Odontiadis, M. Franklin, "Simultaneous determination of catecholamines in rat brain tissue by high-performance liquid chromatography", J. Chromatogr. B 731 (1999) 361.

[73] R.R. Gonzalez, R.F. Fernandez, J.L.M. Vidal, A.G. Frenich, M.L.G. Perez, "Development and validation of an ultra-high performance liquid chromatography–tandem mass-spectrometry (UHPLC–MS/MS) method for the simultaneous determination of neurotransmitters in rat brain samples", J Neurosci Methods 198 (2011) 187.

[74] X. Zhao, Y. Suo, "Simultaneous determination of monoamine and amino acid neurotransmitters in rat endbrain tissues by pre-column derivatization with high-performance liquid chromatographic fluorescence detection and mass spectrometric identification", Talanta 76 (2008) 690.

[75] M. Tsunoda, K. Mitsuhashi, M. Masuda, K. Imai, "Simultaneous determination of 3,4-dihydroxyphenylacetic acid and homovanillic acid using high performance liquid chromatography–fluorescence detection and application to rat kidney microdialysate", Anal. Biochem. 307 (2002) 153.

[76] X. Jia, J.C. Delgado, M. Terrones, V. Meuniere, M.S. Dresselhaus, "Graphene edges: a review of their fabrication and characterization", Nanoscale. 3 (2011) 86.

[77] T. Shimizu, J. Haruyama, D. C. Marcano, D. V. Kosinkin, J. M. Tour, K. Hirose, K. Suenaga, "Large intrinsic energy bandgaps in annealed nanotube-derived graphene nanoribbons", Nat. Nanotechnol. 6 (2011) 45.

[78] A.L. Higginbotham, D.V. Kosynkin, A. Sinitskii, Z. Sun, J.M. Tour, "Lower-Defect Graphene Oxide Nanoribbons from Multiwalled Carbon Nanotubes", ACS nano 4 (2010) 2059.

[79] J. Lin, Z. Peng, C. Xiang, G. Ruan, Z. Yan, D. Natelson, J. M. Tour, "Graphene Nanoribbon and Nanostructured SnO2 Composite Anodes for Lithium Ion Batteries", ACS nano 7 (2013) 6001.

[80] X. Ouyang, L. Luo, Y. Ding, B. Liu, D. Xu, A. Huang, "Simultaneous determination of uric acid, dopamine and ascorbic acid based on poly(bromocresol green) modified glassy carbon electrode", J. Electroanal. Chem. 748 (2015) 1.

[81] G. Ran, X. Chen, Y. Xia, "Electrochemical detection of serotonin based on a poly(bromocresol green) film and Fe3O4 nanoparticles in a chitosan matrix", RSC Adv. 7 (2017) 1847.

[82] H. Juying, A. Shiyun, "Electrochemical Determination of Reduced Glutathione at Multiwalled Carbon Nanotubes/Poly(bromocresol green) Modified Glassy Carbon Electrode", Chem Res Chin Univ. 27 (2011) 934.

[83] D.V. Kosynkin, A.L. Higginbotham, A. Sinitskii, J.R. Lomeda, A. Dimiev, B. K. Price, J.M. Tour, "Longitudinal unzipping of carbon nanotubes to form graphene nanoribbons", Nature 458 (2009) 872.

[84] C.E. Banks, R.G. Compton, "Edge plane pyrolytic graphite electrode", Anal Sci 21 (2005) 1263.

[85] J. Li, S. Ye, T. Li , X. Li, X. Yang, S. Ding, "Preparation of graphene nanoribbons (GNRs) as an electronic component with the multi-walled carbon nanotubes (MWCNTs)", Procedia Eng. 102 (2015) 492.

[86] N.S. Ismaila, Q.H. Le, H. Yoshikawa, M. Saito, E. Tamiya, "Development of Non-enzymatic Electrochemical Glucose Sensor Based on Graphene Oxide Nanoribbon – Gold Nanoparticle Hybrid", Electrochim. Acta 146 (2014) 98.

[87] J.C. Delgado, J.M. Herrera, X. Jia, D.A. Cullen, H. Muramatsu, Y. Kim, T. Hayashi, Z. Ren, D.J. Smith, Y. Okuno, T. Ohba, H. Kanoh, K. Kaneko, M. Endo, H. Terrones, M. S. Dresselhaus, M. Terrones, "Bulk Production of a New Form of sp^2 Carbon: Crystalline Graphene Nanoribbons", Nano letters 8 (2008) 2773.

[88] P. Gupta, R.N. Goyal, Y.B. Shim, "Simultaneous analysis of dopamine and 5-hydroxyindoleacetic acid at nanogold modified screen printed carbon electrodes", Sens. actuators B 213 (2015) 72.

[89] A. Liu, I. Honma, H. Zhou, "Amperometric biosensor based on tyrosinase-conjugated polysaccharide hybrid film: Selective determination of nanomolar neurotransmitters metabolite of 3,4-dihydroxyphenylacetic acid (DOPAC) in biological fluid", Biosens. Bioelectron. 21 (2005) 809.

[90] J. Wang, M. Li, Z. Shi, N. Li, Z. Gu, "Electrocatalytic oxidation of 3,4-dihydroxyphenylacetic acid at a glassy carbon electrode modified with single-wall carbon nanotubes", Electrochim. Acta 47 (2001) 651.

[91] M.L. Mena, V. Carralero, A.G. Cortes, P.Y. Sedeno, J.M. Pingarron, "Laccase Biosensor Based on N-Succinimidyl-3-Thiopropionate-Functionalized Gold Electrodes", Electroanalysis 17 (2005) 2147.

[92] Z. Wu, H. Zhao, Y. Xue, Y. He, X. Li, Z. Yuan, "Poly(pyridine-3-boronic acid)/Multiwalled Carbon Nanotubes Modified Glassy Carbon Electrodes for Simultaneous Determination of Ascorbic Acid, 3,4-Dihydroxyphenylacetic Acid and Uric Acid", Electroanalysis 22 (2010) 2196.

[93] C.R. Raj, T. Ohsaka, "Analytical Applications of Functionalized Self-Assembled Monolayers on Gold Electrode: Voltammetric Sensing of DOPAC at the Physiological Level", Electroanalysis 14 (2002) 679.

[94] S. Liu, Y. Chen, P. Wan, C. Zhou, S. Zhang, H. Mo, "Determination of 5-Hydroxyindole Acetic Acid by Electrochemical Methods with an Oxidized Glassy Carbon Electrode", Electrochim. Acta 216 (2016) 528.

[95] P. Kanyong, S. Rawlinson, J. Davis, "Simultaneous electrochemical determination of dopamine and 5-hydroxyindoleacetic acid in urine using a screen-printed graphite electrode modified with gold nanoparticles", Anal Bioanal Chem (2016) 1.

[96] Y. Liu, Y. Jiang, W. Song, N. Lu, M. Zou, H. Xu, Z. Yu, "Voltammetric determination of 5-hydroxydole-3-acetic acid in human gastric juice", Talanta 50 (2000) 1261.

[97] S. Liu, G. Dai, H. Liu, X. Chen, "Voltammetric behavior of 5-HIAA on a multi-wall carbon nanotubes (MWNT)–Nafion modified electrode", Fenxi Shiyanshi 26 (2007) 99.

Chapter 5

Functionalized SWCNTs based sensor for the determination of ATP metabolites

5.1 INTRODUCTION

Adenosine triphosphate (ATP) is used in cells as a coenzyme and transports chemical energy within cells for metabolism. In the human system, metabolism of ATP occurs by a series of enzymatic reactions (**Scheme 1**). Initially the breakdown leads to cellular accumulation of adenosine diphosphate (ADP) and adenosine monophosphate (AMP) and activates some dormant enzymes including AMP deaminase, 5'-nucleotidase, xanthine oxidase, and purine nucleoside phosphorylase. In this case, inosine (INO) can be produced by two different pathways. In the first path way, AMP deaminase catabolizes AMP into inosine monophosphate (IMP), which is converted by the 5'-nucleotidase to INO. Otherwise, AMP is cleaved by either intra- or extra-cellular 5'-nucleotidase to form adenosine, which is subsequently converted to INO by adenosine deaminase [1,2]. INO is then converted into hypoxanthine (HX) and finally xanthine oxidase converts HX to xanthine (XT) and subsequently to uric acid (UA) [3-5]. INO, the major metabolite of ATP degradation performs various important functions in the human body, such as, participation in tumor necrosis factor, which induces nitric oxide production in cultured sertoli cells, protection against myocardial damage, participation in receptor mediated signaling, having inflammatory and immune modulatory effects, reduction of LPS-induced acute lung injury and association with multiple sclerosis [6-9]. INO is found in the micro molar range (0.75-1.49 μM) in interstitial fluids, whereas the level increases fiercely during ischemia and sepsis interstitial and reaches greater than 1.0 mM [10]. HX, is found in low concentration as 1.47-2.94 μM in blood plasma and is also a potential biomarker for acute cardiac ischemia (AMI), where the concentration of HX elevated in the bloodstream [3,11]. Further conversion of HX to XT, which is found in the physiological fluids as 20 μg/dL is important to measure as the level of xanthine is required for the diagnosis and treatment of Gouty arthritis (gout), hyperuricaemia, and xanthinuria [12]. The final metabolic product UA is produced in liver, intestines and other tissues and is normally excreted via urine. The release of ATP-catabolites was less in newborn than in the adults' hearts during reperfusion, which coincided with lower xanthine oxidase activity [3]. In the patients with AMI, angina pectoris and other ischemic diseases, a significant rise in the intermediates and end products of purine metabolism i.e. INO, HX, XT, and UA can be an indicator of a heart attack [13]. Hence, the simultaneous determination of these four ATP catabolites has been considered of significant importance in biochemical and clinical diagnosis.

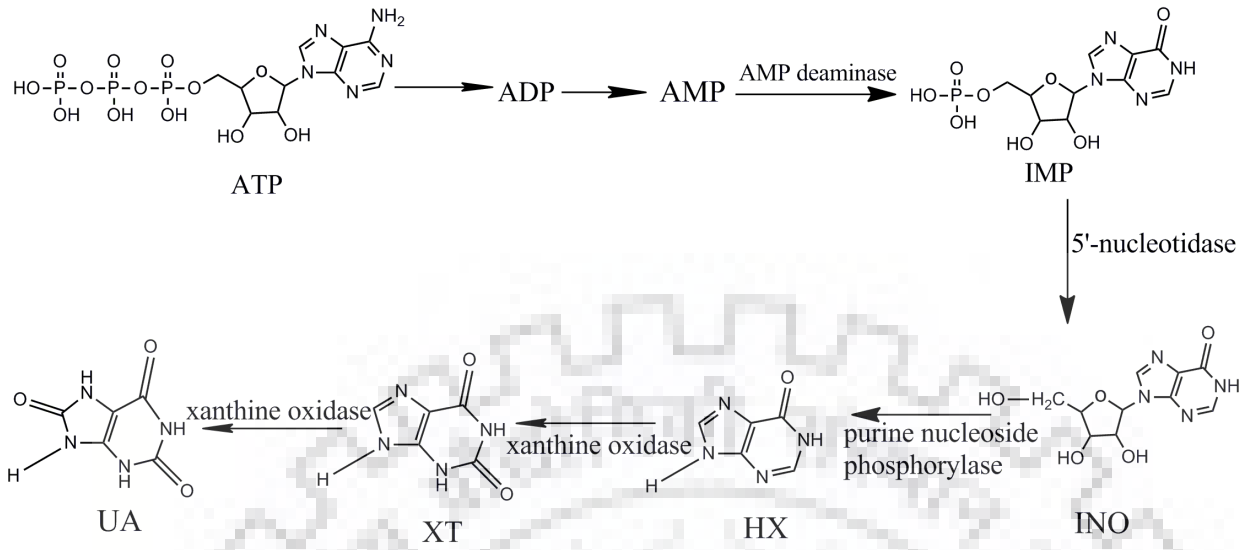

Scheme 1: A series of enzymatic reactions that occur during ATP catabolism.

The determinations of INO, HX, XT, and UA were carried out by several methods, such as high-performance liquid chromatography, reverse-phase chromatography, chemiluminescent, liquid chromatography with a diode array detector, capillary electrophoresis, spectrophotometer, multi-enzyme reactor sensor and many more [14-21]. An enzyme-coupled assay for fluorometric detection of AMP, adenosine, INO, and HX, was reported, however, the procedure required costly apparatus, complicated enzyme reactions, and extensive analysis time [22]. To our knowledge, no attempt has been made to determine these four metabolites simultaneously without any separation technique in the last decade. However, most of the reported methods used for the individual and simultaneous determination of two purines have many limitations, like less sensitivity, long analysis time and poor selectivity, involvement of complex steps for sample preparation and requirement of expensive instruments. Therefore a rapid, less expensive, highly sensitive and selective technique is required for the simultaneous determination of these four metabolites. In the presented approach, amide functionalized SWCNTs (AmSWCNTs) were combined with the film of palladium nanoparticles (PdNPs) and polymer of bromocresol green (pBG) for enhancing the macroscopic mechanical properties of the composite. Amide functionalized SWCNTs were used to improve the nanotube-polymer interface as the amine termination of the nanotubes provides the suitable link for covalent bonding via amide linkage between SWCNTs and biological molecules or pBG layer [23,24]. PdNPs are used as a surface modifier due to the compatibility with biomolecules [25,26]. In the present method, first AmSWCNTs was casted at the pyrolytic graphite surface followed by electro polymerization of BG in the presence of $PdCl_2$. The modified

probe layers were characterized by field emission scanning electron microscopy, high resolution transmission electron microscopy, X-ray photoelectron spectroscopy, electrochemical impedance spectroscopy, cyclic voltammetry, and square wave voltammetry. The modification exhibited excellent electrocatalytic activity, larger effective surface area, good conductivity, improved biocompatibility and helped in the sensitive simultaneous determination of INO, HX, XT, and UA.

5.2 EXPERIMENTAL

5.2.1 Chemicals and Instruments

INO, HX, XT, UA, SWCNTs (code 519308 Sigma), BG, and ethylenediamine and N-[(dimethylamino)-1H-1,2,3-triazolo[4,5,6] pyridin-1-ylmethylene]-N-methylmethanaminium hexafluorophosphate N-oxide (HATU) were purchased from Sigma-Aldrich (USA). Considering the physiological pH, the phosphate buffer of pH 7.4 was used for detailed experimental studies.

The voltammetric measurements and characterization techniques used were essentially similar to that reported in the section A of the chapter 2. High resolution transmission electron microscopy (HR-TEM, JEOL, JEM-300FS) and Fourier-transform infrared spectroscopy (FTIR, PerkinElmer, Inc-L1600300 Spectrum Two LITs/96903) were also used for the characterization of the fabricated surface. The X-ray photoelectron spectroscopy (XPS) was analyzed using VG Scientific XPSLAB 250 XPS spectrometer and a monochromated Al Kα source with charge compensation (KBSI (Busan).

5.2.2 Preparation of amide functionalized SWCNTs

The amide functionalization of SWCNTs involved two steps [23,27]. In the first step, SWCNTs (20 mg) were treated with a 3:1 mixture of conc. H_2SO_4 and HNO_3 solution (30 mL) and reaction mixture was sonicated in an ultrasonic bath at 40°C for 3 h to introduce carboxylic acid (-COOH) groups on the surface of SWCNTs. After 3 h, the reaction mixture was added drop-wise to the cold double distilled water and then filtered using polycarbonate filter paper (10 μm pore size). The residual acid was then removed by washing with double distilled water and the residue was dried at 80°C for 4 h. In the next step, the oxidized SWCNTs (15 mg) were added in 10 mL of ethylenediamine and the mixture was sonicated. The coupling agent HATU (1 mg) was then added to the reaction mixture and sonicated for 4 h. The methanol in excess amount was then added to the mixture and product was filtered using polycarbonate filter paper. The residue was washed with excess of methanol. The prepared amide functionalized SWCNTs (AmSWCNTs) were dried at 80°C for ~24h.

5.2.3 Preparation of polymer nanocomposite modified PdNPs:pBG/AmSWCNTs/EPPG

An unmodified EPPG sensor was prepared by reported method [28]. The optimized volume of 10 µL of prepared AmSWCNTs (1 mg/ml dispersed in dimethylformamide solution was drop-casted at the surface of sensor and allowed to dry overnight in an oven at 110 ^{o}C. The volume of AmSWCNTs was optimized by taking 2 to 20 µL. The voltammograms were recorded in a mixture of all the four analytes at 25 µM concentration. The well-defined peaks with maximum peak current were observed with 10 µL AmSWCNTs. At volume greater than 10 µL, the peaks became broad and the current decreased. Hence, 10 µL was drop casted in subsequent studies. DMF is selected as it is suitable solvent for the dispersion of various functionalized nanotubes because it properly wets the nanotubes [29]. In the next step, 1:1 mixture of 1 mM $PdCl_2$ (prepared in 10% HCl) and 1.0 mM BG (prepared in 0.1 M NaOH) were taken and the AmSWCNTs deposited EPPG sensor was dipped in it and potential was applied from -400 mV to 1800 mV at a sweep rate of 100 mV/s for 20 scans (optimized). Similarly, for polymerization several sweep rates and number of cycles used in different ratios of $PdCl_2$ and BG. When the ratio was increased from 1:1 to 1:4, the peaks of all the analytes showed a tendency to become broad. The sweep rate was changed from 50 to 200 mV/s. Though peak currents of the analytes increased with increase in sweep rate, however, the peak became broad. Hence, a sweep rate of 100 mV/s was used at which best results were observed. The number of scans used for polymerization was in the range 10 to 30. When, number of scans was more than 20, then the peak current decreased probably due to the thickness of polymeric layer. Hence, 20 scans were used during polymerization of $PdCl_2$ and BG. On completion of 20 scans, the resulting surface was thoroughly washed with double distilled water to remove unreacted molecules at the surface of sensor. The modified surface was characterized using FE-SEM and HR-TEM. For recording voltammograms the prepared PdNPs:pBG/AmSWCNTs/EPPG sensor was first stabilized by scanning the potential from 400 mV to -1100 mV for 5 cycles at 100 mV/s sweep rate in 0.1 M NaOH solution to get a steady cyclic voltammogram because pBG gets deprotonation at higher pH to give the dianionic form, which is stabilized by resonance structure [30] as shown in **Fig 5.1.** In another approach, electro-deposition of PdNPs:pBG composite (by scanning the potential from 400 mV to -1100 mV for 5 cycles at 100 mV/s sweep rate) was first achieved, followed by the drop casting of AmSWCNTs. In this case, broad anodic peaks with low currents and higher potential were observed for the analytes. Hence, electro-deposition of PdNPs:pBG was carried out after drop-casting of

AmSWCNTs at the EPPG surface (first approach) to ensure good conductivity and sensitivity, which was used for further studies.

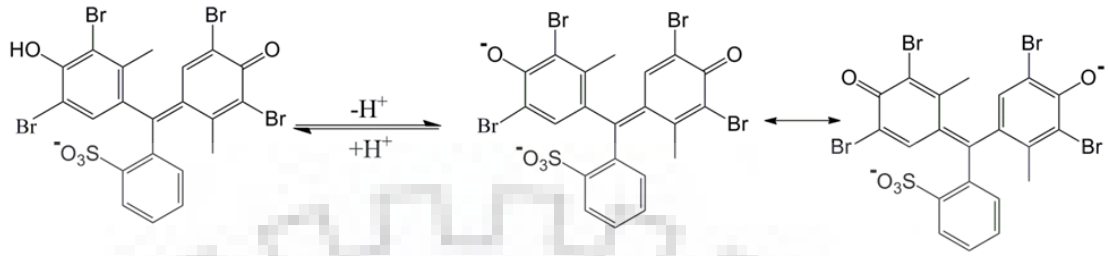

Fig. 5.1: Various structures showing stabilization of p-BG.

5.2.4 Experimental procedure

For the voltammetric studies, 1.0 mM solutions of four analytes INO, HX, XT and UA were prepared in double distilled water. Then 2.0 ml of phosphate buffer (pH 7.4), desired amount of analyte and remaining water (total 4 ml) were used. The optimized parameters used in cyclic voltammetry were initial potential (E_i): 0 mV, switching potential (E): 1500 mV, final potential (E_f): 0 mV, sweep rate (ν): 100 mV/s. The parameters used in square wave voltammetry (SWV) were E_i: 0 mV, E_f: 1500 mV, square wave frequency (f): 15 Hz, square wave amplitude (E_{sw}): 25 mV and potential step (E): 4 mV. To remove the adsorbed material and regenerate the sensing surface at constant potential of -800 mV was applied in the blank solution for 180 s after each scan. The potentials reported are with respect to Ag/AgCl electrode.

To ensure the practical applicability of the modified sensor human urine and blood plasma sample of healthy volunteers were obtained from Indian Institute of Technology (I.I.T.), Roorkee hospital (approved by Institute Human Ethics Committee (IHEC), No: BIOTECH/IHEC/AP/15/1). The collected urine and plasma samples were diluted two times with phosphate buffer of pH 7.4 prior to analysis to minimize matrix complexity. For the validation of results obtained, HPLC was carried out by using Shimadzu LC-2010A HT system equipped with C18 bond pack 125 A^o, 10 µm) reverse phase column. The mobile phase used was 50 mM phosphate buffer (48 mM of KH_2PO_4 and 2 mM K_2HPO_4 with methanol (97:3, v/v) followed by adjusting the pH to 4.0) at the flow rate of 0.5 ml/min. The injection volume of the sample was 40 µL and the absorbance of the eluent was monitored at 285 nm.

5.3 RESULTS AND DISCUSSION

5.3.1 Characterization of sensor

The prepared AmSWCNTs were characterized by recording FT-IR spectrum and the observed results are displayed in **Fig. 5.2**, in which a band at 1665 cm^{-1} corresponding to the amide carbonyl (C=O) stretching was noticed. Two other bands at 1575 cm^{-1} and 1218 cm^{-1} are assigned to the N-H in-plane and C-N bond stretching, respectively and further confirmed the presence of the amide functional group. A broad band at 3398 cm^{-1} is due to the characteristic N-H stretching vibrations and C-H stretches are observed between 2849 cm^{-1} and 2915 cm^{-1}. The observed results are similar to the previously reported in the literature for amide functionalized SWCNTs [23,31].

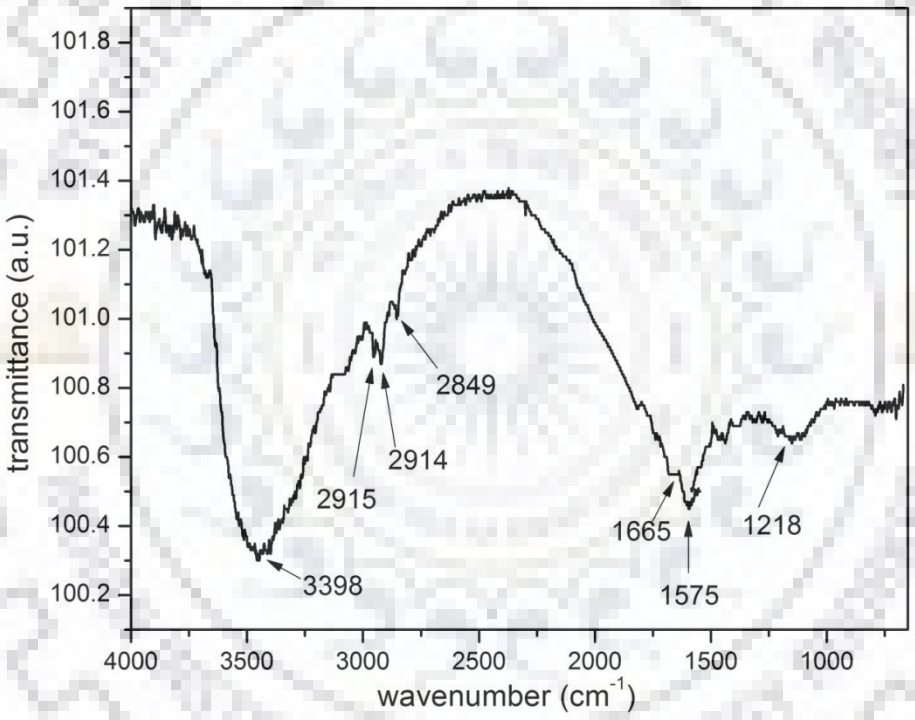

Fig. 5.2: FT-IR spectrum observed for amide-functionalized SWCNTs.

To demonstrate the presence of Pd at the surface, EDX was performed at the modified surface as shown in **Fig. 5.3**, which clearly indicated the presence of Pd in PdNPs:pBG/AmSWCNTs/EPPG sensor.

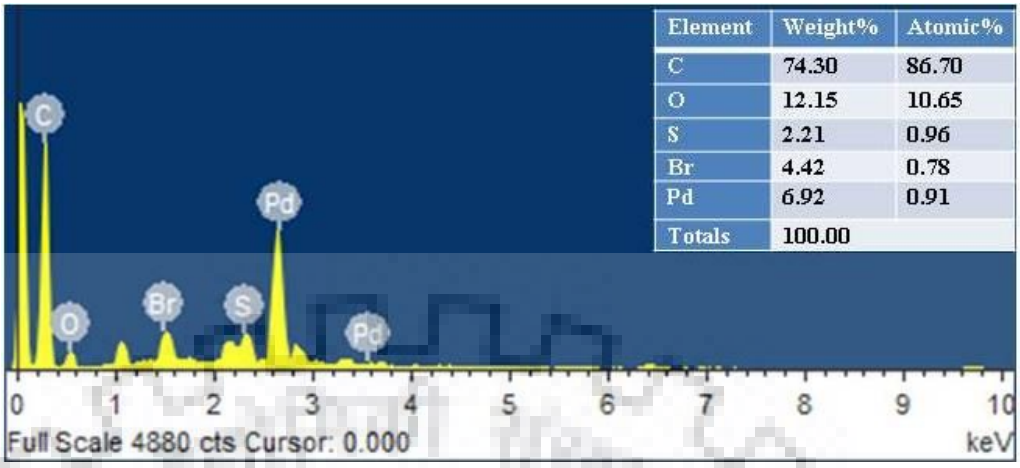

Fig. 5.3: EDX data demonstrating the presence of Pd in PdNPs:pBG/AmSWCNTs/EPPG.

Surface morphology of the modified sensor was carried out by using FE-SEM. Some typical images observed are presented in **Fig. 5.4**. The surface of the unmodified EPPG surface is smooth and flat as represented in the inset of **Fig.5.4**. The surface of PdNPs:pBG/AmSWCNTs/EPPG sensor had herbs like clusters appeared to be interlinked with amino groups and provided increased nanotubes/metal nanoparticle-polymer interface, which facilitate the interaction and electron transfer property between the analyte and modified surface.

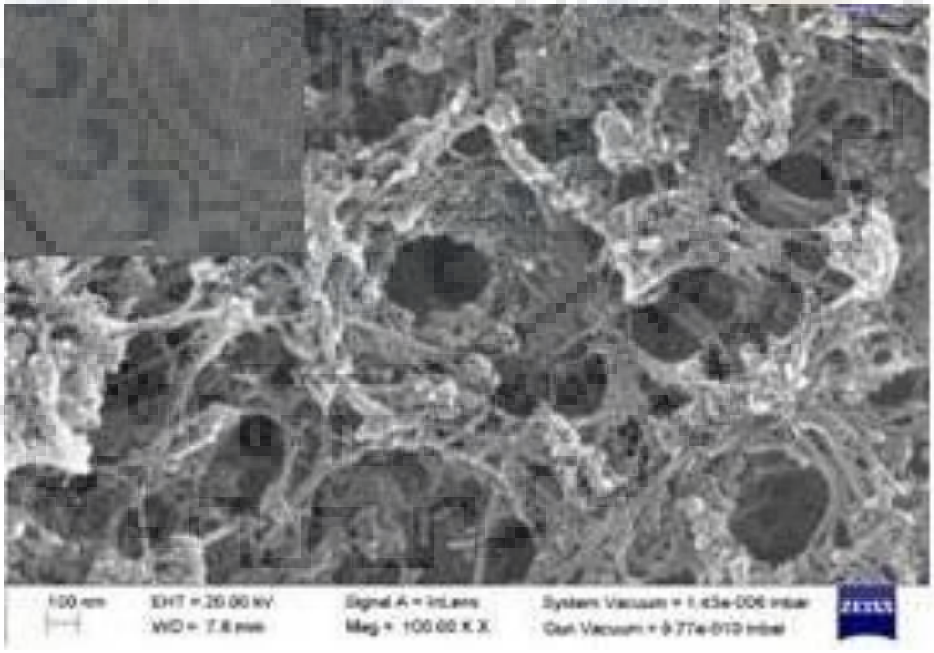

Fig. 5.4: Typical FE-SEM images observed for PdNPs:pBG/AmSWCNTs/EPPG and inset shows the unmodified EPPG.

Fig 5.5 (A) shows the HR-TEM image of PdNPs:pBG layer and **Fig 5.5 (B)** corresponding EDX analysis result, which clearly indicate that small PdNPs (average size of 5nm) were formed on the pBG layer with well distribution and high density. Additionaly, evidence for the presence of PdNPs in the pBG layer was obtained by EDX analysis.

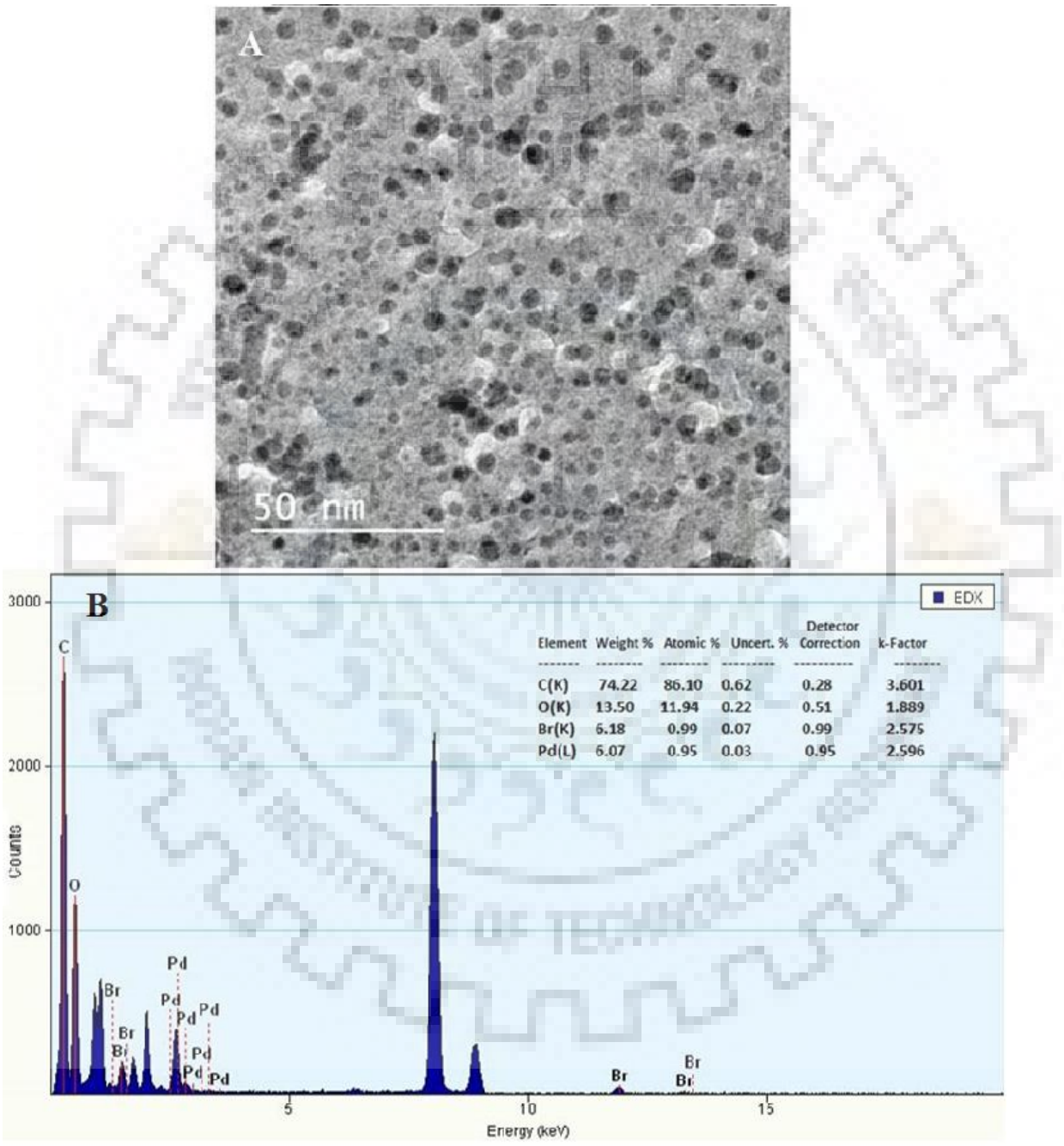

Fig. 5.5: (A) HR-TEM image of PdNPs:pBG layer and **(B)** corresponding EDX analysis.

Fig. 5.6 shows the XPS analysis using (i) AmSWCNTs and (ii) PdNPs:pBG/AmSWCNTs modified layer with survey (**Fig. 5.6 A**), C1s (**Fig. 5.6 B**), S2p (**Fig. 5.6 C**), Br3d (**Fig. 5.6 D**) and Pd3d (**Fig. 5.6 E**). All spectra were internally calibrated with the C1s peak (284.6 eV) before analysis. The deconvoluted C1s spectrum revealed three peaks at 284.6, 285.9, and 288.5 eV, which corresponded to the C-C or C=C, C-N, and C-O or C=O bonds, respectively. The C-N peak was observed, which indicated the presence of C-N bond from the amide functionalized SWCNTs. Moreover, the C-O or C=O peak appeared because of SWCNTs, that comprises abundant of carboxylic acid or carbonyl groups. In addition, S2p (C-S (163.1 eV) and S-O or S=O (168.0 eV)) and Br3d (Br-C (70.2 eV)) peaks were newly obtained for the PdNPs:pBG/AmSWCNTs modified layer, and were originated from pBG. Moreover, XPS spectrum of Pd3d was characterized by two spin-orbit-split doublets (3d5/2 and 3d3/2). The major two peaks at 335.4 and 340.7 eV indicates the bulk metallic Pd (Pd(0)), however, relatively small peaks at 338.0 and 343.0 eV are attributed from the chemically bound Pd (Pd(II)). From the result of S2p, Br3d, and Pd3d spectra, it was confirmed that the PdNPs:pBG layer was successfully immobilized on the AmSWCNTs, while no peaks were observed at S2p, Br3d, and Pd3d for the AmSWCNTs layer due to the absence of each atom.

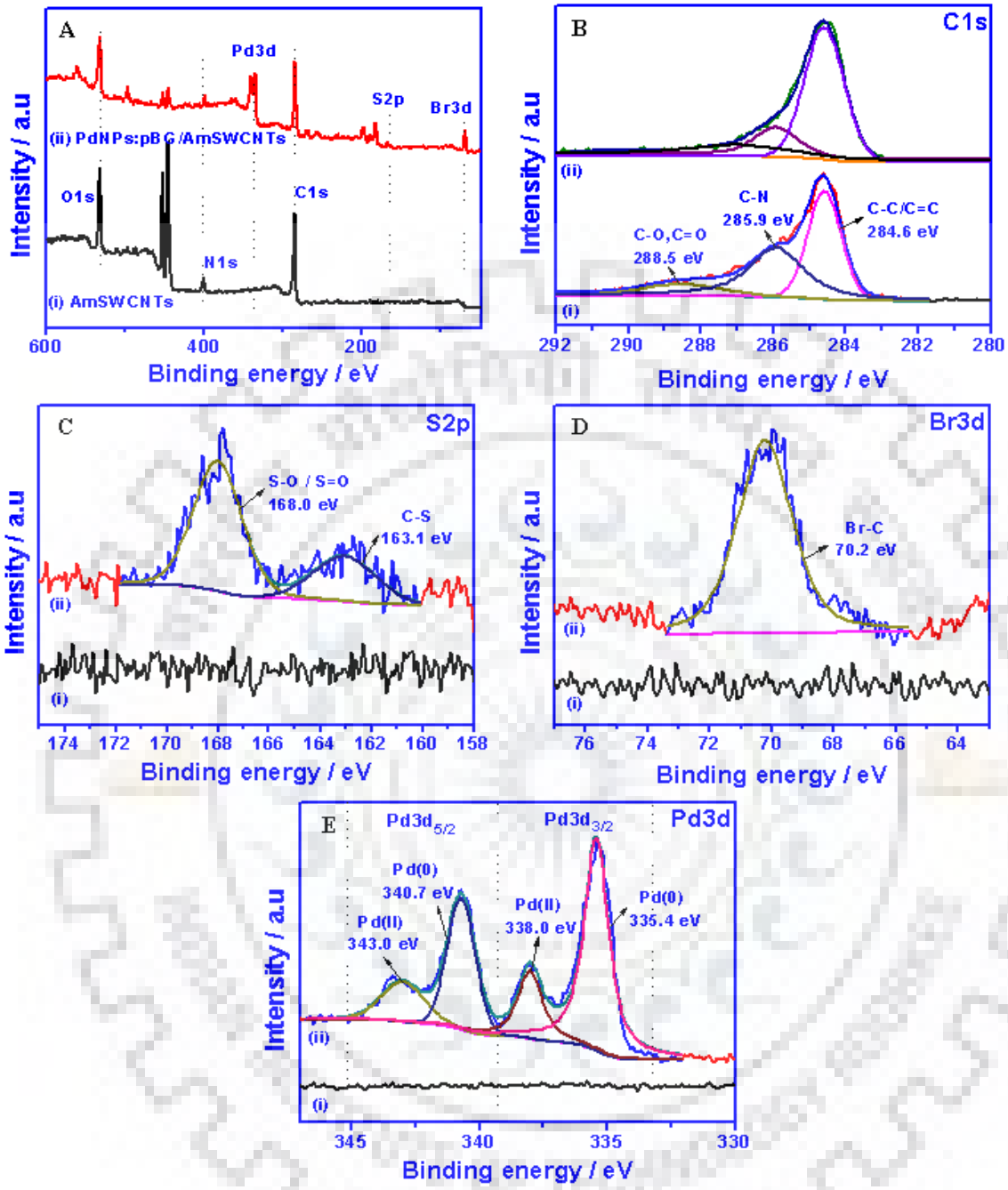

Fig. 5.6: XPS survey spectra of (i) AmSWCNTs and (ii) PdNPs:pBG/AmSWCNTs (**A**), C1s (**B**), S2p (**C**), Br3d (**D**) and Pd3d (**E**).

5.3.2 Electrochemical Impedance Spectroscopy

EIS was used to investigate the electrochemical characteristics of the sensor at different stages of modification. The values of the electron-transfer resistance (R_{CT}) were determined in 0.1 M KCl containing 2.0 mM $K_3Fe(CN)_6$ solutions over a frequency range of 0.1 Hz to 100 Hz with

an applied potential of 50 mV. The EIS curves displayed a semicircle followed by the linear portion (**Fig. 5.7**) in which the semi-circular portion featured an electron transfer limiting process, whereas the charge transfer resistance (R_{CT}) was equal to the diameter of the semicircle. The inset of the (**Fig. 5.7**) shows the Randles equivalent circuit used for simulating the experimental data, where R_s denotes the electrolyte resistance; C_{dl} denotes the double layer capacitance and W stand for Warburg impedance. Unmodified EPPG surface exhibited a large semicircle portion indicating high R_{CT} (1198 Ω) for the $Fe(CN)_6^{3-/4-}$ redox process (**curve a**), whereas the charge transfer rate at electrode/electrolyte surface was higher for modified electrode, hence, the impendence would decrease due to the conductivity of SWCNTs and high electrochemical activity due to amide functionalization [32]. Thus, AmSWCNTs/EPPG exhibited a reduced semi-circular domain with the R_{CT} value as 986 Ω (**curve b**). The observed R_{CT} value for PdNPs/AmSWCNTs/EPPG is 563 Ω (**curve c**) and in the case of PdNPs:pBG/AmSWCNTs/EPPG sensor, the smallest semicircle was witnessed with the R_{CT} value as 188 Ω (**curve d**) indicating lowest resistance for this sensor. Thus, it is concluded that PdNPs:pBG/AmSWCNTs/EPPG sensor has lowest resistance and maximum electron transfer efficiency, which would promote the oxidation of ATP metabolites.

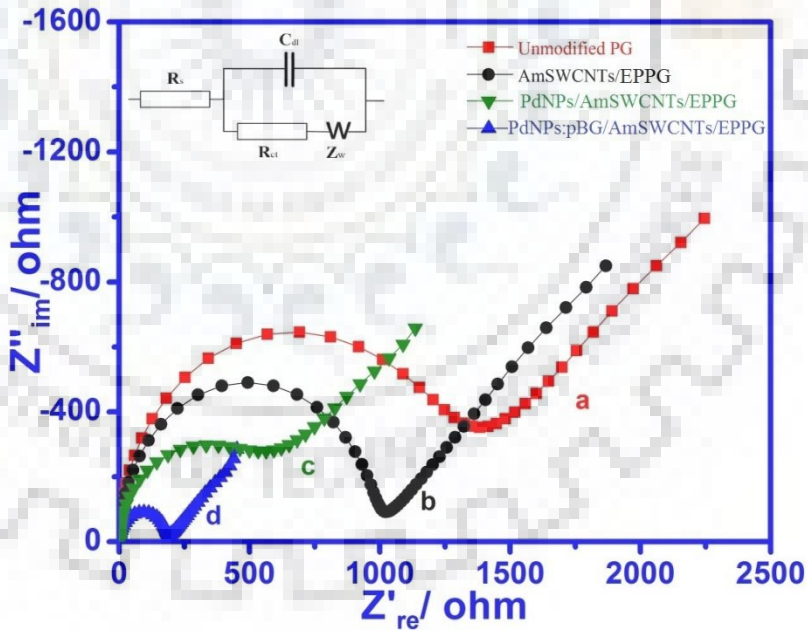

Fig. 5.7: Typical Nyquist plots observed for unmodified EPPG (a), AmSWCNTs/EPPG (b), PdNPs/AmSWCNTs/EPPG (c), and PdNPs:pBG/AmSWCNTs/EPPG (d). The inset shows the Randles equivalent circuit used for the simulation of the EIS data.

5.3.3 Cyclic voltammetry

Cyclic voltammograms were recorded in 1.0 mM $K_3Fe(CN)_6$ containing 0.1 M KCl at different sweep rates (5 mV/s to 225 mV/s). The observed slope of the i_p vs. $\nu^{1/2}$ plots was used to calculate effective surface areas using Randles-Sevcik equation. The calculated value of effective surface areas for unmodified EPPG, AmSWCNTs/EPPG, PdNPs/AmSWCNTs/EPPG, and PdNPs:pBG/AmSWCNTs/EPPG were found as 0.086 cm^2, 1.732 cm^2, 2.988 cm^2, and 3.894 cm^2, respectively. The highest effective surface area was found for the PdNPs:pBG/AmSWCNTs/EPPG sensor, which was nearly 45 times greater than unmodified EPPG and increased the charge transfer kinetics for the electro-oxidation of the targeted analytes.

The voltammograms were then recorded at the fixed concentration of 25 µM of each analyte in the sweep range 5 mV/s to 225 mV/s. It was observed that the peak current (i_p) increased linearly with increasing sweep rate for all the analytes. The plots of i_p versus ν and log i_p versus log ν plots were linear and the relations and R^2 values are summarized below:

For INO $\quad$ **i_p (µA) = 0.0809 ν + 0.2454** $\quad$ **(R^2 = 0.997)**

log i_p = 0.9407 log ν − 0.9564 $\quad$ **(R^2 = 0.999)**

For HX $\quad$ **i_p (µA) = 0.075 ν + 0.5169** $\quad$ **(R^2 = 0.999)**

log i_p = 0.8335 log ν − 0.754 $\quad$ **(R^2 = 0.998)**

For XT $\quad$ **i_p (µA) = 0.2003 ν + 1.4367** $\quad$ **(R^2 = 0.996)**

log i_p = 0.8529 log ν − 0.3658 $\quad$ **(R^2 = 0.997)**

For UA $\quad$ **i_p (µA) = 0.0121 ν+ 0.0743** $\quad$ **(R^2 = 0.999)**

log i_p = 0.8187 log ν − 1.5232 $\quad$ **(R^2 = 0.996)**

The linearity of i_p versus ν plots suggested the involvement of adsorption controlled process for oxidation. Further, the slope of log i_p versus log ν plots were 0.9407, 0.8335, 0.8529, and 0.8187 for INO, HX, XT and UA, respectively, which are sufficiently greater than 0.5 and confirmed adsorption controlled oxidation of these analytes [33,34].

The voltammograms of a mixture of these analytes were recorded having INO, HX, and XT (25µM), and UA (10µM) at unmodified EPPG, AmSWCNTs/EPPG, PdNPs/AmSWCNTs/EPPG and PdNPs:pBG/ AmSWCNTs/EPPG and were as shown in the **Fig. 5.8**. At unmodified EPPG surface, three anodic peaks were observed. The broad peak at 1110 mV was due to INO and HX

(peak a_1) and other two peaks observed at 710 mV (peak a_2) and 307 mV (peak a_3) were due to XT and UA, respectively. Thus, unmodified EPPG surface was unable to separate the four analytes. At the surface of AmSWCNTs/EPPG sensor, four oxidation peak clearly observed with increased peak current and less peak potential at 1329 mV, 1057 mV, 690 mV and 300 mV for INO (peak b_1), HX (peak b_2), XT (peak b_3) and UA (peak b_4), respectively, whereas at the surface of PdNPs/AmSWCNTs/EPPG sensor oxidation peaks were observed at 1320 mV, 1043 mV, 685 mV, and 290 mV for INO (peak c_1), HX (peak c_2), XT (peak c_3) and UA (peak c_4), respectively. At the surface of PdNPs:pBG/AmSWCNTs/EPPG sensor all the four peaks observed had large peak currents and peak potentials shifted to less positive potentials as 1342 mV (peak d_1), 1025 mV (peak d_2), 680 mV (peak d_3) and 293 mV (peak d_4) for INO, HX, XT and UA, respectively.

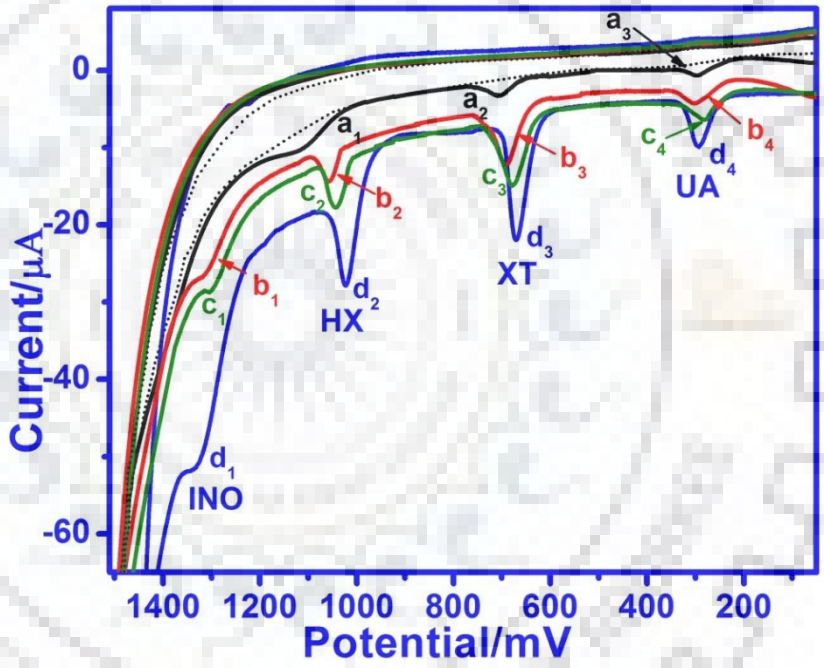

Fig. 5.8: A comparison of observed CVs at unmodified EPPG (curve a), AmSWCNTs/EPPG (curve b) and PdNPs:pBG/AmSWCNTs/EPPG (curve c) for a mixture of INO (25 µM), HX (25 µM), XT (25 µM) and UA (10 µM) in pH 7.4 at a scan rate of 100 mV/s. The background is presented by the dotted line.

5.3.4. Square wave voltammetry

Square wave voltammograms were recorded for a mixture of INO, HX, XT and UA (25 µM each) at pH 7.4. A comparison of voltammograms at unmodified EPPG, AmSWCNTs/EPPG, PdNPs/AmSWCNTs/EPPG and PdNPs:pBG/AmSWCNTs/EPPG sensors is shown in **Fig. 5.9.** At unmodified EPPG (curve a) four peaks were obtained at 1358 mV, 1070 mV, 718 mV and 296 mV

for INO, HX, XT and UA. At the AmSWCNTs/EPPG surface (curve b) and PdNPs/AmSWCNTs/EPPG surface (curve c) the peak potential shifted to more positive values in contrast to unmodified EPPG surface and enhanced peak currents were observed. However, PdNPs:pBG/AmSWCNTs/EPPG sensor surface (curve d) gives excellent results in terms of peak separation with the lowest peak potentials and sensitivity. The shift of E_p to less potential demonstrated the excellent electrocatalytic activity towards the simultaneous determination of these analytes due to the improvement in the interfacial binding, strength and electron transfer properties.

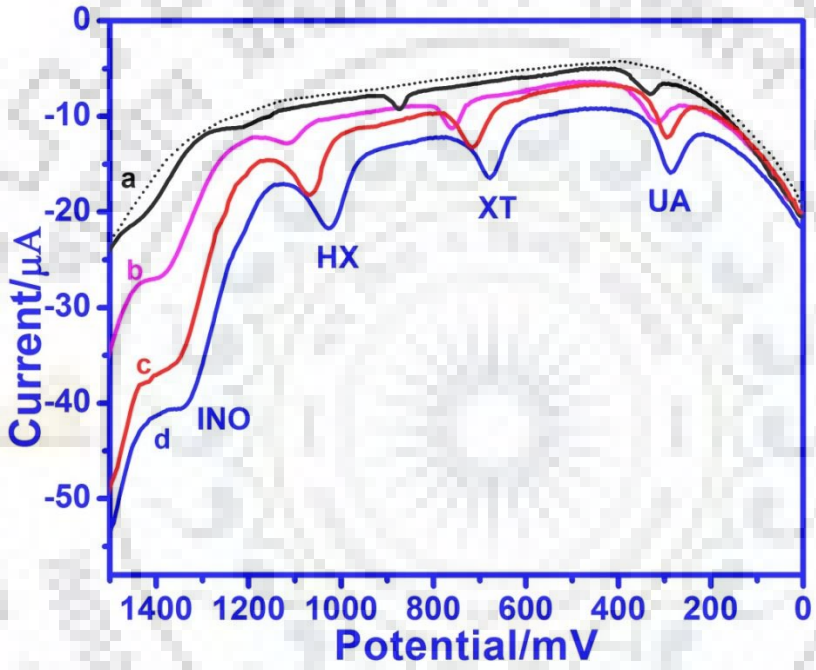

Fig. 5.9: Comparison of square wave voltammograms observed at unmodified EPPG (curve a), AmSWCNTs/EPPG (curve b), PdNPs/AmSWCNTs/EPPG (curve c), and PdNPs:pBG/AmSWCNTs/EPPG sensor (curve d) for a mixture of INO, HX, XT and UA (25 µM each) at pH 7.4. The background is denoted by the dotted line.

5.3.4.1 Effect of concentration

To ensure the sensitivity of the PdNPs:pBG/AmSWCNTs/EPPG sensor toward these analytes, the concentration study was carried out at pH 7.4. The oxidation peak currents were linearly dependent on the concentrations as represented in **Fig. 5.10** and the relations can be represented as:

$$\mathbf{i_p\ (\mu A) = 0.1872\ [C\ 0.001-175\ \mu M] + 1.1332 \quad (R^2 = 0.999); \quad For\ INO}$$

$$i_p\ (\mu A) = 0.1715\ [C\ 0.001 - 200\ \mu M] + 2.3195 \quad (R^2 = 0.998); \quad \textbf{For HX}$$

$$i_p\ (\mu A) = 0.1659\ [C\ 0.001 - 150\ \mu M] + 2.7427 \quad (R^2 = 0.999); \quad \textbf{For XT}$$

$$i_p\ (\mu A) = 0.4109\ [C\ 0.001 - 200\ \mu M] + 4.7192 \quad (R^2 = 0.998); \quad \textbf{For UA}$$

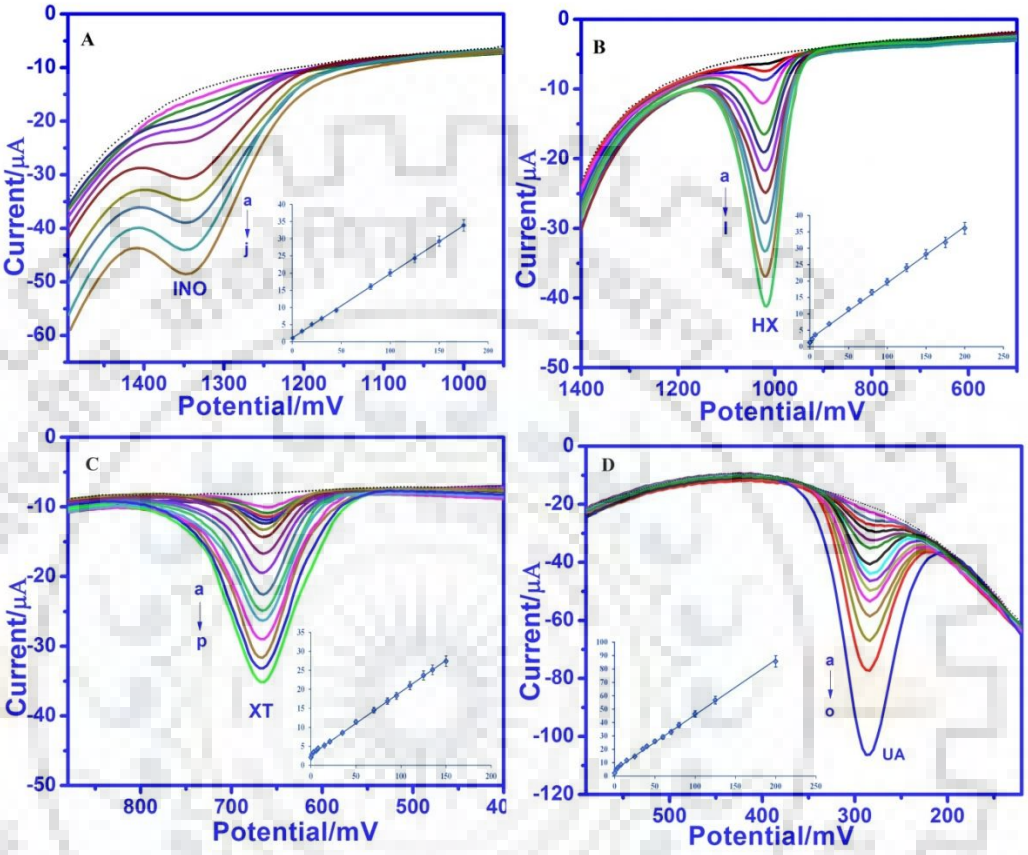

Fig. 5.10: SWVs observed for the increasing concentration of (**A**) INO (0.001-175 µM), (**B**) HX (0.001-200 µM), (**C**) XT (0.001-150 µM), and (**D**) UA (0.001-200 µM) at PdNPs:pBG/AmSWCNTs/EPPG sensor. Each inset figure shows the corresponding calibration plot.

The limit of detection (LOD) and limit of quantification (LOQ) were calculated by the relations 3 σ/b and 10 σ/b, respectively, where σ is the standard deviation of the blank signals and b is the observed slope of the calibration curve. The observed LOD and LOQ for these analytes were found as 0.95, 1.04, 1.07, 0.43 nM and 3.1, 3.4, 3.5, 1.4 nM for INO, HX, XT and UA respectively. The LOD values were much lower than reported in the last few years using different modified sensors **(Table 1)**.

Table 1: A comparison of analysis results of ATP metabolites at PdNPs:pBG/AmSWCNTs/EPPG sensor with previously reported methods.

S.No.	Method/Electrode	Conc. range (μM)	LOD (nM)	Real sample	Ref.
INO					
1.	HPLC	0.93-18.6	372	Yes	[15]
2.	SWNTs/PGE	10-1000	204	Yes	[35]
3.	XO/SPE	1-50	1000	Yes	[36]
4.	PdNPs:pBG/AmSWCNTs/EPPG	0.001-175	0.95	Yes	This work
HX					
1.	P6-TG/GCE	2-800	100	Yes	[37]
2.	(PyTS-NG)/GCE	8-200	231	Yes	[38]
3.	GCE/PLMT	0.02-0.1	7	Yes	[39]
4.	PdNPs:pBG/AmSWCNTs/EPPG	0.001-200	1.04	Yes	This work
XT					
1.	P6-TG/GCE	1-500	300	Yes	[37]
2.	(PyTS-NG)/GCE	8-800	83	Yes	[38]
3.	GCE/PLMT	0.02-0.1	4	Yes	[39]
4.	PdNPs:pBG/AmSWCNTs/EPPG	0.001-150	1.07	Yes	This work
UA					
1.	P6-TG/GCE	2-1600	60	Yes	[37]
2.	poly(BCP)/GCE	0.5-120	200	Yes	[40]
3.	p-(PCV)/mwcntsCOOH/GCE	0.3-80	160	Yes	[41]
4.	PdNPs:pBG/AmSWCNTs/EPPG	0.001-200	0.43	Yes	This work

P6-TG: poly(6-thioguanine) film, **SWCNT**: single walled carbon nanotube, **(PyTS–NG):**1,3,6,8-pyrene tetra sulfonic acid sodium salt functionalized nitrogendoped graphene, **XO**: Xanthine oxidase, **poly (BCP):** poly (bromocresol purple), **poly(PCV):** poly (pyrocatechol violet), **PLMT:** poly(l-methionine), **SPE**: screen printed electrode.

5.3.4.2 Effect of pH

The effect of pH on the electrochemical behavior of different analytes was studied in the pH range 2.4-10.5 (μ=0.5 M) at 25 μM concentration at the surface of PdNPs:pBG/AmSWCNTs/EPPG. The peak potential was dependent on pH and shifted towards less positive value with increasing pH. The E_p versus pH relations were found as linear as follows:

For INO E_p (pH 2.4 – 10.5) = -57.406 pH + 1757.6 mV vs. Ag/AgCl

For HX E_p **(pH 2.4 – 10.5) = -57.422 pH + 1442.2 mV vs. Ag/AgCl**

For XT E_p **(pH 2.4 – 10.5) = -55.691 pH + 1067.9 mV vs. Ag/AgCl**

For UA E_p **(pH 2.4 – 10.5) = -56.034 pH + 695.8 mV vs. Ag/AgCl**

The correlation coefficients for the linear relations were 0.997, 0.997, 0.991, and 0.997, respectively. The value of dE_p/pH for all the analytes was close to 59 mV/pH (theoretical Nernst value), hence, it is concluded that equal number of electrons and protons are involved in the oxidation of these analytes at PdNPs:pBG/AmSWCNTs/EPPG sensor. The variation of peak current with pH for all the four metabolites is presented in **Fig 5.11**.

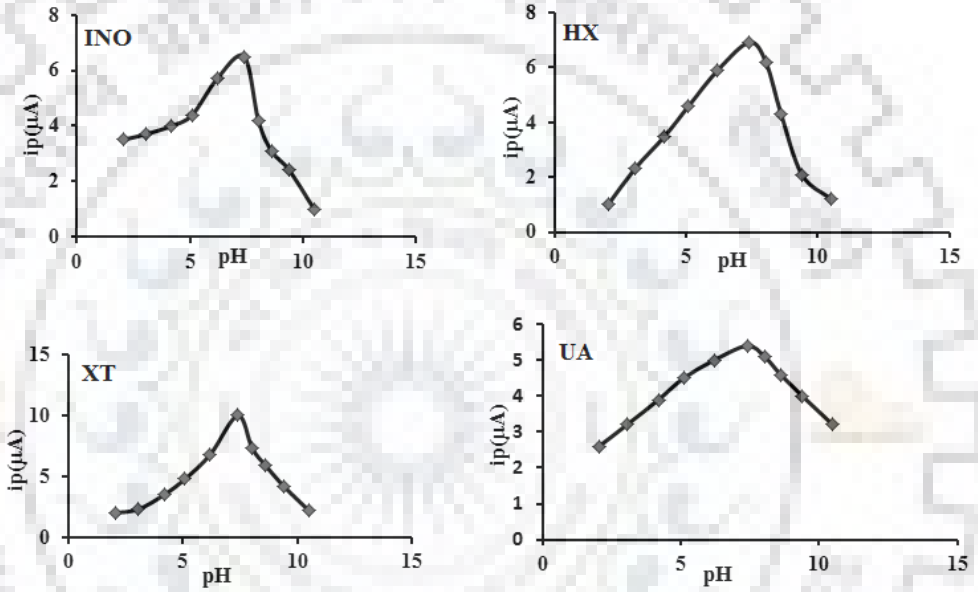

Fig. 5.11: Observed variation of peak current with pH for different metabolites of ATP.

5.3.4.3 Effect of frequency

The effect of square wave frequency on the oxidation peak current was studied over the frequency range 5-40 Hz at pH 7.4. An increase in the frequency induces an increase in the oxidation peak current of these analytes and the linear relations for the peak current (i_p) vs. frequency (f) were observed as:

$i_p/\mu A = 0.4558\ f - 0.8875$ **(For INO)**

$i_p/\mu A = 0.2981\ f + 1.8372$ **(For HX)**

$i_p/\mu A = 0.6064\ f + 0.6902$ **(For XT)**

$i_p/\mu A = 0.4471\ f - 0.8607$ **(For UA)**

The values of correlation coefficient were 0.996, 0.992, 0.998 and 0.993, respectively. The linearity of the above relations suggested the involvement of adsorption in the oxidation.

The adsorption was further confirmed by the linear relation of log i_p versus log f:

$\log i_p = 1.164 \log f - 0.612$ ($R^2 = 0.995$; For INO)

$\log i_p = 0.7161 \log f - 0.0253$ ($R^2 = 0.994$; For HX)

$\log i_p = 0.9086 \log f - 0.072$ ($R^2 = 0.999$; For XT)

$\log i_p = 1.0652 \log f - 0.4855$ ($R^2 = 0.997$; For UA)

In all the case the slope value (dlog f /dlog i_P was sufficiently greater than 0.5, which clearly confirmed that the oxidation process of these analytes was adsorption controlled [32].

5.3.4.4. Simultaneous analysis of INO, HX, XT and UA

The simultaneous determination of INO, HX, XT and UA has great importance due to co-existence of these four analytes; hence, the determination was carried out in three steps. In the first set of experiments, the SWVs were recorded by keeping the concentration of two analytes HX and UA constant as 25 μM and 15 μM, respectively, and the concentration of other two were varied from 25 μM to 150 μM (for INO) and 15 μM to 110 μM (for XT). Four distinguished and sharp oxidation peaks at potentials of 1344 mV, 1020 mV, 667 mV and 284 mV were observed for INO, HX, XT and UA, respectively (**Fig. 5.12 A**). On increasing the concentration of both INO and XT, the peak currents of INO and XT increased without affecting the E_p and i_p of other analytes HX and UA. In the second step, the SWVs were recorded by keeping the concentration of INO and XT constant (25 μM) and concentrations of HX and UA were increased from 25 μM to 150 μM and 10 μM to 70 μM, respectively. In this case, the enhancement in the peak current was observed without affecting the peak potential and peak current of INO and XT as presented in (**Fig. 5.12 B**). Similar results were observed on keeping the concentration of one analyte constant with different concentrations of other three analytes; no influence was seen in the peak current and peak potential of any analyte. In the third step, the SWVs were recorded by increasing the concentration of all the four analytes from 25 μM each (for INO, HX) and 15 μM each (for XT and UA) to 150 μM each (for INO, HX), 110 μM (for XT) and 70 μM (for UA). The increment in the peak currents was observed for all four analyte with increasing concentrations without affecting the peak potential and peak current of any analyte as presented in (**Fig. 5.12 C**). Thus, it is concluded from the observed results that simultaneous determination of these four analytes can be carried out effectively using PdNPs:pBG/AmSWCNTs/EPPG sensor. The anodic peak response and sensitivity for the individual and simultaneous determination of these analytes was found to be similar, which indicated that the presence of other analytes did not affect the simultaneous determination due to their co-existence.

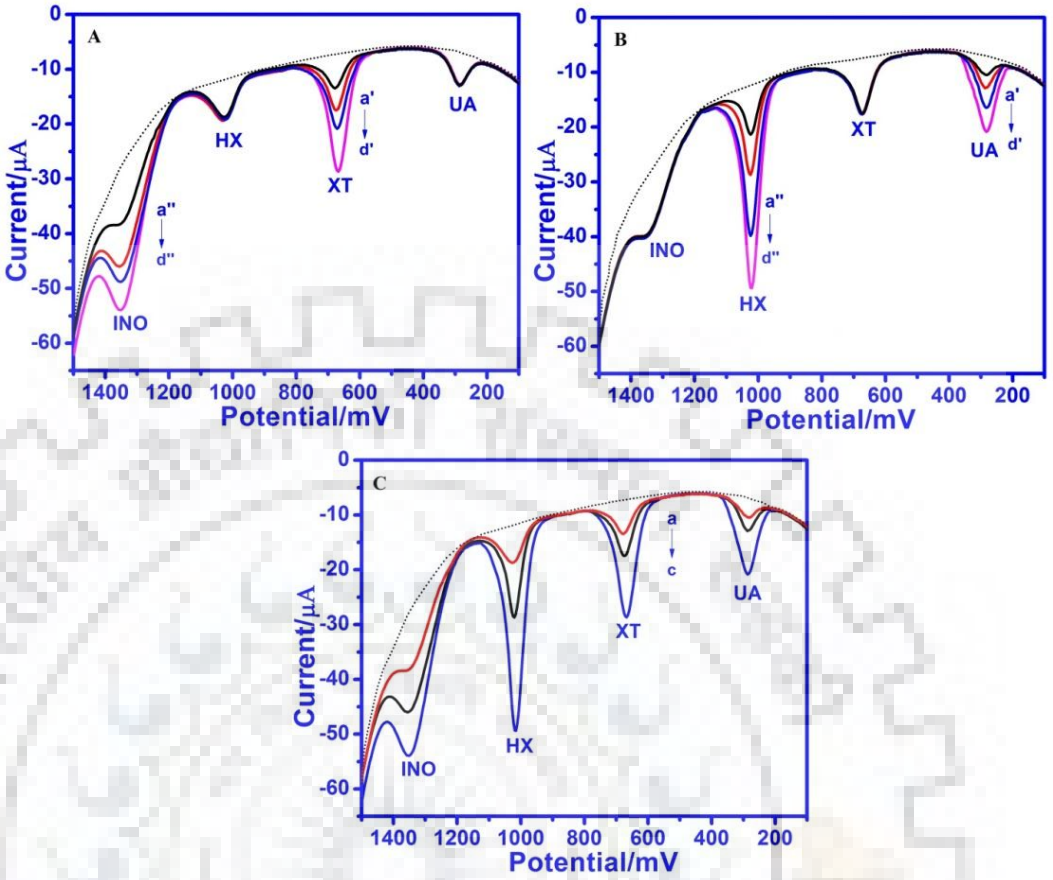

Fig. 5.12: (A) SWVs recorded for a mixture of INO, HX, XT, and UA at PdNPs:pBG/AmSWCNTs/EPPG sensor at pH 7.4 at concentration of INO (a) 25; (b) 70; (c) 110; and (d) 150 µM with the concentration of XT (a) 15; (b) 30; (c) 70; and (d) 110 µM. The concentrations of HX and UA were constant as 25 µM and 15 µM, respectively.

(B) SWVs recorded for a mixture of INO, HX, XT and UA at pH 7.4 at concentration of HX (a) 25; (b) 40; (c) 100; and (d) 150 µM with the concentration of UA (a) 15; (b) 25; (c) 40; and (d) 70 µM. The concentrations of INO and XT were constant (25 µM each).

(C) SWVs recorded for a mixture of INO, HX, XT and UA at pH 7.4, 25 µM each for INO, HX and 15 µM each for XT and UA (curve a); 70 µM, 40 µM, 30 µM, and 25 µM for INO, HX, XT, and UA, respectively (curve b) and 150 µM each for INO, HX, 110 µM XT and 70 µM UA (curve c). The background is shown by the dotted line.

5.3.5 Interference study

Under optimized conditions, the interference studies were performed in the presence of ascorbic acid (AA), dopamine (DA), adenosine monophosphate (AMP), and inosine monophosphate (IMP) and the observed results are presented in **Fig. 5.13**. **Fig. 5.13 A** shows a

voltammograms recorded for a mixture of INO, HX, XT (35 µM each) and UA (20 µM) in the presence of increasing concentration of AA and DA up to 400 µM. The results observed from the **Fig. 5.13 A** clearly demonstrate that presence of AA and DA does not interfere with the oxidation of these analytes. In another set of voltammetric studies, voltammograms were recorded for a mixture of INO (20 µM) and HX, XT, UA (35 µM each) in the presence of increasing concentration of AMP from 100 µM to 300 µM as shown in the **Fig. 5.13 B**. It was observed that AMP did not cause interference in the oxidation of INO, HX, XT and UA, whereas oxidation of IMP occurred at 1298 mV and interfered with INO. It was tolerated only up to 75 µM concentration in these studies.

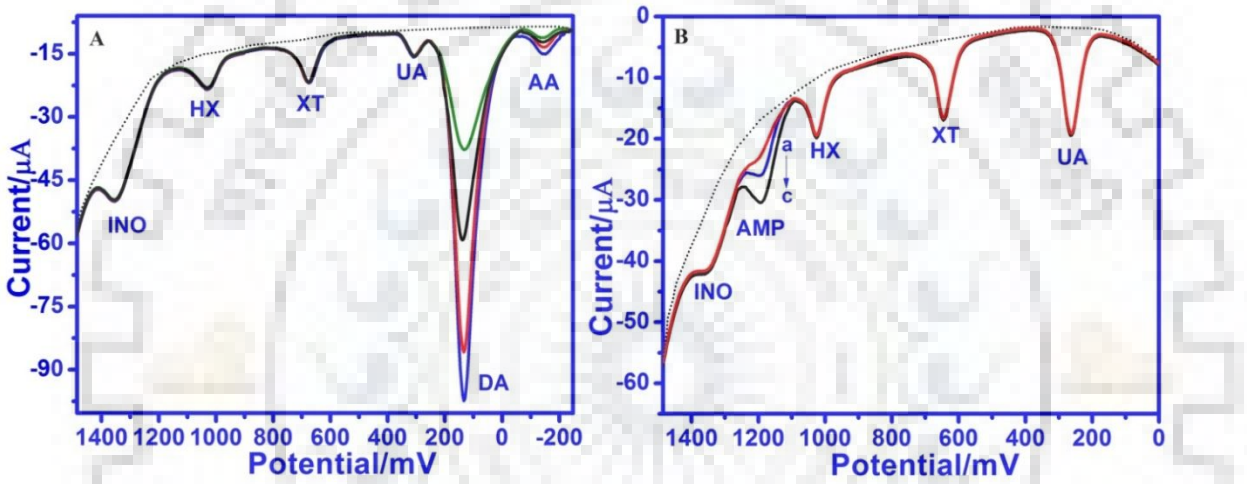

Fig. 5.13: (A) SWVs observed for INO, HX, XT (35 µM each) and UA (20 µM) with increased concentration of AA and DA (100-400 µM each) at the PdNPs:pBG/AmSWCNTs/EPPG sensor at pH 7.4. The dotted line represents the background. **(B)** SWVs observed for INO (20 µM), HX, XT, and UA (35 µM each) in the presence of adenosine monophosphate (AMP) with increasing concentration from 100 to 300 µM; at the PdNPs:pBG/AmSWCNTs/EPPG sensor at pH 7.4.

5.3.6 Analytical applicability

5.3.6.1 Analysis in human plasma samples

Purines can pass through the cell membrane in the human blood and enter to the blood stream. In general, purines are found in lower concentrations, but in the case of AMI, angina pectoris, and other ischemic diseases, the concentration of these analytes increase in blood plasma [17]. Thus, the applicability of the modified sensor was examined for the determination of INO, HX, XT and UA in the blood plasma by standard addition method. The voltammograms were recorded and recovery studies were carried out after adding known concentration of different analytes. The recovery values were determined in the range 99.07-100.75% for INO, 99.44-

101.56% for HX, 99.49-100.65% for XT and 99.96-100.25% for UA and are summarized in **Table 2.**

5.3.6.2 Analysis in human urine samples

A typical voltammogram of diluted urine sample is presented in **Fig. 5.14 A**, which demonstrates the presence of all four analyte in the human urine sample. The concentration of the four targeted analytes was determined and reported in **Table 3**. The exogenous INO, HX, XT and UA were then spiked in the urine sample and the SWVs were again recorded. The observed results are summarized in **Table 3** and clearly demonstrated the acceptable range of recoveries as 99.87-100.29% for INO, 98.43-101.56% for HX, 99.89-100.3% for XT and 99.96-100.05% for UA. The observed results in the human urine samples were also validated using HPLC studies. Four peaks were clearly observed at 30.95, 36.36, 38.40, and 43.21 min in the HPLC for UA, HX, XT and INO, respectively as represented in **Fig. 5.14 B**. Some other peaks were also observed, which were not identified in this study. All target analytes were then studied at different concentrations and the area under the peaks were plotted against concentration to get a calibration curve. The concentrations of UA, HX, XT and INO in the urine sample were then calculated from the calibration curve and found as 275.27 µM, 2.57 µM, 19.38 µM and 31.01 µM for UA, HX, XT and INO, respectively. Thus, the practically similar values obtained for these four analytes by the two methods in the simultaneous determination demonstrated the sensitivity and practical applicability of the presented approach.

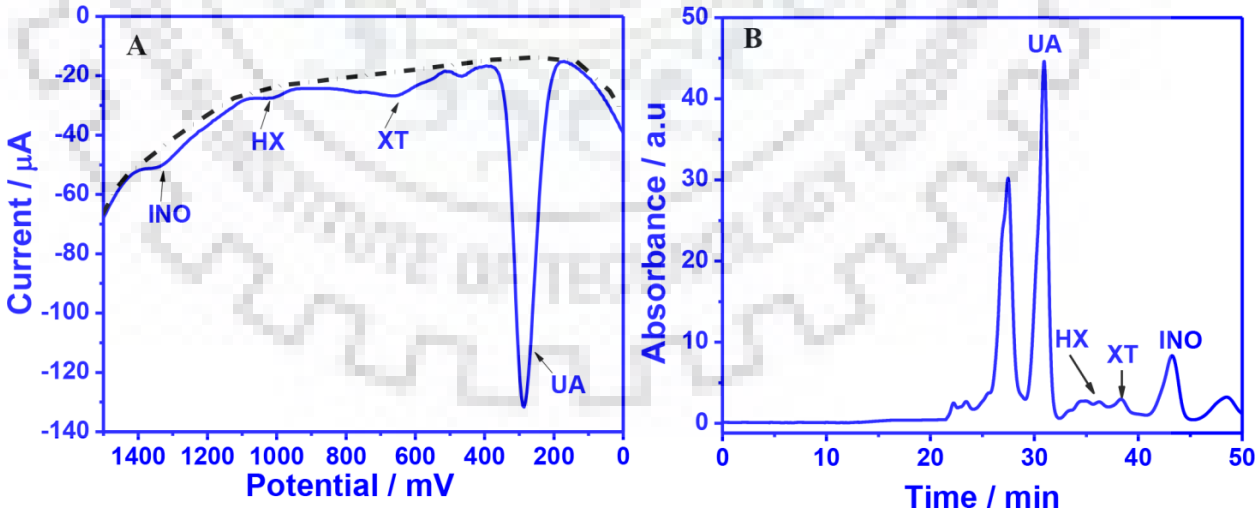

Fig. 5.14: (A) SWV observed for human urine samples of a healthy volunteer at the modified PdNPs:pBG/AmSWCNTs/EPPG sensor. **(B)** HPLC chromatogram observed for the human urine sample of a healthy volunteer.

Table 2: Analysis of ATP metabolites in the human plasma samples of healthy volunteers at the modified PdNPs:pBG/AmSWCNTs/EPPG sensor.

	INO		HX		XT		UA	
Amount added (μM)	**Amount Detected (μM)**	**Recovery* (%)**	**Amount Detected (μM)**	**Recovery* (%)**	**Amount Detected (μM)**	**Recovery* (%)**	**Amount Detected (μM)**	**Recovery* (%)**
Plasma samples								
Sample 1								
0	**14.24**	-	**1.40**	-	**4.60**	-	**56.15**	-
5	19.32	100.56	6.42	101.42	9.63	100.65	61.14	**99.98**
10	24.13	99.22	11.39	99.28	14.62	100.43	66.13	**99.96**
15	29.20	99.71	16.38	98.57	19.59	99.78	77.17	**100.03**
Sample 2								
0	**11.92**	-	**1.28**	-	**3.96**	-	**50.15**	-
10	22.01	100.75	11.26	98.43	13.98	100.63	60.14	**99.98**
20	31.94	100.16	21.29	100.78	23.94	99.49	70.19	**100.07**
30	41.81	99.07	31.30	101.56	33.97	100.25	80.28	**100.25**

*The R.S.D. values for plasma was less than ±2.04 for n = 3. The detected values are sum of metabolite present + added amount

Table 3: Analysis of ATP metabolites in the human urine samples of healthy volunteers at the modified PdNPs:pBG/AmSWCNTs/EPPG sensor.

	INO		HX		XT		UA	
Amount added (μM)	Amount Detected (μM)	Recovery* (%)	Amount Detected (μM)	Recovery * (%)	Amount Detected (μM)	Recovery* (%)	Amount Detected (μM)	Recovery* (%)
Urine samples								
Sample								
0	31.01	-	2.56	-	19.39	-	275.27	-
5	36.022	100.03	7.52	98.43	24.43	100.2	280.31	99.97
25	55.97	99.87	27.55	99.60	44.45	100.3	300.49	100.05
50	81.10	100.29	52.60	101.56	69.37	99.89	325.26	99.96

*The R.S.D. values for urine determination was less than ±2.12 for n = 3. The detected values are sum of metabolite present + added amount.

5.3.7 Stability and reproducibility of modified sensor

The stability of the proposed method was evaluated at the 25 µM concentration of each analyte in a solution over a period of 30 days at pH 7.4. It was found that the peak currents of INO, HX, XT and UA remained unchanged for the first 15 days with relative standard deviation (R.S.D.) as ± 1.79%, ± 2.16%, ± 1.92% and ± 2.42%. After 15 days, a deviation in the peak current was noticed with increase in variations in R.S.D. values, therefore it is concluded that the sensor can be successfully used for the first 15 days. The intraday reproducibility of the PdNPs:pBG/AmSWCNTs/EPPG sensor was examined by recording at least eight replicate voltammograms at an interval of 1 h in the blank solution as well as in the mixture of INO, HX, XT, and UA (25 µM each). The R.S.D. values (n = 4) were observed as ± 0.56%, ± 1.44%, ± 0.72% and ± 1.58% for INO, HX, XT and UA, respectively, which indicated the good accuracy and reproducibility of prepared sensor.

5.4 CONCLUSION

A fabricated novel sensitive and selective sensor based on polymer nanocomposite (PdNPs:pBG/AmSWCNTs/EPPG) has been efficiently used for the simultaneous detection of the four ATP metabolites, INO, HX, XT and UA with excellent peak separation and enhanced sensitivity. At the EPPG surface, AmSWCNTs were effectively interlinked with the PdNPs and pBG composite film and exhibited excellent electrocatalytic activity with the larger surface area and increased electron transfer properties. The linear calibration curves were obtained for INO, HX, XT and UA in the linear range as 0.001-175 µM, 0.001-200 µM, 0.001-150 µM and 0.001-200 µM, respectively, with the detection limits of 0.95 nM, 1.04 nM, 1.07 nM and 0.43 nM for INO, HX, XT and UA, respectively. The common compounds AMP, AA, DA present in the physiological fluids have no interference in the oxidation of INO, HX, XT and UA at the modified sensor, whereas IMP was tolerated only upto 75 µM. The simultaneous determination of these analytes in the human urine and plasma samples was carried out and the observed results were validated using HPLC studies.

5.5 REFERENCES

[1] G. Hasko, M.V. Sitkovsky, C. Szabo, "Immuno modulatory and neuro-protective effects of inosine", Trends Pharmacol. Sci. 25 (2004) 152.

[2] K.K. Hussain, M.H. Akhtar, M.H. Kim, D.K. Jung, Y.B. Shim, "Performance comparison between multienzymes loaded single and dual electrodes for the simultaneous electrochemical detection of adenosine and metabolites in cancerous cells", Biosens. Bioelectron. 109 (2018) 263.

[3] D.E. Farthing, C.A. Farthing, L. Xi, "Inosine and hypoxanthine as novel biomarkers for cardiac ischemia: From bench to point-of-care", Exp. Biol. Med. 240 (2015) 821.

[4] A.M. Pedley, S.J. Benkovic, "A new view into the regulation of purine metabolism: The Purinosome", Trends Biochem Sci. 42 (2017) 141.

[5] A.M Amorini, A. Petzold, B. Tavazzi, J. Eikelenboom, G. Keir, A. Belli, G. Giovannoni, V.D. Pietro, C. Polman, S. D'Urso, R. Vagnozzi, B. Uitdehaag, G. Lazzarino, "Increase of uric acid and purine compounds in biological fluids of multiple sclerosis patients", Clin. Biochem. 42 (2009) 1001.

[6] L.F. Souza, A.P. Horn, D.P. Gelain, F.R. Jardim, G. Lenz, E.A. Bernard, "Extracellular inosine modulates ERK 1/2 and p38 phosphorylation in cultured Sertoli cells: Possible participation in TNF-alpha modulation of ERK 1/2", Life Sci. 77 (2005) 3117.

[7] L. Liaudet, J.G. Mabley, P. Pacher, L. Virag, F.G. Soriano, A. Marton, G. Hasko, E.A. Deitch, C. Szabo, "Inosine exerts a broad range of anti-inflammatory effects in a murine model of acute lung injury", Ann. Surg. 235 (2001) 568.

[8] S. Buckley, L. Barsky, K. Weinbergand, D. Warburton, "In vivo inosine protects alveolar epithelial type 2 cells against hyperoxia-induced DNA damage through MAP kinase signaling", Am. J. Physiol.-Lung Cell. Mol. Physiol. 288 (2005) L569.

[9] S.B. Revin, S.A. John, "Selective determination of inosine in the presence of uric acid and hypoxanthine using modified electrode", Anal. Biochem. 421 (2012) 278.

[10] A.A. Welihinda, M. Kaur, K. Greene, Y. Zhai, E.P Amento, "The adenosine metabolite inosine is a functional agonist of the adenosine A2A receptor with a unique signalling bias", Cell. Signal 28 (2016) 552.

[11] J.R. Docherty, A. Camba, E. Lendoiro, C. Cordeiro, I.M. Silva, M.S.R. Calvo, D.N. Vieira, J.I.M. Barus, "High variation in hypoxanthine determination after analytical treatment of vitreous humor samples", Forensic Sci. Med. Pathol. 10 (2014) 627.

[12] S.Z. Bas, H. Gulce, S. Yildiz, A. Gulce, "Amperometric biosensors based on deposition of gold and platinum nanoparticles on polyvinylferrocene modified electrode for xanthine detection", Talanta 87 (2011) 189.

[13] A.P.M Farias, A.A. Castro, "Determination of xanthine in the presence of hypoxanthine by adsorptive stripping voltammetry at the mercury film electrode", Anal. Chem. Insights 9 (2004) 49.

[14] N. Cooper, R. Khosravan, C. Erdmanna, J. Fiene, J.W. Lee, "Quantification of uric acid, xanthine and hypoxanthine in human serum by HPLC for pharmacodynamic studies", J. Chromatogr. B 837 (2006) 1.

[15] D.E. Farthing, D. Sica, T. Gehr, B. Wilson, I. Fakhry, T. Larus, C. Farthing, H.T. Karnes, "An HPLC method for determination of inosine andhypoxanthine in human plasma from healthy volunteers and patients presenting with potential acute cardiac ischemia", J. Chromatogr. B 854 (2007) 158.

[16] D.E. Farthing, D. Sica, M. Hindle, L. Edinboro, L. Xi, T.W.B. Gehr, L. Gehr, C.A. Farthing, T.L. Larus, I. Fakhrya, H.T. Karnes, "A rapid and simple chemiluminescence method for screening levels of inosine and hypoxanthine in nontraumatic chest pain patients", Luminescence 26 (2011) 65.

[17] J. Maiuolo, F. Oppedisano, S. Gratteri, C. Muscoli, V. Mollace, "Regulation of uric acid metabolism and excretion", Int. J. Cardiol. 213 (2016) 8.

[18] H.H. Hamzah, Z.M. Zain, N.L.W. Musa, Y.C. Lin, E. Trimbee, "Spectrophotometric determination of uric acid in urine based-enzymatic method uricase with 4-aminodiphenylamine diazonium sulfate (variamine blue RT salt)", J. Anal. Bioanal. Tech. S7 (2013) 1.

[19] T. Richter, L.L.S. Lockyear, R.D. Oleschuk, U. Bilitewski, D.J. Harrison, "Bi-enzymatic and capillary electrophoretic analysis of non-fluorescent compounds in microfluidic devices determination of xanthine", Sens. Actuators B 81 (2002) 369.

[20] H. Okuma, E. Watanabe, "Flow system for fish freshness determination based on double multi-enzyme reactor electrodes", Biosens. Bioelectron. 17 (2002) 367.

[21] S. Wang, F.Yang, K. Feng, D. Li, J. Zhao, S.P. Li, "Simultaneous determination of nucleosides, myriocin, and carbohydrates in Cordyceps by HPLC coupled with diode array detection and evaporative light scattering detection", J. Sep. Sci. 32 (2009) 4069.

[22] M. Helenius, S. Jalkanen, G.G. Yegutkin, "Enzyme-coupled assays for simultaneous detection of nanomolar ATP, ADP, AMP, adenosine, inosine and pyrophosphate concentrations in extracellular fluids", Biochim. Biophys Acta A 182 (2012) 1967.

[23] T. Ramanathan, F.T. Fisher, R.S. Ruoff, L.C. Brinson, "Amino-functionalized carbon nanotubes for binding to polymers and biological systems", Chem. Mater. 17 (2005) 1290.

[24] D.M. Kim, M.Y. Kim, S.S. Reddy, J. Cho, C.H. Cho, S. Jung, Y.B. Shim, "Electron-Transfer Mediator for a NAD-Glucose Dehydrogenase-Based Glucose Sensor", Anal. Chem. 85 (2013) 11643.

[25] F. Atta, M.F.E Kady, "Novel poly(3-methylthiophene)/Pd, Pt nanoparticle sensor: Synthesis, characterization and its application to the simultaneous analysis of dopamine and ascorbic acid in biological fluids", Sens. Actuators B 145 (2010) 299.

[26] P.K. Rastogi, V. Ganesan, S. Krishnamoorthi, "Palladium nanoparticles incorporated polymer-silica nanocomposite based electrochemical sensing platform for nitrobenzene detection", Electrochim. Acta 147 (2014) 442.

[27] C. Ciobotaru, C.M. Damian, H. Iovu, "Single-wall carbon nanotubes purification and oxidation", UPB. Sci. Bull. Series B 75 (2013) 55.

[28] R.N. Goyal, S.K. Srivastava, R. Agarwal, "Electrochemical behavior and aggregation number of pyridinol azo dyes", Bull. Soc. Chim. Fr. 4 (1985) 656.

[29] A.L. Vaisman, H.D. Wagner, G. Marom, "The role of surfactants in dispersion of carbon nanotubes", Adv. Colloid Interface Sci. 128 (2006) 37.

[30] A. Shokrollahi, F. Firoozbakht, "Determination of the acidity constants of neutral red and bromocresol green by solution scanometric method and comparison with spectrophotometric results", Beni-Seuf Univ. J. Appl. 5 (2016) 13.

[31] W. Chidawanyika, T. Nyokong, "Characterization of amine-functionalized single-walled carbon nanotube-low symmetry phthalocyanine conjugates", Carbon 48 (2010) 2831.

[32] W. Wang, L. Wang, L. Zou, G. Li, B. Ye, "Electrochemical behavior of arctigenin at a novel voltammetric sensor based on Iodide/SWCNTs composite film modified electrode and its sensitive determination", J. Electroanal. Chem. 772 (2016) 17.

[33] J.M. Zen, Y.Y. Lai, H.H. Yang, A.S. Kumar "Multianalyte sensor for the simultaneous determination of hypoxanthine, xanthine and uric acid based on a preanodized nontronite-coated screen-printed electrode", Sens. Actuators B 84 (2002) 237.

[34] M. Raj, P. Gupta, R.N. Goyal, Y.B. Shim, "Graphene/conducting polymer nano-composite loaded screen printed carbon sensor for simultaneous determination of dopamine and 5-hydroxytryptamine", Sens. Actuators B 239 (2017) 993.

[35] R.N. Goyal, V.K. Gupta, S. Chatterjee, "Simultaneous determination of adenosine and inosine using single-wall carbon nanotubes modified pyrolytic graphite electrode", Talanta 76 (2008) 662.

[36] M.A. Carsol, G. Volpe, M. Mascini, "Amperometric detection of uric acid and hypoxanthine with Xanthine oxidase immobilized and carbon based screen-printed electrode. Application for fish freshness determination", Talanta 44 (1997) 2151.

[37] D. Lan, L. Zhang, "Electrochemical synthesis of a novel purine-based polymer and its use for the simultaneous determination of dopamine, uric acid, xanthine and hypoxanthine", J. Electroanal. Chem. 757 (2015) 107.

[38] A. Luo, Q. Lian, Z. An, Z., Li, Y. Guo, D. Zhang, Z. Xue, X. Zhou, X. Lu, "Simultaneous determination of uric acid, xanthine and hypoxanthine based on sulfonic groups functionalized nitrogen-doped graphene", J. Electroanal. Chem. 756 (2015) 22.

[39] R. Ojani, A. Alinezhad, Z. Abedi, "A highly sensitive electrochemical sensor for simultaneous detectionof uric acid, xanthine and hypoxanthine based on poly(l-methionine)modified glassy carbon electrode", Sens. Actuators B 188 (2013) 621.

[40] Y. Wang, L. Tong, "Electrochemical sensor for simultaneous determination of uric acid, xanthine and hypoxanthine based on poly (bromocresol purple) modified glassy carbon electrode", Sens. Actuators B 150 (2010) 43.

[41] Y. Wang, "Simultaneous determination of uric acid, xanthine and hypoxanthine at poly(pyrocatechol violet)/functionalized multi-walled carbon nanotubes composite film modified electrode", Colloid Surf. B 88 (2011) 614.

Chapter 6

AgNPs:ErGO modified sensor to determine the effect of caffeine on Estradiol release

6.1 INTRODUCTION

Estradiol, 1,3,5 (10)-estratrien-3, 17 β-diol (EST), a major female sex hormone is one of the most potent endogenous estrogen steroids. In human body estradiol is synthesized from cholesterol through different pathways. A common pathway includes the formation of testosterone by the aromatization of androstenedione, which can be converted into EST [1,2]. EST acts primarily as a growth hormone for the female reproductive organs. Secondary role, such as breast development, alteration of body shape and maintenance of female reproductive tissues are also driven by estradiol [3]. Normal EST level presents in the childbearing aged women (18–35 yr) is in the range 55 pM to 2.84 nM, whereas for postmenopausal women the normal EST level is lower than 40 pM [4]. The irregularity in these levels can cause several abnormalities in the female system. Approximately 90% of women of child-bearing age (18–35 yr) consume an average of 165 mg caffeine/day from different sources. Caffeine consumption has been found to decrease estradiol in white women, whereas, the increase was found in asian women by nonlinear mixed models [5]. In a recent study caffeinated drinks have been found to affect estrogen metabolism in premenopausal women [6]. Caffeine, 1,3,7-trimethylxanthine, (CAF) is a natural psychoactive drug, which stimulates central nervous system and cardiovascular systems. This is one of the most widely consumed foods and supplements in the world, which is mainly found in common beverages, i.e. coffee, tea, soft drinks, numerous foods and drugs. CAF has some positive physiological effects, such as diuresis, increased metabolic rate, gastric acid secretion and lower risk of diabetes but it also produces many severe adverse effects on the human health [7-9]. In postmenopausal women, the risk of Parkinson's disease is reduced by CAF intake but an increased risk is associated among estrogen users and middle age females [10]. CAF consumption for the long time can influence the women's EST level and these variations in EST level over a long period of time may lead to many disorders, such as breast cancer, endometriosis, endometrial, ovarian cancers, increased blood pressure, plasma homocysteine concentrations, osteoporosis, serum total and low-density lipoprotein cholesterol concentrations [11-14]. Due to the associations of CAF intake with serum EST concentration, the accurate and rapid simultaneous determination has been considered of significant importance in biochemical and clinical diagnosis.

Therefore, various approaches have been reported for the individual and simultaneous determination of EST and CAF, such as enzyme immunoassay, UV spectrophotometry, high-performance liquid chromatography, liquid chromatography and liquid chromatography–mass spectrometry [15-20]. However, most of the methods used have limitations, such as involvement of

complex steps for sample preparation, requirement of expensive instruments, less sensitivity and long analysis time. In a recent paper Pd/N doped reduced GO has also been used for the determination of EST [18]. The N-RGO was prepared by using hydrothermal method and the sensor showed high catalytic activity to the oxidation of EST. An aptamer based determination of EST has been reported [21], however, selection, preparation and cost has limited the use of aptamers in analysis. However, no voltammetric attempt has been made to study effect of CAF on the release of EST. Therefore; an advanced, rapid, less expensive, highly sensitive and selective technique is required for the simultaneous analysis of EST and CAF. In the presented approach, one step synthesis and electro-deposition of silver nanoparticles (AgNPs) and electrochemically reduced graphene oxide (ErGO) at the pyrolytic graphite surface were carried out. ErGO have number of surface defects and oxygen functionalities, such as hydroxides, carboxylates and epoxides due to which ErGO disperse easily and strongly interacts with other materials [22-24]. AgNPs with the ErGO surface defects increases the sensitivity, catalytic properties, active surface area and functional sites for the adsorption of analytes and helps the electron transfer processes for the oxidation of analytes. The synergetic effect of Ag nano particles and reduced GO has been found to exhibit electrocatalytic effect due to storage capability of electrons and provide electrons on demand [25]. The present manuscript proposes a single step; green electrochemical method for the synthesis of AgNPs combined ErGO biosensor for the determination of EST and CAF. The applicability of the biosensor in human biological fluids is also demonstrated.

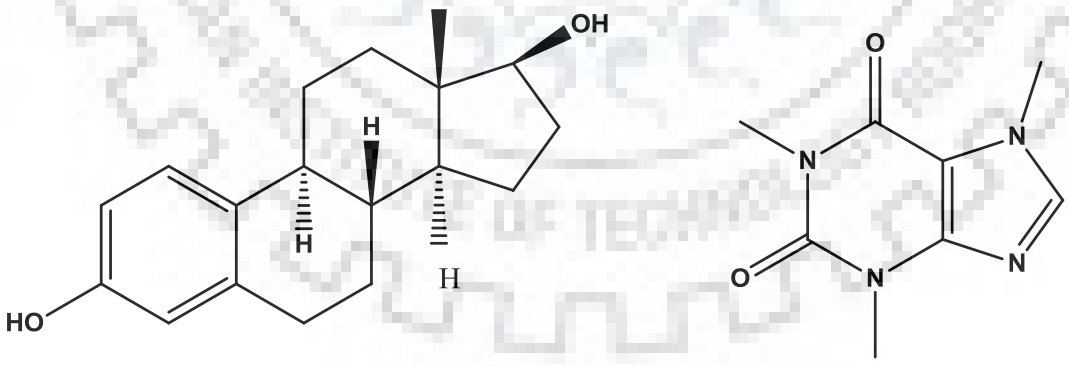

Estradiol Caffeine

Scheme 1: Chemical structure of Estradiol and Caffeine.

6.2 EXPERIMENTAL

6.2.1 Instrumentation

X-ray diffraction (Bruker D8-advance X-ray powder diffractometer), Fourier-transform infrared spectroscopy (FTIR, PerkinElmer, Inc), Raman Spectroscopy (Renishaw invia Raman microscopy at 540 nm), Transmission Electron Microscopy (TEM, model; Technai G2 20S-TWIN) were used for the characterization of the modified surface. HPLC studies for validation were carried out by using Shimadzu LC-2010A HT system equipped with C18 bondapack (125 Ao, 10 µm) reverse phase column. Methanol (HPLC grade) and water in the ratio of 1:1 was used as the solvent at the flow rate of 0.8 ml/min. The injection volume was 10 µL and the wave length of eluent was monitored at 254 nm. All other characterization techniques and electrochemical observations techniques were similar to that described in the section A of the chapter 2.

6.2.2 Chemicals and reagents

Estradiol (EST), caffeine (CAF), graphite powder (GO <20 nm), silver nitrate ($AgNO_3$) H_2SO_4 and $KMNO_4$ were purchased from Sigma-Aldrich (USA). All solvents and reagents used in the experiments were of analytical grade.

6.2.3 Preparation of graphene oxide

Graphene oxide (GO) was synthesized using graphite powder (>20 µm) by following improved Hummers method [26]. Briefly, graphite powder (2 g) was suspended for 2 h in the mixture of H_3PO_4 and H_2SO_4 (20:180). The mixture was stirred and $KMnO_4$ (8 g) was drop-wise added followed by heating the solution for 12 h at 50 °C. A brown colored suspension was obtained, which changed into yellow on the addition of 100 ml water followed by drop wise addition of 3 ml of 30% H_2O_2. The final mixture was then centrifuged and the sediment was thoroughly washed with 150 ml of water followed by 150 ml of HCl and 150 ml of ethanol to get freshly prepared GO, which was dried and characterized.

6.2.4 Preparation of modified AgNPs:ErGO/EPPG

Initially glassy carbon, which is commonly available, was used as a substrate for the modification; however, for EST it showed less sensitivity and broad peaks with high oxidation potential as compared to EPPG. For CAF, the peak merged with the background due to its high oxidation potential. Hence, EPPG was used as a substrate throughout the studies of these analytes. An unmodified EPPG sensor, was prepared by embedding of edge plane of pyrolytic graphite

piece [27] was first cleaned by rubbing it on a P-400 emery paper and carefully cleaned with double distilled water. Two approaches for the fabrication of sensor were used for step wise electro-deposition of AgNPs and ErGO. In the first approach, electro-deposition of AgNPs was first achieved, followed by the ErGO, whereas in another approach electro-deposition of ErGO was first achieved followed by the AgNPs. In both the cases, broad anodic peaks with low peak currents and higher potential were observed for both the analytes. Even on changing the ratio of AgNPs and ErGO upto 1:3 by varying the volume did not show significant change. Hence, electro-deposition of AgNPs:ErGO was carried out in a single step approach. The optimization studies were performed to get the maximum sensitivity of the sensor by varying the concentration ratio of both $AgNO_3$ and GO upto five times. It was found that the highest peak current of the prepared sensor was achieved, when the electro-deposition was carried out in the 1:1 mixture of both $AgNO_3$ and GO. Hence, 1:1 mixture of AgNPs and ErGO was used for electro-deposition. To deposit the composite on the surface, the sensor was dipped in 1:1 mixture of 1 mM $AgNO_3$ and GO (1 mg/ml in phosphate buffer solution of pH 7.4 which was uniformly dispersed by 40 min sonication) and the potential was applied from −1500 mV to 1500 mV at a sweep rate of 100 mVs^{-1} for 10 scans (optimized). After completion of 10 scans, the resulting modified surface was thoroughly rinsed with double distilled water to remove adsorbed molecules at the surface and was characterized. The prepared AgNPs:ErGO/EPPG biosensor was then stabilized by sweeping the potential from 400 mV to -1100 mV for 4 cycles (optimized) at 100 mV/s at pH 7.4 to get a steady cyclic voltammogram.

6.2.5 Procedure

The voltammetric studies of EST and CAF were carried out by using cyclic voltammetry (CV) and square wave voltammetry (SWV). For this purpose, separate solutions of two analytes EST and CAF (1 mM) were prepared by dissolving the required amount of each analyte in double distilled water. To carry out the voltammetric studies, 4 ml of the solution containing 2 ml of phosphate buffer of pH 7.4 and desired amount of analyte and water was used after bubbling the nitrogen gas for 10 min. The optimized parameters used in cyclic voltammetry were initial potential (E_i): 100 mV, switching potential (E): 1500 mV, final potential (E_f): 100 mV, sweep rate (v):100 mVs^{-1}, whereas parameters used in square wave voltammetry were, initial potential (E_i): 200 mV, final potential (E_f): 1430 mV, square wave frequency (f): 15 Hz, SW amplitude (E_{sw}): 25 mV and potential step (E): 4 mV. To remove the adsorbed material and regenerate the surface of

the senor a constant potential of −600 mV was applied in the blank solution for 150 s after each scan. The studies were carried out at an ambient temperature of 25 ± 2°C using Ag/AgCl electrode.

Biological samples: To check the practical applicability of the modified AgNPs:ErGO/EPPG biosensor, human urine and blood serum samples were obtained from I.I.T. hospital, Roorkee after the Ethical clearance committee approval. To collect the samples of healthy women of childbearing age (18–35 y) having regular menstrual cycle and not currently using hormonal contraception were given 2 cups caffeinated coffee (equivalent to ~200 mg caffeine/d) and the samples of urine and serum were collected before and after ~5 h of consumption of coffee. The anthropometric data of the women were F-1, 18 y, 48 kg; F-2, 22 y, 50 kg; F-3, 26 y, 46 kg; F-4, 30 y, 51 kg and F-5, 34 y, 45 kg. The collected urine and serum samples were diluted two times with phosphate buffer of pH 7.4 prior to analysis to minimize matrix complexity.

6.3 RESULTS AND DISCUSSION

6.3.1 Characterization of AgNPs:ErGO/EPPG biosensor

The Raman spectra of prepared GO, ErGO and AgNPs:ErGO are presented in **Fig. 6.1**, in which G-band represents the planar configuration of sp^2 bonded carbon, whereas D-band (defect band or disorder band) shows the breathing mode from sp^2 carbon rings or the level of defects in the material. Raman spectrum of GO (curve a) displays the bands associated at ~1352 cm^{-1} and ~1589 cm^{-1} corresponding to D and G modes respectively. These bands shifted to ~1348 cm^{-1} and ~1604 cm^{-1}, respectively with a new 2D band at 2705 cm^{-1} in the case of ErGO (curve b) with increase in intensity. Hence, the intensity ratio (I_D/I_G) increased for ErGO as compared to GO, which is attributed to the increased defects in ErGO. The I_D/I_G ratio of AgNPs:ErGO (curve c) is also larger than that of ErGO due to increased defects after the deposition of AgNPs. Moreover, a significant enhancement in the intensities of these three bands has also been witnessed in this case because AgNPs with ErGO increases the Raman signal via the Surface-Enhanced Raman Spectroscopy effect [24].

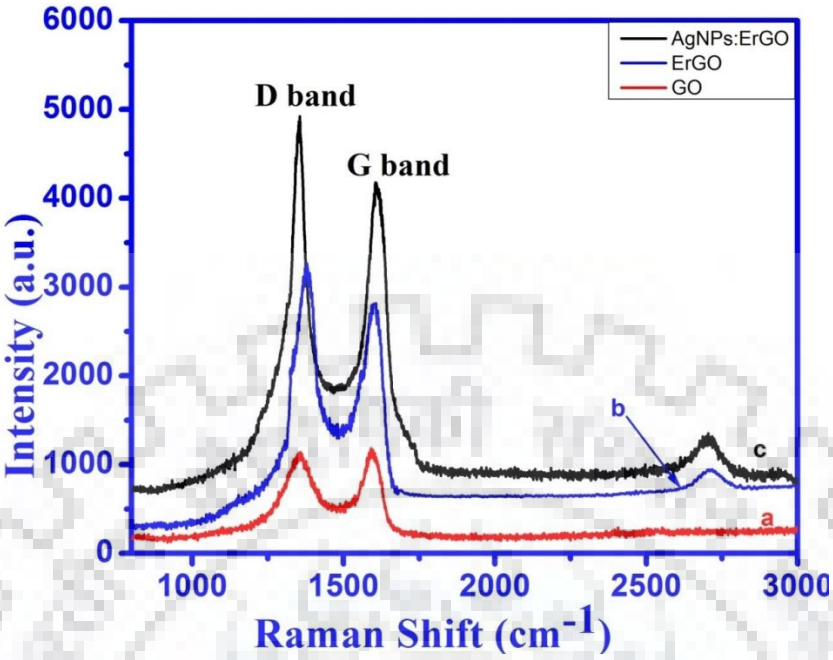

Fig. 6.1: Raman spectrum observed at various stages of modification.

The XRD pattern of AgNPs:ErGO nanocomposite was recorded and presented in **Fig. 6.2**. The prominent peaks observed at 37.9, 44.4 and 64.4 are assigned to the (111), (200) and (220) crystallographic planes of AgNPs, respectively. A broad diffraction peak is also observed at 24.6 (002) representing the presence of graphitic carbon in the AgNPs:ErGO nanocomposites [28]. Thus, it was concluded that the crystalline AgNPs decorated electrochemically reduced graphene oxide was successfully electro-deposited at the surface of EPPG.

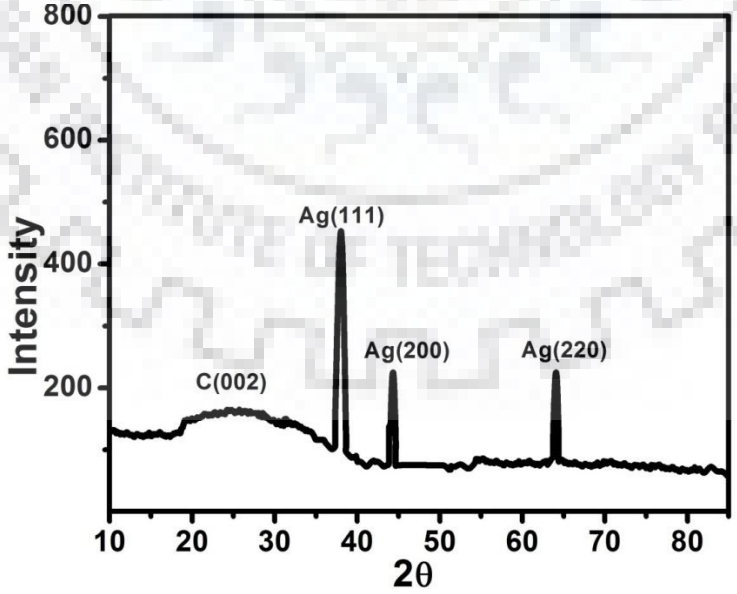

Fig. 6.2: Observed XRD pattern for AgNPs:ErGO.

The morphology of the modified surface AgNPs:ErGO/EPPG was examined by FE-SEM and a typical image observed for AgNPs:ErGO/EPPG is presented in **Fig. 6.3 (A).** The unmodified EPPG surface is smooth and clear, which has very less effective surface area (in inset) whereas, after the modification AgNPs were homogenously distributed on the crumpled and wrinkled multi-layers of ErGO, which demonstrated a strong interaction between them, hence, provided large effective surface area for the electro-oxidation of analytes. **Fig. 6.3 (B)** exhibited the EDX data of the AgNPs:ErGO/EPPG, where the results demonstrated the presence of AgNPs in the final modified surface.

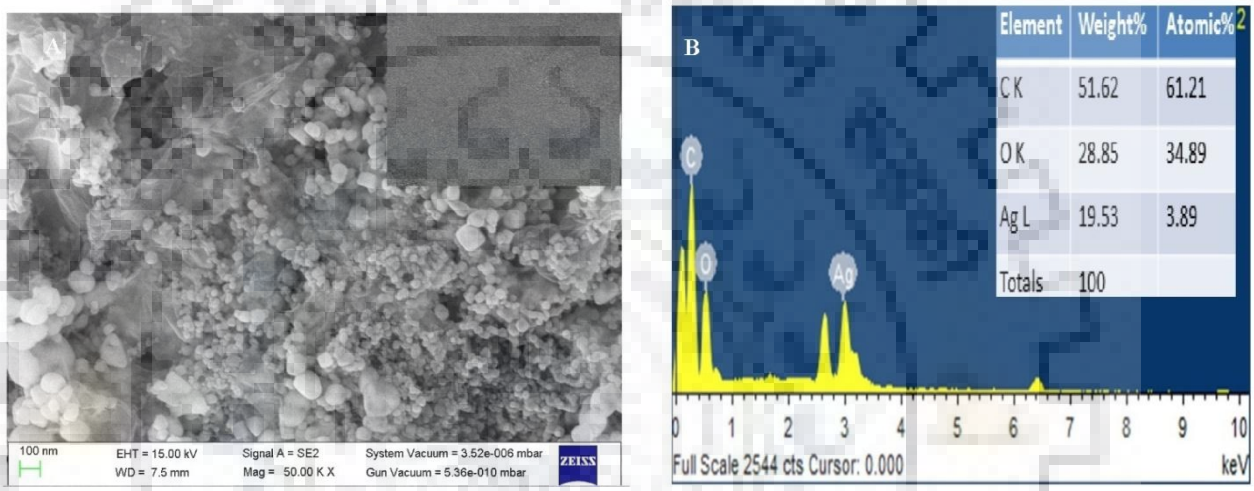

Fig. 6.3: (A) Typical FE-SEM images observed for AgNPs:ErGO /EPPG and inset shows the unmodified EPPG. **(B)** EDX data demonstrating the presence of Ag in AgNPs:ErGO/EPPG.

A representative TEM image of AgNPs:ErGO nanocomposite indicating the attachment of AgNPs with the ErGO nanosheets is presented in **Fig. 6.4 (A)**, which contributes to the high electrochemical activity of the AgNPs:ErGO/EPPG biosensor. **Fig. 6.4 (B)** represents the EDX data collected for the TEM image and demonstrated the highly dispersed AgNPs on the ErGO nanosheets.

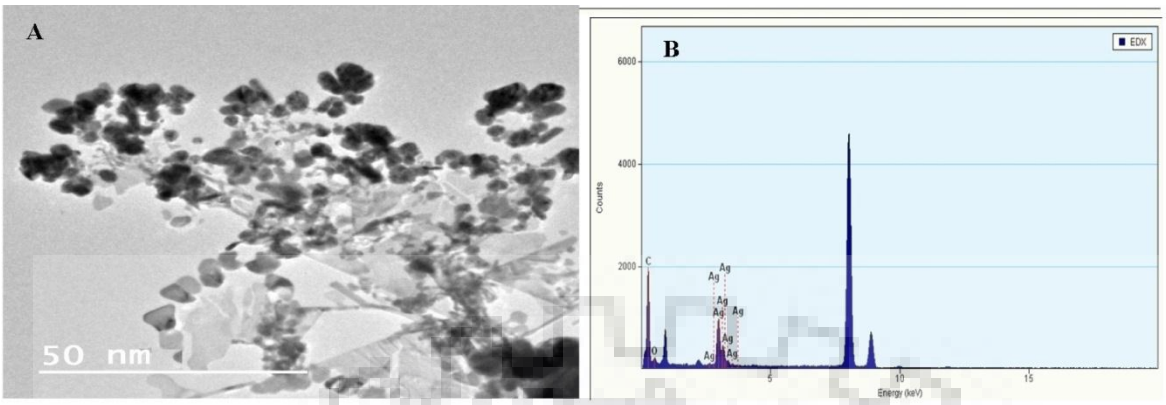

Fig. 6.4: (A) A typical TEM image observed for AgNPs:ErGO. **(B)** EDX data demonstrating the presence of Ag.

Electrochemical impedance spectroscopy (EIS) was then used to calculate the values of the electron-transfer resistance (R_{CT}) for unmodified EPPG, ErGO/EPPG, AgNPs/EPPG and AgNPs:ErGO/EPPG sensors in 0.1 M KCl containing 1.0 mM $K_3Fe(CN)_6$ solution over a frequency range of 0.1 Hz to 100 Hz with an applied potential of 50 mV. **Fig. 6.5** represents four EIS curves for different stages of modification of the sensor in which a semicircle followed by the linear portion.

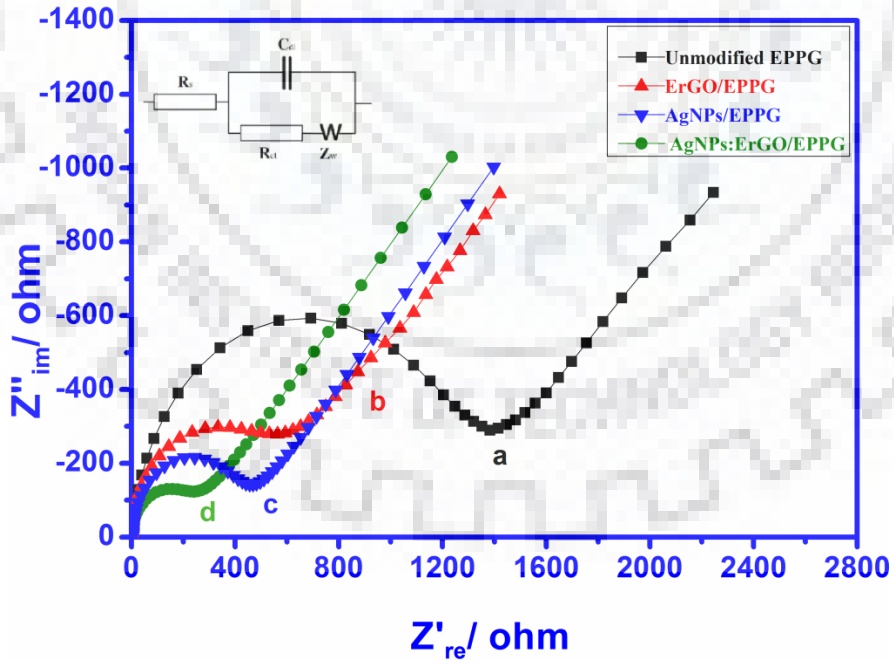

Fig. 6.5: Nyquist plots observed for unmodified EPPG (a), ErGO/EPPG (b), AgNPs/EPPG (c), and AgNPs:ErGO/EPPG (d). The Randles equivalent circuit used for the simulation of the EIS data is displayed in inset.

The semi-circular portion displayed an electron transfer limiting process, whereas the diameter of the semicircle indicated the charge transfer resistance (R_{CT}), which controls the electron-transfer kinetics at the electrode interface. The linear portion indicates the mass transfer effects at lower frequency. The inset of the **Fig. 6.5** shows the Randles equivalent circuit used for simulating the experimental data, where R_s is the electrolyte resistance; C_{dl} is the double layer capacitance and Z_w represents the Warburg impedance. The surface of unmodified EPPG exhibits a large semicircle portion indicating high R_{CT} for the $Fe[CN]_6^{3-/4-}$ redox process as 1228 Ω (curve a), whereas ErGO/EPPG exhibited a reduced semicircle and R_{CT} value as 558 Ω (curve b). In the case of AgNPs/EPPG surface (curve c), the R_{CT} value decreased to 440 Ω, whereas, the smallest semicircle with the lowest R_{CT} value 220 Ω is found for AgNPs:ErGO/EPPG sensor (curve d). Thus, the lowest resistance and maximum electron transfer efficiency was observed for AgNPs:ErGO/EPPG.

To study the change in the effective surface areas for unmodified EPPG, ErGO/EPPG, AgNPs/EPPG and AgNPs:ErGO/EPPG, cyclic voltammograms were recorded in 1 mM $K_3Fe(CN)_6$ containing 0.1 M KCl (supporting electrolyte) at different sweep rates from 5 mVs^{-1} to 225 mVs^{-1}. The observed slope of the i_P vs. $\nu^{1/2}$ polts was used to calculate effective surface areas using Randles-Sevcik equation:

$$\mathbf{i_p = 0.4463\ (F^3/RT)^{1/2}\ A\ n^{3/2}\ D_R^{1/2} C_0.\ \nu^{1/2}}$$

where i_p (peak current in ampere), F (Faraday's constant; 96,485 C mol^{-1}), R is the universal gas constant as 8.314 $JK^{-1}mol^{-1}$, A (surface area of electrode in cm^2), n (number of electron; 1 in this case), ν sweep rate in Vs^{-1}, D_R diffusion coefficient as 7.6×10^{-6} cm^2s^{-1}, T is the absolute temperature (298 K is taken in this case) and C_0 (concentration in mol L^{-1}). The effective surface areas for unmodified EPPG, ErGO/EPPG, AgNPs/EPPG and AgNPs:ErGO/EPPG were calculated as 0.092 cm^2, 1.524 cm^2, 2.785 cm^2 and 3.645 cm^2, respectively. Thus, the modified AgNPs:ErGO/EPPG biosensor exhibited highest effective surface area (~40 times larger than bare) which stimulated the charge transfer kinetics for the electro-oxidation of the EST and CAF.

6.3.2 Cyclic voltammetry

The determination of 30 μM EST or CAF was carried out at pH 7.4 by recording the cyclic voltammograms at AgNPs:ErGO/EPPG and a single well-defined sharp oxidation peak was observed at 616 mV and 1275 mV for EST and CAF. For the simultaneous determination of these

compounds voltammograms in a mixture of EST (30 μM) and CAF (10 μM) were recorded at unmodified EPPG and AgNPs:ErGO/EPPG at pH 7.4 and are shown in the **Fig. 6.6**. At unmodified EPPG surface, a small bump (626 mV) and broad anodic peak was observed at 1286 mV (curve a) with low peak current of CAF, whereas at AgNPs:ErGO/EPPG (curve b) two peaks at 616 mV and 1275 mV were observed corresponding to EST and CAF. Thus, the strong interaction of nanoparticles and graphene sheets were able to catalyse the oxidation of these molecules.

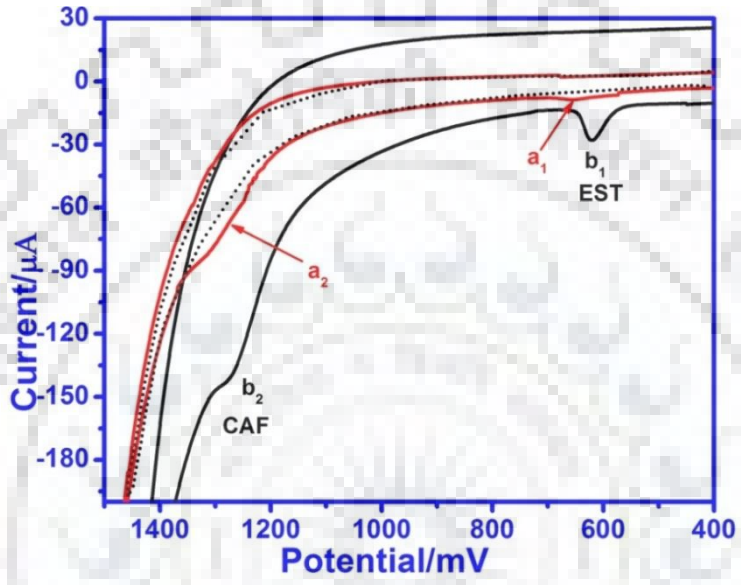

Fig. 6.6: A comparison of CVs observed for the mixture of EST (30 μM), and CAF (10 μM) at unmodified EPPG (curve a) and AgNPs:ErGO/EPPG (curve b) at pH 7.4. The dotted line represents the background.

To establish the nature of the electron transfer process involved in the electrocatalytic oxidation of EST and CAF at AgNPs:ErGO/EPPG biosensor, the sweep rate studies were performed at pH 7.4 and CVs were recorded in the scan rate range (5 mVs^{-1} to 225 mVs^{-1}) at the fixed concentration of 30 μM of EST and CAF. The peak current (i_p) increased linearly with increasing sweep rate for both the analytes and the plots of i_p vs. ν and log i_p vs log ν were linear. The relations observed are:

For EST $i_p\,(\mu A) = 0.0488\,\nu + 0.2686$ $(R^2 = 0.999)$

$\log i_p = 0.831 \log \nu - 0.9364$ $(R^2 = 0.994)$

For CAF $i_p\,(\mu A) = 0.1319\,\nu + 0.6265$ $(R^2 = 0.999)$

$\log i_p = 0.902 \log \nu - 0.6538$ $(R^2 = 0.999)$

The dependence of i_p versus ν plots for both the analytes suggested the involvement of adsorption controlled process for the oxidation of EST and CAF. The slope of log i_p versus log ν

plots were 0.831 and 0.902 (sufficiently > 0.5) for EST and CAF respectively, which further confirmed adsorption controlled oxidation for EST and CAF [29]. The detailed studies were then carried out using square wave voltammetry.

6.3.3 Square wave voltammetry

Square wave voltammetry was carried out for a mixture of EST and CAF (30 µM of each analyte) at pH 7.4 at different stages of surface modification i.e. unmodified EPPG, ErGO/EPPG, AgNPs/EPPG and AgNPs:ErGO/EPPG and the observed results for this comparison is shown are **Fig. 6.7**. At the unmodified EPPG, two oxidation peaks at 742 mV (EST) and 1318 mV were observed (curve a). Curve b shows the results observed at the ErGO/EPPG sensor, which exhibited shifting of the peak potentials to the less positive values with increased peak currents. At the AgNPs /EPPG surface (curve c) the peak potential shifted to more positive values (656 mV and 1286 mV) for EST and CAF, respectively with enhanced peak current. However, highest peak current and lowest peak potentials with enough separation for EST and CAF (540 mV and 1264 mV) was observed at AgNPs:ErGO/EPPG biosensor, which demonstrated an excellent electrocatalytic activity of AgNPs:ErGO/EPPG surface towards the simultaneous determination of EST and CAF.

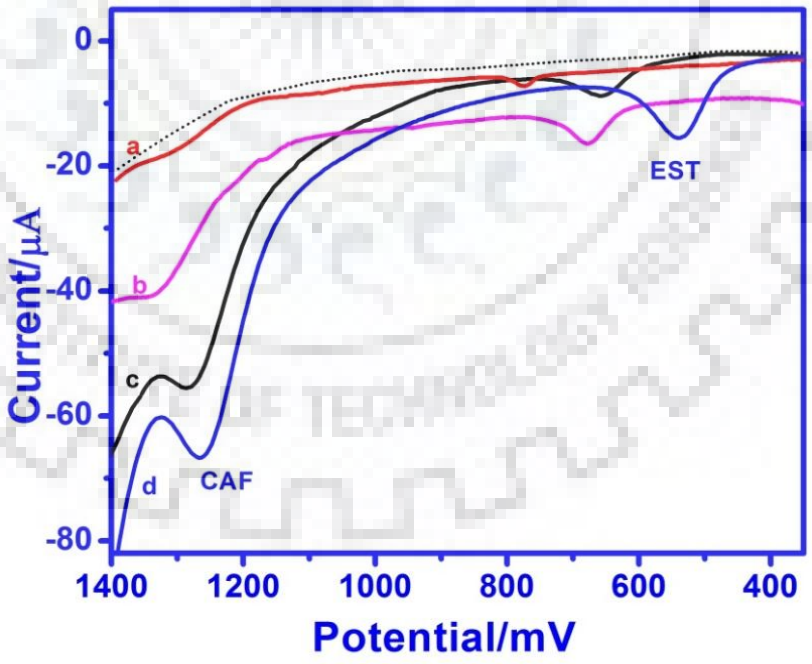

Fig. 6.7: A comparison of SWVs observed for the mixture of EST (30 µM), and CAF (30 µM) at unmodified EPPG (curve a), ErGO/EPPG (curve b), AgNPs/EPPG (curve c), and AgNPs:ErGO/EPPG (curve d) at pH 7.4. The dotted line represents the background.

6.3.3.1 Electrochemical investigations of EST

The influence of pH on the electrochemical behaviour of EST was studied in 0.1 M buffer of different pH 2.4–10.5 for EST (20 μM) at the AgNPs:ErGO/EPPG by recording square wave voltammograms. A significant shifting of peak potential of EST to less positive potentials has been witnessed with increasing pH of the solution. The observed E_p versus pH plot was linear and the dependence of E_p on pH can be represented as:

$$\mathbf{E_p\ (pH\ 2.4 - 10.5) = -58.78\ pH + 972.2\ mV \quad vs.\ Ag/AgCl \qquad (R^2 = 0.998)}$$

where R^2 represents the correlation coefficient. The observed slope of dE_p/dpH (58.78 mV/pH) was close to the theoretical Nernst value (~59 mV/pH) and suggested the involvement of equal number of electrons and protons in the oxidation of EST at the AgNPs:ErGO/EPPG. The variation of peak current with pH of phosphate buffer for EST is presented in **Fig 6.8 (A)**. The effect of ionic strength of buffers on the E_p of EST was studied in the range 0.01 to 1.0 M. It was observed that peak current increases with increasing ionic strength from 0.01 to 0.5 M and slightly decreases from 0.5 M to 1 M ionic strength of phosphate buffer. Hence, phosphate buffer of 0.5 M ionic strength was used throughout the studies.

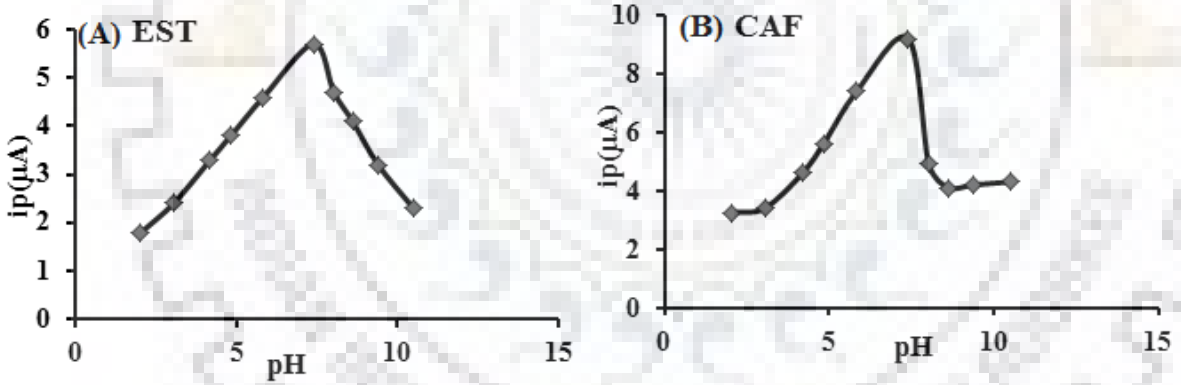

Fig. 6.8: Observed variation of peak current with pH for EST (**A**) and CAF (**B**) in phosphate buffer of pH 7.4.

The effect of increase in square wave frequency on the peak current of EST was studied at AgNPs:ErGO/EPPG and the voltammograms were recorded for EST (20 μM) over the frequency range 5-40 Hz at pH 7.4. The increase in the square wave frequency resulted an increase in the peak current of EST and a linear dependence of peak current (i_p) vs. frequency (f) was noticed.

$$\mathbf{i_p/\mu A = 0.3114\ f + 0.8014 \qquad (R^2 = 0.996)}$$

$$\mathbf{\log i_p = 0.9051 \log f - 0.3245 \qquad (R^2 = 0.992)}$$

where, R^2 represents the correlation coefficient and f denotes the square wave frequency in Hz. The linearity of the above relation suggested an adsorption controlled pathway for the oxidation of EST, which has also been confirmed by the linear relation between log i_p versus log f, having a slope > 0.5 [29]. Thus, it is concluded that the oxidation processes of EST was adsorption controlled.

SWVs were also recorded at pH 7.4 for various concentrations of EST. The observed results show that the peak current of EST was linearly dependent on the EST concentrations, over the range 0.001-175 μM as displayed in **Fig. 6.9 A**. The peak current is calculated by subtracting the background current and the reported value is an average of minimum three replicate voltammograms. The linear calibration curve exhibited a break at around 1 μM, the observed linear relations at lower (0.001−1 μM) and higher (3−175 μM) concentration range can be represented as:

$$\mathbf{i_p\ (\mu A) = 1.2482\ [C\ (0.001{-}1)\ \mu M] + 1.158 \qquad (R^2 = 0.999)}$$

$$\mathbf{i_p\ (\mu A) = 0.2014\ [C\ (3{-}\ 175)\ \mu M] + 1.9524 \qquad (R^2 = 0.999)}$$

The value of 3σ/b and 10 σ/b were used to calculate the limit of detection (LOD) and limit of quantification (LOQ), respectively for EST, where σ is the standard deviation of the blank signals and b is the observed slope of the calibration curve. At the proposed AgNPs:ErGO/PG biosensor, the observed LOD and LOQ for EST were found as 0.046 nM and 0.80 nM, respectively.

6.3.3.2 Electrochemical investigations of CAF

The effect of pH on the oxidation of CAF was studied by recording SWVs for 10 μM concentration of CAF in the phosphate buffers of pH 2.4–10.5 at fabricated AgNPs:ErGO/EPPG. The peak potential of CAF was shifted towards less positive value with increasing pH of the solution and Ep versus pH relation was found to be linear:

$$\mathbf{E_p\ (pH\ 2.4 - 10.5) = -55.46\ pH + 1674.5\ mV\ \ vs.\ Ag/AgCl \qquad (R^2 = 0.9971)}$$

The observed slope of dE_p/pH (55.4 mV/pH) indicated the involvement of equal number of protons and electrons in the electro-oxidation of CAF. The variation of peak current with pH of phosphate buffer for CAF is presented in **Fig. 6.8 (B).**

The frequency study was carried out for 10 μM CAF over the frequency range 5-40 Hz. The peak current of CAF increased with the increase in the square wave frequency and the linear relation of peak current (i_p) vs. frequency (f) and log i_p versus log f can be represented as:

$$\mathbf{i_p/\mu A = 0.4212\ f + 0.5357 \qquad (R^2 = 0.998)}$$

$$\log i_p = 0.924 \log f - 0.2447 \qquad (R^2 = 0.998)$$

where, f is square wave frequency (Hz). The linearity of i_p vs. f indicated that oxidation of CAF is adsorption controlled, which was further confirmed by the slope of d log f/d log i_p (> 0.5).

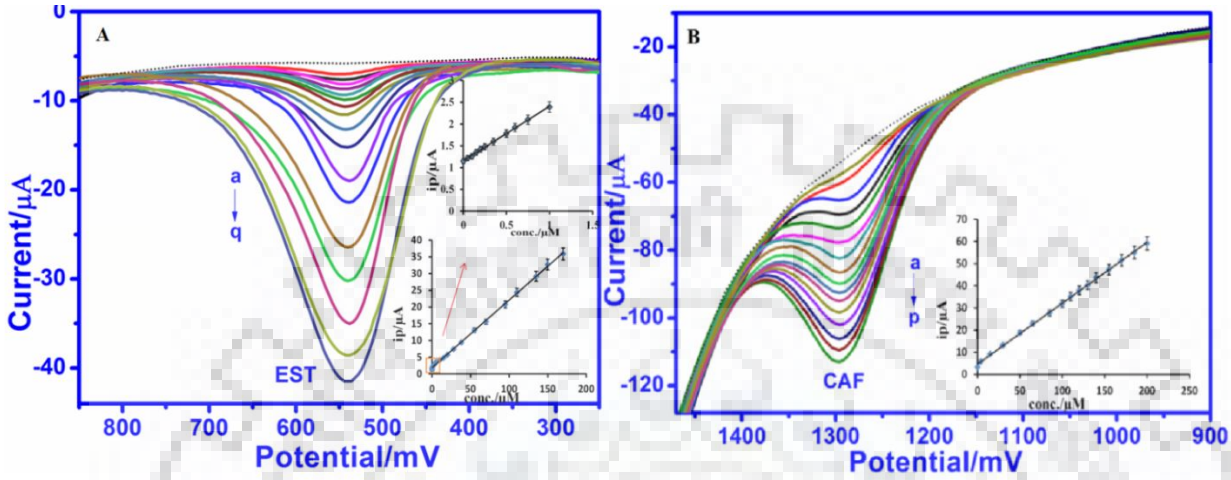

Fig. 6.9: (A). SWVs observed at pH 7.4 for the increasing concentration of EST at AgNPs:ErGO/PG (a) 0.001, (b)0.005, (c) 1, (d) 3, (e) 5, (f) 10, (g) 15, (h) 20, (i) 30, (j) 38, (k) 55, (l) 70, (m) 95, (n) 110, (o) 135, (p) 150 and (q) 175 µM; inset is the calibration plot, in which zoom portion shows increasing concentration of EST as 0.001, 0.005, 0.05, 0.15, 0.2, 0.25, 0.35, 0.5, 0.6, 0.75 and 1 µM. **(B)**. SWVs observed for the increasing concentration of CAF at pH 7.4 (a) 0.001, (b) 4, (c) 15, (d)30, (e) 50, (f) 65, (g) 85, (h) 100, (i) 110, (j) 120, (k) 130, (l) 140, (m) 155, (n) 170, (o) 185 and (p) 200 µM; inset is the calibration plot.

The modified AgNPs:ErGO/EPPG sensor was then used for the quantification of CAF. SWVs were recorded in the concentration range 0.001 to 200 µM of CAF at pH 7.4 and observed response in terms of oxidation peak current is shown in **Fig. 6.9 (B)**. The observed results demonstrate an increase in peak current with the increase in the concentration of CAF under the optimum conditions and displayed a linear calibration over the wide concentration range 0.001-200 µM. The observed relation can be represented as:

$$i_p\,(\mu A) = 0.275\,[C\ 0.001 - 200\ \mu M] + 4.6244 \qquad (R^2 = 0.999)$$

The LOD and LOQ were found as 0.54 nM and 1.2 nM, respectively.

6.3.3.3 Simultaneous analysis of EST and CAF

A long term CAF intake has the potential to influence EST concentration in women, which lead to many abnormalities, hence the simultaneous determination of EST and CAF was carried

out. As the peak current for EST and CAF were maximum at pH 7.4, hence the studies were carried out at this pH using AgNPs:ErGO/PG sensor. The experiment has been carried out in two sets, in the first set of experiments, the voltammograms were recorded by keeping the fixed concentration of EST as 30 µM and the concentration of CAF was increased from 15 µM to 100 µM. Two distinguished oxidation peaks at potentials 540 and 1264 mV for EST and CAF, were observed as displayed in **Fig. 6.10A**, which clearly demonstrated that on increasing the concentration of CAF, the oxidation peak current of CAF increased without affecting the peak potential and peak current of EST. Similar results were found in the second set of experiments, where voltammograms were recorded with increasing concentration of EST from 10 µM to 95 µM at fixed concentration of CAF (30 µM). The increase in peak current was observed with increasing EST, whereas the oxidation peak current and peak potential of CAF remain unchanged as presented in **Fig. 6.10B**. The linear relations for EST and CAF were essentially similar to that observed for the individual determination. Hence, it is concluded that simultaneous determination of the two analytes can be achieved effectively at the AgNPs:ErGO/PG.

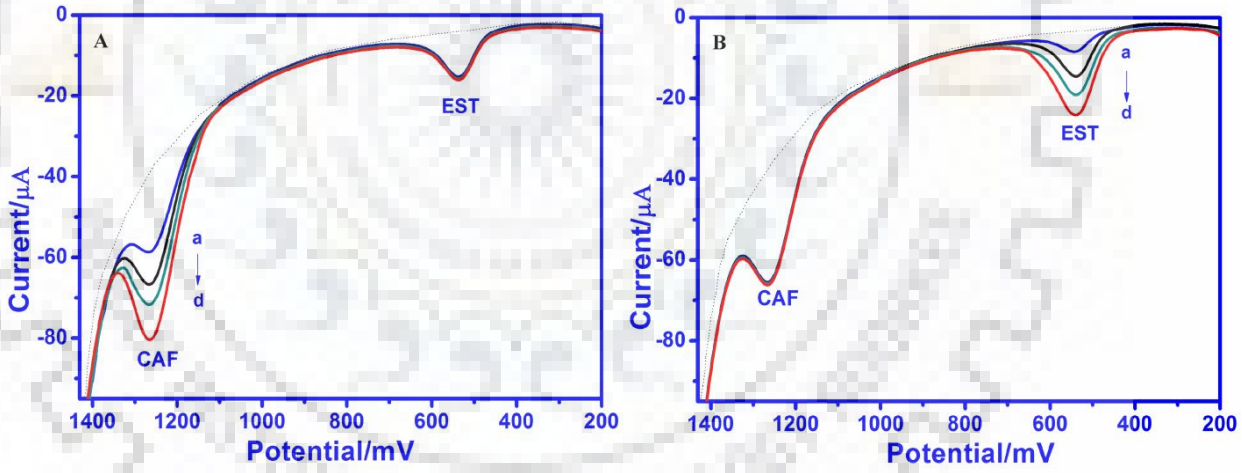

Fig. 6.10: (A) SWVs of a mixture of EST and CAF at AgNPs:ErGO/EPPG sensor at pH 7.4 at concentration of CAF (a) 15; (b) 50; (c) 85 and (d) 100 µM. The concentration of EST was constant (30 µM). The background is shown by the dotted line.

(B) SWVs observed for a mixture of EST and CAF at AgNPs:ErGO/EPPG sensor at pH 7.4 at concentration of EST (a) 10; (b) 28; (c) 38 and (d) 95 µM. The concentration of CAF was constant (30 µM). The background is shown by the dotted line.

6.3.4 Interference, Stability and Reproducibility studies

The interference studies were performed by recording SWVs under optimized conditions in the presence of common interfering substances, such as ascorbic acid (AA), uric acid (UA), xanthine (XT) and hypoxanthine (HX). The observed results are presented in **Fig. 6.11**, where the concentration of AA, UA, XT and HX was increased upto 600 µM and the concentration of EST and CAF was constant at 30 µM. It was noticed that AA, UA, XT and HX had no interference (even in the presence of higher amount) in the oxidation of EST and CAF at modified AgNPs:ErGO/PG. The interference of glucose and H_2O_2 was also determined at the AgNPs:ErGO/PG sensor, where the oxidation peaks were observed at the -374 mV and 98 mV for glucose and H_2O_2, respectively and were similar to the previously reported work [30,31]. As these oxidation potential were well separated they did not interfere in the determination of EST and CAF.

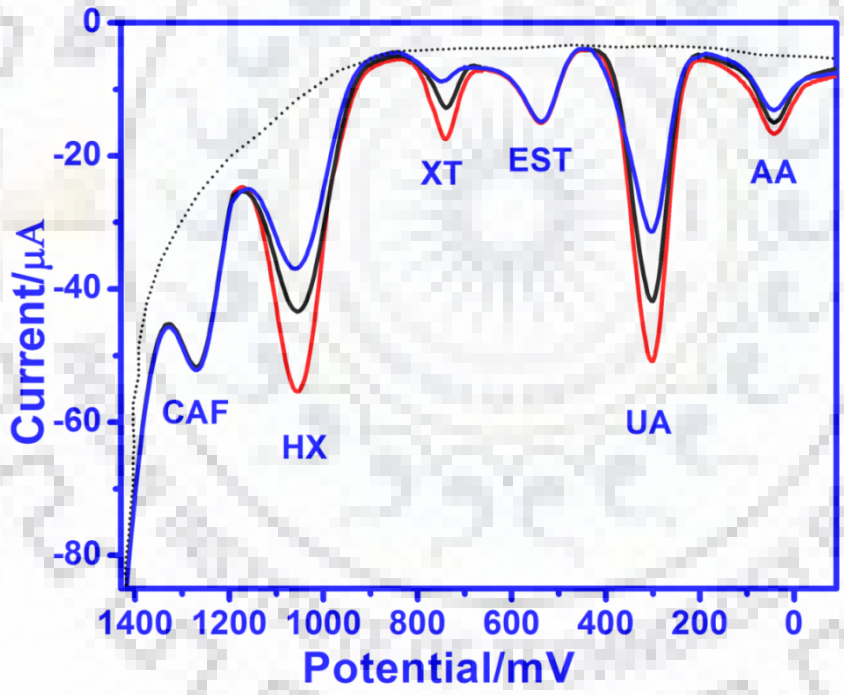

Fig. 6.11: SWVs recorded for 30 µM EST and 30 µM CAF in the presence of ascorbic acid (AA), uric acid (UA), xanthine (XT) and hypoxanthine (HX) at the AgNPs:ErGO/EPPG sensor at pH 7.4. The background is displayed by the dotted line.

To demonstrate the stability of the proposed biosensor, the response of the sensor was monitored at 30 µM concentration of both the analytes over a period of 30 days at pH 7.4. The voltammograms for each analyte were recorded every day and after the use; the sensor was kept

under the ambient conditions. It was observed that the peak current response for EST and CAF remained unchanged for first 15 days with relative standard deviation (R.S.D.) as ± 1.65% and ±1.94%. After 15 days, the peak current decreased significantly. Therefore; the presented sensor can be successfully applied for first 15 days for the simultaneous determination of EST and CAF. The intraday reproducibility of the presented sensor was then checked by recording at least six replicate voltammograms during same day at an interval of 1 h in the blank solution as well as in the mixture of EST and CAF (30 μM each). The observed R.S.D. values for n = 6 were ± 0.94% and ± 1.06% for EST and CAF, respectively, which clearly indicated the good accuracy and reproducibility of modified AgNPs:ErGO/EPPG sensor.

6.3.5 Analytical Application

The intake of caffeinated drinks by women of childbearing age (18–35 yr) is common now a days. Approximately 90% of women of this category consume an average of 2 to 3 cups caffeinated coffee (equivalent to 165 mg caffeine/day). In addition varieties of other sources mostly from caffeinated beverages are also consumed. Consumption of CAF for a long time can influence the women's EST level and the variation in EST level over a long period may lead to many disorders such as breast cancer, endometriosis and ovarian cancers. Thus, the applicability of the biosensor was examined for the determination of EST and CAF in the blood serum and urine by standard addition method. The samples were collected before consumption of CAF and after 5 h (half-life of caffeine in the circulation) [32] of consumption of ~2 cups of coffee (equivalent to 200 mg caffeine) by women of child bearing age having regular menstrual cycle and not currently using hormonal contraception. Prior to analysis, the collected urine and serum samples were diluted two times with phosphate buffer of pH 7.4 prior to analysis to minimize matrix complexity. Typical SWV of serum of F-1 is represented in **Fig. 6.12** and two clear peaks of EST and CAF (E_p 540 and 1264 mV) were observed. Several other peaks were also noticed, however, no attempt was made to identify them.

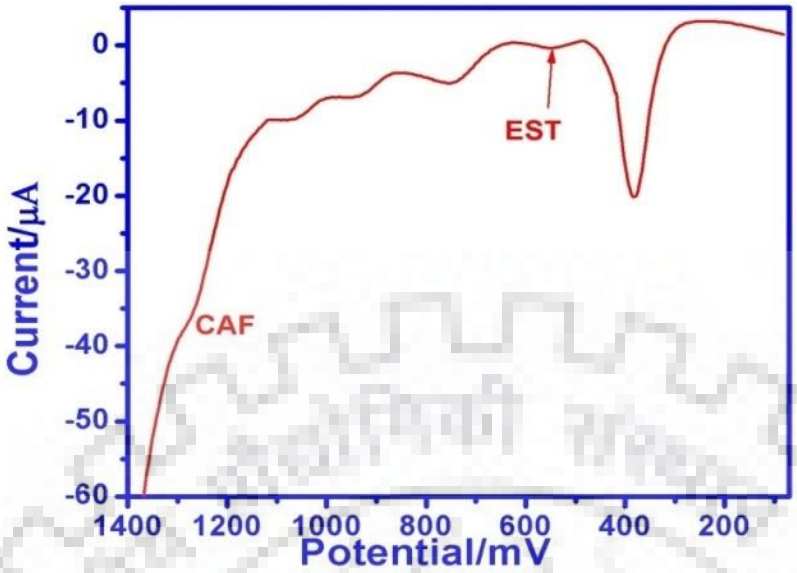

Fig. 6.12: A SWV recorded for blood serum of F-1 at pH 7.4.

The EST content was determined using the standard addition method and the results are summarized in **Table 1.** The recoveries after spiking were found in the acceptable range (99.41 to 100.41%). Similarly the estradiol content was determined in other urine samples using the standard addition method and the results are summarized in **Table 2.** Typical SWV of urine sample of F-1 is represented in **Fig. 6.13 (A)** and two clear peaks of EST and CAF (E_p 540 and 1264 mV) were observed. The studies demonstrate that the presented approach can be successfully employed for the selective determination of EST and CAF in physiological samples.

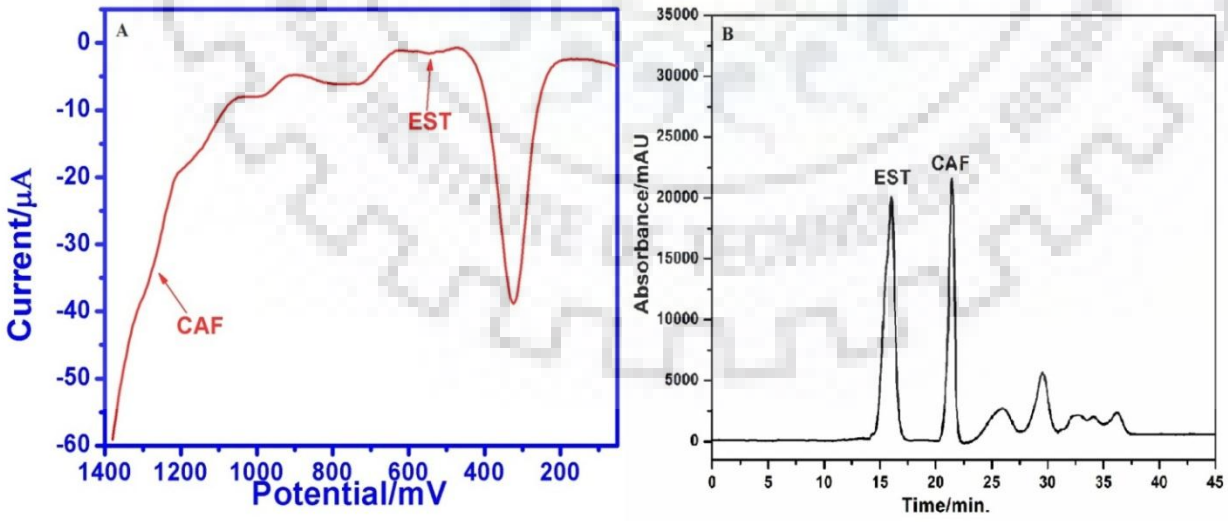

Fig. 6.13: (**A**) A SWV recorded for urine sample of F-1 at pH 7.4. (**B**) HPLC chromatogram observed for urine sample of F-1.

Table 1: Analysis of CAF and EST in the woman serum samples at the modified sensor after 5 h of consuming coffee.

Serum No.	CAF (µM)	EST Before CAF intake (nM)	EST After CAF intake (nM)	EST Spiked (nM)	EST observed[a] (nM)	Recovery (%)*
F-1	10.5	1.36	1.72	0	1.72	-
				10	11.73	100.58
				20	21.71	99.41
F-2	15.3	2.04	2.42	0	2.42	-
				10	12.41	99.58
				20	22.43	100.41
F-3	17.2	2.23	2.59	0	2.59	-
				10	12.58	99.61
				20	22.60	101.56
F-4	12.4	1.84	2.01	0	2.01	-
				10	12.02	100.49
				20	21.99	99.12
F-5	8.6	0.95	1.35	0	1.35	-
				10	11.36	100.71
				20	21.34	99.25

*The R.S.D. value for determination was less than 1.98 for n = 3.
[a]The observed values are sum of metabolite present + spiked amount.

The analysis results of EST were validated by using HPLC. In the HPLC chromatogram, EST exhibited a sharp peak at 16.023 min, whereas a sharp peak was observed at 21.461 min for CAF. Different concentrations of EST and CAF were then analyzed under same conditions and the areas under the peaks observed were plotted against concentration. The F-1 urine sample was then injected in HPLC and the observed chromatogram is presented in **Fig. 6.13 (B)**. Area of the peaks observed at 16.023 min and 21.461 min were determined. The concentrations of EST and CAF

were then calculated from the calibration plot and found to be 1.42 nM and 12.2 µM for EST and CAF, respectively. Thus, the practically similar values of EST by using the sensor and HPLC indicated that the sensor is sufficiently sensitive.

Table 2: Analysis of CAF and EST in the woman urine samples at the modified sensor after 5 h of consuming coffee.

Urine No.	CAF (µM)	EST Before CAF intake (nM)	EST After CAF intake (nM)	EST Spiked (nM)	EST observed[a] (nM)	Recovery (%)*
				0	1.42	-
F-1	12.2	1.26	1.42	5	6.43	100.70
				10	11.41	99.29
				0	0.94	-
F-2	9.5	0.68	0.94	5	5.95	101.06
				10	10.93	98.93
				0	1.21	-
F-3	11.6	1.03	1.21	5	6.22	100.82
				10	11.20	99.17
				0	1.65	-
F-4	13.6	1.48	1.65	5	6.64	99.39
				10	11.66	100.60
				0	0.68	-
F-5	7.8	0.54	0.68	5	5.67	98.52
				10	10.69	101.47

*The R.S.D. value for determination was less than 1.90 for n = 3.
[a]The observed values are sum of metabolite present + spiked amount.

6.4 CONCLUSION

A sensitive one step electro-deposition of AgNPs:ErGO nanocomposite at the pyrolytic graphite surface has been successfully achieved and efficiently used for the simultaneous determination of the EST and CAF. An increase in effective surface area (~40 times) as compared to unmodified and the synergetic effect of Ag nano particles and reduced GO, due to storage capability of electrons and providing electrons on demand, has been found to exhibit electrocatalytic effect for the oxidation of EST. The linear calibration curves were obtained for EST and CAF in the linear range of 0.001-175 µM and 0.001-200 µM, respectively. The limits of detection were found as 0.046 nM and 0.54 nM for EST and CAF, respectively with quantification limits as 0.80 nM and 1.2 nM for EST and CAF, respectively. A comparison of limit of detection observed for EST and CAF with present sensor was made with the sensors reported in recent years (**Table 3**). It is noticed that the prepared sensor is more sensitive than reported earlier.

Table 3: A comparison of analysis results of EST and CAF at AgNPs:ErGO/EPPG biosensor with previously reported methods.

S.No.	Method/Electrode	Conc. range (µM)	LOD (nM)	Real sample	Ref.
	EST				
1.	Pd/N doped red GO	0.1-400	1.8	Yes	[18]
2.	poly(L-serine)/GCE	0.03-10	20	Yes	[33]
3.	RGO–DHP/GCE	0.2-40	77	No	[34]
4.	MWNT–GNP/PGE	0.4-700	10	Yes	[35]
5.	MWNTs/GCE	0.001-1	5	No	[36]
6.	AgNPs:ErGO/EPPG	0.001-175	0.046	Yes	This work
	CAF				
1.	AQMCPE	2-800	143	Yes	[7]
2.	Nafion–Gr/GCE	40-600	120	Yes	[8]
3.	BDD	40-25	150	Yes	[9]
4.	AuNP-GCPE	25-1000	96	No	[37]
5.	AgNPs:ErGO/EPPG	0.001-200	0.54	Yes	This work

DHP:dihexadecylphosphate film (DHP)., **RGO:** reduced graphene oxide, **MWNT–GNP:** multi-walled carbon nanotube–gold nanoparticle composite, **AQMCPE:** Anthraquinone Modified Carbon Paste Electrode, **BDD**: boron-doped diamond electrode, **AuNP-GCPE:** gold nanoparticle-glassy carbon paste composite electrode.

The common interfering compounds, such as AA, UA XT and HX present in the physiological fluids did not show any interference in the determination. The presented approach can be efficiently applied to determine the effect of CAF on the concentration of EST in women of child bearing age. The present studies demonstrate that the approach is simple, reproducible, highly selectivity and good sensitivity with long term stability of the modified sensor. It is noticed that the increase in EST level after the intake of ~200 mg caffeine in blood serum and urine is in the range 10 to 42% and 11 to 38% respectively. The studies indicate that CAF intake more than 200 mg/day on regular basis should be avoided.

6.5 REFERENCES

[1] K.J. Ryan, "Biochemistry of aromatase: significance to female reproductive physiology", Cancer Res. 42 (1982) 3342s.

[2] J. Cui, Y. Shen, R. Li, "Estrogen synthesis and signaling pathways during ageing: from periphery to brain", Trends Mol Med. 19 (2013) 197.

[3] F. Kordi, H. Khazali, "The effect of ghrelin and estradiol on mean concentration of thyroid hormones", Int J Endocrinol Metab. 13 (2015) e17988.

[4] H.T. Depypere, S. Bolca, M. Bracke, J. Delanghe, F. Comhaire, P. Blondeel, "The serum estradiol concentration is the main determinant of the estradiol concentration in normal breast tissue", Maturitas 81 (2015) 42.

[5] K.C. Schliep, E.F. Schisterman, S.L. Mumford, A.Z. Pollack, C. Zhang, A. Ye, J.B. Stanford, A.O. Hammoud, C.A. Porucznik, J.W. Wende, "Caffeinated beverage intake and reproductive hormones among premenopausal women in the biocycle study", Am J Clin Nutr. 95 (2012) 488.

[6] J.S. Sisti, S.E. Hankinson, N.E. Caporaso, F. Gu, R.M. Tamimi, B. Rosner, X. Xu, R. Ziegler, A.H. Eliassen, "Caffeine, coffee and tea intake and urinary estrogens and estrogen metabolites in premenopausal women", Cancer Epidemiol Biomarkers Prev. 8 (2015) 1174.

[7] Y. Tadesse, A. Tadese, R.C. Saini, R. Pal, "Cyclic voltammetric investigation of caffeine at anthraquinone modified carbon paste electrode", Int. J. Electrochem. Sc. 2013 (2013) 1.

[8] J.Y. Sun, K.J. Huang, S.Y. Wei, Z.W. Wu, F.P. Ren, "A graphene-based electrochemical sensor for sensitive determination of caffeine", Colloids Surf. B 84 (2011) 421.

[9] L. Svorc, P. Tomcik, J. Svitkova, M. Rievaj, D. Bustin, "Voltammetric determination of caffeine in beverage samples on bare boron-doped diamond electrode", Food Chem. 135 (2012) 1198.

[10] A. Ascherio, M.G. Weisskopf, E.J. O'Reilly, M.L. McCullough, E.F. Calle, C. Rodriguez, M.J. Thun, "Coffee consumption, gender, and parkinson's disease mortality in the cancer prevention study ii cohort: the modifying effects of estrogen", Am J Epidemiol 160 (2004) 977.

[11] C. Nagata, M. Kabuto, H. Shimizu, "Association of coffee, green tea, and caffeine intakes with serum concentrations of estradiol and sex hormone-binding globulin in premenopausal japanese women", Nutr. Cancer 30 (1998) 21.

[12] D.R. Lee, J. Lee, M. Rota, J. Lee, H.S. Ahn, S.M. Park, D. Shin, "Coffee consumption and risk of fractures: A systematic review and dose–response meta-analysis", Bone 63 (2014) 20.

[13] M. Fujimaki, S. Saiki, Y. Li, N. Kaga, H. Taka, T. Hatano, K.I. Ishikawa, Y. Oji, A. Mori, A. Okuzumi, T. Koinuma, S.I. Ueno, Y. Imamichi, T. Ueno, Y. Miura, M. Funayama, N. Hattori, "Serum caffeine and metabolites are reliable biomarkers of early Parkinson disease", Neurology 90 (2018) e404.

[14] K. Xu, Y. Xu, D.B. Jermyn, J.F. Chen, A. Ascherio, D.E. Dluzen, M.A. Schwarzschild, "Estrogen Prevents Neuroprotection by Caffeine in the Mouse 1-Methyl-4-Phenyl-1,2,3,6-Tetrahydropyridine Model of Parkinson's Disease", J. Neurosci. 26 (2006) 535.

[15] C.J. Munro, G.H. Stabenfeldt, J.R. Cragun, L.A. Addiego, J.W. Overstreet, B.L. Lasley, "Relationship of serum estradiol and progesterone concentrations to the excretion profiles of their major urinary metabolites as measured by enzyme immunoassay and radioimmunoassay", Clin. Chem. 37 (1991) 838.

[16] B. Yilmaz, Y. Kadioglu, "Determination of 17 b-estradiol in pharmaceutical preparation by UV spectrophotometry and high performance liquid chromatography methods", Arab. J. Chem. 10 (2017) S1422.

[17] B.E.P. Fajara, H. Susanti, "HPLC determination of caffeine in coffee beverage", Mater. Sci. Eng. C 259 (2017) 1.

[18] J. Li, J. Jiang, D. Zhao, Z. Xu, M. Liu, P. Deng, X. Liu, C. Yang, D. Qian, H. Xie, "Facile synthesis of Pd/N-doped reduced graphene oxide via a moderate wet-chemical route for non-enzymatic electrochemical detection of estradiol", J. Alloys Comp. 769 (2018) 566.

[19] Y. Shi, D.D. Penga, C.H. Shi, X. Zhang, Y.T. Xie, B. Lu, "Selective determination of trace 17b-estradiol in dairy and meat samples by molecularly imprinted solid-phase extraction and HPLC", Food Chem. 126 (2011) 1916.

[20] J. Ganan, D.P. Quintanilla, S.M. Zarcero, I. Sierra, "Comparison of different mesoporous silicas for off-line solid phase extraction of 17-estradiol from waters and its determination by hplc-dad", J. Hazard. Mater. 260 (2013) 609.

[21] X. Chen, Z. Shi, Y. Hu, X. Xiao, G. Li, "A novel electrochemical sensor based on Fe3O4-doped nanoporous carbon for simultaneous determination of diethylstilbestrol and 17β-estradiol in toner", Talanta 188 (2018) 81

[22] G.K. Ramesha, S. Sampath, "Electrochemical Reduction of Oriented Graphene Oxide Films: An in Situ Raman Spectroelectrochemical Study", J. Phys. Chem. C 113 (2009) 7985.

[23] A.A. Nafiey, P. Subramanian, A. Addad, B. Sieber, S. Szunerits, R. Boukherroub, "Green synthesis of reduced graphene oxide-silver nanoparticles using environmentally friendly l-arginine for H_2O_2 detection", ECS J. Solid State Sci. Technol. 5 (2016) M3060.

[24] H.L. Guo, X.F. Wang, Q.Y. Qian, F.B. Wang, X.H. Xia, "A Green Approach to the Synthesis of Graphene Nanosheets", Acs nano 9 (2009) 2653.

[25] I.V. Lightcap, T.H. Kosel, P.V. Kamat, "Anchoring semiconductor and metal nanoparticles on a two-dimensional catalyst mat. storing and shuttling electrons with reduced graphene oxide", Nano Lett. 10 (2010) 577.

[26] W.S. Hummers, R.E. Offeman, "Preparation of Graphitic Oxide", J. Am. Chem. Soc. 80 (1958) 1339.

[27] R.N. Goyal, S.K. Srivastava, R. Agarwal, "Electrochemical behavior and aggregation number of pyridinol azo dyes", Bull. Soc. Chim. Fr. 4 (1985) 656.

[28] R.K. Das, S. Saha, V.R. Chelli, A.K. Golder, "Bio-inspired AgNPs, multilayers-reduced graphene oxide and graphite nanocomposite for electrochemical H_2O_2 sensing", Bull. Mater. Sci. 41 (2018) 1.

[29] J.M. Zen, Y.Y. Lai, H.H. Yang, A.S. Kumar, "Multianalyte sensor for the simultaneous determination of hypoxanthine, xanthine and uric acid based on a preanodized nontronite-coated screen-printed electrode", Sens. Actuators B 84 (2002) 237.

[30] S. Daniele, D. Battistel, S. Bergamin, C. Bragato, "Voltammetric determination of glucose at bismuth-modified mesoporous platinum microelectrodes", Electroanalysis 22 (2010) 1511.

[31] J.A. Cox, R.K. Jaworski, "Voltammetric reduction and determination of hydrogen peroxide at an electrode modified with a film containing palladium and iridium", Anal. Chem. 61 (1989) 2176.

[32] T.M. McLellan, J.A. Caldwell, H.R. Lieberman, "A review of caffeine's effects on cognitive, physical and occupational performance", Neurosci. Biobehav. Rev.71 (2016) 294.

[33] J. Song, J. Yang, X. Hu, "Electrochemical determination of estradiol using a poly(L-serine) film-modified electrode", J. Appl. Electrochem. 38 (2008) 833.

[34] B.C. Janegitz, F.A. DosSantos, R.C. Faria, V. Zucolotto, "Electrochemical determination of estradiol using a thin film containing reduced graphene oxide and dihexa decylphosphate", Mater. Sci. Eng. C. 37 (2014) 14.

[35] G. Hao, D. Zheng, T. Gan, C. Hua, S. Hu, "Development and application of estradiol sensor based on layer-by-layer assembling technique", J. Exp. Nanosci. 6 (2011) 13-28.

[36] H. Tao, W. Wei, X. Zeng, X. Liu, X. Zhang, Y. Zhang, "Electrocatalytic oxidation and determination of estradiol using an electrode modified with carbon nanotubes and an ionic liquid", Microchim Acta 166 (2009) 53.

[37] T. Oren, U. Anik, "Voltammetric determination of caffeine by using gold nanoparticle-glassy carbon paste composite electrode", Measurement 106 (2017) 26.